Free Vibration Analyses of Stationary and Rotating Tapered Composite Beams with Delamination

Puneet Jagpaul

A thesis

in

the Department

of

Mechanical, Industrial and Aerospace Engineering (MIAE)

Presented in Partial Fulfillment of the Requirements

For the Degree of

Master of Applied Science (Mechanical Engineering) at

Concordia University

Montreal, Quebec, Canada

March 2021

CONCORDIA UNIVERSITY

School of Graduate Studies

This is to certify that the thesis prepared

By: Puneet Jagpaul

Entitled: Free Vibration Analyses of Stationary and Rotating Tapered Composite Beams with Delamination

and submitted in partial fulfillment of the requirements for the degree of

Master of Applied Science (Mechanical Engineering)

complies with the regulations of the University and meets the accepted standards with respect to originality and quality.

Signed by the final Examining Committee:

Dr. Farjad Shadmehri	Chair
Dr. Farjad Shadmehri	Examiner
Dr. Adel M. Hanna	Examiner
Dr. R. Ganesan	Supervisor

Approved by Dr. Mamoun Medraj
Chair of Department or Graduate Program Director

Dr. Mourad Debbabi
Dean of Faculty

Date March 30, 2021

ABSTRACT

Free Vibration Analyses of Stationary and Rotating Tapered Composite Beams with Delamination

Puneet Jagpaul

The exceptional engineering properties and customizability of the laminated composites have enabled their use in the design of the stationary and rotating tapered structures in the aerospace and energy sectors. The tailoring capabilities of the composite material can be used to stiffen the structure at one location while being flexible at other location and consequently reduce the weight, as required in specific applications such as helicopter rotor blade, windmill blade and turbine blade. The vibration characteristics (natural frequencies and mode shapes) of the stationary and rotating structures differ substantially and must be well identified in the design stage. The composite structures are prone to failures such as delamination and fiber-matrix debonding caused during their fabrication or in service, especially when used as blades and beams in various stationary and rotating applications. Delamination reduces the overall stiffness and the strength of the laminates, which may lead to local or sudden structural failures. The delaminated structure has reduced natural frequencies and exhibits different mode shapes than that of the intact structure.

In the present thesis, the free vibration analyses of stationary and rotating tapered composite beams with delamination are conducted. The influence of the delamination on the vibration characteristics of the stationary and rotating tapered composite beams is comprehensively studied. The Finite Element Analysis tool ANSYS® is used to develop three-dimensional models of the intact and delaminated composite beams. The natural frequencies of the stationary and rotating intact cantilever composite beams are determined for uniform, thickness-tapered and doubly tapered beam profiles using modal analysis and the results are compared with the results available in the literature. The Mode-I and Mode-II delamination tests are performed on the numerical models of the double cantilever beam and end notch flexure test samples based on cohesive zone modeling and the results of the tests are verified with the available results. The critically stressed locations prone to delamination in the stationary and rotating composite beams are determined using the first-ply failure analyses based on Tsai-Wu failure criterion. The free vibration responses of the stationary and rotating composite beams with end and mid-span delaminations of different lengths and with different stacking sequences are obtained and they are verified wherever possible. The

delamination length that has minimal effect on the first three natural frequencies of the uniform and thickness-tapered composite beams is determined and is found to be 5% of the total beam length. Higher modes should be investigated for the composite structures with smaller delamination. A basis for the non-destructive evaluation is suggested for the stationary thickness-tapered simply supported composite beams with end and mid-span delaminations. The influences of the delamination length, delamination location, fiber orientation angle, thickness-tapering, double tapering, layer reduction and taper angle on the free vibration response of the stationary and rotating delaminated composite beams are investigated for uniform, thickness-tapered and doubly tapered beam profiles through various parametric studies. The influences of the rotational velocity and hub radius on the natural frequencies of the rotating doubly tapered composite beams with delamination are thoroughly examined. The present thesis contributes towards the safe design of the composite structures. The studies performed are helpful for developing delamination detection techniques based on the free vibration response of tapered composite beams and can aid designers to model optimised tapered composite structures by considering the influences of delamination on their vibrational characteristics.

ACKNOWLEDGEMENT

First and foremost, I would bow down and express my invaluable gratitude to almighty god who gave me the ability to complete this thesis and to my late grandparents for showering their blessings on me.

I cannot express enough thanks to my supervisor, Dr. Rajamohan Ganesan for his continued support and encouragement. I offer my sincere appreciation for the learning opportunities he provided and for inspiring each student to go beyond their limits and to dream for the best. I am very grateful to him for being very patient and for all his time that he spared in discussing the various subjects of this thesis, and for going through the numerous versions of this dissertation. I benefited enormously form his excellence as a mentor.

I would like to dedicate this accomplishment to my respected parents, Mrs. Shakti Bhardwaj and Mr. Kamaldeep Jagpaul, and to my sister Dr. Dimple and my brother-in-law Dr. Damandeep. I am grateful for their love, invaluable encouragement, unconditional support, and their sacrifice to shape me into what I am today. I would like to thank my significant other for her constant affection, understanding and immense patience.

I would also like to thank Pramod Kumar, Ajeesh Nair, Prateek Arora and all my friends at the graduate research office EV 13.167 who supported me during my research studies by sharing ideas and discussions. There are no words to express my gratitude to all my friends for their constant moral support throughout.

I gratefully acknowledge the funding support for my research provided by NSERC and Concordia University.

Thank you.

Table of Contents

List of Figures

List of Tables

Chapter 1

Introduction, literature review and scope of the thesis

1.1 Vibration analysis in mechanical design

Mechanical vibration is the interaction of inertia and restoring forces in a structure resulting in fluctuating motion from a state of equilibrium. The inertia tends to maintain the current state of the object, whereas the restoring force pushes the object back to its equilibrium position. In general, vibration results in the wastage of energy, reduction in performance, unpleasant motion and noise. Vibration induces dynamic stresses and fatigue in the structure and leads to progressive and localized structural damage. If the structure is allowed to vibrate near its natural frequency, it may lead to unpredictable failure due to the resonance which accelerates the vibration excessively. Therefore, the vibration analysis of the machines and structures becomes important to maintain the operating performance and to prevent the sudden failures.

1.2 Free vibration analysis of rotating structures

The high-speed rotating structures are widely used in the aerospace and energy sectors. The rotating structures such as wind turbines, helicopter rotors and aircraft propellers are often idealized as rotating beams. The rotating unbalance and uneven distribution of load displace the center of pressure which results in unpleasant vibration.

The vibration characteristics of the rotating structures differ substantially from that of the stationary structures. The basic difference between the stationary and rotating structures is the presence of centrifugal force and Coriolis effect in the rotating structures due to rotational velocity, which is absent in the latter. The centrifugal force increases the bending stiffness of the rotating structure and consequently increases its natural frequencies. For their proper design, the vibration characteristics of the rotating structures must be well identified.

The free vibration of a rotating element is the vibration due to the initial displacement and initial speed. Whenever the natural frequency of the free vibration of a rotating element coincides with the frequency of the external load (forced vibration), resonance may occur which accelerates the vibration excessively and may result in the structure failure.

1.3 Composite material in rotating structures

Composite material can be defined as a synthetic assembly of two or more inorganic materials to acquire desirable material properties, such as high strength/stiffness to weight ratio, favourable thermal and fatigue characteristics, corrosion resistance and damage tolerance. One component of the composite material is usually a continuous phase, called matrix and the other is a discontinuous phase, called reinforcement material that could be in the form of fibres, particles or flakes. The matrix binds the reinforcement together and keeps them in the proper orientation. The matrix also transfers the load to and in between the reinforcement. Fiber reinforced composite materials are generally manufactured as a thin layer, called lamina. Different lamina layers are irreversibly bonded under high pressure and temperature using a hot press or autoclave. The orientation of the fibers in each lamina and the stacking sequence of the layers can be selected to attain the intended strength and stiffness for the specific applications.

Due to the outstanding engineering properties, the composite materials are extensively used in the aerospace, automotive and construction industries. The thickness reduction of the laminated structure is implemented by terminating plies at discrete locations, which reduces the weight of the structure and provides the ability to be stiff at one location while flexible at the other as required in some specific rotating structures like helicopter rotor blade, windmill blade, turbine blades, etc. The elastic and weight tailoring properties of the composite structures make them suitable to be used in the commercial and military aircrafts. The Bell Helicopter engineered the first commercial composite rotor yoke assembly made of glass-fiber (S-2 glass)/epoxy composite material, which is safer and lasts far more flight hours than the traditional titanium or steel yoke.

1.4 Vibration analysis of delaminated composite structures

With the increase in the use of the composite materials in many vital industries, the failure analyses of the composite structures have acquired the attention of many researchers. Detailed experimental and theoretical studies based on the failure analyses of the delaminated composite structures are being conducted globally. Delamination is the separation or debonding of the adjacent plies in the composite laminate and may cause serious structural degradation. Delamination in the composite structure can occur during the manufacturing (due to incomplete

wetting and air entrapment) and/or in the service (due to fatigue, low velocity impact and bird strikes).

Delamination embedded in the laminate is generally barely visible, but its presence degrades the stiffness and the strength of the composite structure and changes the vibration characteristics of the structure. The presence of delamination decreases the natural frequencies and changes the points of inflection of the mode shapes of the composite structure. Delamination in the composite structures must be detected to avoid structural collapse due to resonance at reduced natural frequencies. In the present thesis, the influences of the delamination length and location on the natural frequencies of the stationary and rotating composite beams are comprehensively studied.

1.5 Finite element method (FEM)

With the advancement in the structural configurations, the existing methods became insufficient to deal with the complexity of the new structural shapes. Nowadays, the structural study of the complex designs depends heavily on computer simulations. Finite Element Method (FEM) is a numerical approach for the analyses of the complicated designs where analytical formulations are complex and may give inaccurate results.

Finite Element Method (FEM) subdivides a complex structure into smaller and simpler pieces called finite elements, which is accomplished by complex spatial discretization in the dimensions of space. This is achieved by the construction of the mesh of the object that is the numerical domain for the solution. The speed of convergence and accuracy of results obtained using FEM depend on the type and the size of the finite element.

Conventional FEM considers two nodes at the ends of the beam element where each node has two degrees of freedom (displacement and rotation), so the beam must be divided into large number of elements to get the accurate results which lowers the speed of convergence. Higher-order Finite Element (HOFE) overcomes this difficulty by considering four degrees of freedom (displacement, rotation, curvature and gradient of curvature) per node.

In the present thesis, commercial Finite Element Analysis (FEA) tool ANSYS® is used to perform the vibration analyses of the uniform and tapered composite beams with delamination.

1.6 Literature review

In this section, a detailed literature survey is presented to explore the contributions of researchers for analyzing the vibrational characteristics of the rotating, stationary and delaminated composite beams that have uniform, thickness-tapered and doubly tapered beam profiles.

1.6.1 Vibration analysis of stationary and rotating beams

At the early stage of rotating beam research, Peters [1] presented simple expressions to obtain natural frequencies and mode shapes of the rotating uniform cantilever beams and to determine the relation between the mass and stiffness parameters. Boyce and Handelman [2] studied the free vibration of the rotating beams with tip mass using Rayleigh-Ritz and Southwell methods. They showed that presence of tip mass depressed the lowest frequency. They also showed that the effect of tip mass on the kinetic energy outweighed the contribution to the potential energy produced by centrifugal force. Putter and Manor [3] obtained the natural frequencies and the mode shapes of the radial beam mounted on the rotating disc at a 90° setting angle by using the finite element technique. Swaminathan and Rao [36] performed the vibration analysis of the rotating pre-twisted and tapered cantilever beams with rectangular cross-section using Rayleigh-Ritz method. They examined the influences of pre-twist, rotation and width-tapering on the first three natural frequencies of the considered beams. Lately, more efficient modeling methods were introduced by Yoo et al. [4] and by Kuo and Lin [5].

Some work has also been done on the vibration analysis of the uniform rotating composite beams. Aksencer and Aydogdu [6] studied the out-of-plane bending vibration of the rotating composite beams based on Euler-Bernoulli and Timoshenko beam theories. They used Ritz method to obtain the solution. Chandra and Chopra [7] presented experimental-cum-theoretical study of the free vibration characteristics of the thin-walled rotating composite box beams with bending-twist and extension-twist coupling under rotating conditions. Qin et al. [8] investigated the effects of the hygrothermal environment, aerodynamic force, rotational velocity and fiber orientation angle on the out-of-plane free vibration characteristics of the thin-walled rotating composite beam. Carrera et al. [9] established a refined structural theory called Carrera Unified Formulation to conduct the free vibration analysis of the rotating composite beam. Bekhoucha et al [35] conducted nonlinear forced vibration analysis of the rotating anisotropic uniform beams by

coupling Galerkin method with harmonic balance method. They obtained the response curves and investigated the non-linearity for various geometrical conditions. Pavankishore and Behera [10] evaluated the modal characteristics of the marine propeller blade using finite element approach and obtained the optimum stacking sequence for the optimum modal characteristics of the blade. Khosravi et al. [37] performed the vibration analysis of rotating composite beams reinforced with carbon nanotubes and discussed the influences of uniform temperature elevation on its free vibration response which may lead to instability.

Recently, Seraj [11] studied the free vibration response and conducted dynamic instability analysis of the rotating doubly tapered cantilever composite beam using Rayleigh-Ritz method and Finite Element Analysis (FEA) tool ANSYS®. He investigated the effects of the rotational velocity, hub radius, double taper ratio, taper configuration and laminate's configuration on the out-of-plane bending, in-plane bending and axial vibrations. He also identified the first critical speed, maximum displacement and the width of the instability region of the rotating doubly tapered composite beam.

In the past a lot of work was done on the free vibration response of the stationary uniform composite beams. Abarcar and Cunniff [12] investigated the experimental results for the natural frequencies and the mode shapes of graphite-epoxy and boron-epoxy composite beams for various fiber orientation angles. Their results gave indication of the interaction between bending and twisting for the beams with 15° and 30° fiber orientation angles. Chandrashekhara et al. [13] studied the free vibration of the composite beams by including rotary inertia and shear deformation effects. They demonstrated the effects of shear deformation, material anisotropy and boundary conditions on the natural frequencies of the advanced composite beams. Abramovich et al. [14] obtained the solutions for the natural frequencies of the laminated beams by including the effects of rotary inertia and shear deformations using exact element method. They found the effect of shear deformation more significant in the laminated beams than in that of the homogeneous beams. Miller and Adams [15] studied the vibration characteristics of the orthotropic clamped-free beams using the classical laminate theory without including the effect of shear deformation. The exact solutions of the simply supported composite beam based on the classical laminate theory was obtained by Vinson and Sierakowski [16] by neglecting the effects of rotary inertia and shear deformation. Krishnaswamy et al. [17] developed the dynamic equations governing the free vibration of the laminated composite beams using the Hamilton's principle. They included the

effects of rotary inertia and transverse shear in the energy formulation. Shafei et al. [38] performed non-linear vibration analysis of anisotropic composite beams using iso-geometric third order shear deformation theory. They integrated the governing nonlinear equations of vibration with the Newton-Raphson method. They concluded that nonlinear vibration and flutter characteristics of the anisotropic composite beams are completely different from those for the orthotropic and isotropic ones.

Recently, researchers started analyzing the tapered composite beams and plates due to their extensive use in various industries. Nabi and Ganesan [18] developed a general finite element formulation based on the first order shear deformation theory, to study the free vibration characteristics of the laminated composite beams. Zabihollah [19] conducted the free vibration and buckling analyses of the tapered composite beams with different taper configurations using conventional and advanced finite element formulations which gave more accurate results by using fewer elements. He presented the advanced finite element models with eight degrees of freedom based on Euler-Bernoulli theory and Timoshenko beam theory. Eftakher [20] used Rayleigh-Ritz method along with conventional and advanced finite element formulations to conduct the free and forced vibration analyses of uniform-width thickness-tapered laminated composite beams. Ganesan and Seraj [21] conducted the dynamic instability analysis of the doubly tapered cantilever composite beams rotating at periodic rotational velocity for out-of-plane bending, in-plane bending, and axial vibrations. They applied Bolotin's method to obtain the unstable regions and studied the effects of the taper configuration, double tapering, stacking sequence, rotational velocity and hub radius on the dynamic instability characteristics of the composite beams. Babu et al. [39] investigated the dynamic properties of the thickness-tapered composite plates for different tapered configurations under the harmonic excitation. They presented the governing differential equations of motion in finite element formulation using classical laminated plate theory. They investigated the influences of taper configurations, aspect ratio, taper angle and fiber orientation angle on the free vibration response of composite plates. Ashok and Jeyaraj [40] conducted static deflection and thermal stress analysis of the non-uniformly heated thickness-tapered composite plates using finite element analysis. They observed that the static deflection of the tapered plate was significantly influenced by the nature of temperature field. They also observed large variation of stresses at the resin pockets. Arab [22] investigated the free vibration response of the thickness-tapered laminated composite square plates using the Ritz method, based on classical laminated

plate theory and first order shear deformation theory. He also studied the forced vibration response of undamped and damped thickness-tapered laminated composite square plates using assumed modes method. Kumar [23] carried out free and forced vibration analyses for the doubly tapered composite beam using Ritz and assumed modes methods. He studied the influences of the various parameters on the dynamic response of the doubly tapered composite beams subjected to general periodic and non-periodic loadings.

1.6.2 Composite beams with delamination

The extensive use of the composite materials has challenged engineers with the new problems in recent decades. Delamination is one of the critical problems in this field. Kanninen [24] was the first to develop analytical model of the Double Cantilever Beam (DCB) specimen to study crack propagation and crack arrest. He treated the specimen as a finite length beam, which was partly free and partly supported by an elastic foundation. He used Euler–Bernaulli beam model for formulating the problem. Rybicki et al. [25] were the first to show that the strain energy release rate near the delamination tip remains constant during the delamination growth and therefore, it can be used as a criterion for predicting the delamination growth. He used the concepts of linear elastic fracture mechanics to study the delamination growth in the composite material. Penado [26] extended the work done by Kanninen [24] to obtain closed form solution for the energy release rate of the DCB specimen with an adhesive layer. He showed that shear deformation must be considered in addition to the elastic foundation effect. He verified his closed form solution results using the finite element method. Arakawa and Takahashi [27] introduced an analytical model for the analysis of interlaminar fracture and deformation ahead of the crack front in DCB specimen with simple unidirectional layup. They included the effect of the material stiffness ahead of the crack front in the calculation of fracture parameters. Sun and Zheng [28] studied delamination characteristics and analysed the distribution of strain energy release rate at the crack fronts of the Double Cantilever Beam (DCB) and End Notch Flexure (ENF) specimens by using the plate finite element. Krueger and et al [29] obtained a finite element technique with mixed 3D and shell elements for the analysis of delaminated composites. They computed the distribution of strain energy release rates across the width of the specimen by using virtual crack closure technique (VCCT). Hassan et al. [43] investigated the effect of pre-rolling temperature on the interfacial properties and formability of steel-steel bilayer sheet in single point incremental forming.

Harper and Hallet [31] showed that the accuracy of the composite delamination analysis using interface elements relies on having sufficient elements within the cohesive zone, ahead of the crack tip. They modified the existing formulae for the better prediction of the cohesive zone length and gave clarification regarding the minimum number of interface elements required within the cohesive zone length. Their work helped researchers to choose appropriate mesh size while preserving the numerical accuracy and minimizing the computational expense.

Alfano and Crisfield [30] developed the finite element models of the DCB specimen to perform delamination analysis of the laminated composite beams using interface elements. They discussed the influence of interface strength on the convergence properties and on the final results of the numerical solution of the delamination problem. Supreeth and Manjunath [32] conducted the analysis of Mode-I and Mode-II delamination onset in composite laminates. They studied the effects of material properties, fiber orientation and crack length on the delamination onset. They found that the laminates with unidirectional fibers were more resistant to the applied displacement and force. They also found that with the increase in the delamination length, lesser force was required for crack opening and initiation. Callioglu and Atlihan [33] conducted the vibration analysis of the delaminated composite beams using analytical and numerical models. They developed the analytical model using Timoshenko beam theory. They investigated the effect of the penalty stiffness of the contact elements at the delaminated interface on the natural frequencies of the delaminated beam. They also showed that the natural frequencies of the delaminated beams decrease with the increase in the delamination length. Talookolaei and Della [34] studied the dynamic behavior of the rotating delaminated composite beams including rotary inertia and shear deformation effects. Imran et al. [46] investigated the effects of delamination size, stacking sequence and boundary conditions on the vibration behavior of composite plate using finite element analysis tool ABAQUS®. Babu et al. [47] studied the free and forced vibration responses of rotating thickness-tapered delaminated composite plates. They conducted various parametric studies to investigate the influences of delamination length and location, different thickness-tapered configurations and rotational speed on the dynamic characteristics of tapered composite plates. Alidoost and Rezaeepazhand [45] studied the vibration, buckling and flutter instability of the delaminated composite beam subjected to concentrated follower force. They studied the influences of delamination length and location on the fundamental frequency, buckling load and flutter load. Zhang et al. [44] conducted the vibration-based delamination detection in the curved

composite plates. They employed two algorithms based on computer intelligence, namely artificial neural network and surrogate assisted genetic algorithm for predicting the location, size and interface of the delamination. Munian et al. [41] conducted elastic guided wave-based evaluation to detect delamination in composites by studying the wave scattering due to different delamination positions. They modeled guided wave interaction with delamination in laminated composite using time domain spectral finite element method. Mekonnen et al. [42] studied post buckling and delamination propagation behavior of composite laminates with embedded delamination experimentally and numerically. They found that buckling mode determined the growth direction of the delamination propagation, and that the stacking sequence influenced the extent of propagation area, while the orientation of the delamination affected the buckling loads.

1.7 Objective and scope of the thesis

The cited references mostly investigated the dynamics of delaminated uniform composite beams. However, the free vibration analysis of stationary and rotating thickness-tapered and doubly tapered delaminated composite beams has not been addressed. In the present thesis, the free vibration analyses of the stationary and rotating intact and delaminated composite beams are conducted for uniform, thickness-tapered and doubly tapered beam profiles. The lack of research work on the free vibration of tapered composite beams with delamination has encouraged to thoroughly study the influences of various geometrical and design parameters on the free vibration response of the stationary and rotating thickness-tapered and doubly tapered composite beams with end and mid-span delaminations. Furthermore, consideration of rotating doubly tapered cantilever composite beams with delamination would be more representative of real situations such as delamination in helicopter and windmill blades due to impact loading and/or fatigue.

The pictorial representation of the applications of stationary and rotating composite beams are provided in Appendix A. In Figure A.3, the cross-section view of the helicopter blade with honeycomb core is shown. The honeycomb core is wrapped by composite material. The aerospace industries analyze the composite protypes at the design phase of the helicopter blades.

The objective of the present thesis is to investigate the free vibration response of stationary and rotating thickness-tapered and doubly tapered composite beams with end and mid-span delaminations using FEA tool ANSYS®. Various parametric studies are conducted to

investigate the influences of the delamination length and location, fiber orientation angle, layer reduction, thickness-tapering and taper angle on the vibration characteristics of stationary thickness-tapered and uniform simply supported composite beams with delamination. The delamination length having minimal effect on the natural frequencies of the stationary composite beams is determined. The influences of the rotational velocity, delamination length and location, stacking sequence, double taper ratio, hub radius and taper angle on the vibrational characteristics of rotating doubly tapered cantilever composite beams with delamination are also investigated. The vibration characteristics of the end and mid-span delaminated stationary and rotating composite beams are compared.

The delaminations are modelled at the critically stressed locations in the stationary and rotating composite beams which are determined using first-ply failure analyses based on Tsai-Wu failure criterion. The numerical model of the delaminated beam with cohesive interface is finalised after verifying the Mode-II delamination test results with the available results. The natural frequencies of the stationary and rotating intact and delaminated composite beams have been determined and they are verified wherever possible.

The studies performed in the present thesis are helpful for developing delamination detection techniques based on the free vibration response of stationary and rotating tapered composite beams. The variations in the natural frequencies due to the presence of delamination of different sizes at critically stressed locations in the stationary and rotating tapered composite beam studied in the present thesis, can be used as reference for the delamination detection in aircraft airfoils, helicopter blades, turbine blades and windmill blades. Even smaller delaminations can be detected by studying the higher modes. The delamination detection technique based on the free vibration is effective and cost efficient.

1.8 Layout of the thesis

The present chapter provides brief introduction and literature survey on the free vibration analysis of stationary and rotating intact and delaminated composite beams for uniform, thickness-tapered and doubly tapered beam profiles.

In the first part of Chapter-2, the first three out-of-plane bending natural frequencies of the stationary and rotating cantilever composite beams with uniform, thickness-tapered and doubly tapered beam profiles are determined and compared with the results available in the literature. A numerical investigation called "layer reduction test" has been implemented to compare the first three natural frequencies of the uniform and thickness-tapered beams with simply supported and cantilever boundary conditions. In the second part of Chapter-2, the first-ply failure analyses are conducted to determine the critically stressed locations in the uniform composite beams undergoing static and rotational loadings. The Double Cantilever Beam (DCB) and the End Notch Flexure (ENF) test samples are modeled using FEA tool ANSYS® to simulate the Mode-I and Mode-II delamination tests, respectively. The load vs displacement curves for DCB and ENF test samples are obtained from ANSYS® and are compared with the results available in the literature. The natural frequencies of the stationary and rotating uniform composite beams with end and mid-span delaminations, respectively, are obtained using ANSYS® and are verified with the results available in the literature.

In Chapter-3, the free vibration response of the stationary uniform and thickness-tapered simply supported composite beams with end and mid-span delaminations of different lengths and at different locations are investigated for various fiber orientation angles. The influences of the layer reduction, thickness-tapering and taper angle (due to change in the beam length and number of plies dropped-off) on the natural frequencies of the delaminated composite beams are investigated for various fiber orientation angles.

In Chatper-4, the free vibration analyses of the rotating thickness-tapered and doubly tapered cantilever composite beams with end and mid-span delaminations are conducted for different rotational velocities. Various numerical studies are conducted to analyze the influences of the delamination length, delamination location, stacking sequence, double tapering, hub radius and taper angle (due to change in the beam length) on the natural frequencies of the rotating doubly tapered cantilever composite beams for different rotational velocities.

Chapter 5 brings the thesis to its end by providing the overall conclusions of the present work and some future recommendations for the future work.

Chapter 2

Free vibration response of stationary and rotating intact and delaminated composite beams

2.1 Introduction

The free vibration response of a rotating laminated composite beam is an engineering research field of extensive interest. The laminated composite beam has the property to have the required strength even with less weight, which has foremost importance in aerospace, mechanical, and automotive structures. Recently, composite beams with tapered profile are extensively used in the aerospace industry and wind energy sector as a rotating element such as a helicopter blade or wind turbine blade. Rotating composite beams are distinctly different from the stationary beams, so extensive research is required to study the free vibration response of rotating composite beams. Geometric non-linearity in the composite beam provides the provision to control the vibration.

In this chapter, the free vibration analysis for out-of-plane bending of thickness-and-width-tapered laminated composite beam, called as "doubly tapered composite beam" is conducted using commercial Finite Element Analysis (FEA) tool ANSYS® and the modeling and analysis are verified with the results available in the literature where possible. Rotating composite beams are prone to delamination, due to which the free vibration analyses of rotating beams with internal flaws become very important. In the present work, the critically stressed locations prone to delamination in stationary and rotating composite beams are determined from first-ply failure analysis. The load vs displacement curves of the uniform composite beams undergoing Mode-I and Mode-II delamination tests are determined and are verified with the results available in the literature. The free vibration response of stationary and rotating uniform composite beams with end and mid-span delaminations are determined and are verified with the results available in the literature. The composite beams made of different materials are considered to verify obtained results with the existing references.

2.2 Description of the rotating beam

Consider a laminated composite beam of length L, which is attached to a hub of radius R, as shown in Figure 2.1. The hub rotates about its axis at a constant angular velocity Ω rad/s. The origin of the coordinates is taken at the center of the face of the beam fixed to the hub. The x-axis coincides with the centroidal axis of the beam, the z-axis is parallel to the axis of rotation and the y-axis lies in the plane of rotation.

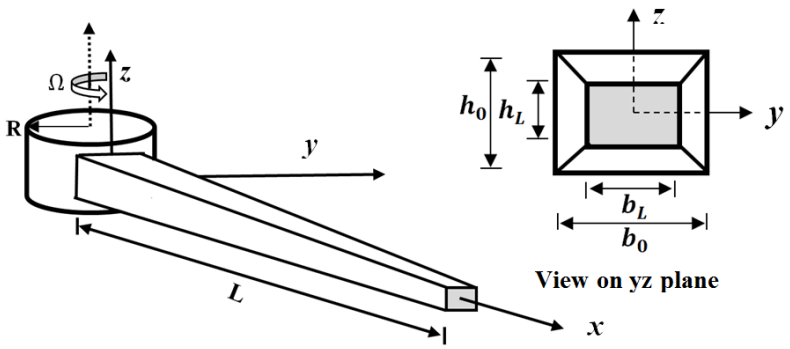

Figure 2.1 Rotating doubly tapered composite beam [11]

The view on y-z plane illustrates the beam with the change in the thickness from h_0 to h_L and with the change in the width from b_0 to b_L over the length L. The laminated composite beam consists of N layers, numbered from the lower to the upper face. To study the out-of-plane bending vibration, the x-y plane is chosen as the mid-surface and reference plane. Half of the layers of the laminated beam is in positive z-direction and the other half is in negative z-direction. Half of the width is in positive y-direction and the other half is in negative y-direction.

2.3 Finite element analysis software ANSYS®

The commercial finite element analysis program ANSYS® 19.0 Workbench platform is chosen to perform the modal analysis. Modal analysis of a rotating beam is a pre-stressed analysis where static analysis must be done before modal analysis to set up the boundary condition and rotational load. ANSYS® Composite Prep Post (ACP) has been used to model the taper configuration of the laminated composite beam. In the present thesis, the stationary and rotating intact and delaminated composite beams are discretized using the finite element SOLID185 that is shown in Figure 2.2. The natural frequencies of the stationary intact uniform composite beams

modeled using SOLID185 and SHELL181 finite elements are compared in Table 2.4, for the result verification. The geometry of the finite element SHELL181 is shown in Figure 2.3.

SOLID185 element has eight nodes (I, J, K, L, M, N, O and P as shown in Figure 2.2) and three degrees of freedom at each node: translations in the x, y, and z directions. The circled number in Figure 2.2 represents the element face. The SOLID185 element is used for three-dimensional modeling of rotating delaminated beams due to its stress stiffening and large deflection capabilities.

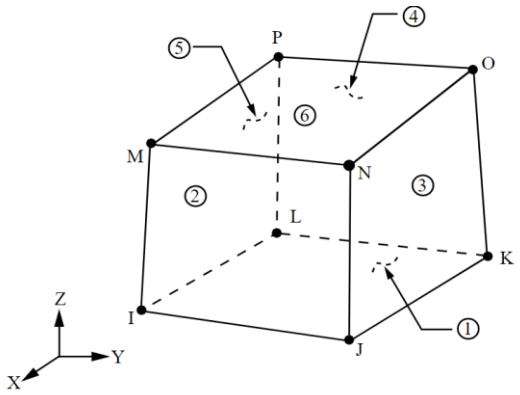

Figure 2.2 Geometry of finite element – SOLID185 [50]

SHELL181 has 4 nodes (I, J, K and L as shown in Figure 2.3) and six degrees of freedom at each node: translations in the x, y and z directions and rotations about the x, y, and z-axes. The circled number in Figure 2.3 represents the element face. Shell elements are used to model structures in which one dimension is significantly smaller than the other dimensions. SHELL181 is suitable for layered applications, for modeling composite shells or/and sandwich construction.

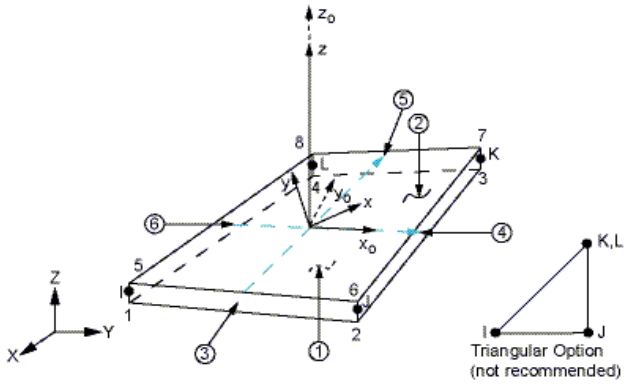

Figure 2.3 Geometry of finite element – SHELL181 [49]

2.4 Verification of natural frequencies of composite beams

In the present section, the first three out-of-plane bending natural frequencies of stationary and rotating uniform, thickness-tapered and doubly tapered cantilever composite beams determined using FEA tool ANSYS® are compared with the results available in Ref. [11]. NCT-301 graphite-epoxy composite material is considered to conduct the numerical analyses. The mechanical properties of NCT-301 graphite-epoxy composite and resin material are given in Tables 2.1 and 2.2, respectively, whereas the geometric parameters of the beam are given in Table 2.3. The mechanical properties of the composite material are defined in 1-2-3 coordinate system in this thesis, where the 1 direction is the fiber direction, while the 2 and 3 are the matrix or transverse directions.

Mechanical properties of NCT-301 graphite-epoxy	
Longitudinal modulus (E_1)	113.9 GPa
Transverse modulus (E_2)	7.985 GPa
$E_3 = E_2$	7.985 GPa
In-plane shear modulus (G_{12})	3.137 GPa
Out-of-plane shear modulus (G_{23})	2.852 GPa
Density of ply (ρ_p)	1480 kg/m^3
Major Poisson's ratio (υ_{12})	0.288
Minor Poisson's ratio (υ_{21})	0.018

Table 2.1 Mechanical properties of NCT-301 graphite-epoxy [11]

Mechanical properties of the resin material	
Elastic modulus (E)	3.93 GPa
Shear modulus (G)	1.034 GPa
Density of resin (ρ_r)	1000 kg/m^3
Poisson's ratio (υ)	0.37

Table 2.2 Mechanical properties of the resin material [11]

Geometric properties of the beam	
Length of the beam (L)	250 mm
Individual ply thickness (t_{ply})	0.125 mm
Width of the beam at the fixed end (b_0)	20 mm

Table 2.3 Geometric parameters of the beam [11]

The verification of the natural frequencies of the composite beam are performed in three steps as illustrated in Figure 2.4.

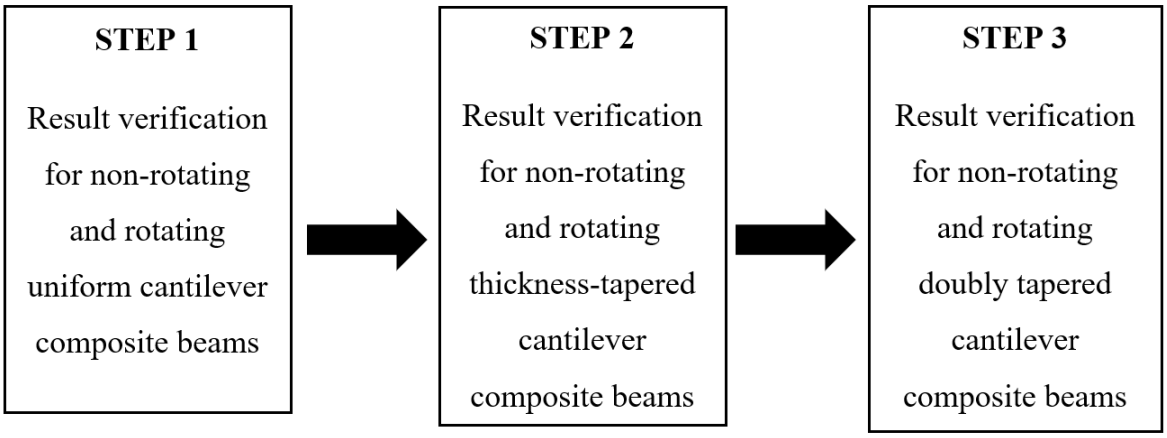

Figure 2.4 Flowchart for the required verification steps

In this thesis, thickness-tapering in the laminated beam is described by the number of ply drop-offs (S). Thickness-taper angle (φ) and number of ply drop-offs (S) are related by the following equation:

$$\varphi = tan^{-1}\left(\frac{(S/2)t_{ply}}{L}\right) \tag{2.1}$$

where, φ is the thickness-taper angle, S is the number of ply drop-offs, L is the length of the beam and t_{ply} is the individual ply thickness. Width-tapering is described by width-ratio (r_b) as:

$$r_b = \frac{b_L}{b_0} \tag{2.2}$$

where, b_L is the width of the beam at the free end and b_0 is the width of the beam at the fixed end.

2.4.1 Verification step 1: Stationary and rotating uniform cantilever composite beam

In this verification step, the first three out-of-plane bending natural frequencies of stationary and rotating uniform cantilever composite beams determined using FEA tool ANSYS® are compared with the results available in Ref. [11] in Tables 2.4 and 2.5, respectively. The composite beams with four different stacking sequences are considered for both the analyses. The mechanical properties of composite material used are given in Table 2.1 and the geometric properties of the beam are given in Table 2.3. The hub radius of 25 mm is considered for all the rotating composite beams considered in this thesis.

The convergence study of uniform composite beams for $[0]_{8s}$ stacking sequence is presented in Table B.1 of Appendix B. The composite beam with 7200 SOLID185 finite elements shows excellent convergence with the results available in Ref. [11]. The natural frequencies of stationary cantilever composite beam are obtained using SOLID185 and SHELL181 finite elements. The mesh of element size 2 mm and a total of 45000 SOLID185 and 1250 SHELL181 finite elements are used to get the results presented in Table 2.4.

Stacking sequence	Mode number	Results obtained using ANSYS® based on SOLID185 finite element	Results obtained using ANSYS® based on SHELL181 finite element	Results from Ref. [11] using ANSYS®
$[0/90]_{9s}$	1	77.33	77.33	77.34
	2	479.95	479.91	481.20
	3	1323.50	1323.30	1333.40
$[90]_{18s}$	1	27.01	27.01	27.02
	2	169.02	169.02	169.50
	3	472.17	472.17	476.20
$[0]_{18s}$	1	101.78	101.78	101.80
	2	627.66	627.56	629.00
	3	1714.40	1713.80	1725.50
$[0/45/-45]_{6s}$	1	69.62	69.64	69.78
	2	432.96	433.10	434.90
	3	1198.90	1199.30	1211.00

Table 2.4 Natural frequencies (in Hz) of the 250-mm-long stationary uniform cantilever composite beam based on SOLID185 and SHELL181 finite elements

The natural frequencies of rotating composite beams obtained using mesh of element size 2 mm and a total of a total of 45000 SOLID185 finite elements and are presented and compared with the results available in Ref. [11] in Table 2.5.

Stacking sequence	Mode number	Ω = 0 rad/s	Ω = 50 rad/s		Ω = 100 rad/s		Ω = 200 rad/s	
		Results obtained using ANSYS® based on SOLID185 finite element	Results obtained using ANSYS® based on SOLID185 finite element	Results from Ref. [11] using ANSYS®	Results obtained using ANSYS® based on SOLID185 finite element	Results from Ref. [11] using ANSYS®	Results obtained using ANSYS® based on SOLID185 finite element	Results from Ref. [11] using ANSYS®
$[0]_{18s}$	1	101.78	102.18	102.20	103.42	103.50	108.25	108.30
	2	627.66	627.94	629.40	629.16	630.50	632.84	634.90
	3	1714.40	1714.86	1725.80	1715.23	1726.90	1719.89	1731.40
$[90]_{18s}$	1	27.01	28.54	28.50	32.71	32.72	45.57	45.60
	2	169.02	170.53	170.90	174.57	174.90	189.84	190.20
	3	472.17	474.65	477.50	478.69	481.50	494.45	497.30
$[0/90]_{9s}$	1	77.33	77.88	77.89	79.50	79.52	85.69	85.70
	2	479.95	480.57	481.70	482.01	483.13	487.73	488.90
	3	1323.50	1325.50	1334.00	1326.90	1335.40	1332.70	1341.20
$[0/45/-45]_{6s}$	1	69.62	70.26	70.30	72.07	72.19	78.88	78.90
	2	432.96	433.82	435.50	435.42	437.10	441.76	443.40
	3	1198.90	1201.30	1211.50	1202.90	1213.10	1209.20	1219.50

Table 2.5 Natural frequencies (in Hz) of the 250-mm-long rotating uniform cantilever composite beams based on SOLID185 finite element

From Table 2.4, it can be observed that the natural frequencies of stationary uniform cantilever composite beams obtained using SOLID185 and SHELL181 finite elements are in good agreement with the results available in Ref. [11]. The natural frequencies of the composite beam with $[0]_{18s}$ stacking sequence are the highest, whereas the natural frequencies of the composite beam with $[90]_{18s}$ stacking sequence are the lowest.

From Table 2.5, it can be observed that the natural frequencies of rotating uniform cantilever composite beams obtained using SOLID185 finite element are in good agreement with

the results available in Ref. [11]. The natural frequencies of the composite beams increase with the increase in the rotational velocity.

The first three mode shapes of stationary uniform cantilever composite beams with $[0]_{18s}$ stacking sequence are illustrated in Figure 2.5.

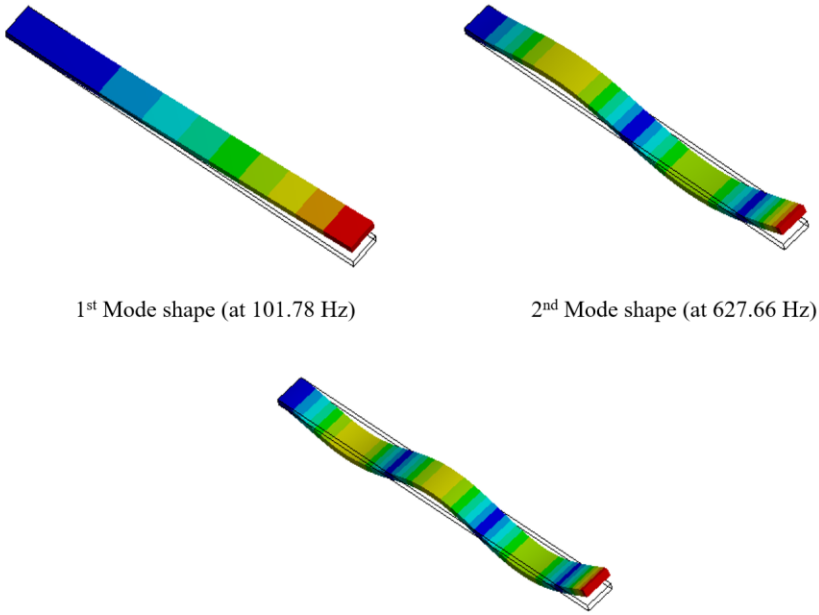

Figure 2.5

Figure 2.5 Pictorial representation of the first three mode shapes of the 250-mm-long stationary uniform cantilever composite beam with $[0]_{18s}$ stacking sequence

2.4.2 Verification step 2: Rotating thickness-tapered cantilever composite beam

In this verification step, the first three out-of-plane bending natural frequencies of rotating thickness-tapered cantilever composite beam determined using FEA tool ANSYS® are compared with the results available in Ref. [11] in Table 2.6. The available results were obtained using Rayleigh-Ritz (R-R) method. The composite beams with $[90]_{18s}$ stacking sequence are considered for the analysis. The mechanical properties of the composite and resin material are given in Tables 2.1 and 2.2, respectively, whereas the geometric properties of the beam are given in Table 2.3.

The thickness-tapered beams are modeled by dropping-off the plies in a staircase arrangement. The half of the plies are dropped-off from the top half of the beam, and the other half

are dropped-off from the bottom half of the beam, as shown in Figure 2.6. The triangular resin pockets are formed due to dropping-off the plies. There are a total of 36 plies at the fixed end of the cantilever beam, whereas at the free end there could be a total of 30 or 26 plies depending on the number of plies dropped-off. The screenshots of the important steps required for modeling doubly tapered composite beams are given in Appendix C. The cut-off geometry is created in design modular and is linked to ACP (Pre) to generate CAD geometry which is further used in cut-off selection rule to drop the plies.

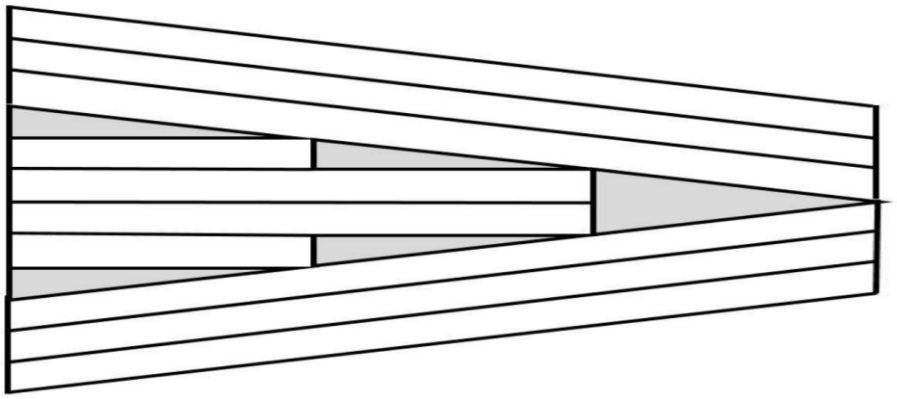

Figure 2.6 Geometry of taper configuration

The natural frequencies of the rotating thickness-tapered cantilever composite beams with 6 and 10 plies dropped-off are obtained using a total of 73762 and 60580 SOLID185 finite elements, respectively. The results are compared with results available in Ref. [11] in Table 2.6.

umber of plies		Mode number	Ω = 0 rad/s		Ω = 50 rad/s		Ω = 200 rad/s	
At fixed end	At free end		Results obtained using ANSYS®	Results from Ref. [11] using ANSYS®	Results obtained using ANSYS®	Results from Ref. [11] using ANSYS®	Results obtained using ANSYS®	Results from Ref. [11] using ANSYS®
36	30	1	27.58	27.61	29.12	29.21	46.14	46.19
		2	160.06	163.60	161.46	162.50	181.08	182.00
		3	437.42	442.80	438.79	444.20	458.87	464.20
	26	1	28.06	28.09	29.59	29.70	46.60	46.67
		2	153.84	154.80	155.25	156.20	175.09	176.00
		3	413.39	418.40	414.77	419.70	435.03	439.00

Table 2.6 First three natural frequencies (in Hz) of the 250-mm-long rotating thickness-tapered cantilever composite beams with $[90]_{18s}$ stacking sequence

From Table 2.6, it can be observed that the results obtained using ANSYS® are in good agreement with the results available in Ref. [11]. The natural frequencies increase with increase in the rotational velocity, as was observed in the previous sub-section. It can also be observed that the 1st natural frequency increases, whereas the 2nd and 3rd natural frequencies decrease with the increase in number of plies dropped-off.

The first three natural frequencies of the rotating thickness-tapered cantilever composite beams with $[0]_{18s}$ and $[0/90]_{9s}$ stacking sequences are illustrated in Table 2.7.

Stacking sequence	Number of plies		Mode number	Rotational velocity (in rad/s)		
	At fixed end	At free end		0	100	200
$[0/90]_{9s}$	36	30	1	79.24	81.33	87.48
			2	456.95	458.63	464.44
			3	1235.80	1237.00	1242.80
	36	26	1	82.67	84.78	90.78
			2	449.61	451.54	457.29
			3	1194.00	1195.90	1201.60
	36	18	1	85.19	87.27	93.30
			2	407.00	409.01	415.00
			3	1041.50	1043.50	1049.40
$[0]_{18s}$	36	30	1	104.01	105.66	110.47
			2	596.04	597.53	601.99
			3	1598.00	1599.50	1604.00
	36	26	1	105.81	107.46	112.26
			2	572.86	574.37	578.89
			3	1509.70	1511.20	1515.80
	36	18	1	110.62	112.45	117.20
			2	525.34	526.90	531.55
			3	1333.40	1335.00	1339.60

Table 2.7 First three natural frequencies (in Hz) of the 250-mm-long rotating thickness-tapered cantilever composite beams with $[0]_{18s}$ and $[0/90]_{9s}$ stacking sequence

From Tables 2.6 and 2.7, it can be observed that the composite beams with $[0]_{18s}$ stacking sequence have the highest natural frequencies, whereas the composite beams with $[90]_{18s}$ stacking sequence have the lowest natural frequencies. The natural frequencies of the beams with $[0/90]_{9s}$ stacking sequence fall in between the natural frequencies of the beams with $[0]_{18s}$ and $[90]_{18s}$ stacking sequences.

2.4.3 Verification step 3: Rotating doubly tapered cantilever composite beam

In this verification step, the first three out-of-plane bending natural frequencies of rotating doubly tapered cantilever composite beam determined using FEA tool ANSYS® are compared with the results available in Ref. [11]. The available results were obtained using ANSYS® and Rayleigh-Ritz (R-R) method. The composite beams with $[90]_{18s}$ stacking sequence are considered for the analysis. The mechanical properties of the composite and resin material are given in Tables 2.1 and 2.2, respectively, whereas the geometric properties of the beam are given in Table 2.3.

To model the doubly tapered composite beam, in addition to the thickness-tapering, the plies are tailored along the length to get different widths at fixed and free ends of the cantilever beam. The width-tapering is described by width-ratio (r_b). The free vibration analysis is conducted on rotating doubly tapered cantilever composite beams with 18 plies dropped-off for three different width-ratio values. A total of 60788, 49104 and 37998 SOLID185 finite elements are used to model the doubly tapered beams of width-ratio values 1, 0.5 and 0.1, respectively.

The first three natural frequencies of rotating doubly tapered cantilever composite beam with $[90]_{18s}$ stacking sequence are presented and compared with the results available in Ref. [11] in Table 2.8. Table 2.9 illustrates the first three natural frequencies of rotating doubly tapered cantilever composite beams with $[0]_{18s}$ and $[0/90]_{9s}$ stacking sequences and with 18 plies dropped-off for three different width-ratio values.

Number of plies		Width-ratio value	Mode number	Ω = 0 rad/s			Ω = 200 rad/s		
At fixed end	At free end			Results obtained using ANSYS®	Results from Ref. [11] using ANSYS®	Results from Ref. 11] using R-R solution	Results obtained using ANSYS®	Results from Ref. [11] using ANSYS®	Results from Ref. 11] using R-R solution
36	18	0.1	1	49.1	49.3	49.6	62.8	62.9	63.0
			2	185.5	175.6	187.0	188.9	189.6	201.2
			3	403.3	406.4	440.9	417.1	420.1	455.0
		0.5	1	35.5	35.7	35.1	52.4	52.3	51.9
			2	157.3	150.9	160.5	169.5	158.8	180.1
			3	372.4	375.7	408.2	394.3	391.2	427.9
		1	1	29.4	29.4	28.9	47.9	47.9	47.4
			2	146.5	141.4	150.5	162.4	163.1	173.5
			3	362.3	366.4	397.5	384.5	388.4	421.1

Table 2.8 First three natural frequencies (in Hz) of the 250-mm-long rotating doubly tapered cantilever composite beams with $[90]_{18s}$ stacking sequence

From Table 2.8, it can be observed that the natural frequencies increase with the increase in the rotational velocity, as was observed in the previous sub-sections. Another observation, that can be drawn is that with the decrease in the width-ratio value, the natural frequencies of the composite beams increase.

Stacking sequence	Number of plies		Width-ratio value	Mode number	Rotational velocity (in rad/s)		
	At fixed end	At free end			0	100	200
$[0/90]_{9s}$	36	18	0.1	1	142.12	143.47	147.43
				2	504.77	506.03	509.78
				3	1156.40	1157.60	1161.30
			0.5	1	102.96	104.89	111.64
				2	430.35	432.48	439.79
				3	1070.96	1073.34	1081.64
			1	1	84.80	87.33	93.41
				2	407.00	409.01	415.00
				3	1041.50	1043.50	1049.40
$[0]_{18s}$	36	18	0.1	1	184.58	185.62	188.71
				2	650.33	651.30	654.22
				3	1477.80	1478.70	1481.60
			0.5	1	133.80	135.26	139.35
				2	560.08	561.40	565.35
				3	1369.20	1370.50	1374.40
			1	1	110.62	112.45	117.20
				2	526.34	527.90	532.55
				3	1333.40	1335.00	1339.60

Table 2.9 First three natural frequencies (in Hz) of the 250-mm-long rotating doubly tapered cantilever composite beams with $[0]_{18s}$ and $[0/90]_{9s}$ stacking sequences

Table 2.9 illustrates the first three out-of-plane bending natural frequencies of rotating doubly tapered cantilever composite beams with $[0]_{18s}$ and $[0/90]_{9s}$ stacking sequences. It can be observed that the natural frequencies of the beam with $[0]_{18s}$ stacking sequence are higher than the natural frequencies of the beam with $[0/90]_{9s}$ stacking sequence. The natural frequencies of the beam increase with the decrease in width-ratio value.

2.5 Layer reduction test

In this section, a numerical investigation called herein as the "layer reduction test" has been implemented to compare the first three natural frequencies of the uniform and thickness-tapered beams with simply supported and cantilever boundary conditions obtained using FEA tool ANSYS®. A three-stepped layer reduction test is implemented on the uniform composite beam. Three identical uniform composite beams with $[\theta]_{8s}$ stacking sequence (where θ is fiber orientation angle) and made of Metyx® 600 Tex graphite-epoxy composite material are presented in Figure 2.7 (a). The mechanical properties of the composite material and the geometric properties of the beam are given in Table 2.10 and 2.11, respectively.

In Figure 2.7, the uniform beams on the left and right sides have same lengths as that of middle beam but are displayed only in part due to insufficient horizontal space. The uniform beams at the left side are called as thick beams, whereas the uniform beams at the right side are called as thin beams. The beams shown at the center are called as thickness-tapered beams.

The thickness-tapered beam profile is obtained by dropping-off the plies in a staircase arrangement. At each step of the layer reduction test, the thickness of left end of the beam remains the same, whereas the thickness of right end of the beam is reduced and taper angle comes into existence. In the first step of the layer reduction test two plies are dropped-off, out of which one is dropped-off above the mid-plane and other one is dropped-off below the mid-plane as shown in Figure 2.7 (b). In the second step of the layer reduction test four plies are dropped-off, out of which two are dropped-off above the mid-plane and other two are dropped-off below the mid-plane as shown in Figure 2.7 (c). In the third step of layer reduction test six plies are dropped-off in a similar manner as in that of the first and second steps of the test. The arrangement of the plies in the third step of the test is shown in Figure 2.7 (d). The triangular resin pockets are formed due to dropping-off the plies.

The thick beam has 16 plies both at the left and right ends. A ply is removed from the top and bottom halves of the beam at each step of the three-stepped layer reduction test that results in a uniform thin beam. The removed plies are not replaced with resin and therefore, the thin beam stays uniform during the test.

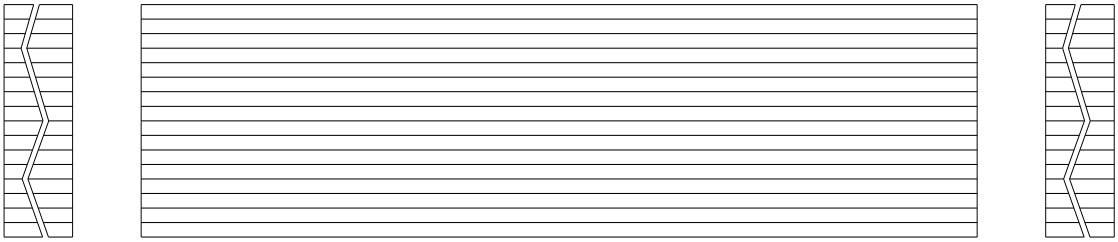

Figure 2.7 (a) Identical beams considered for layer reduction test (no ply drop-off)

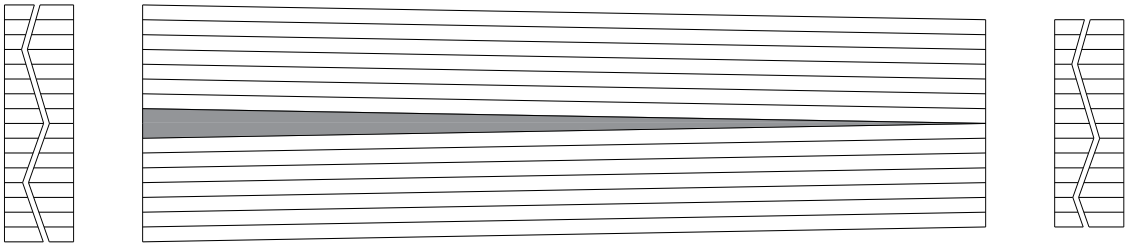

Figure 2.7 (b) Step 1: 2 plies dropped-off

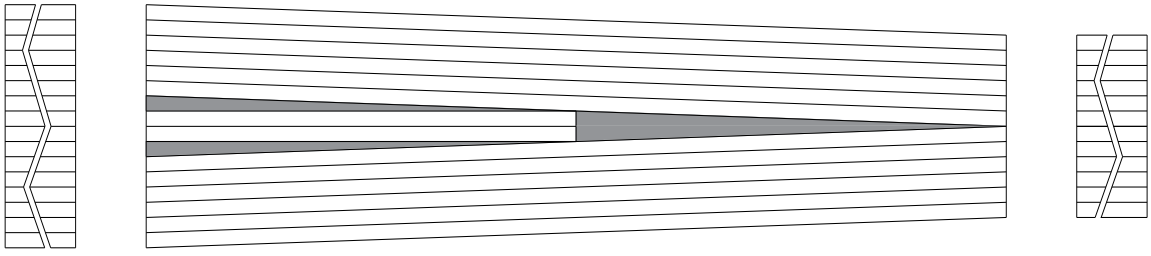

Figure 2.7 (c) Step 2: 4 plies dropped-off

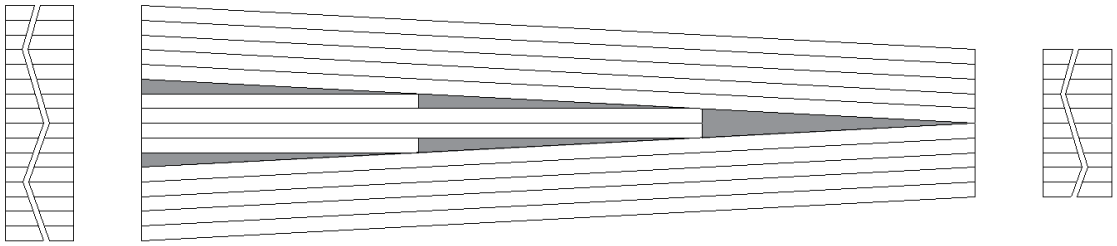

Figure 2.7 (d) Step 3: 6 plies dropped-off

Figure 2.7 Three-stepped layer reduction test

Mechanical properties of Metyx® 600 Tex graphite-epoxy	
Longitudinal modulus (E_1)	44.15 GPa
Transverse modulus (E_2)	12.30 GPa
$E_3 = E_2$	12.30 GPa
In-plane shear modulus (G_{12})	4.09 GPa
$G_{13} = G_{12}$	4.09 GPa
Density of a ply (ρ_p)	2026 kg/m^3
Major Poisson's ratio (υ_{12})	0.20
Minor Poisson's ratio (υ_{21})	0.018

Table 2.10 Mechanical properties of Metyx® 600 Tex graphite-epoxy [33]

Geometric properties of the beam	
Length of the beam	400 mm
Width	20.5 mm
Individual ply thickness	0.206 mm
Number of plies at the left end of the beam	16
Thickness at the left end of the beam	3.3 mm

Table 2.11 Geometric properties of the beam [33]

The natural frequencies of the thick, thin and thickness-tapered simply supported composite beams are obtained and presented in Table 2.12.

Beam type	Number of plies		Mode number	Stacking sequence			
	At left end	At right end		$[0]_{8s}$	$[30]_{8s}$	$[60]_{8s}$	$[90]_{8s}$
Thick	16	16	1	43.07	29.92	21.47	22.74
			2	172.11	104.26	85.89	90.94
			3	386.56	239.69	193.35	204.49
Tapered	16	14	1	40.40	28.11	20.14	21.33
			2	161.53	97.86	80.60	85.33
			3	362.92	225.08	181.47	191.92
Thin	14	14	1	38.19	26.60	19.04	20.16
			2	152.67	92.48	76.17	80.64
			3	343.13	212.84	171.54	181.42
Tapered	16	12	1	37.33	26.00	18.61	19.70
			2	149.56	90.65	74.62	78.99
			3	336.05	208.48	168.00	177.66
Thin	12	12	1	32.74	22.87	16.32	17.28
			2	130.92	79.31	65.31	69.14
			3	294.41	182.71	147.13	155.59
Tapered	16	10	1	34.26	23.85	17.08	18.09
			2	137.89	83.67	68.79	72.82
			3	309.72	192.23	154.80	163.70
Thin	10	10	1	26.93	18.86	13.42	14.22
			2	107.72	65.26	53.73	56.88
			3	242.35	150.48	121.08	128.02

Table 2.12 First three natural frequencies (in Hz) of 400-mm-long thick, thin and thickness-tapered simply supported composite beams

Table 2.12 illustrates the first three natural frequencies of thick, thin, and thickness-tapered simply supported composite beams. The uniform composite beam with 16 plies is considered as the thick beam, whereas the uniform composite beams with 14, 12, or 10 plies are considered as thin beams. The composite beams with dropped-off plies are considered as thickness-tapered beams. It can be observed that the natural frequencies of the thick beam are the highest and that of the thin beam with 10 plies are the lowest. The natural frequencies of the thickness-tapered beams fall in between the natural frequencies of thick and thin beams. For instance, considering the 0° fiber orientation angle, the 1st natural frequency of the thick beam is 43.07 Hz, whereas the 1st the natural frequency of the thickness-tapered beam with 2 plies dropped-off is 40.40 Hz, the 1st natural frequency of the thin beam with 14 plies is 38.19 Hz and is the lowest among the three.

The natural frequencies of thick, thin and thickness-tapered beams decrease due to change in fiber orientation angle from 0° to 60°. A slight increase is seen in the natural frequencies due to change in fiber orientation angle from angle 60° to 90°. The lowest natural frequencies are observed for the composite beams with 60° fiber orientation angle. The variation of the natural frequencies with the change in the fiber orientation angle is due to change in the effective stiffness in the longitudinal direction of the beam and is discussed in detail in section 2.7. The natural frequencies of thickness-tapered and thin simply supported composite beams decrease at each step of the layer reduction test.

The natural frequencies of the thick, thin and thickness-tapered cantilever composite beams are obtained and presented in Table 2.13.

Beam type	**Number of plies**		**Mode number**	**Stacking sequence**			
	At left end	**At right end**		$[0]_{8s}$	$[30]_{8s}$	$[60]_{8s}$	$[90]_{8s}$
Thick	16	16	1	15.36	9.45	7.69	8.10
			2	96.16	59.20	48.20	50.78
			3	268.97	165.97	135.04	142.22
Tapered	16	14	1	15.41	9.48	7.72	8.13
			2	92.13	56.69	46.17	48.65
			3	254.26	156.84	127.61	134.40
Thin	14	14	1	13.61	8.38	6.82	7.18
			2	85.28	52.52	42.75	45.03
			3	238.64	147.30	119.78	126.12
Tapered	16	12	1	15.54	9.55	7.78	8.20
			2	87.60	53.88	43.89	46.26
			3	237.61	146.51	119.22	125.58
Thin	12	12	1	11.67	7.19	5.85	6.16
			2	73.12	45.05	36.66	38.60
			3	204.67	126.38	102.72	108.13
Tapered	16	10	1	15.89	9.75	7.95	8.39
			2	83.46	51.29	54.91	44.06
			3	221.60	136.56	111.15	117.09
Thin	10	10	1	9.60	5.92	4.81	5.07
			2	60.15	37.08	31.16	31.75
			3	168.43	104.04	84.53	88.94

Table 2.13 First three natural frequencies (in Hz) of 400-mm-long thick, thin, and thickness-tapered cantilever composite beams

Table 2.13 illustrates the first three natural frequencies of thick, thin, and thickness-tapered cantilever composite beams. It can be observed that the natural frequencies of the thick beams are the highest and that of the thin beams with 10 plies are the lowest. The 1st natural frequency of the thickness-tapered beam increases with the increase in the number of plies

dropped-off, whereas the 2nd and 3rd natural frequencies decrease with the increase in number of plies dropped-off. For instance, considering 0° fiber orientation angle, the 1st and 2nd natural frequencies of thick beam are 15.36 Hz and 96.16 Hz, respectively, whereas the 1st and 2nd natural frequencies of the thickness-tapered beam with 2 plies dropped-off are 15.41 Hz and 92.13 Hz, respectively.

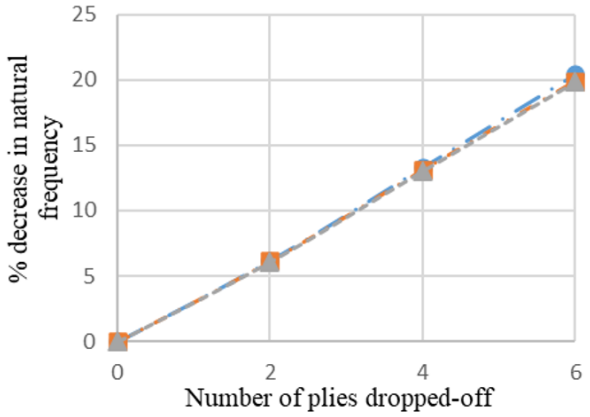

Figure 2.8 (a) Percentage decrease in the natural frequencies of thickness-tapered beam w.r.t. that of thick beam for simply supported boundary condition

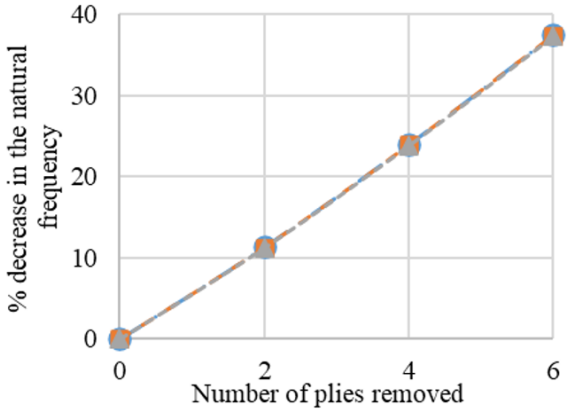

Figure 2.8 (b) Percentage decrease in the natural frequencies of thin beam w.r.t. that of thick beam for simply supported boundary condition

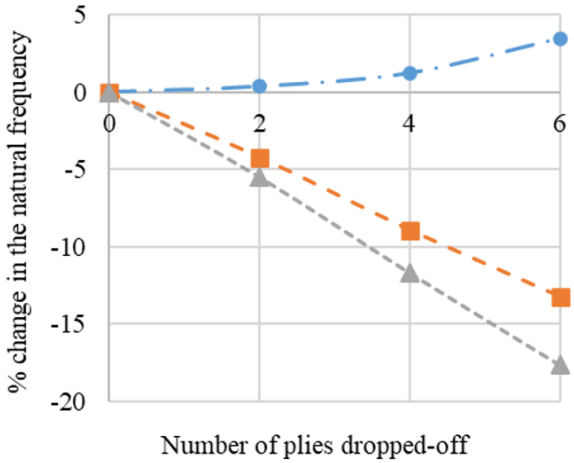

Figure 2.8 (c) Percentage change in the natural frequencies of thickness-tapered beam w.r.t. that of thick beam for cantilever boundary condition

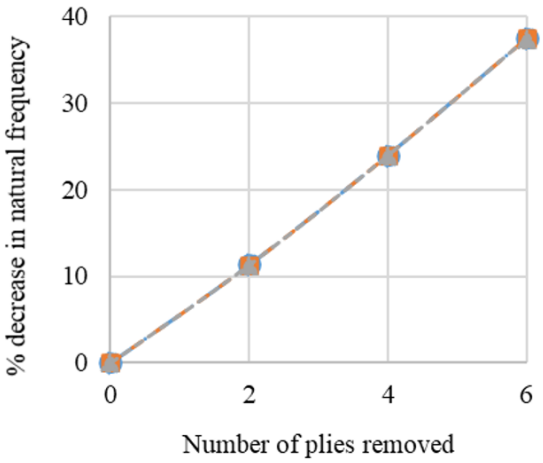

Figure 2.8 (d) Percentage decrease in the natural frequencies of thin beam w.r.t. that of thick beam for cantilever boundary condition

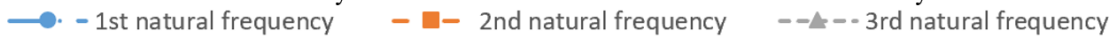

Figure 2.8 Percentage changes in the first three natural frequencies of thickness-tapered and thin beams w.r.t. that of 400-mm-long thick beam for simply supported and cantilever boundary conditions and for $[0]_{8s}$ stacking sequence

Figure 2.8 illustrates the percentage changes in the natural frequencies of thickness-tapered and thin beams with respect to that of the thick beam for simply supported and cantilever boundary conditions. The analysis is done for $[0]_{8s}$ stacking sequence.

From Figures 2.8 (a) and 2.8 (b) it can be observed that the natural frequencies of the thickness-tapered and thin beams for simply supported boundary condition decrease with each step of the layer reduction test. It can also be observed that the curves representing the percentage decrease in the natural frequencies are linear and are close enough to coincide. The decline in the natural frequencies of the thin beam with each step of the layer reduction test is higher in comparison to that of the thickness-tapered beam.

In Figure 2.8 (c), the 1st natural frequency of thickness-tapered beam increases slightly, whereas 2nd and 3rd natural frequencies decrease with each step of the layer reduction test and a higher decrease is seen in the 3rd natural frequency as compared to that of the 2nd natural frequency. From Figure 2.8 (d), it can be observed that all three natural frequencies of the thin beam are decreasing with the increase in the number of removed plies. The curves representing the percentage decrease in the natural frequencies of the thin beam are close enough to coincide.

2.6 First–ply failure analyses

In this section, the first-ply failure analyses are conducted using FEA tool ANSYS® to determine the critically stressed location in the rotating uniform cantilever composite beam based on Tsai-Wu failure criterion. AS4/3502 graphite-epoxy composite material is considered to conduct the first-ply failure analyses.

To determine the critically stressed location in rotating cantilever beam the first-ply failure analysis is initially conducted on uniform simply supported composite beam with concentrated static load at the mid span and the result is compared with the result available in Ref. [48]. Afterward, another first-ply failure analysis is conducted on the same beam but for cantilever boundary condition and with a concentrated static load at the end, to determine the critically stressed location in the uniform cantilever composite beam. The cantilever beam is then subjected to rotation, to determine the critical rotational velocity at which first-ply failure occurs and critically stressed location in the beam prone to delamination.

The mechanical properties of the composite material and the geometric properties of the beam are presented in Tables 2.14 and 2.15, respectively.

Mechanical properties of AS4/3502 graphite-epoxy	
Longitudinal modulus (E_1)	141.2 GPa
Transverse modulus ($E_2 = E_3$)	11.5 GPa
Shear modulus (G_{12})	6.0 GPa
Major Poisson's ratio (υ_{12})	0.3
Minor Poisson's ratio (υ_{21})	0.024
Tensile stress limit in the longitudinal direction (X_t)	2.343 GPa
Compressive stress limit in the longitudinal direction (X_c)	1.723 GPa
Tensile stress limit in transverse direction ($Y_t = Z_t$)	0.051 GPa
Compressive stress limit in transverse direction ($Y_c = Z_c$)	0.223 GPa
Shear stress limit ($S_{12} = S_{13} = S_{23}$)	0.086 GPa

Table 2.14 Mechanical properties of AS4/3502 graphite-epoxy [48]

Geometric properties of the beam	
Length	127.0 mm
Width	24.13 mm
Thickness	4.593 mm

Table 2.15 Geometric properties of the beam considered for first-ply failure analyses [48]

2.6.1 First–ply failure analysis of stationary uniform simply supported composite beam

In this sub-section, the first-ply failure analysis of a uniform simply supported composite beam with a concentrated static load at the mid-span of the beam is conducted using the FEA tool ANSYS®. The uniform composite beam with $[0_8/90_8]_s$ stacking sequence is considered for the analysis. The first-ply failure load obtained using Tsai-Wu failure criterion is compared in Table 2.16 with the results available in the Ref. [48] which were obtained using FEA tool ABAQUS® and Classical Laminate Theory (CLT).

	Results obtained using ANSYS®	ABAQUS® results from Ref. [48]	CLT results from Ref. [48]
First-ply failure load (N)	3125 N	2986 N	3248 N

Table 2. 16 First-ply failure load of the uniform composite beam with simply supported boundary condition using Tsai-Wu failure criterion

The pictorial illustration of first-ply failure of the considered uniform simply supported composite beam with a concentrated static load at the mid-span of the beam is shown in Figure 2.9.

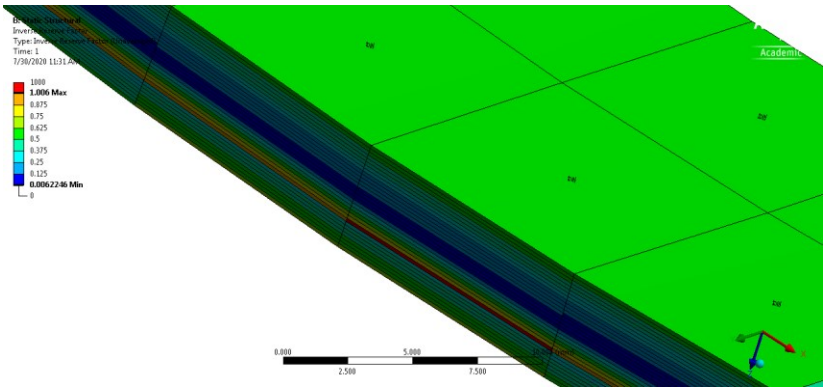

Figure 2.9 Pictorial illustration of first-ply failure of a uniform simply supported composite beam with a concentrated static load at the mid-span of the beam

From Table 2.16, it can be observed that the result obtained using ANSYS® is in good agreement with the results available in Ref. [48]. Figure 2.9 illustrates the pictorial representation of the failing ply. The 9th ply from the bottom with 90° fiber orientation angle is the first ply to fail at the mid-span of the beam.

2.6.2 First–ply failure analysis of stationary uniform cantilever composite beam

In this sub-section, the first-ply failure analysis of a uniform cantilever composite beam with a concentrated static load at the end of the beam is conducted using the FEA tool ANSYS®. The uniform composite beam with $[0_8/90_8]_s$ stacking sequence is considered for this analysis. The first-ply failure load is obtained using Tsai-Wu failure criterion and is found to be 748 N.

The pictorial representations of the loaded cantilever beam and the failing ply are illustrated in Figure 2.10.

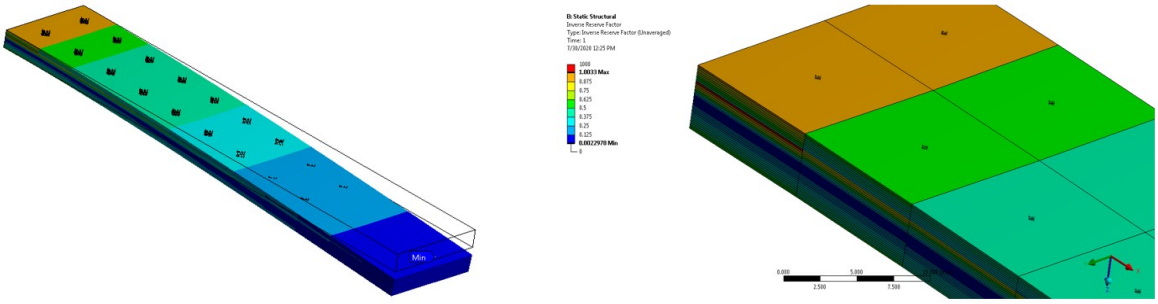

Figure 2.10 Pictorial representations of the loaded cantilever composite beam subjected to concentrated static load at the end and that of the first-ply failure

From Figure 2.10 it can be observed that the 24th ply from the bottom with 90° fiber orientation angle is the first ply to fail at the fixed end of the beam.

2.6.3 First–ply failure of rotating uniform cantilever composite beam

In this sub-section, the first-ply failure analysis of a rotating uniform cantilever composite beam is conducted using the FEA tool ANSYS®. The critical rotational speed responsible for the first-ply failure obtained using Tsai-Wu failure criterion is found to be 4908 rad/s. The pictorial representations of the deformed beam and the failing plies, while rotating at critical velocity are illustrated in Figure 2.11.

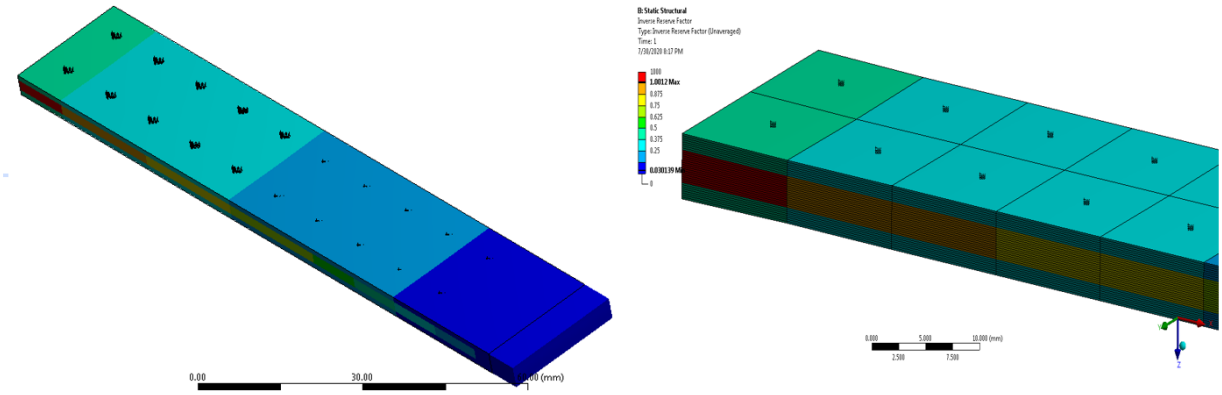

Figure 2.11 Pictorial representation of deformed beam and that of the first-ply failure while rotating at critical velocity

In Figure 2.11, the axial deformation is observed in the composite beam because of the centrifugal force due to the rotation of the beam. The axial deformation is responsible for the failure of 16 plies at the fixed end of the beam while rotating at critical rotational velocity. All the failed plies have 90° fiber orientation angle. It can be concluded that the fixed end of the rotating uniform cantilever composite beam is the critically stressed location.

2.7 Mode-I and Mode-II delamination tests

The separation of two adjacent plies in composite beams, represents one of the most critical failure in composite structures known as delamination. The composite beams are prone to delamination initiation and growth. The Finite Element Method (FEM) appears to be the best tool

to simulate delamination growth in composite structures. Mode-I and Mode-II delamination tests are conducted using Double cantilever beam (DCB) and end notch flexure (ENF) test samples to verify the values of the parameters of cohesive interface, which are used in performing further studies in the present thesis. The numerical models of DCB and ENF test samples are modeled ANSYS® and are based on Cohesive Zone Modeling (CZM). The contact elements (CONTAC174 finite element) are used for modeling of the bonded interface. The fracture energy method of CZM available in ANSYS® is used to model the cohesive interface of DCB and ENF test samples. The fracture energy method of CZM follows bilinear traction-separation law for delamination initiation and growth. The behavior of the contact element is characterized by the maximum traction in between interface elements and the critical energy release rate at which crack growth initiates. The area under the load vs displacement graph obtained from Mode-I and Mode-II tests gives critical energy release rate and indicates the fracture toughness.

An adequate mesh size must be chosen for modeling Mode-I delamination. The small mesh size can increase the computational time, whereas the large mesh size can lead to oscillations in the load vs displacement curve and therefore will result in unconverging solution. An artificial damping coefficient has been used to avoid oscillations in the load vs displacement curve. The artificial damping coefficient of value 0.01 is found to be adequate to obtain the reliable result with low computational time.

The pictorial representations of Mode-I and Mode-II failure modes are presented in Figure 2.12.

(a) Mode-I failure mode (b) Mode–II failure mode

Figure 2.12 Pictorial representations of Mode-I and Mode-II failure modes

The fracture energy based debonding approach is used for modeling the cohesive interface. The geometries of DCB and ENF test samples are created in Design Modeler, whereas

meshing is done in the mechanical module of Static Structural analysis system. The delaminated and cohesive interfaces were defined in Static Structural analysis system as frictionless and bonded regions. The appropriate boundary condition and loading are further applied to the test samples before running the simulation. The screenshots of the important steps required for the modeling of cohesive zone for Mode-II delamination test are presented in Appendix D.

2.7.1 Mode-I delamination test

In this sub-section, Mode-I delamination test is performed on a DCB test sample using FEA tool ANSYS®. The mechanical properties of the composite material along with the cohesive interface parameters are given in Table 2.17, whereas geometric properties of the DCB test sample are given in Table 2.18.

Mechanical properties of composite material	
Longitudinal modulus (E_1)	135 GPa
Transverse modulus (E_2)	9 GPa
$E_3 = E_2$	9 GPa
In-plane shear modulus (G_{12})	5.2 GPa
Major Poisson's ratio (υ_{12})	0.24
Poisson's ratio ($\upsilon_{23} = \upsilon_{32}$)	0.46
Cohesive interface parameters	
Maximum normal traction	1.7 MPa
Critical energy release rate	250 J/m^2
Artificial damping coefficient	0.01

Table 2.17 Mechanical properties of the composite material and cohesive interface parameters of DCB test sample [30]

Geometric properties of the beam	
Length (L)	100 mm
Width (b)	20 mm
Thickness of the laminate (t)	3 mm
Delamination length (a)	30 mm

Table 2.18 Geometric properties of the DCB test sample [30]

From Tables 2.17 and 2.20 it can be observed that the value of Poisson's ratio υ_{23} is higher than that of the value of the major Poisson's ratio υ_{12}, which is due to the softness of the material in the matrix direction resulting in easier extension and contraction in the 2 and 3 directions.

The delamination is modeled at the free end of the DCB test sample. For performing Mode-I delamination test, the displacements (δ) of 10 mm are given to the top and bottom edges of the DCB test sample at its free end to facilitate the crack opening. The given displacements are opposite to each other and are perpendicular to mid-plane of the DCB test sample as shown in Figure 2.13. As the crack growth initiates, the loads at the top and the bottom edges at the free end of DCB test sample are determined and are plotted against the given displacement. In Figure 2.14, the load vs displacement curve obtained from ANSYS® is compared with the load vs displacement graph available in Ref. [30]. The mesh of element size 1.2 mm is used to model DCB test sample. Test sample with $[0]_{10s}$ stacking sequence is considered for this test.

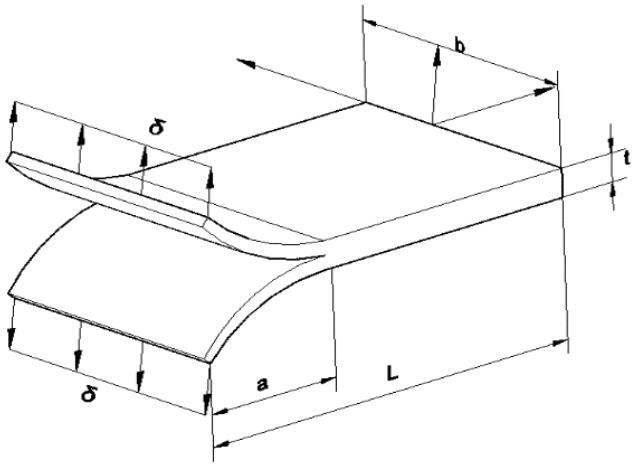

Figure 2.13 Pictorial representation of the DCB test sample undergoing Mode-I delamination test

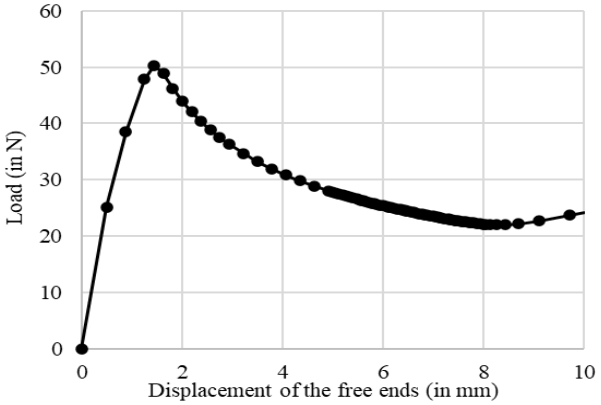

Figure 2.14 (a) Curve of load vs displacement of the free ends of DCB test sample undergoing Mode-I delamination test obtained using ANSYS®

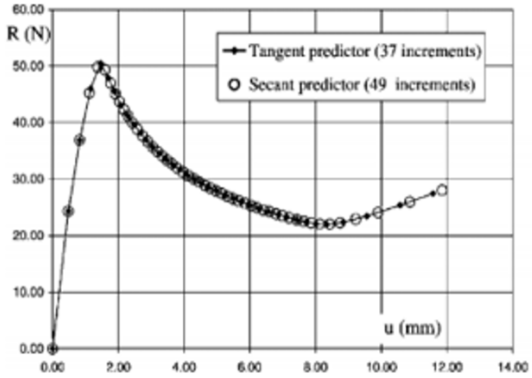

Figure 2.14 (b) Curve of load vs displacement of the free ends of DCB test sample undergoing Mode-I delamination test available in Ref. [30] obtained using FEA

Figure 2.14 Curves of load vs displacement of the free ends of the DCB test sample undergoing Mode-I delamination test obtained using ANSYS® and that available in Ref. [30] obtained using FEA

It can be observed from Figure 2.14 that the load vs displacement curve of DCB test sample undergoing Mode-I delamination test obtained using ANSYS® is in good agreement with the load vs displacement curve available in Ref. [30]. The peak in the load vs displacement curve represents the critical load and the corresponding displacement represents the critical displacement for the crack growth. The three-dimensional pictorial representation of the DCB test sample undergoing Mode-I delamination test is a shown in Figure 2.15.

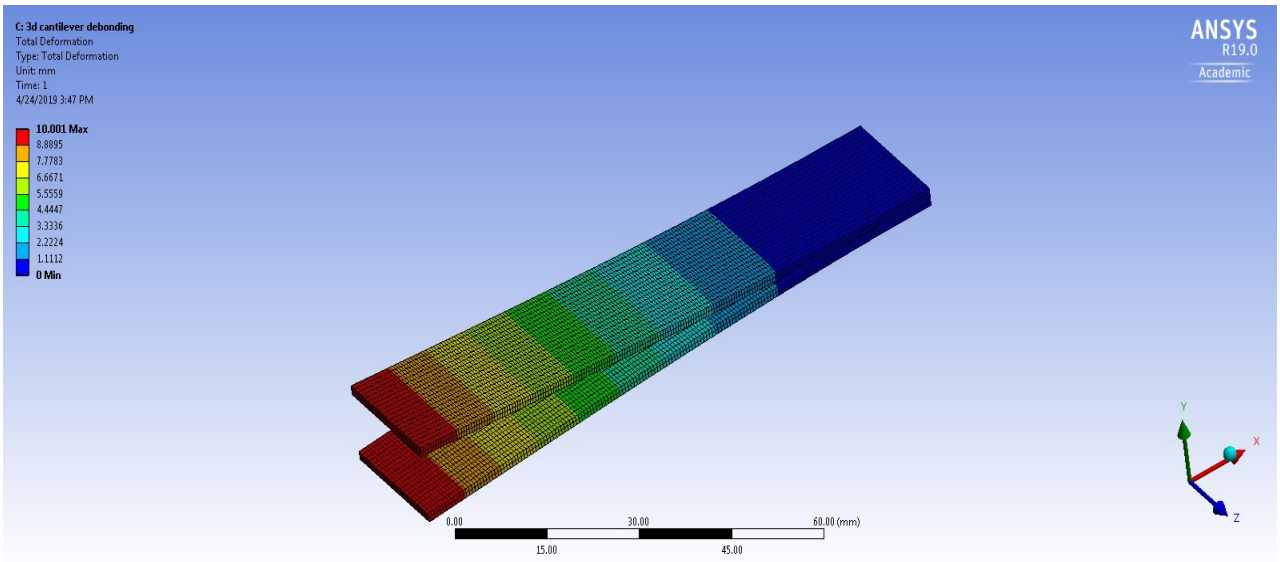

Figure 2.15 The three-dimensional pictorial illustration of the DCB test sample undergoing Mode-I delamination test using FEA tool ANSYS®

2.7.2 Mode-II delamination test

In this sub-section, Mode-II delamination test is performed on a ENF test sample using FEA tool ANSYS®. IM7/8852 graphite-epoxy composite material is considered for this analysis. The mechanical properties of the composite material along with interface properties are given in Table 2.19 whereas geometric properties of ENF test sample are given in Table 2.20.

The meshing of the test sample is done using edge meshing. The edge meshes of size 1 mm, 2 mm and 1.125 mm are used to mesh the edges along the length, width and thickness of the ENF test sample, respectively. Test sample with $[0]_{12s}$ stacking sequence is considered for this test.

Figure 2.16 illustrates the two-dimensional pictorial representation of ENF test sample undergoing Mode-II delamination test.

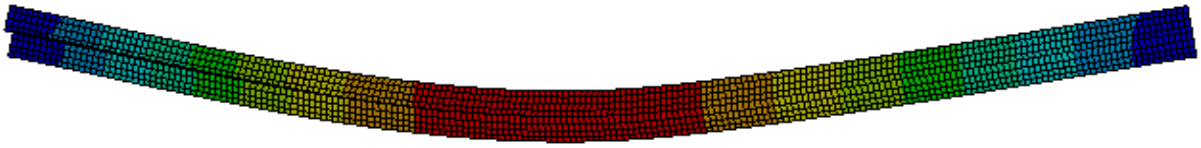

Figure 2.16 Two-dimensional pictorial representation of the ENF test sample undergoing Mode-II delamination test using FEA tool ANSYS®

Mechanical properties of IM7/8852 graphite-epoxy	
Longitudinal modulus (E_1)	161 GPa
Transverse modulus (E_2)	11.38 GPa
$E_3 = E_2$	11.38 GPa
In-plane shear modulus (G_{12})	5.2 GPa
Major Poisson's ratio (υ_{12})	0.32
Poisson's ratio ($\upsilon_{23} = \upsilon_{32}$)	0.48
Cohesive interface parameters	
Maximum tangential traction	29.8 MPa
Critical energy release rate	774 J/m^2
Artificial damping coefficient	0.01

Table 2.19 Mechanical properties of IM7/8852 graphite-epoxy and cohesive interface parameters of the ENF test sample [32]

Geometric properties of the ENF test sample	
Length (L)	101.1 mm
Width (b)	25.4 mm
Thickness of the laminate (t)	4.5 mm
Delamination length (a)	25.4 mm

Table 2.20 Geometric properties of the ENF test sample [32]

The delamination is modeled at the end of the ENF test sample, supported on rollers. For performing Mode-II delamination test, the displacement (δ) of 2 mm is given at the center of the ENF test sample in the downward direction to facilitate the crack growth as shown in Figure 2.17. When the central displacement attains the critical value the upper part of the beam slides over the interface indicating the crack progression. The load at the center of the ENF test sample is determined and is plotted against the given displacement. The obtained load vs displacement curve is presented in Figure 2.18. The critical displacement and critical load at which the crack growth initiates are given in Table 2.21 and are compared with the results available in Ref. [32].

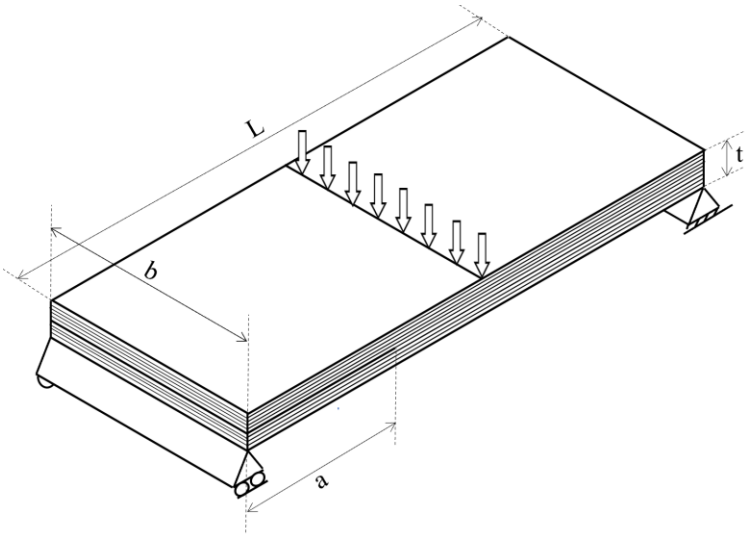

Figure 2.17 Pictorial representation of the End Notch Flexure (ENF) test sample undergoing Mode-II delamination test

	Results obtained using ANSYS®	Results from Ref. [32] using ANSYS®
Critical Load (in N)	1304.1	1372.7
Critical displacement (in mm)	1.33	1.31

Table 2.21 Comparison of critical load and critical displacement of the ENF test sample undergoing Mode-II delamination test

From Table 2.21 it can be observed that the results obtained using ANSYS® are in good agreement with the results available in Ref. [32].

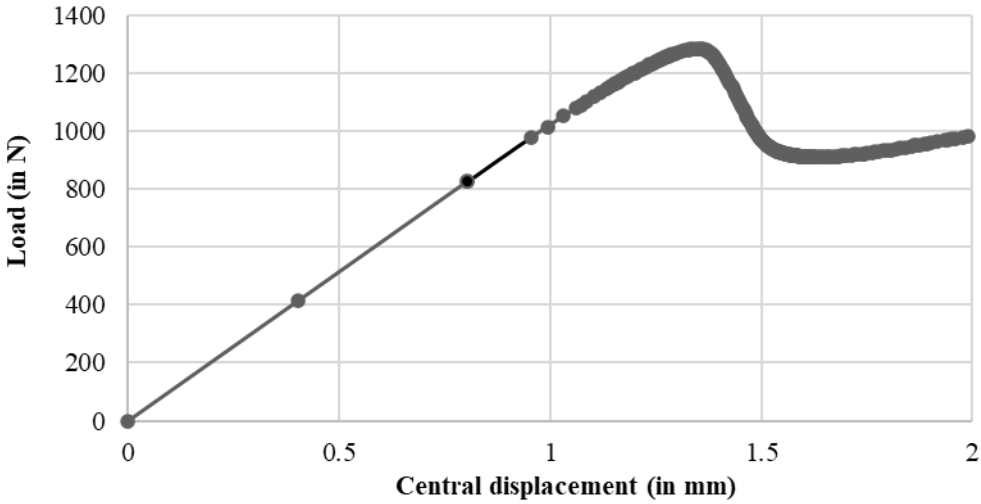

Figure 2.18 Curve of load vs. central displacement obtained for the ENF test sample undergoing Mode-II delamination test using ANSYS®

In Figure 2.18, the peak in the load vs displacement curve represents the critical load and the corresponding displacement represents the critical displacement at which the crack growth initiates. The trough in load vs displacement curve represents the crack arrest load, and corresponding displacement represents crack arrest displacement. The crack progression occurs for the displacement values lying in between the critical displacement and crack arrest displacement.

The three-dimensional pictorial representation of the delaminated beam undergoing Mode-II delamination test is presented in Figure 2.19.

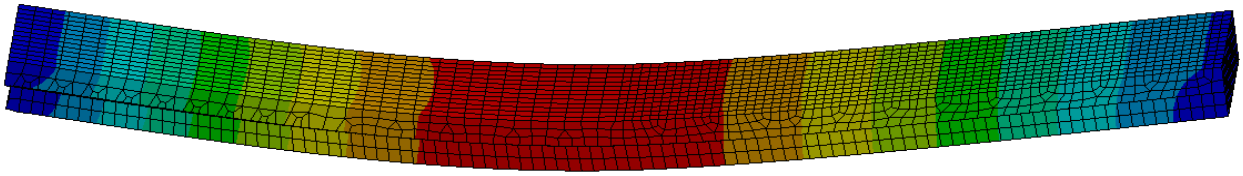

Figure 2.19 Three-dimensional pictorial representation of a simply supported beam with end delamination undergoing Mode-II delamination test

2.8 Free vibration response of uniform simply supported composite beams with end delamination

In the present section, uniform simply supported composite beams with end delamination and $[\theta]_{8s}$ stacking sequence (where θ is the fiber orientation angle), which are made up of Metyx® 600 Tex graphite-epoxy prepreg, are considered for the verification of natural frequencies. The geometric properties of the beam and the mechanical properties of the composite material are given in Tables 2.22 and 2.23, respectively whereas the interface parameters of cohesive and delaminated region are given in Table 2.24.

Geometric properties	
Length	400 mm
Width	20.5 mm
Individual ply thickness	0.206 mm
Number of plies	16
Thickness of the laminate	3.3 mm

Table 2.22 Geometric properties of the beam [33]

Mechanical properties of Metyx® 600 Tex graphite-epoxy [33]	
Longitudinal modulus (E_1)	44.15 GPa
Transverse modulus (E_2)	12.30 GPa
$E_3 = E_2$	12.30 GPa
In-plane shear modulus (G_{12})	4.09 GPa
G_{13}=G_{12}	4.09 GPa
Density of a ply (ρ_p)	2026 kg/m^3
Major Poisson's ratio (υ_{12})	0.20
Minor Poisson's ratio (υ_{21})	0.018

Table 2.23 Mechanical properties of Metyx® 600 Tex graphite-epoxy [33]

Cohesive interface parameters [4]	
Maximum tangential traction	29.8 MPa
Critical energy release rate	774 J/m^2
Artificial damping coefficient	0.01
Delaminated interface parameters [5]	
Penalty stiffness of the delaminated interface (N/mm^2)	10^5

Table 2.24 Interface parameters of cohesive and delaminated regions [32,33]

The finite element model of the delaminated beam is developed using FEA tool ANSYS®. The SOLID185 finite element is used for three-dimensional modeling of delaminated beam and CONTAC174 contact finite element is used for modeling the cohesive interface. The mesh of 8 mm is used to perform the analysis. A total of 2400 SOLID185 finite elements are used to get the desired results. The total number of CONTAC174 contact finite elements used in the analysis depends on the length of the bonded interface. The natural frequencies of the uniform simply supported composite beams with end delamination of different lengths are determined from the modal analysis and are compared in Table 2.25 with the results available in Ref. [33]. The results in Ref. [30] were obtained by using Timoshenko beam theory.

Crack length (in mm)	Mode number	Stacking sequence							
		$[0]_{8s}$		$[45]_{8s}$		$[60]_{8s}$		$[90]_{8s}$	
		Results obtained using ANSYS®	Results from Ref. [33]	Results obtained using ANSYS®	Results from Ref. [33]	Results obtained using ANSYS®	Results from Ref. [33]	Results obtained using ANSYS®	Results from Ref. [33]
0	1	44.17	45.00	23.67	24.00	21.76	21.00	23.04	23.00
	2	174.31	175.00	90.99	95.00	87.01	90.00	92.10	93.00
	3	391.29	390.00	206.01	204.00	195.76	200.00	207.01	205.00
40	1	43.64	43.00	22.90	23.00	21.59	21.00	22.48	22.00
	2	168.10	170.00	87.36	90.00	83.97	84.00	89.20	90.00
	3	361.43	360.00	189.35	193.00	182.28	190.00	194.23	195.00
320	1	23.78	22.00	11.82	11.00	11.15	11.00	11.81	12.00
	2	93.40	92.00	48.13	50.00	46.37	47.00	49.12	50.00
	3	216.52	208.00	112.76	114.00	108.89	110.00	115.41	115.00

Table 2.25 First three natural frequencies (in Hz) of 400-mm-long stationary uniform simply supported composite beams with end delamination

From Table 2.25, it can be observed that the results obtained using ANSYS® are in good agreement with the results available in Ref. [33]. The natural frequencies of the uniform composite beam decrease with increase in delamination length and for fiber orientation angles up to 60°. A substantial decline is observed in the natural frequencies of the delaminated and non-delaminated composite beams due to the change in the fiber orientation angle from 0° to 45°, whereas a slight increase is seen in their natural frequencies due to change in fiber orientation angle from 60° to 90°. The highest natural frequencies are observed for the non-delaminated beam with 0° fiber orientation angle, whereas the lowest natural frequencies are observed for the composite beam

with 320 mm end delamination and 60° fiber orientation angle. The effective bending stiffnesses in the longitudinal and transverse directions of the beam change due to change in the fiber orientation angle, which leads to change in the natural frequencies. The values of the effective bending stiffness in the longitudinal direction of the intact beam determined for various fiber orientation angles are presented in Figure 2.20.

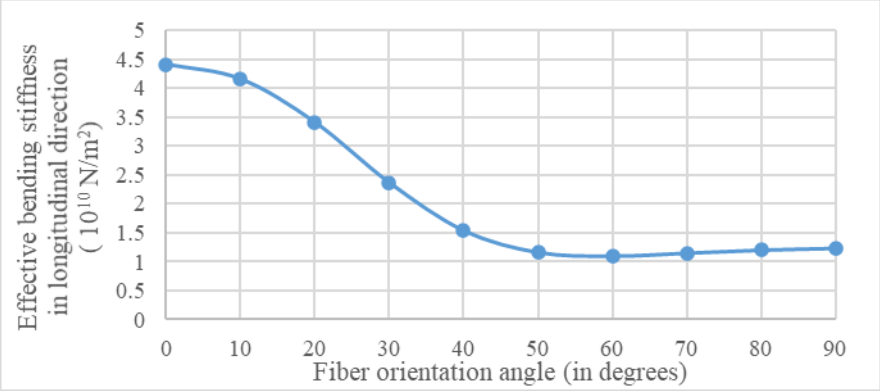

Figure 2.20 The Influence of fiber orientation angle on the effective bending stiffness in the longitudinal direction of the 400-mm-long intact composite beam

The effective bending stiffness in the longitudinal direction of the beam (in x x-axis direction) for various fiber orientation angles shown in Figure 2.20 is calculated using MATLAB®. The following equation derived from ABD matrix presented in Ref. [51] is used to determine the effective stiffness in the longitudinal direction of the beam.

$$E_x = \frac{12}{h^3 \, D_{11}^*}$$

From Figure 2.20, it can be observed that the composite beam with $[0]_{8s}$ stacking sequence has the highest effective stiffness in the longitudinal direction of the beam, whereas the composite beam with $[60]_{8s}$ stacking sequence has the lowest. The effective bending stiffness of the composite beam in the longitudinal direction of the beam decreases with the increase in the fiber orientation angle up to 60°. The effective stiffness in the longitudinal direction of the beam decreases sharply due to the change in fiber orientation angle from 0° to 45°, whereas it increases slightly when the fiber orientation angle changes from 60° to 90°.

The composite beams with $[45]_{8s}$ and $[90]_{8s}$ stacking sequences have similar values of their effective bending stiffness in the longitudinal direction of the beam, resulting in close values

of their natural frequencies. The effective bending stiffness in the longitudinal direction of the intact beam with $[90]_{8s}$ stacking sequence is 1.29×10^{10} N/m^2, which is slightly higher than that of the effective bending stiffness in the longitudinal direction of the intact beam with $[60]_{8s}$ stacking sequence i.e. 1.23×10^{10} N/m^2.

2.9 Free vibration response of stationary and rotating uniform cantilever composite beams with mid-span delamination

In the present section, stationary and rotating uniform cantilever composite beams with mid-span delamination are considered for the verification of fundamental frequency. The beams are made up of T300/934 graphite/epoxy prepreg. The mechanical properties of the composite material and the cohesive interface parameters are given in Tables 2.26 and 2.27, respectively. The geometric properties of the stationary and rotating cantilever composite beams are given in Tables 2.28 and 2.29, respectively. The delaminated beams are modeled using FEA tool ANSYS®.

Mechanical properties of T300/934 graphite/epoxy		
	Imperial standard units	**International standard units**
Longitudinal modulus (E_1)	19.5 ×10^6 Psi	134.44 GPa
Transverse modulus (E_2)	1.5×10^6 Psi	10.34 GPa
$E_1 = E_2$	1.5×10^6 Psi	10.34 GPa
In-plane shear modulus (G_{12})	0.725×10^6 Psi	4.998 GPa
Density of a ply (ρ_n)	1.382×10^{-6} lb-s/in^4	1471.32 kg/m^3
Major Poisson's ratio (υ_{12})	0.33	0.33

Table 2.26 Mechanical properties of T300/934 graphite/epoxy [34]

Cohesive interface parameters	
Maximum tangential traction	29.8 MPa
Critical energy release rate	774 J/m^2
Artificial damping coefficient	0.01

Table 2. 27 Cohesive interface parameters [34]

Geometric properties of stationary cantilever composite beam	
Length	127 mm
Width	12.7 mm
Individual ply thickness	0.127 mm
Number of plies	8
Thickness of the laminate	1.016 mm
Stacking sequence	[0/90/0//90/90/0/90/0]

Table 2.28 Geometric properties and stacking sequence of the stationary cantilever composite beam [34]

Geometric properties of rotating cantilever composite beam	
Length	127 mm
Width	12.7 mm
Individual ply thickness	0.254 mm
Number of plies	4
Thickness of the laminate	1.016 mm
Stacking sequences	[0/0/0//0], [45/-45/-45//-45], [90/90/90//90]

Table 2.29 Geometric properties and stacking sequences of the rotating cantilever composite beam [34]

In Tables 2.28 and 2.29 while illustrating the stacking sequence, double slash is used to indicate thickness wise location of the mid-span delamination between the plies. The formulations of non-dimensional parameters L^* and η [6] are given in equations (2.3) and (2.4), respectively. The non-dimensional parameters are converted to dimensional form and are illustrated as delamination length (in mm) in Table 2.30 and as rotational velocity (in rad/s) in Table 2.31.

$$L^* = \frac{L_1}{L} \tag{2.3}$$

$$\eta = \Omega L^2 \sqrt{\frac{\rho_p}{h^2 E_{11}}} \tag{2.4}$$

The terminologies used in equations (2.3) and (2.4) are given below:

L_1 - Delamination length (in mm) L - Beam length (in mm)

Ω - Rotational velocity (in rad/s) h - Thickness of the laminate (in mm)

E_{11} - Young's modulus in the axial direction (in GPa) ρ_p - Density of ply(in Kg/m^3)

The fundamental frequencies of stationary uniform cantilever composite beams with mid-span delamination of different lengths are determined and compared in Table 2.29 with the results available in the literature. The fundamental frequencies of mid-span delaminated stationary and rotating cantilever composite beams are obtained using FEA tool ANSYS®. The results in Ref. [34] were obtained using finite element approach whereas the results in Ref. [35] were obtained analytically by considering shear effect, rotary inertia and bending-extension coupling in the governing equations of vibration.

L*	Delamination length (in mm)	Fundamental frequency (in Hz) obtained using ANSYS®	Results from Ref. [34]	Results from Ref. [35]
0.2	25.4	81.30	80.38	82.01
0.4	50.8	79.72	79.09	80.79
0.6	76.2	75.76	76.05	77.52

Table 2.30 Fundamental frequencies (in Hz) of the 127-mm-long stationary cantilever composite beams with mid-span delamination

From Table 2.30, it can be observed that the results obtained from ANSYS® are in good agreement with the results available in the literature.

Table 2.31 illustrates the fundamental frequencies of intact stationary uniform cantilever composite beam with $[0]_{2s}$ stacking sequence and rotating uniform cantilever composite beam with mid-span delamination for three different stacking sequences. The mid-span delamination of 25.4 mm is considered in this analysis.

The terminologies used in Table 2.31 are given below:

ω_s - Fundamental frequency of stationary intact beam with $[0]_{2s}$ stacking sequence

ω - Fundamental frequency of rotating composite beam with [0/0/0//0], [45/45/45//45], [90/90/90//90] stacking sequences and with mid-span delamination

η - Non-dimensional parameter of rotational velocity as per equation (2.4)

Stacking sequence $[0]_{2s}$	**Stacking sequence [0/0/0//0]**				
Intact stationary beam	**Delaminated rotating beam**				
(ω_s) using ANSYS®	**η**	**Rotational velocity (in rad/s)**	**(ω) using ANSYS®**	**ω/ω_s**	**ω/ω_s Ref. [34]**
99.60	0.001	6.02	96.86	0.97	0.98
99.60	1	602.10	142.22	1.43	1.45
99.60	2	1204.20	227.47	2.28	2.31
99.60	3	1806.40	320.16	3.21	3.28
Stacking sequence $[0]_{2s}$	**Stacking sequence [45/45/45//45]**				
Intact stationary beam	**Delaminated rotating beam**				
ANSYS® (ω_s)	**η**	**Rotational velocity (in rad/s)**	**ANSYS® (ω)**	**ω/ω_s**	**ω/ω_s Ref. [34]**
99.60	0.001	6.02	32.76	0.33	0.33
99.60	1	602.10	107.83	1.08	1.11
99.60	2	1204.20	203.25	2.04	2.1
99.60	3	1806.40	304.61	3.05	3.12
Stacking sequence $[0]_{2s}$	**Stacking sequence [90/90/90//90]**				
Intact stationary beam	**Delaminated rotating beam**				
ANSYS® (ω_s)	**η**	**Rotational velocity (in rad/s)**	**ANSYS® (ω)**	**ω/ω_s**	**ω/ω_s Ref. [34]**
99.60	0.001	6.02	27.02	0.27	0.28
99.60	1	602.10	104.88	1.05	1.06
99.60	2	1204.20	200.32	2.01	2.09
99.60	3	1806.40	301.05	3.02	3.10

Table 2.31 Fundamental frequencies (in Hz) of the 127-mm-long intact stationary and 127-mm-long rotating cantilever composite beams with 25.4 mm mid-span delamination

In Table 2.31, the values of the ratio (ω/ω_s) of the fundamental frequencies of rotating cantilever composite beam with mid-span delamination and intact stationary cantilever composite beam with $[0]_{2s}$ stacking sequence are obtained and are compared with the results available in Ref. [34]. It can be observed that the results presented in Table 2.31 are in good agreement with the results available in Ref. [34].

2.10 Conclusion

In this chapter, the free vibration analysis of uniform, thickness-tapered, and doubly tapered composite beams under rotational loading has been conducted using the FEA tool ANSYS® in the first stage. The results for the first three out-of-plane bending natural frequencies were verified with the existing references. The influence of plies dropped-off and width-ratio on the natural frequencies of rotating composite beams has been investigated. From the results obtained, it can be concluded that with increase in number of plies dropped-off, the 1st natural frequency of the rotating thickness-tapered composite beam increases, whereas 2nd and 3rd natural frequencies decrease. The natural frequencies of rotating doubly tapered composite beam increase with the decrease in the width-ratio value. A layer reduction test has been performed on simply supported and cantilever composite beams. For the simply supported beams, the natural frequencies of the tapered laminate were higher than those of thin beams and lower than those of a thick beam. For cantilever beams due to asymmetry in the boundary condition, the 1st natural frequency of tapered beam was higher than those of thin and thick uniform beams, but 2nd and 3rd natural frequencies of tapered beam were higher than those of thin uniform beam but lower than those of the thick uniform beam.

In the second stage, the first-ply failure analyses were conducted to determine the critically stressed location prone to delamination in the stationary and rotating cantilever composite beams with a concentrated load at the end and in stationary simply supported beam with a concentrated load at the mid-span. In stationary and rotating cantilever composite beams, the plies with 90° fiber orientation angles were the first to fail at the fixed end. In a stationary simply supported beam, the ply with 90° fiber orientation angle was the first to fail at the mid-span. Further in the thesis, the influence of delamination size on the natural frequencies of the composite beams has been investigated by modeling the delamination at the critically stressed location.

Mode-I and Mode-II delamination tests have been conducted to simulate delamination growth in DCB and ENF test samples. The critical load and critical displacement at which the delamination growth initiates have been determined and compared with the existing references.

The free vibration response of uniform simply supported composite beam with end delamination has been determined and is compared with the results available in the literature. The free vibration response of stationary and rotating uniform cantilever composite beams with mid-span delamination have been determined and compared with the results of an existing reference.

Chapter 3

Free vibration response of stationary uniform and thickness-tapered composite beams with delamination

3.1 Introduction

In chapter 2, the first three out-of-plane bending natural frequencies of uniform, thickness-tapered and doubly tapered composite beams determined using FEA tool ANSYS® were verified with the results available in the literature where possible. The first-ply failure analyses were conducted to determine the critically stressed locations prone to delamination in stationary and rotating uniform composite beams. The load vs displacement curves of DCB and ENF test samples undergoing Mode-I and Mode-II delamination tests were discussed and compared with the results available in the literature. The first three out-of-plane bending natural frequencies of stationary and rotating uniform composite beams with end and mid-span delamination were compared with the available results for simply supported and cantilever boundary conditions.

In this chapter, the free vibration response of the uniform and thickness-tapered composite beams with end and mid-span delamination of different lengths is determined and the influences of delamination length and fiber orientation angle on the natural frequencies are investigated. The delamination lengths having minimal effect on the natural frequencies of the uniform and thickness-tapered composite beams with end delamination are determined. The natural frequencies of thickness-tapered composite beams with end and mid-span delamination are compared. In another study, the free vibration analysis of uniform composite beams with mid-span delamination between different plies is conducted. The influences of the layer reduction and taper angle on the natural frequencies of end delaminated composite beams are also investigated. The simply supported boundary condition and Metyx® 600 Tex graphite-epoxy composite material are considered for all the beams considered in this chapter.

The commercial finite element analysis software ANSYS® 19.0 Workbench platform is chosen to perform this study. ANSYS® Composite PrepPost (ACP) is used to model composite beams. The SOLID185 and CONTAC174 finite elements are used for the three-dimensional modeling of the delaminated beams and the cohesive interface, respectively. The behavior of the contact element is characterized by the maximum tangential traction between the interface elements and the critical energy release rate at which crack growth initiates.

3.2 Influences of the delamination length and fiber orientation angle on the natural frequencies of uniform composite beam with end mid-plane delamination

In this section, the influences of delamination length and fiber orientation angle on the first three out-of-plane bending natural frequencies of uniform simply supported composite beam with end mid-plane delamination are investigated. The numerical model of the delaminated beam is developed using FEA tool ANSYS®. The mesh of element size 4 mm is used to model the uniform delaminated beam. The mechanical properties of the composite material are given in Table 3.1, whereas the interface parameters are given in Table 3.2. The geometric properties of the beam are given in Table 3.3.

Mechanical properties of Metyx® 600 Tex graphite-epoxy	
Longitudinal modulus (E_1)	44.15 GPa
Transverse modulus (E_2)	12.30 GPa
$E_3 = E_2$	12.30 GPa
In-plane shear modulus (G_{12})	4.09 GPa
$G_{13} = G_{12}$	4.09 GPa
Density of a ply (ρ_p)	2026 kg/m^3
Major Poisson's ratio (υ_{12})	0.20
Minor Poisson's ratio (υ_{21})	0.018

Table 3.1 Mechanical properties of Metyx® 600 Tex graphite-epoxy [33]

Cohesive interface parameters [32]	
Maximum tangential traction	29.8 MPa
Critical energy release rate	774 J/m^2
Artificial damping coefficient	0.001
Delaminated interface parameters [33]	
Penalty stiffness of the delaminated interface (N/mm^2)	10^5

Table 3.2 Interface parameters of cohesive and delaminated regions [32, 33]

Geometric properties of the beam	
Length	400 mm
Width	20.5 mm
Individual ply thickness	0.20625 mm
Number of plies	16
Thickness of the laminate	3.3 mm

Table 3.3 Geometric properties of the beam [33]

The natural frequencies of the intact and end delaminated uniform simply supported composite beams are compared in Figure 3.1.

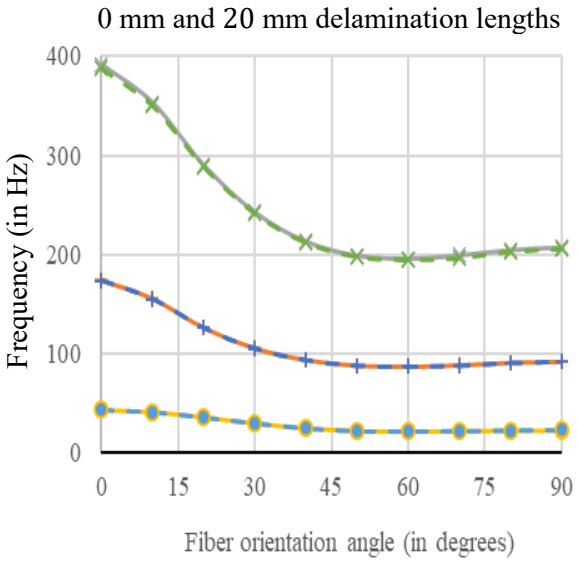

Figure 3.1 (a)

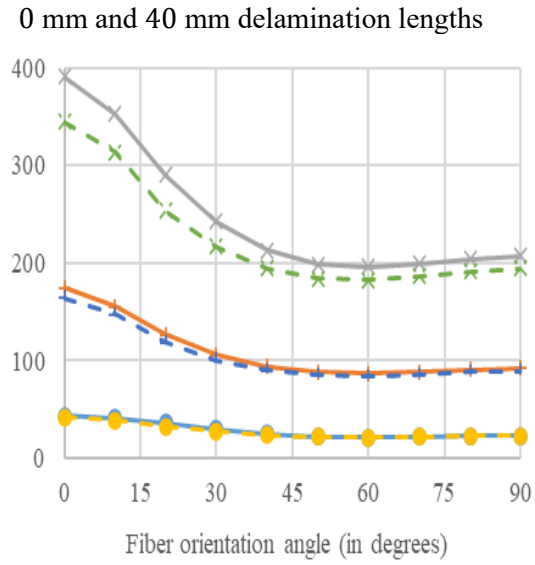

Figure 3.1 (b)

0 mm and 80 mm delamination lengths

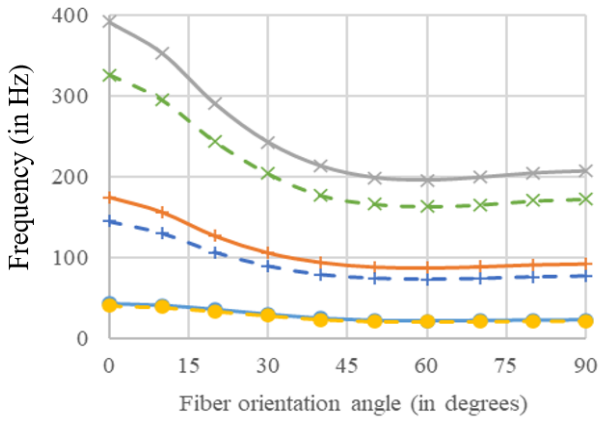

Figure 3.1 (c)

0 mm and 160 mm delamination lengths

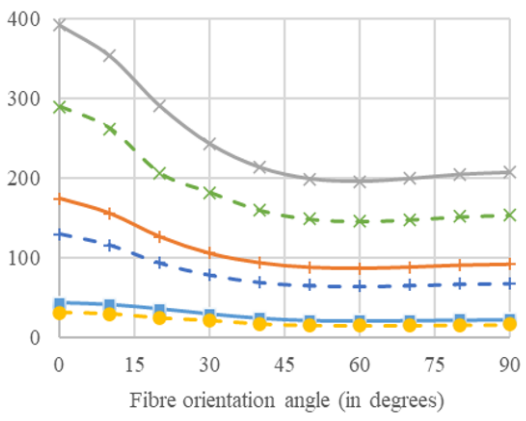

Figure 3.1 (d)

0 mm and 240 mm delamination lengths

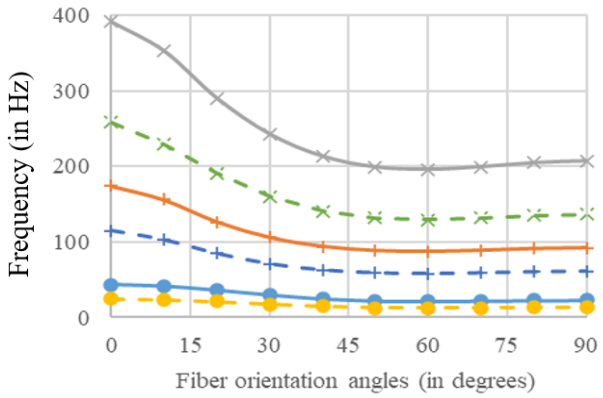

Figure 3.1 (e)

0 mm and 320 mm delamination lengths

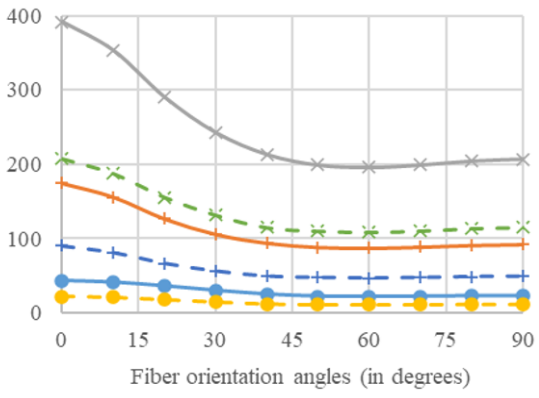

Figure 3.1 (f)

Figure 3.1 Comparison of the first three natural frequencies (in Hz) of the 400-mm-long intact and end delaminated uniform simply supported composite beams

Figure 3.1 illustrates the comparison of the first three natural frequencies of the intact and end delaminated uniform simply supported composite beams over a range of 0° to 90° fiber orientation angles. The solid curves represent natural frequencies of the intact beam, whereas the dotted curves represent natural frequencies of the end delaminated beam. A similar variation is observed in all the three natural frequencies due to the change in fiber orientation angle. The natural frequencies decrease with the increase in delamination length.

From Figure 3.1 (a) it is observed that all the three natural frequencies of the intact and end delaminated composite beams are overlapping, hence up to 20 mm delamination length there is minimal effect of the delamination on the natural frequencies of the end delaminated beam.

Figures 3.2 and 3.3 illustrate the percentage decrease in the natural frequencies of the end delaminated beams with respect to that of the intact beams. The analysis is done for different delamination lengths and fiber orientation angles. The following equation is used to calculate the percentage decrease in the natural frequencies.

$$\text{Percentage decrease} = \frac{\text{Natural frequency of intact beam} - \text{Natural frequency of delaminated beam}}{\text{Natural frequency of intact beam}} \times 100$$

The analysis is conducted on two different geometries of the beam, with same width-to-beam-length ratio and delamination-length-to-beam-length ratio values. The results are expressed using the delamination-length-to-beam-length ratio. The mechanical properties of the composite material are given in Table 3.1 and the geometric properties of composite beams are given in Tables 3.3 and 3.4. For convenience, the delamination lengths of both the geometries with the corresponding delamination-length-to-beam-length ratio values are provided in Table 3.5.

Geometric properties	
Length	500 mm
Width	25.625 mm
Individual ply thickness	0.2062 mm
Number of plies	16
Thickness of the beam	3.3 mm

Table 3.4 Geometric properties of 500-mm-long beam

Delamination lengths and the corresponding delamination-length-to-beam-length ratio values									
Delamination-length-to-beam-length ratio value	0.05	0.1	0.2	0.3	0.4	0.5	0.6	0.7	0.8
Delamination lengths (in mm) of 400-mm-long beam	20	40	80	120	160	200	240	280	320
Delamination lengths (in mm) of 500-mm-long beam	25	50	100	150	200	250	300	350	400

Table 3.5 Delamination lengths and the corresponding delamination-length-to-beam-length-ratio values

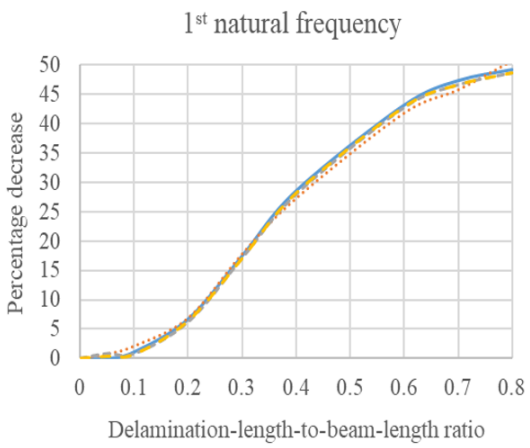

Figure 3.2 (a)

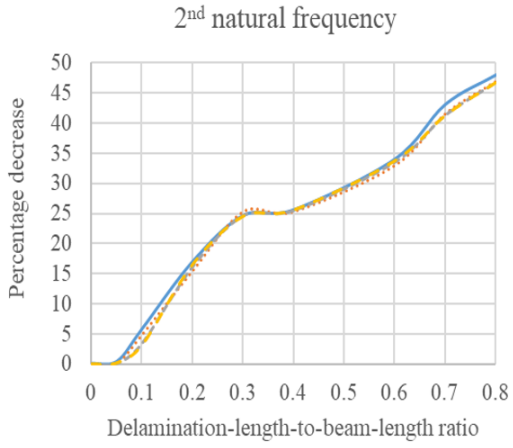

Figure 3.2 (b)

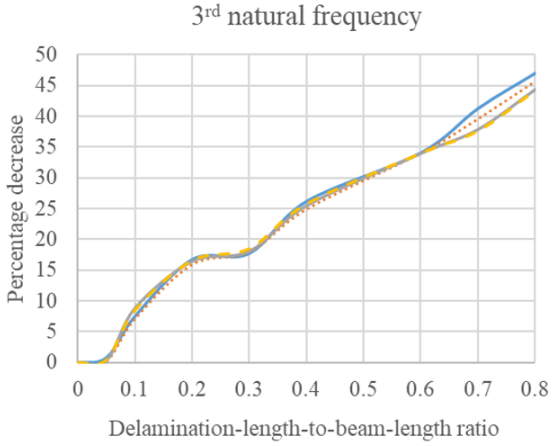

Figure 3.2 (c)

Stacking sequence $[0]_{8s}$ $[30]_{8s}$ $[60]_{8s}$ $[90]_{8s}$

Figure 3.2 Percentage decrease in the first three natural frequencies of the end delaminated uniform composite beams w.r.t. that of the intact composite beams for 400 mm beam length and simply supported boundary condition

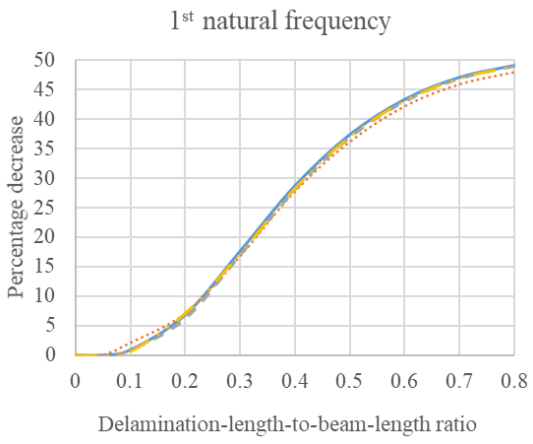

Figure 3.3 (a)

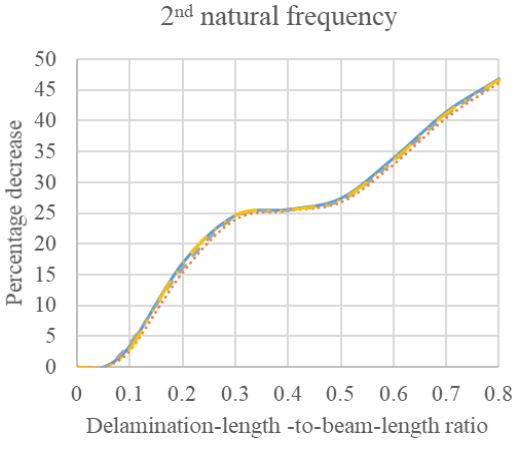

Figure 3.3 (b)

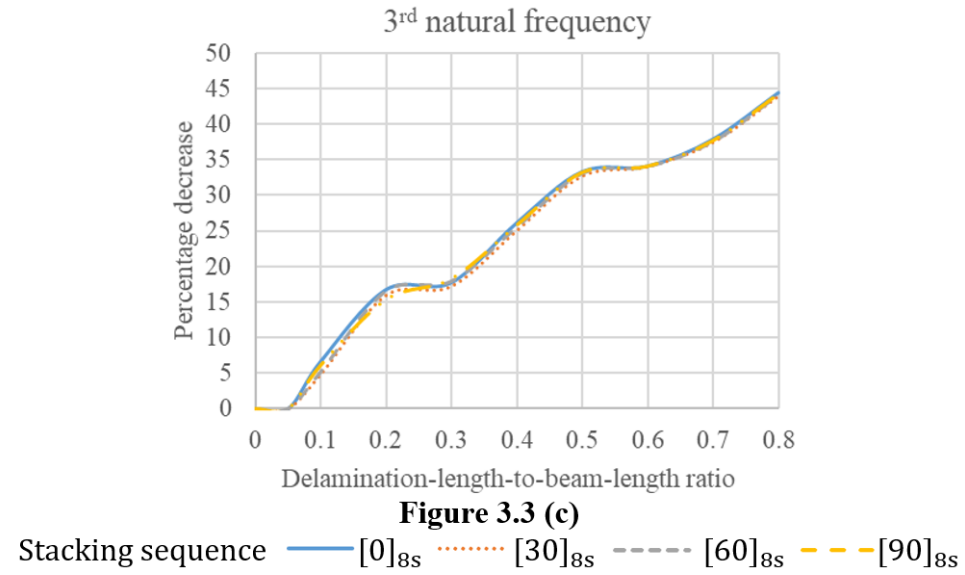

Figure 3.3 Percentage decrease in the first three natural frequencies of the end delaminated uniform composite beams w.r.t. that of the intact composite beams for 500 mm beam length and simply supported boundary condition

From Figures 3.2 and 3.3, it is observed that with the increase in delamination length, both the geometries show similar variation of the percentage decrease in the first three natural frequencies for all the considered stacking sequences. The percentage decrease in all the three natural frequencies is almost 0% up to the delamination-length-to-beam-length ratio value of 0.05.

In Figures 3.2 (a) and 3.3 (a), a steep increase is seen in the percentage decrease of 1st, 2nd and 3rd natural frequencies from 0.05 to 0.7, from 0.05 to 0.3 and from 0.05 to 0.2 delamination-length-to-beam-length ratio values, respectively. The slope of inclination for the percentage decrease in 2nd and 3rd natural frequencies decreases from 0.3 to 0.5 and from 0.2 to 0.3 delamination-length-to-beam-length ratio values, respectively. An increase is seen in the slope of the percentage decrease in 2nd and 3rd natural frequencies from delamination-to-beam-length ratio values of 0.5 to 0.8 and 0.3 to 0.5, respectively.

From Figures 3.2 and 3.3, it is observed that the percentage decrease in the 1st, 2nd, and 3rd natural frequencies for the delamination-length-to-beam-length ratio of value 0.8 is in between 45% to 50% for both the considered geometries.

Figure 3.4 illustrates the first three mode shapes of 400-mm-long uniform simply supported composite beam with 320 mm end delamination and $[0]_{8s}$ stacking sequence, whereas

Figure 3.5 illustrates the first three mode shapes of 400-mm-long uniform simply supported composite beam with 320 mm end delamination and $[90]_{8s}$ stacking sequence.

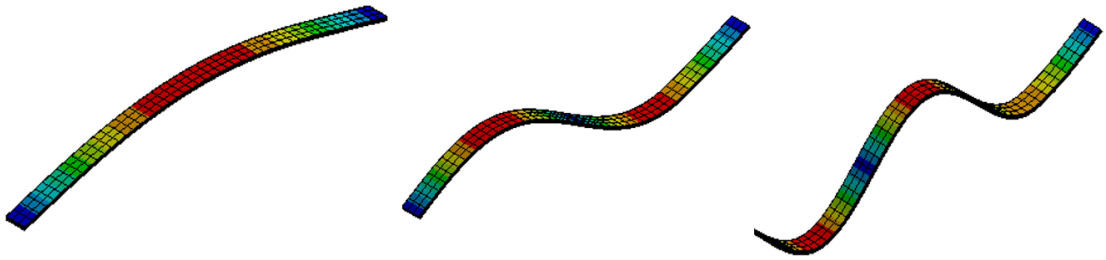

1st Mode 33.68 Hz 2nd Mode 106.38 Hz 3rd Mode 243.25 Hz

Figure 3.4 First three mode shapes of the 400-mm-long uniform simply supported composite beam with 320 mm end delamination and $[0]_{8s}$ stacking sequence

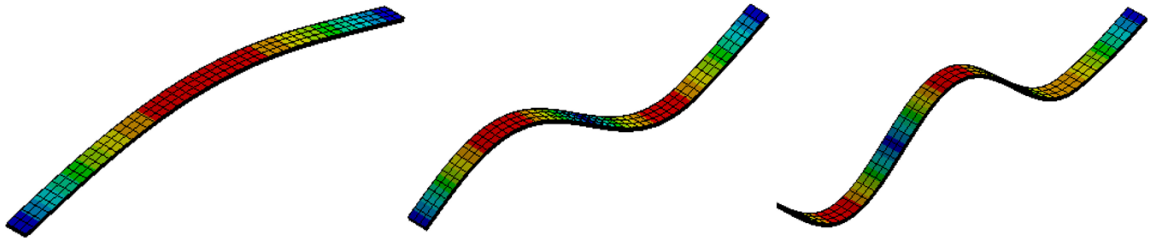

1st Mode 11.80 Hz 2nd Mode 49.20 Hz 3rd Mode 103.86 Hz

Figure 3.5 First three mode shapes of the 400-mm-long uniform simply supported composite beam with 320 mm end delamination and $[90]_{8s}$ stacking sequence

From Figures 3.4 and 3.5, it is observed that for the same delamination length, the composite beams with $[0]_{8s}$ and $[90]_{8s}$ stacking sequences have similar mode shapes. The points of inflection of the mode shapes are measured from the left end of the beams and are presented in Table 3.6.

Mode	Points of inflection of the mode shapes shown in Figure 3.4	Points of inflection of the mode shapes shown in Figure 3.5
1st Mode	200 mm	200 mm
2nd Mode	100 mm, 295 mm	100 mm, 295 mm
3rd Mode	65 mm, 190 mm, 315 mm	65 mm, 190 mm, 315 mm

Table 3.6 Points of inflection of the mode shapes illustrated in Figures 3.4 and 3.5

From Table 3.6, it is understood that for the same delamination length, the composite beams with $[0]_{8s}$ and $[90]_{8s}$ stacking sequences have same points of inflection measured from the left end of the beam.

3.3 Influences of the delamination length and fiber orientation angle on the natural frequencies of thickness-tapered composite beam with end mid-plane delamination

In this section, the influences of delamination length and fiber orientation angle on the first three out-of-plane bending natural frequencies of thickness-tapered simply supported composite beam with end mid-plane delamination are investigated. The thickness-tapered composite beam with a total of 16 plies at the left end and 10 plies at the right end is considered for this analysis. A total of 6 plies are dropped-off in a staircase arrangement as shown in Figure 2.6 of chapter 2 to obtain thickness-tapered beam profile. The mechanical properties of the composite material are given in Table 3.1, whereas the interface parameters are given in Table 3.2. The geometric properties of the beam are given in Table 3.3. The number of plies and the thickness of the beam mentioned in Table 3.3 refer to the number of plies and the thickness on the thick side (at the left end) of the thickness-tapered beam.

The finite element model of the delaminated beam is developed using FEA tool ANSYS®. The natural frequencies of thickness-tapered simply supported composite beams with end delamination determined from the modal analysis for different delamination lengths and fiber orientation angles are illustrated in Figure 3.6. The mesh of element size 4 mm is used to perform the analysis.

Figure 3.6 illustrates the comparison of the first three natural frequencies of the intact and end delaminated thickness-tapered simply supported composite beams, over a range of 0° to 90° fiber orientation angles. In Figure 3.6, the solid curves represent the natural frequencies of the intact beam, whereas the dotted curves represent the natural frequencies of the delaminated beam.

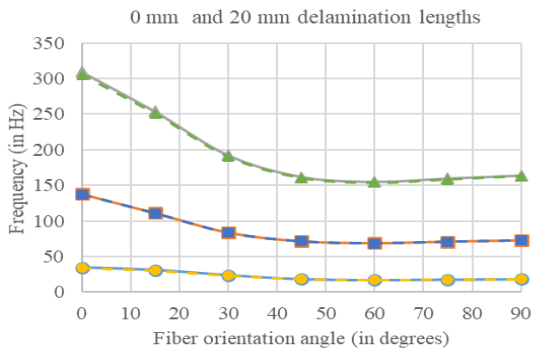

Figure 3.6 (a)

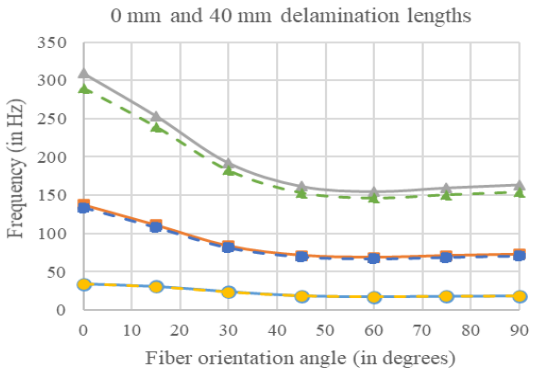

Figure 3.6 (b)

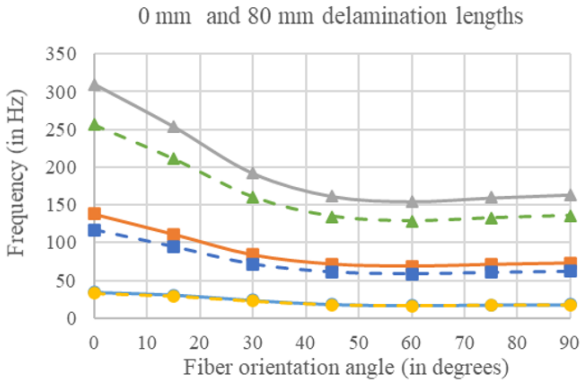

Figure 3.6 (c)

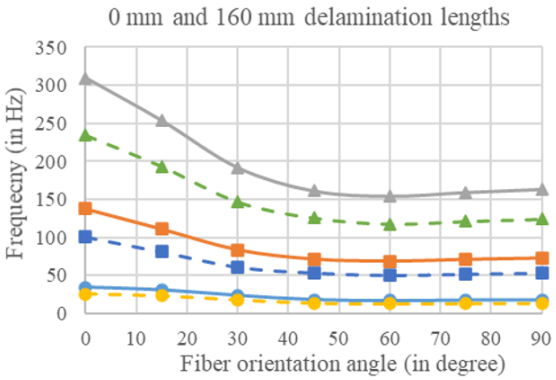

Figure 3.6 (d)

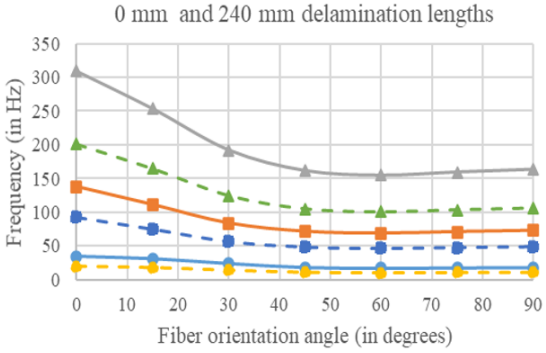

Figure 3.6 (e)

Figure 3.6 Comparison of the first three natural frequencies (in Hz) of the 400-mm-long intact and end delaminated thickness-tapered simply supported composite beams

From Figure 3.6 (a) it is observed that all three natural frequencies of the intact beam and that of the end delaminated thickness-tapered composite beams are overlapping, hence up to 20 mm delamination length there is minimal effect of delamination on the natural frequencies of the end delaminated thickness-tapered beam as was observed in the case of uniform beam in the previous section.

From Figures 3.1 and 3.6, it is observed that the natural frequencies of the end delaminated thickness-tapered composite beam are lower than that of the end delaminated uniform composite beam that has the same number of plies as that of the thick side of the tapered beam (presented in Figure 3.1) for simply supported boundary condition. A similar variation is observed in all the three natural frequencies of the thickness-tapered composite beam due to the change in the fiber orientation angle as was observed in the case of the uniform beams in the previous section. The

highest and lowest natural frequencies are observed at 0° and 60° fiber orientation angle, respectively. For instance, the highest and the lowest fundamental frequencies of the uniform beam with 80 mm end delamination are 40.66 Hz and 20.24 Hz respectively, for 0° and 60° fiber orientation angles, whereas the highest and the lowest fundamental frequencies of the thickness-tapered composite beam with 80 mm end delamination are 32.59 Hz and 16.30 Hz, respectively for 0° and 60° fiber orientation angles.

Due to the change in the fiber orientation angle, the effective stiffnesses in the longitudinal direction and the natural frequencies of the uniform and thickness-tapered composite beams change in the similar proportion. The pictorial illustration of the percentage decrease in the fundamental frequencies of the end delaminated uniform composite beams and thickness-tapered composite beams with 6 plies dropped-off due to the change in the fiber orientation angle is shown in Figure 3.7. The percentage decrease in the fundamental frequencies is calculated w.r.t. that of the fundamental frequencies of the end delaminated uniform and thickness-tapered composite beams with 0° fiber orientation angle. The analysis is conducted for 160 mm end delamination length.

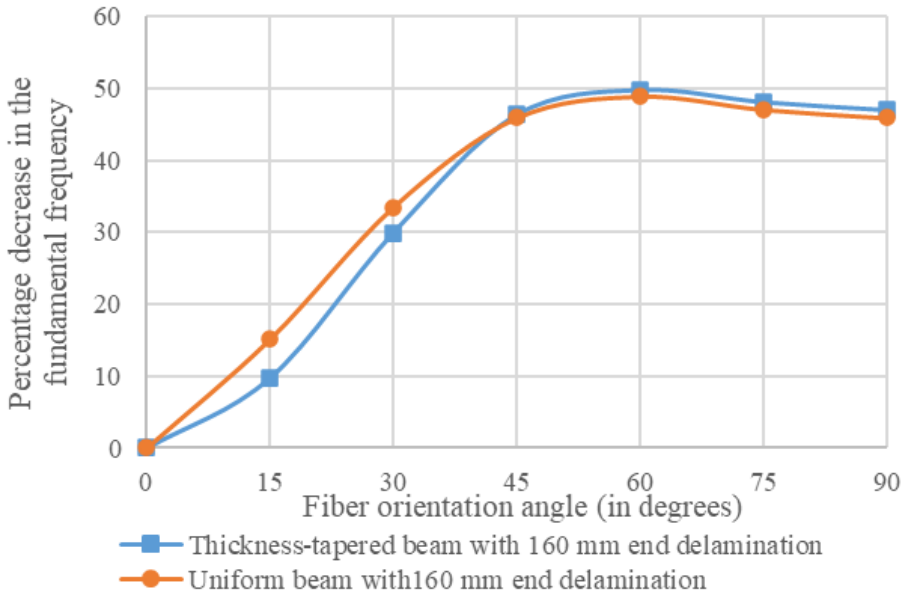

Figure 3.7 Percentage decrease in the fundamental frequencies of the end delaminated uniform and thickness-tapered composite beams due to the change in the fiber orientation angle w.r.t. that of the uniform and thickness-tapered beams with 0° fiber orientation angle for 160 mm delamination length

From Figure 3.7, a similar non-linear variation is observed in the percentage decrease of the fundamental frequencies of end delaminated uniform and thickness-tapered composite beams due to the change in the fiber orientation angle. From 0° to 45° fiber orientation angle, the percentage decrease in the fundamental frequency of the end delaminated thickness-tapered composite beam is lower than that of the uniform composite beam. From 45° to 60° fiber orientation angle, the percentage decrease in the fundamental frequency of the end delaminated uniform composite beam is slightly lower than that of the thickness-tapered composite beam.

The fundamental frequencies of the end delaminated uniform and thickness-tapered composite beams decrease by 33.5% and 29.9%, respectively from 0° to 30° fiber orientation angle and decrease by 48.9% and 49.8%, respectively from 0° to 60° fiber orientation angle. With further increase in the fiber orientation angle the percentage decrease in the fundamental frequencies of both the considered beams decreases slightly.

The pictorial illustration of the percentage decrease in the fundamental frequencies of the end delaminated uniform and thickness-tapered composite beams with 6 plies dropped-off due to the change in the delamination length for 0° fiber orientation angle is shown in Figure 3.8. The percentage decrease in the fundamental frequencies is calculated w.r.t. that of the fundamental frequencies of the intact uniform and thickness-tapered composite beams with 0° fiber orientation angle.

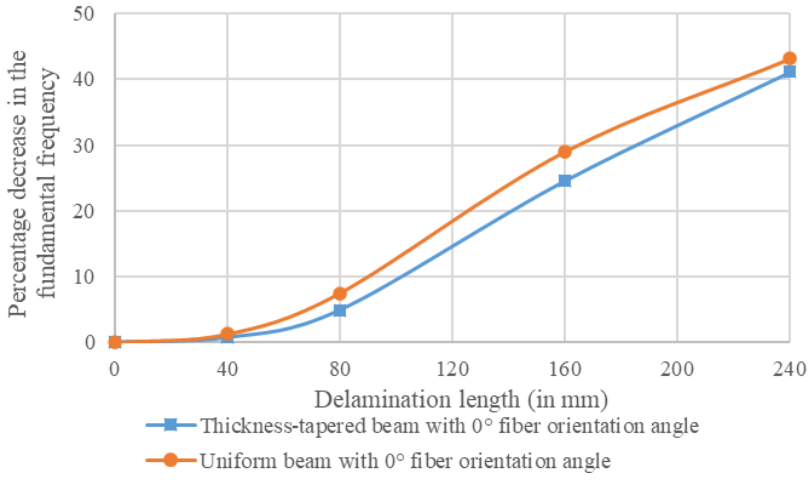

Figure 3.8 Percentage decrease in the fundamental frequencies of the end delaminated uniform and thickness-tapered composite beams due to the change in the delamination length w.r.t. that of the end delaminated intact uniform and thickness-tapered composite beams for 0° fiber orientation angle

From Figure 3.8, a similar variation is observed in the percentage decrease of the fundamental frequencies of the end delaminated uniform and thickness-tapered composite beams due to the change in the delamination length. Up to 40 mm delamination length there is minimal increase in the percentage decrease in the fundamental frequencies of the end delaminated uniform and thickness-tapered composite beams, but with further increase in the delamination length a significant increase is seen in the percentage decrease of the fundamental frequencies of both the considered beams. The percentage decrease in the fundamental frequency of the uniform beam is higher than that of the thickness-tapered beams.

In Figure 3.8 the fundamental frequencies of the end delaminated uniform and thickness-tapered composite beams decreases by 1.2% and 0.7%, respectively up to 40 mm delamination length, and decrease by 7.4% and 4.8%, respectively up to 80 mm delamination length. With further increase in the delamination length the percentage decrease in fundamental frequencies of the end delaminated uniform and thickness-tapered composite beams decreases by 29.0% and 24.5%, respectively up to 160 mm delamination length, and decrease by 43.1% and 41.0%, respectively up to 240 mm delamination length. The maximum difference between the percentage decreases in the fundamental frequencies of both the considered beams is observed for the 160 mm delamination length.

Figure 3.9 illustrates first three mode shapes of the intact thickness-tapered composite beam with $[0]_{8s}$ stacking sequence, whereas Figure 3.10 illustrates the first three mode shapes of the thickness-tapered composite beam with 80 mm end delamination and $[0]_{8s}$ stacking sequence. The points of inflection of both the beams are compared in Table 3.7.

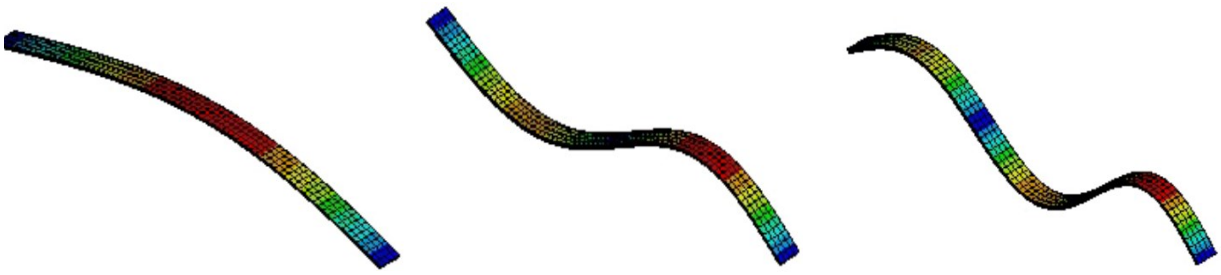

1st Mode (at 34.25 Hz) 2nd Mode (at 137.89 Hz) 3rd Mode (at 309.25 Hz)

Figure 3.9 First three mode shapes of the 400-mm-long intact thickness-tapered simply supported composite beam with $[0]_{8s}$ stacking sequence

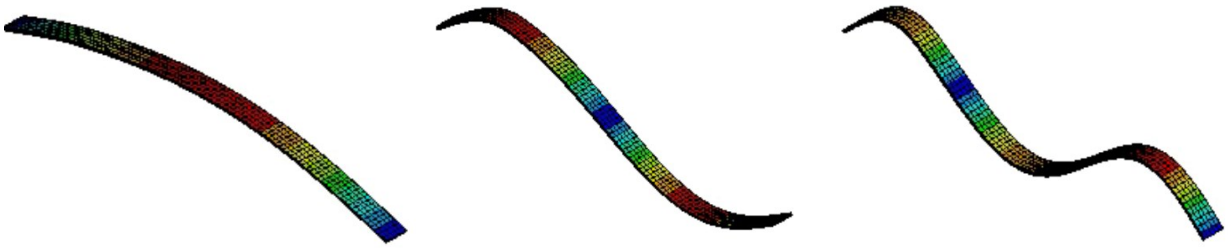

1st Mode (at 32.58 Hz) 2nd Mode (at 116.67 Hz) 3rd Mode (at 256.26 Hz)

Figure 3.10 First three mode shapes of the 400-mm-long thickness-tapered simply supported composite beam with 80 mm end delamination and $[0]_{8s}$ stacking sequence

Mode	Points of inflection of the mode shapes shown in Figure 3.9	Points of inflection of the mode shapes shown in Figure 3.10
1st Mode	205 mm	205 mm
2nd Mode	105 mm, 310 mm	75 mm, 300 mm
3rd Mode	75 mm, 205 mm, 340 mm	60 mm, 190 mm, 340 mm

Table 3.7 Points of inflection of the mode shapes shown in Figures 3.9 and 3.10

Table 3.7 illustrates the points of inflection of the mode shapes shown in Figures 3.9 and 3.10 measured from the left end of the beams. The point of inflection of 1st mode is the same for both the beams but for the higher modes the points of inflection of the delaminated beam are closer to the left end of the beam as compared to that of the non-delaminated beam.

3.4 Influences of the delamination length and fiber orientation angle on the natural frequencies of uniform composite beam with mid-span mid-plane delamination

In this section, the influences of delamination length and fiber orientation angle on the first three out-of-plane bending natural frequencies of 400-mm-long uniform simply supported composite beam with mid-span mid-plane delamination are investigated. The mechanical properties of the composite material are given in Table 3.1, whereas the interface parameters are given in Table 3.2. The geometric properties of the beam are given in Table 3.3.

The finite element model of the delaminated beam is developed using FEA tool ANSYS®. The mesh of element size 4 mm is used to perform the analysis. The natural frequencies of uniform simply supported composite beam with mid-span delamination determined from the modal analysis for different delamination lengths and fiber orientation angles are illustrated in Table 3.8.

0 mm mid-span delamination							
Mode number	**Stacking sequence**						
	$[0]_{8s}$	$[15]_{8s}$	$[30]_{8s}$	$[45]_{8s}$	$[60]_{8s}$	$[75]_{8s}$	$[90]_{8s}$
1	43.63	39.15	30.21	23.67	21.76	22.55	23.04
2	174.31	140.40	105.63	90.99	87.01	89.78	92.10
3	391.29	320.49	242.54	206.01	195.76	201.92	207.01
80 mm mid-span delamination							
Mode number	**Stacking sequence**						
	$[0]_{8s}$	$[15]_{8s}$	$[30]_{8s}$	$[45]_{8s}$	$[60]_{8s}$	$[75]_{8s}$	$[90]_{8s}$
1	43.61	38.09	29.04	23.07	21.75	22.51	23.03
2	160.64	130.63	98.73	84.36	81.01	83.37	85.45
3	385.26	313.85	237.78	201.78	193.64	199.62	204.65
160 mm mid-span delamination							
Mode number	**Stacking sequence**						
	$[0]_{8s}$	$[15]_{8s}$	$[30]_{8s}$	$[45]_{8s}$	$[60]_{8s}$	$[75]_{8s}$	$[90]_{8s}$
1	43.43	37.21	28.31	22.86	21.67	22.41	22.94
2	122.72	100.45	76.11	64.89	62.12	63.80	65.35
3	318.97	261.95	199.68	169.60	162.02	166.34	170.35
240 mm mid-span delamination							
Mode number	**Stacking sequence**						
	$[0]_{8s}$	$[15]_{8s}$	$[30]_{8s}$	$[45]_{8s}$	$[60]_{8s}$	$[75]_{8s}$	$[90]_{8s}$
1	42.34	35.87	27.24	22.25	21.16	21.86	22.39
2	98.17	79.95	60.40	51.52	49.40	50.82	52.08
3	242.24	198.92	151.25	128.13	122.35	125.71	128.77
320 mm mid-span delamination							
Mode number	**Stacking sequence**						
	$[0]_{8s}$	$[15]_{8s}$	$[30]_{8s}$	$[45]_{8s}$	$[60]_{8s}$	$[75]_{8s}$	$[90]_{8s}$
1	39.35	33.03	25.05	20.68	19.72	20.35	20.84
2	88.66	71.72	54.03	46.14	44.35	45.71	46.87
3	218.67	178.70	135.30	114.32	109.43	112.75	115.59

Table 3.8 First three natural frequencies (in Hz) of the 400-mm-long uniform simply supported composite beam with mid-span mid-plane delamination

From Table 3.8, it is observed that the first three natural frequencies of uniform simply supported composite beam decrease with increase in mid-span delamination length and that the decrease in 2nd and 3rd natural frequencies is more significant as compared to the decrease in the 1st natural frequency. For instance, the percentage decreases in the natural frequencies of the delaminated beam with 320 mm mid-span delamination and $[0]_{8s}$ stacking sequence w.r.t. that of the intact beam with the same stacking sequence are 9.8 %, 49.13 % and 44.11 % for 1st, 2nd and 3rd natural frequencies, respectively.

In the case of mid-span delaminated beams, the upper and lower parts of the beam are bonded together at the interface plane at left and right sides of the delamination. These bonded sides of the mid-span delaminated beam restrict the slipping of upper and lower parts over the interface plane and this provides additional stiffness while vibrating at 1st natural frequency as compared to the case of the end delaminated beam for the same delamination length.

In case of end delaminated beams, the upper and lower parts of the beam are bonded together at the interface plane at the right end of the beam, whereas delamination is at the left end of the beam. The delaminated end of the beam allows the upper and lower parts of the beam to slip over the interface while vibrating at 1st natural frequency. This results in a lower 1st natural frequency than that of the mid-span delaminated beam for the same delamination length.

Figure 3.11 illustrates the pictorial representation of the plies slipping over the interface of mid-span and end delaminated simply supported composite beams while vibrating at 2nd natural frequency.

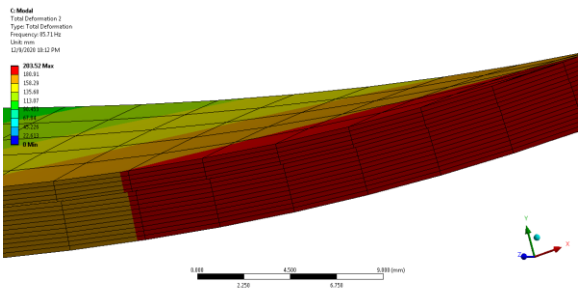

Figure 3.11 (a) Visual of the plies slipping over the interface at the mid-span of the composite beam with 160 mm mid-span delamination at the interface between 11th and 12th plies and with $[30]_{8s}$ stacking sequence while vibrating at 2nd natural frequency of 84.5 Hz

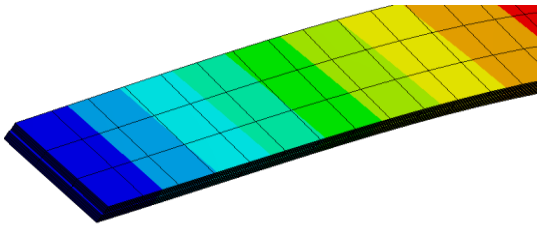

Figure 3.11 (b) Visual of the plies slipping over the interface at the left end of the composite beam with 160 mm end delamination at the interface between 8th and 9th plies and with $[30]_{8s}$ stacking sequence while vibrating at the 2nd natural frequency of 78.85 Hz

Figure 3.11 Visuals of the plies slipping over the interface of mid-span and end delaminated simply supported uniform composite beams

The beams shown in Figures 3.11 (a) and (b) have the same thickness and the same number of plies as that given in the Table 3.3. The snapshots of the visuals of both the beams are taken at different angles, due to which the thicknesses of both the beams may appear to be different. Figure 3.11 (a) illustrates a small cross-section of the mid-span of the mid-span delaminated beam while

vibrating at the 2nd natural frequency, whereas Figure 3.11 (b) illustrates the left end side (with delamination) of the end delaminated beam while vibrating at the 2nd natural frequency.

Figure 3.12 illustrates the first three natural frequencies of the uniform simply supported composite beam with mid-span mid-plane delamination.

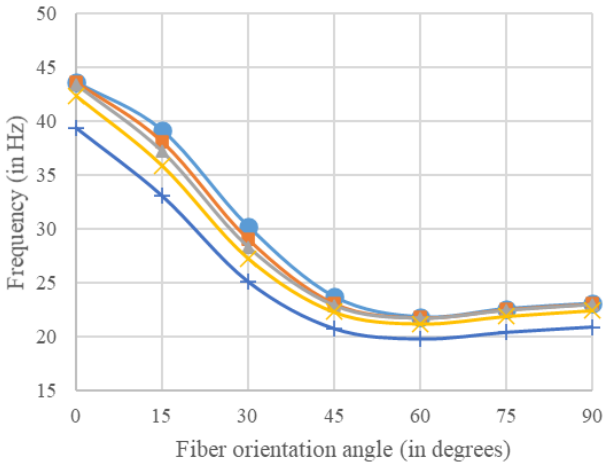

Figure 3.12 (a) Graphical illustration of 1st natural frequencies of uniform simply supported composite beams with mid-span delamination

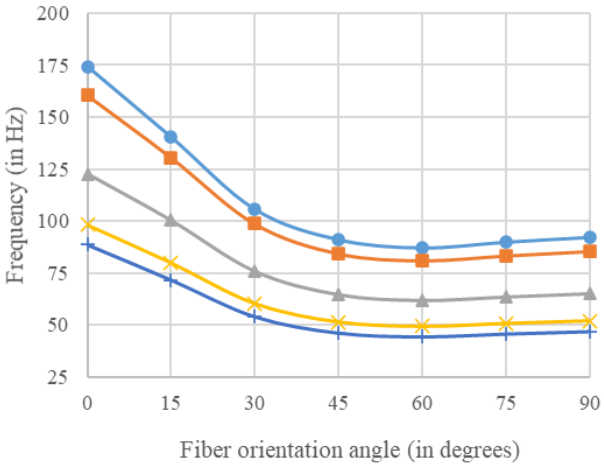

Figure 3.12 (b) Graphical illustration of 2nd natural frequencies of uniform simply supported composite beams with mid-span delamination

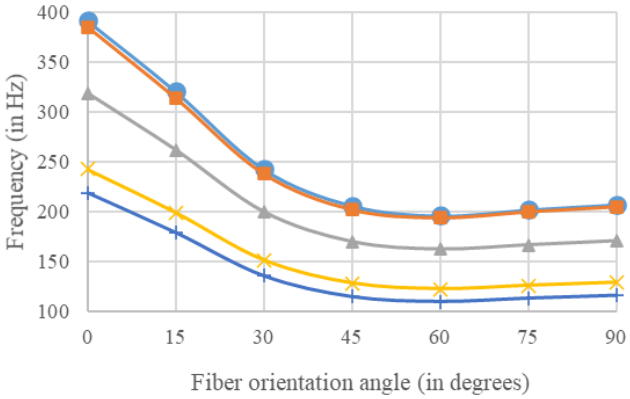

Figure 3.12 (c) Graphical illustration of 3rd natural frequencies of uniform simply supported composite beams with mid-span delamination

Figure 3.12 Graphical illustration of the natural frequencies of the 400-mm-long uniform simply supported composite beams with mid-span mid-plane delamination

From Figure 3.12 (a), it is observed that mid-span delamination length mildly affects the 1st natural frequency of the beam. For instance, at 0° fiber orientation angle there is negligible

difference between the 1st natural frequencies of the composite beams with 80 mm mid-span delamination and that of the intact beam. With the increase in fiber orientation angle from 0° to 30°, a percentage difference of 3.8 % is observed between the 1st natural frequencies of the composite beams with 80 mm mid-span delamination and that of the intact beam. The 1st natural frequencies of the composite beams with 0 mm, 80 mm, and 160 mm mid-span delamination are close enough to coincide from 45° to 90° fiber orientation angle.

In Figure 3.12 (b) the percentage differences between the 2nd natural frequencies of the uniform beams with mid-span delaminations of lengths 80 mm, 160 mm, 240 mm and 320 mm w.r.t. that of the intact uniform beam for 0° fiber orientation angle are 7.8%, 29.6%, 43.8%, and 49.2%, respectively.

In Figure 3.12 (c), the 3rd natural frequencies of the 400-mm-long intact uniform composite beam and that of the 400-mm-long uniform composite beam with 80 mm mid-span delamination almost coincide. Therefore, up to 80 mm mid-span delamination length, there is a negligible effect on the 1st and 3rd natural frequencies of the mid-span delaminated uniform composite beam. Similar observations are noted for the 1st and 3rd natural frequencies of the 500-mm-long uniform simply supported composite beam with 100 mm mid-span delamination, when compared to that of the 500-mm-long intact uniform simply supported composite beam. For instance, the percentage differences between the 1st, 2nd, and 3rd natural frequencies of 500-mm-long intact uniform composite beam and 500-mm-long uniform composite beam with 100 mm mid-span delamination are 0.94%, 9.20% and 1.63%, respectively for 0° fiber orientation angle.

All the frequency curves shown in Figure 3.12 have similar variation due to the change in the fiber orientation angle. The minimum values of the natural frequencies are observed at 60° fiber orientation angle for any considered delamination length.

3.5 Influences of the delamination length and fiber orientation angle on the natural frequencies of thickness-tapered composite beam with mid-span mid-plane delamination

In this section, the influences of delamination length and fiber orientation angle on the first three out-of-plane bending natural frequencies of thickness-tapered simply supported composite beam with mid-span mid-plane delamination are investigated. The mechanical

properties of the composite material are given in Table 3.1, whereas the interface parameters are given in Table 3.2. The geometric properties of the beam are given in Table 3.3. The number of plies and the thickness of the beam mentioned in Table 3.3 refer to the number of plies and the thickness at the left side (thick side) of the thickness-tapered beam.

The thickness-tapered composite beams have $[\theta]_{8s}$ stacking sequence (where θ is fiber orientation angle) on the thick side, whereas on the thin side the stacking sequences could be $[\theta]_{7s}$, $[\theta]_{6s}$, $[\theta]_{5s}$and $[\theta]_{4s}$ with 2, 4, 6, and 8 plies dropped-off, respectively.

The finite element model of the delaminated beam is developed using FEA tool ANSYS®. The mesh of element size of 4 mm is used to perform the analysis. The natural frequencies of thickness-tapered simply supported composite beam with mid-span delamination for different delamination lengths and fiber orientation angles are illustrated in Tables 3.9 - 3.12. The graphical illustration of natural frequencies of thickness-tapered simply supported composite beam with mid-span delamination and 8 plies dropped-off is shown in Figure 3.13.

Number of plies		**Mode number**	**Stacking sequence on the thick side (at the left end)**						
At the left end	**At the right end**		**$[0]_{8s}$**	**$[15]_{8s}$**	**$[30]_{8s}$**	**$[45]_{8s}$**	**$[60]_{8s}$**	**$[75]_{8s}$**	**$[90]_{8s}$**
16	14	1	40.20	35.14	26.80	21.27	20.05	20.75	21.23
		2	148.26	120.55	91.10	77.83	74.73	76.91	78.82
		3	355.34	289.48	219.30	186.04	178.51	184.01	188.65
16	12	1	37.30	32.63	24.90	19.75	18.60	19.26	19.70
		2	138.13	112.30	84.86	72.49	69.60	71.66	73.41
		3	329.47	268.54	203.48	172.53	165.49	170.59	174.86
16	10	1	34.80	30.46	23.26	18.43	17.35	17.96	18.38
		2	130.10	105.78	79.93	68.24	65.51	67.42	69.10
		3	306.33	250.05	189.57	160.58	153.93	158.60	162.57
16	8	1	30.36	26.60	20.32	16.08	15.14	15.67	16.03
		2	114.80	93.31	70.50	60.15	57.74	59.43	60.91
		3	266.80	218.02	165.36	139.91	134.01	138.03	141.47

Table 3.9 First three natural frequencies (in Hz) of the 400-mm-long thickness-tapered simply supported composite beams with 80 mm mid-span mid-plane delamination

Number of plies		Mode number	Stacking sequence on the thick side (at the left end)						
At the left end	At the right end		$[0]_{8s}$	$[15]_{8s}$	$[30]_{8s}$	$[45]_{8s}$	$[60]_{8s}$	$[75]_{8s}$	$[90]_{8s}$
16	14	1	40.02	34.31	26.11	21.07	19.97	20.65	21.14
		2	113.30	92.74	70.27	59.89	57.33	58.88	60.31
		3	294.38	241.72	184.24	156.45	149.43	153.41	157.11
16	12	1	37.13	31.85	24.24	19.55	18.52	19.15	19.61
		2	105.76	86.56	65.59	55.89	53.49	54.94	56.27
		3	273.62	224.62	171.19	145.33	138.79	142.49	145.93
16	10	1	34.60	30.82	22.63	18.23	17.26	17.85	18.28
		2	100.10	112.52	62.07	52.89	50.62	51.98	53.25
		3	255.77	254.60	159.95	135.72	129.61	133.09	136.30
16	8	1	30.15	25.93	19.76	15.90	15.04	15.56	15.93
		2	88.94	72.77	55.13	46.97	44.94	46.15	47.28
		3	224.00	183.74	140.01	118.72	113.36	116.41	119.23

Table 3.10 First three natural frequencies (in Hz) of the 400-mm-long thickness-tapered simply supported composite beams with 160 mm mid-span mid-plane delamination

Number of plies	Number of plies	Mode number	Stacking sequence on the thick side (at the left end)						
At the left end	At the right end		$[0]_{8s}$	$[15]_{8s}$	$[30]_{8s}$	$[45]_{8s}$	$[60]_{8s}$	$[75]_{8s}$	$[90]_{8s}$
16	14	1	39.02	33.07	25.12	20.51	19.50	20.15	20.63
		2	90.60	73.79	55.75	47.54	45.58	46.89	48.05
		3	223.53	183.55	139.57	118.22	112.87	115.95	118.78
16	12	1	36.20	30.69	23.32	19.03	18.09	18.69	19.14
		2	84.49	68.82	52.00	44.34	42.51	43.72	44.80
		3	208.08	170.86	129.93	110.04	105.04	107.90	110.53
16	10	1	33.74	28.63	21.76	17.74	16.86	17.41	17.83
		2	79.84	65.05	49.16	41.91	40.17	41.30	42.33
		3	195.54	160.57	122.11	103.40	98.69	101.35	103.84
16	8	1	29.40	24.98	18.99	15.46	14.69	15.18	15.54
		2	70.83	57.73	43.64	37.19	35.63	36.64	37.55
		3	172.39	141.57	107.68	91.14	86.97	89.33	91.51

Table 3.11 First three natural frequencies (in Hz) of the 400-mm-long thickness-tapered simply supported composite beams with 240 mm mid-span mid-plane delamination

Number of plies	Number of plies	Mode number	Stacking sequence on the thick side (at the left end)						
At the left end	At the right end		$[0]_{8s}$	$[15]_{8s}$	$[30]_{8s}$	$[45]_{8s}$	$[60]_{8s}$	$[75]_{8s}$	$[90]_{8s}$
16	14	1	36.27	30.46	23.10	19.06	18.17	17.41	19.21
		2	81.76	66.15	49.84	42.56	40.90	39.22	43.22
		3	201.65	164.80	124.79	105.43	100.91	96.65	106.58
16	12	1	33.68	28.29	21.45	17.70	16.87	17.41	17.83
		2	76.09	61.58	46.41	39.61	37.83	39.22	40.22
		3	187.48	153.23	116.05	98.03	38.07	96.65	99.07
16	10	1	31.47	26.44	20.05	16.54	15.76	16.26	16.66
		2	71.52	57.96	43.68	37.26	35.79	36.87	37.81
		3	175.72	143.76	108.82	91.91	87.94	90.59	92.86
16	8	1	27.51	23.12	17.54	14.46	13.77	14.21	14.56
		2	63.09	51.16	38.59	32.89	31.57	32.53	33.35
		3	154.44	126.30	95.70	80.81	77.29	79.61	81.59

Table 3.12 First three natural frequencies (in Hz) of the 400-mm-long thickness-tapered simply supported composite beams with 320 mm mid-span mid-plane delamination

From Tables 3.9 - 3.12, it is observed that the natural frequencies decrease with increase in mid-span delamination length. The drop in 2nd and 3rd natural frequencies is more significant as compared to the drop in the 1st natural frequency. For instance, at 0° fiber orientation angle reductions of 9.38%, 45.04% and 42.11% are observed in the 1st, 2nd and 3rd natural frequencies, respectively, of thickness-tapered composite beam with 320 mm mid-span delamination, when compared to that of the natural frequencies of thickness-tapered composite beam with 80 mm mid-span delamination.

The bonded sides of the mid-span delaminated beam restrict the slipping of the upper and lower parts over the interface plane and this provides additional stiffness while vibrating at the 1st natural frequency as compared to the case of the end delaminated beam for the same delamination length. For instance, in Tables 3.11 and 3.22, the 1st natural frequencies of 400-mm-long thickness-tapered composite beams with 6 plies dropped-off and with 240 mm mid-span and end delaminations are 33.74 Hz and 20.09 Hz, respectively for 0° fiber orientation angle.

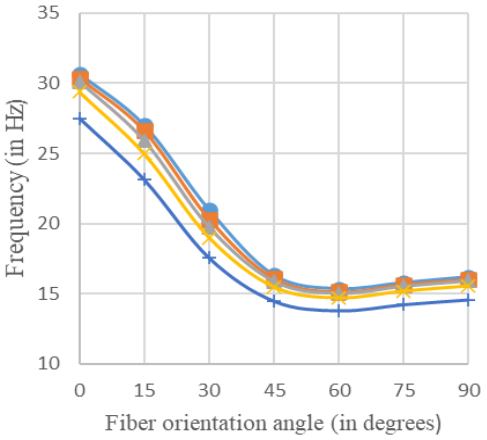

Figure 3.13 (a) Graphical illustration of 1st natural frequency of thickness-tapered simply supported composite beams with mid-span delamination

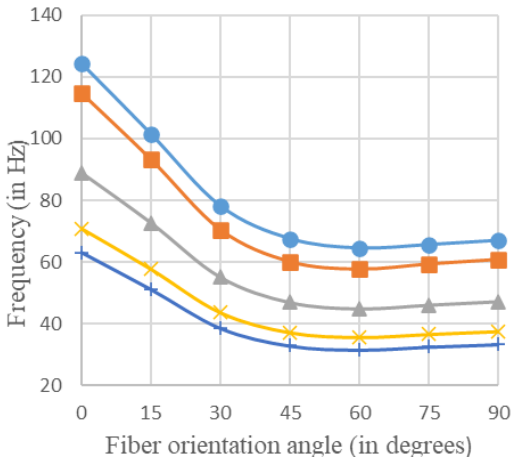

Figure 3.13 (b) Graphical illustration of 2nd natural frequency of thickness-tapered simply supported composite beams with mid-span delamination

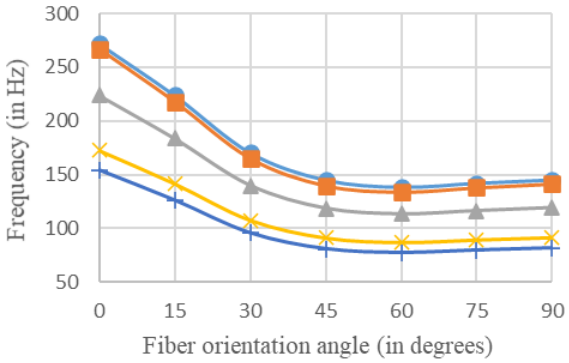

Figure 3.13 (c) Graphical illustration of 3rd natural frequency of thickness-tapered simply supported composite beams with mid-span delaminations

Mid-span delamination length — 0 mm — 80 mm — 160 mm — 240 mm — 320 mm

Figure 3.13 Graphical illustration of the first three natural frequencies of the 400-mm-long thickness-tapered simply supported composite beams with mid-span delamination and 8 dropped-off plies

Figure 3.13 shows the graphical illustration of the natural frequencies of 400-mm-long thickness-tapered simply supported composite beam with mid-span delamination and 8 dropped-off plies. From Figure 3.13 (a) it is observed that the mid-span delamination length mildly affects the 1st natural frequency of the thickness-tapered composite beam as was observed in the case of uniform composite beam. For instance, at 0° fiber orientation angle there is negligible difference between the 1st natural frequency of the thickness-tapered beam with 80 mm mid-span delamination and that of the 1st natural frequency of the intact thickness-tapered beam. With increase in fiber orientation angle from 0° to 30°, a percentage difference of 2.75% is observed between the 1st natural frequency of the thickness-tapered beam with 80 mm mid-span delamination, and the 1st natural frequency of the intact thickness-tapered beam. The 1st natural

frequencies of the composite beams with 0 mm, 80 mm and 160 mm mid-span delamination are close enough to coincide from 45° to 90° fiber orientation angles.

In Figure 3.13 (b) the percentage differences between the 2nd natural frequencies of the 400-mm-long thickness-tapered composite beams with mid-span delaminations of lengths 80 mm, 160 mm, 240 mm and 320 mm w.r.t. that of the 400-mm-long intact thickness-tapered beam for 0° fiber orientation angle are 6.6%, 27.6%, 42.4%, and 48.7%, respectively.

In Figure 3.13 (c), the 3rd natural frequencies of the 400-mm-long intact thickness-tapered composite beam and that of the 400-mm-long thickness-tapered composite beam with 80 mm mid-span delamination almost coincide. Therefore, up to 80 mm mid-span delamination length, there is a negligible effect on the 1st and 3rd natural frequencies of the mid-span delaminated thickness-tapered composite beam. Similar observations are noted for the 1st and 3rd natural frequencies of the 500-mm-long thickness-tapered simply supported composite beam with 100 mm mid-span delamination, when compared to that of the 500-mm-long intact thickness-tapered simply supported composite beam. For instance, the percentage differences between the 1st, 2nd, and 3rd natural frequencies of 500-mm-long intact thickness-tapered composite beam and 500-mm-long thickness-tapered composite beam with 100 mm mid-span delamination are 1.15%, 10.21% and 1.78%, respectively for 0° fiber orientation angle.

In Figure 3.13, all the frequency curves show similar variation due to the change in the fiber orientation angle. The minimum values of the natural frequencies are observed at 60° fiber orientation angle for any considered delamination length.

3.6 Influences of the delamination location on the natural frequencies of thickness-tapered composite beam

In this section, the natural frequencies of thickness-tapered simply supported composite beams with end and mid-span delaminations are shown in Figures 3.14 (a), (b) and (c) for 0° fiber orientation angle. The data representation for the plots presented in Figures 3.14 (a), (b) and (c) is done in Tables 3.19 - 3.22 for the thickness-tapered beams with end delamination and in Tables 3.9 - 3.12 for the thickness-tapered beam with mid-span mid-plane delamination. The finite element models of the delaminated beams are developed using FEA tool ANSYS®. The analysis

is conducted on six thickness-tapered composite beams with different number of plies drop-off, out of which three beams are end delaminated and the rest three are mid-span delaminated. The thickness-tapered composite beams have $[0]_{8s}$ stacking sequence on the thick end of the beam, whereas $[0]_{7s}$, $[0]_{6s}$, $[0]_{5s}$ could be the stacking sequence on the thin end of the beam depending on the number of plies dropped-off. Therefore, there are a total of 16 plies at the thick end of the beam and at the thin end the total number of plies could be 14, 12 or 10.

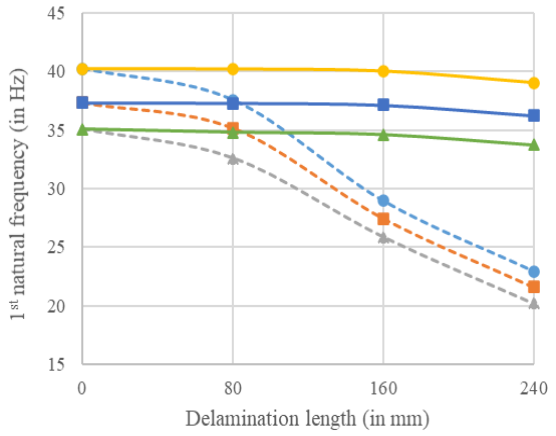

Figure 3.14 (a) Graphical illustration of the 1st natural frequencies of thickness-tapered simply supported composite beams with end and mid-span delaminations for $[0]_{8s}$ stacking sequence

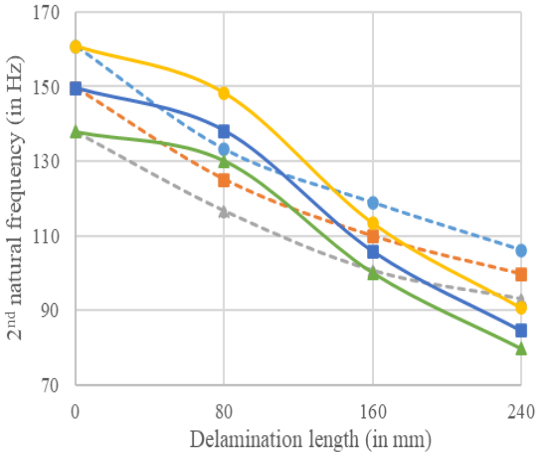

Figure 3.14 (b) Graphical illustration of the 2nd natural frequencies of thickness-tapered simply supported composite beams with end and mid-span delaminations for $[0]_{8s}$ stacking sequence

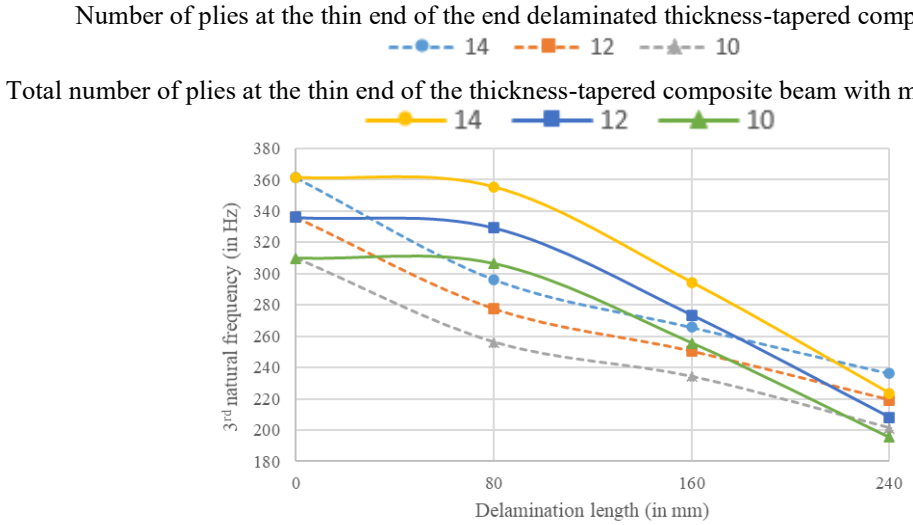

Figure 3.14 (c) Graphical illustration of the 3rd natural frequencies of thickness-tapered simply supported composite beams with end and mid-span delaminations for $[0]_{8s}$ stacking sequence

Figure 3.14 Graphical illustration of the first three natural frequencies of the thickness-tapered simply supported composite beams with end and mid-span delaminations for $[0]_{8s}$ stacking sequence

From Figure 3.14 (a), (b) and (c), it is observed that with the increase in delamination length, the natural frequencies of the thickness-tapered composite beams with end and mid-span delamination are decreasing in different trends.

In Figure 3.14 (a), a significant decrease is observed in the 1st natural frequency of the end delaminated thickness-tapered composite beam as compared to that of the mid-span delaminated thickness-tapered composite beam. A sharp decline is seen in the 1st natural frequency of the end delaminated beam from 80 mm to 240 mm delamination length. There is negligible change in the 1st natural frequency of the mid-spam delaminated beam up to 160 mm delamination length.

In Figures 3.14 (b) and 3.14 (c), the 2nd and 3rd natural frequencies of the mid-span delaminated beams decrease slightly up to 80 mm delamination length, but a sharp decrease is seen in both the natural frequencies with the further increase in mid-span delamination length.

A significant decrease is observed in the 2nd and 3rd natural frequencies of the end delaminated composite beam up to 80 mm delamination length, but with further increase in end delamination length, a slight decrease is observed in the 2nd and 3rd natural frequencies of the composite beam.

Table 3.13 illustrates the equations for the first three natural frequencies of the thickness-tapered delaminated beams characterizing the influence of delamination length and delamination location. Composite beams with $[0]_{8s}$ stacking sequence are considered for this study. The relation between the delamination length and the natural frequencies of the thickness-tapered composite beams with mid-span and end delaminations is represented by equations given in Table 3.13. The 'y' in the equations represents the natural frequency, whereas 'x' in the equations represents the delamination length.

The equations presented in Table 3.13 are formulated from the graphs illustrated in Figure 3.14 (a), (b) and (c) using curve fitting technique. The data representation for this analysis is done in Tables 3.19 - 3.22 for the end delaminated beams and in Tables 3.9 - 3.12 for the mid-span delaminated beams.

Equations for the 1st natural frequency		
End delamination		
Total number of plies		**Equation**
At the left end	**At the right end**	
16	14	$y = 3E\text{-}06x^3 - 0.0011x^2 + 0.0393x + 40.222$
16	12	$y = 2E\text{-}06x^3 - 0.001x^2 + 0.0388x + 37.327$
16	10	$y = 2E\text{-}06x^3 - 0.0009x^2 + 0.0362x + 34.26$
Mid-span delamination		
Total number of plies		**Equation**
At the left end	**At the right end**	
16	14	$y = -4E\text{-}05x^2 + 0.0044x + 40.188$
16	12	$y = -4E\text{-}05x^2 + 0.004x + 37.297$
16	10	$y = -2E\text{-}05x^2 + 0.0004x + 35.02$
Equations for the 2nd natural frequency		
End delamination		
Total number of plies		**Equation**
At the left end	**At the right end**	
16	14	$y = 0.0006x^2 - 0.3627x + 160.23$
16	12	$y = 0.0006x^2 - 0.34x + 149.34$
16	10	$y = 0.0005x^2 - 0.3156x + 138.05$
Mid-span delamination		
Total number of plies		**Equation**
At the left end	**At the right end**	
16	14	$y = 1E\text{-}05x^3 - 0.0045x^2 + 0.1274x + 160.82$
16	12	$y = -0.0004x^2 - 0.1922x + 151.16$
16	10	$y = -0.0005x^2 - 0.1383x + 139.49$
Equations for the 3rd natural frequency		
End delamination		
Total number of plies		**Equation**
At the left end	**At the right end**	
16	14	$y = 0.0006x^2 - 0.3627x + 160.23$
16	12	$y = 0.0011x^2 - 0.7273x + 334.29$
16	10	$y = 0.0008x^2 - 0.6272x + 307.61$
Mid-span delamination		
Total number of plies		**Equation**
At the left end	**At the right end**	
16	14	$y = 1E\text{-}05x^3 - 0.0078x^2 + 0.4563x + 361.34$
16	12	$y = 1E\text{-}05x^3 - 0.0069x^2 + 0.3906x + 336.05$
16	10	$y = 1E\text{-}05x^3 - 0.0066x^2 + 0.4087x + 309.72$

Table 3.13 Equations for the natural frequencies of the thickness-tapered simply supported composite beams with end and mid-span delaminations

3.7 The free vibration response of uniform composite beams with mid-span delamination between different plies

In this section, uniform simply supported composite beams with mid-span delamination between different plies are considered for the free vibration analysis. The mechanical properties of the composite material are given in Table 3.1, whereas the interface parameters are given in Table 3.2. The geometric properties of the beam are given in Table 3.3. The natural frequencies of the uniform simply supported beams are determined from the modal analysis and are presented in

Tables 3.14 - 3.17 for various fiber orientation angles considering mid-span delamination of four different lengths at the interfaces between different plies on the top-half of the beam. The mesh of element size 4 mm is used to perform this analysis. The influence of mid-span delamination location between different plies on the 1st natural frequency is illustrated in Figure 3.15.

Mid-span delamination at the interface between 9th and 10th plies							
Mode number	**Stacking sequence**						
	$[0]_{8s}$	**$[15]_{8s}$**	**$[30]_{8s}$**	**$[45]_{8s}$**	**$[60]_{8s}$**	**$[75]_{8s}$**	**$[90]_{8s}$**
1	43.61	38.13	29.09	23.08	21.75	22.51	23.03
2	161.35	131.13	99.08	84.67	81.33	83.71	85.80
3	385.56	314.15	237.98	201.90	193.76	199.74	204.78
Mid-span delamination at the interface between 10th and 11th plies							
Mode number	**Stacking sequence**						
	$[0]_{8s}$	**$[15]_{8s}$**	**$[30]_{8s}$**	**$[45]_{8s}$**	**$[60]_{8s}$**	**$[75]_{8s}$**	**$[90]_{8s}$**
1	43.62	38.24	29.20	23.11	21.75	22.52	23.03
2	163.17	132.42	99.99	85.48	82.15	84.60	86.72
3	386.35	314.95	238.54	202.23	194.05	200.07	205.11
Mid-span delamination at the interface between 11th and 12th plies							
Mode number	**Stacking sequence**						
	$[0]_{8s}$	**$[15]_{8s}$**	**$[30]_{8s}$**	**$[45]_{8s}$**	**$[60]_{8s}$**	**$[75]_{8s}$**	**$[90]_{8s}$**
1	43.62	38.39	29.36	23.14	21.76	22.52	23.04
2	165.54	134.10	101.17	86.52	83.20	85.73	87.89
3	387.33	316.04	239.29	202.67	194.43	200.48	205.53
Mid-span delamination at the interface between 12th and 13th plies							
Mode number	**Stacking sequence**						
	$[0]_{8s}$	**$[15]_{8s}$**	**$[30]_{8s}$**	**$[45]_{8s}$**	**$[60]_{8s}$**	**$[75]_{8s}$**	**$[90]_{8s}$**
1	43.63	38.57	29.55	23.18	21.76	22.53	23.04
2	167.95	135.80	102.37	87.56	84.26	86.85	89.06
3	388.40	317.20	240.11	203.12	194.81	200.89	205.88
Mid-span delamination at the interface between 13th and 14th plies							
Mode number	**Stacking sequence**						
	$[0]_{8s}$	**$[15]_{8s}$**	**$[30]_{8s}$**	**$[45]_{8s}$**	**$[60]_{8s}$**	**$[75]_{8s}$**	**$[90]_{8s}$**
1	43.63	38.75	29.75	23.23	21.76	22.53	23.04
2	170.10	137.33	103.44	88.49	85.22	87.84	90.09
3	389.35	318.32	240.90	203.53	195.27	201.26	206.20
Mid-span delamination at the interface between 14th and 15th plies							
Mode number	**Stacking sequence**						
	$[0]_{8s}$	**$[15]_{8s}$**	**$[30]_{8s}$**	**$[45]_{8s}$**	**$[60]_{8s}$**	**$[75]_{8s}$**	**$[90]_{8s}$**
1	43.64	38.92	29.94	23.27	21.76	22.54	23.04
2	171.89	138.61	104.35	89.26	85.95	88.66	90.94
3	390.29	319.30	241.62	203.90	195.43	201.56	206.48
Mid-span delamination at the interface between 15th and 16th plies							
Mode number	**Stacking sequence**						
	$[0]_{8s}$	**$[15]_{8s}$**	**$[30]_{8s}$**	**$[45]_{8s}$**	**$[60]_{8s}$**	**$[75]_{8s}$**	**$[90]_{8s}$**
1	43.64	39.08	30.11	23.31	21.76	22.54	23.04
2	173.31	139.65	105.08	89.89	86.56	89.30	91.60
3	390.97	320.11	242.22	204.20	195.65	201.79	206.87

Table 3.14 First three natural frequencies (in Hz) of the 400-mm-long uniform simply supported composite beams with 80 mm mid-span delamination between different plies

Mid-span delamination at the interface between 9th and 10th plies							
Mode number	Stacking sequence						
	$[0]_{8s}$	$[15]_{8s}$	$[30]_{8s}$	$[45]_{8s}$	$[60]_{8s}$	$[75]_{8s}$	$[90]_{8s}$
1	43.44	37.27	28.36	22.87	21.67	22.41	22.95
2	124.60	101.93	77.21	65.84	63.05	64.77	66.35
3	322.31	264.57	201.59	171.24	163.63	168.05	172.11
Mid-span delamination at the interface between 10th and 11th plies							
Mode number	Stacking sequence						
	$[0]_{8s}$	$[15]_{8s}$	$[30]_{8s}$	$[45]_{8s}$	$[60]_{8s}$	$[75]_{8s}$	$[90]_{8s}$
1	43.47	37.44	28.53	22.92	21.69	22.431	22.96
2	129.78	105.98	80.22	68.45	65.60	67.437	69.09
3	331.23	271.58	206.77	175.59	167.93	172.57	176.77
Mid-span delamination at the interface between 11th and 12th plies							
Mode number	Stacking sequence						
	$[0]_{8s}$	$[15]_{8s}$	$[30]_{8s}$	$[45]_{8s}$	$[60]_{8s}$	$[75]_{8s}$	$[90]_{8s}$
1	43.51	37.69	28.77	22.98	21.70	22.45	22.98
2	137.16	111.73	84.48	72.14	69.22	71.21	72.96
3	343.21	280.96	213.72	181.39	173.62	178.58	182.94
Mid-span delamination at the interface between 12th and 13th plies							
Mode number	Stacking sequence						
	$[0]_{8s}$	$[15]_{8s}$	$[30]_{8s}$	$[45]_{8s}$	$[60]_{8s}$	$[75]_{8s}$	$[90]_{8s}$
1	43.54	37.98	29.05	23.05	21.72	22.48	23.00
2	145.44	118.21	89.30	76.28	73.28	75.44	77.32
3	354.92	291.09	221.23	187.40	179.51	184.79	189.33
Mid-span delamination at the interface between 13th and 14th plies							
Mode number	Stacking sequence						
	$[0]_{8s}$	$[15]_{8s}$	$[30]_{8s}$	$[45]_{8s}$	$[60]_{8s}$	$[75]_{8s}$	$[90]_{8s}$
1	43.57	38.30	29.37	23.13	22.77	22.50	23.00
2	153.77	124.67	94.03	80.39	80.60	79.65	81.53
3	364.58	300.44	227.85	192.90	192.30	190.43	174.14
Mid-span delamination at the interface between 14th and 15th plies							
Mode number	Stacking sequence						
	$[0]_{8s}$	$[15]_{8s}$	$[30]_{8s}$	$[45]_{8s}$	$[60]_{8s}$	$[75]_{8s}$	$[90]_{8s}$
1	43.60	38.63	29.68	23.20	21.74	22.52	23.02
2	161.54	130.67	98.45	84.19	80.98	83.53	85.54
3	373.28	308.61	233.79	197.59	188.39	195.17	189.45
Mid-span delamination at the interface between 15th and 16th plies							
Mode number	Stacking sequence						
	$[0]_{8s}$						
1	43.62						
2	168.41						
3	314.62						

Table 3.15 First three natural frequencies (in Hz) of the 400-mm-long uniform simply supported composite beams with 160 mm mid-span delamination between different plies

Mid-span delamination at the interface between 9th and 10th plies							
Mode number	Stacking sequence						
	$[0]_{8s}$	$[15]_{8s}$	$[30]_{8s}$	$[45]_{8s}$	$[60]_{8s}$	$[75]_{8s}$	$[90]_{8s}$
1	42.41	35.98	27.33	22.29	21.19	21.90	22.43
2	100.22	81.59	61.64	52.58	50.43	51.88	53.16
3	246.56	202.45	153.91	130.39	124.53	127.97	131.08
Mid-span delamination at the interface between 10th and 11th plies							
Mode number	Stacking sequence						
	$[0]_{8s}$	$[15]_{8s}$	$[30]_{8s}$	$[45]_{8s}$	$[60]_{8s}$	$[75]_{8s}$	$[90]_{8s}$
1	42.60	36.27	27.59	22.41	21.28	22.00	22.52
2	105.99	86.25	65.13	55.58	53.34	54.89	56.24
3	258.72	212.43	161.45	136.77	130.70	134.34	137.58
Mid-span delamination at the interface between 11th and 12th plies							
Mode number	Stacking sequence						
	$[0]_{8s}$	$[15]_{8s}$	$[30]_{8s}$	$[45]_{8s}$	$[60]_{8s}$	$[75]_{8s}$	$[90]_{8s}$
1	42.829	36.694	27.956	22.569	21.389	22.115	22.636
2	114.68	93.27	70.398	60.102	57.715	59.42	60.824
3	276.91	227.19	172.69	146.27	139.86	143.84	147.25
Mid-span delamination at the interface between 12th and 13th plies							
Mode number	Stacking sequence						
	$[0]_{8s}$	$[15]_{8s}$	$[30]_{8s}$	$[45]_{8s}$	$[60]_{8s}$	$[75]_{8s}$	$[90]_{8s}$
1	43.045	37.184	28.392	22.74	21.494	22.232	22.752
2	125.15	101.88	76.845	65.642	63.081	64.976	66.553
3	298.89	245.37	186.23	157.68	150.88	155.26	158.93
Mid-span delamination at the interface between 13th and 14th plies							
Mode number	Stacking sequence						
	$[0]_{8s}$	$[15]_{8s}$	$[30]_{8s}$				
1	43.214	37.701	28.33				
2	135.82	111.38	82.731				
3	321.79	264.82	197.84				
Mid-span delamination at the interface between 14th and 15th plies							
Mode number	Stacking sequence						
	$[0]_{8s}$	$[15]_{8s}$					
1	43.412	38.221					
2	149.46	121.25					
3	349.71	284.53					

Table 3.16 First three natural frequencies (in Hz) of the 400-mm-long uniform simply supported composite beams with 240 mm mid-span delamination between different plies

Mid-span delamination at the interface between 9th and 10th plies							
Mode number	Stacking sequence						
	$[0]_{8s}$	$[15]_{8s}$	$[30]_{8s}$	$[45]_{8s}$	$[60]_{8s}$	$[75]_{8s}$	$[90]_{8s}$
1	39.57	33.26	25.22	20.80	19.82	20.46	20.95
2	90.68	73.35	55.26	47.19	45.36	46.75	47.94
3	222.62	181.95	137.76	116.39	111.42	114.80	117.69
Mid-span delamination at the interface between 10th and 11th plies							
Mode number	Stacking sequence						
	$[0]_{8s}$	$[15]_{8s}$	$[30]_{8s}$	$[45]_{8s}$	$[60]_{8s}$	$[75]_{8s}$	$[90]_{8s}$
1	40.14	33.86	25.70	21.11	20.10	20.75	21.25
2	96.48	78.02	58.77	50.19	48.26	49.74	51.01
3	234.03	191.34	144.88	122.38	117.15	120.72	123.75
Mid-span delamination at the interface between 11th and 12th plies							
Mode number	Stacking sequence						
	$[0]_{8s}$	$[15]_{8s}$	$[30]_{8s}$	$[45]_{8s}$	$[60]_{8s}$	$[75]_{8s}$	$[90]_{8s}$
1	40.881	34.682	26.371	21.52	20.454	21.128	21.633
2	105.41	85.201	64.162	54.815	52.72	54.349	55.689
3	251.75	205.92	155.92	131.67	126.05	129.89	132.61

Table 3.17 First three natural frequencies (in Hz) of the 400-mm-long uniform simply supported composite beams with 320 mm mid-span delamination between different plies

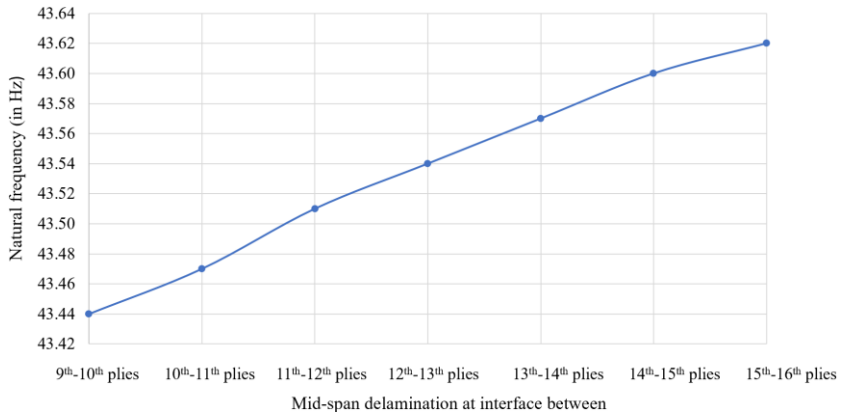

Figure 3.15 The influence of mid-span delamination location between different plies on the fundamental frequency of the 400-mm-long uniform composite beam with 160 mm mid-span delamination

From Figure 3.15 it is observed that the 1st natural frequency of the uniform simply supported composite beam with 160 mm mid-span delamination is higher when the delamination is away from the mid-plane. From Table 3.15 similar variations are observed in the 2nd and 3rd natural frequencies of the beam as that seen in the 1st natural frequency upon moving mid-span delamination away from the mid-plane in Figure 3.15, but the increases in the 2nd and 3rd natural frequencies are higher as compared to that of the increase in the 1st natural frequency. For instance, in Table 3.15 the percentage increases in the 1st, 2nd and 3rd natural frequencies of the uniform

beam with 160 mm mid-span delamination due to the change in mid-span delamination location from the interface between 9th and 10th plies to the interface between 14th and 15th plies are 2.6%, 28.6% and 15.8%, respectively for 0° fiber orientation angle and 2.8%, 24.23% and 14.78 %, respectively for 45° fiber orientation angle.

The large mid-span delamination located away from mid-plane leads to local buckling of the beam and convergence difficulties in the modal analysis. The mid-span delamination of 240 mm at the at the interface of 13th and 14th ply or above, or the mid-span delamination of 320 mm at the at the interface of 12th and 13th ply or above leads to the local buckling of the beam and convergence difficulties in the modal analysis. The converged results for the natural frequencies obtained from modal analysis are presented in Tables 3.14 - 3.17.

Figure 3.16 illustrates the graphical representation of the natural frequencies of uniform simply supported composite beams with mid-span delamination between different plies for $[0]_{8s}$ stacking sequence. In this analysis, the influence of delamination location on the natural frequencies of the composite beam is investigated by modeling mid-span delamination at the interface between different plies of the beam.

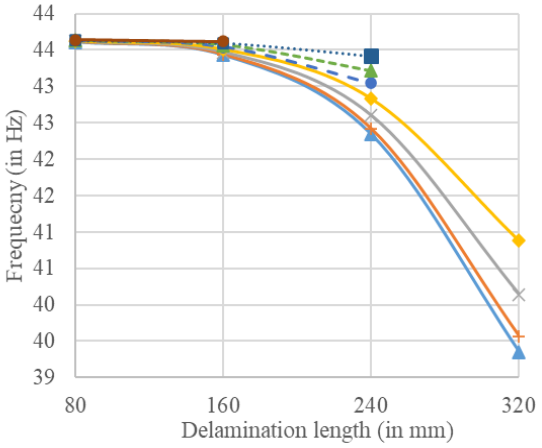

Figure 3.16 (a) Graphical illustration of the 1st natural frequencies of the uniform simply supported composite beams with mid-span delamination between different plies for $[0]_{8s}$ stacking sequence

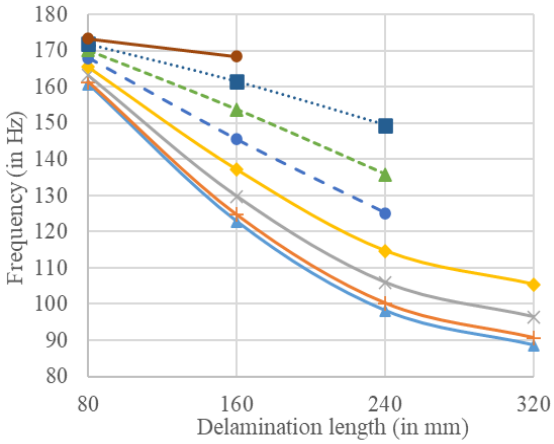

Figure 3.16 (b) Graphical illustration of the 2nd natural frequencies of the uniform simply supported composite beams with mid-span delamination between different plies for $[0]_{8s}$ stacking sequence

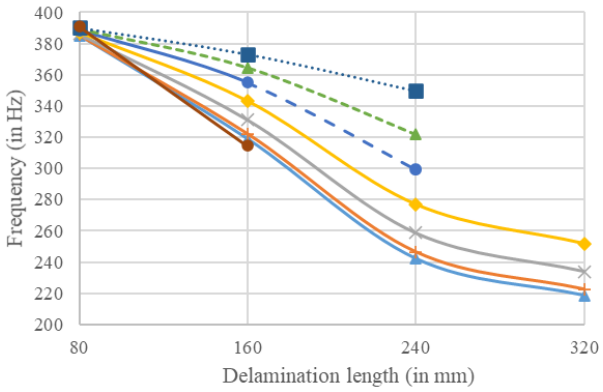

Figure 3.16 (c) Graphical illustration of the 3rd natural frequencies of the uniform simply supported composite beams with mid-span delamination between different plies for $[0]_{8s}$ stacking sequence

Figure 3.16 Graphical illustration of the first three natural frequencies of the 400-mm-long uniform simply supported composite beams with mid-span delamination between different plies for $[0]_{8s}$ stacking sequence

From Figure 3.16, it is observed that the natural frequencies are higher when the delamination is away from the mid-plane and with the increase in delamination length the natural frequencies decrease. The natural frequencies of the beam with delamination at the mid-plane or at the interface between 8th and 9th plies are the lowest, whereas the natural frequencies of the beam with delamination at the interface between 15th and 16th plies are the highest.

From Figures 3.16 (a), (b), and (c), it is observed that the natural frequency curves of the beams with mid-span delamination at the interface between 12th and 13th plies, 13th and 14th plies and 14th and 15th plies get terminated at 240 mm delamination length due to local buckling and convergence difficulties in the modal analysis. In Figure 3.16 (c), there is a sudden drop in the 3rd natural frequency of the beam with mid-span delamination at the interface between 15th and 16th plies due to the local buckling. From Figure 3.16 (a) it is observed, that up to 160 mm delamination, there is minimal effect of delamination length on the 1st natural frequency of the 400-mm-long beam.

Figures 3.17 and 3.18 illustrate the first three mode shapes of the uniform simply supported composite beam with 80 mm and 240 mm mid-span delamination at the interface between 14th and 15th plies for $[0]_{8s}$ stacking sequence.

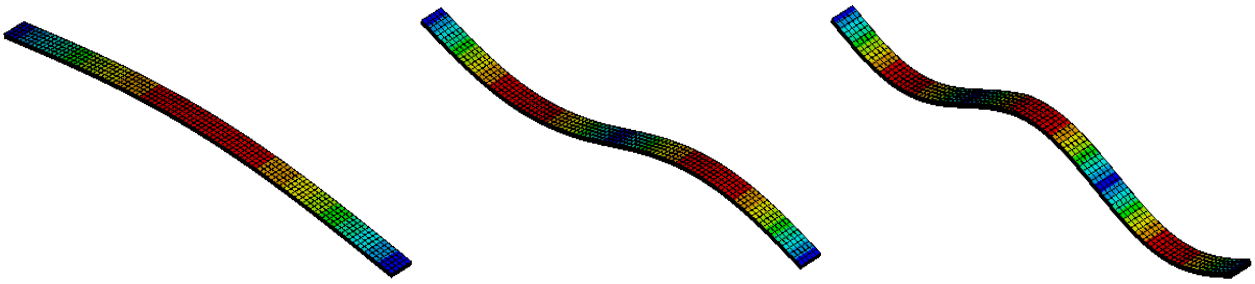

1st Mode 43.63 Hz 2nd Mode 171.89 Hz 3rd Mode 390.29Hz

Figure 3.17 First three mode shapes of the uniform simply supported composite beam with 80 mm mid-span delamination at the interface between 14th and 15th plies for $[0]_{8s}$ stacking sequence

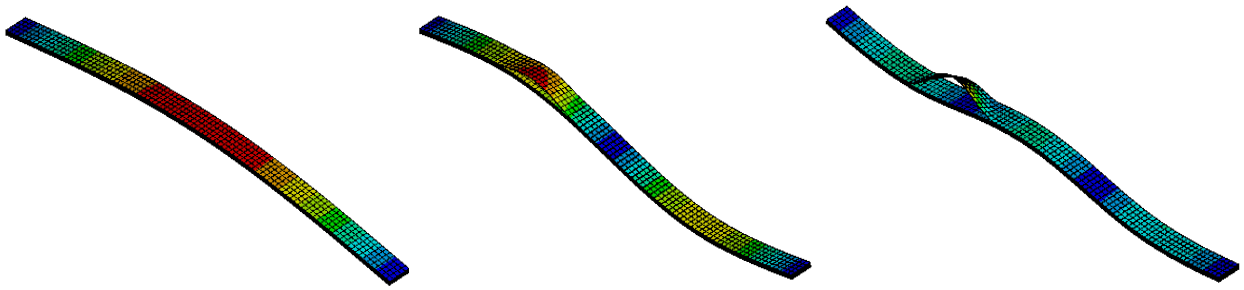

1st Mode 43.41 Hz 2nd Mode 149.46 Hz 3rd Mode 349.71 Hz

Figure 3.18 First three mode shapes of the uniform simply supported composite beam with 240 mm mid-span delamination at the interface between 14th and 15th plies for $[0]_{8s}$ stacking sequence

The points of inflection of the mode shapes shown in Figures 3.17 and 3.18 are measured from left end of the beams and are presented in Table 3.18. In Figure 3.18, the local buckling of the composite beam can be observed while vibrating at 2nd and 3rd natural frequencies. From Table 3.18 it is observed that the mid-span delaminated beams of different delamination lengths but with the same mid-span delamination location and stacking sequence have similar points of inflection of their mode shapes.

Mode	Points of inflection of the mode shapes presented in Figure 3.17	Points of inflection of the mode shapes presented in Figure 3.18
1st Mode	200 mm	200 mm
2nd Mode	110 mm, 290 mm	110 mm, 290 mm
3rd Mode	70 mm, 200 mm, 330 mm	70 mm, 200 mm, 330 mm

Table 3.18 Points of inflection of the mode shapes shown in Figures 3.17 and 3.18

3.8 Layer reduction effect

In Chapter 2, layer reduction test was conducted to compare the first three natural frequencies of uniform and thickness-tapered simply supported composite beams. In this section, the effect of layer reduction on the natural frequencies of the end delaminated simply supported composite beams is analyzed. A 3-stepped layer reduction is implemented on the 400-mm-long composite beams with end delamination for four different delamination lengths. The terms "thick beam", "thin beam" and "tapered beam" used in this section are as defined in the previous chapter in section 2.5.

The mechanical properties of the composite material are given in Table 3.1, whereas the interface parameters are given in Table 3.2. The geometric properties of the beam are given in Table 3.3. Tables 3.19 - 3.22 illustrate the first three natural frequencies of end delaminated thick, thin and thickness-tapered simply supported composite beams for different delamination lengths and fiber orientation angles obtained using FEA tool ANSYS®. The mesh of element size 4 mm is used to perform the analysis.

Beam type	Number of plies		Mode number	Stacking sequence on the thick side (at the left end)						
	At the left end	At the right end		$[0]_{8s}$	$[15]_{8s}$	$[30]_{8s}$	$[45]_{8s}$	$[60]_{8s}$	$[75]_{8s}$	$[90]_{8s}$
Thick	16	16	1	42.52	36.08	27.45	22.70	21.59	22.21	22.88
			2	158.31	130.64	100.44	86.76	83.97	84.21	89.20
			3	325.49	276.37	217.15	188.04	182.28	184.93	194.23
Tapered	16	14	1	39.81	35.23	26.98	21.24	19.88	20.58	21.04
			2	154.43	124.77	94.14	80.59	77.51	79.87	81.89
			3	323.63	275.88	210.18	176.60	168.46	173.36	177.57
Thin	14	14	1	37.35	31.85	24.24	19.92	18.91	19.59	20.03
			2	140.43	115.36	88.32	76.13	73.59	76.07	78.09
			3	291.91	246.32	192.11	165.51	159.99	165.70	170.11
Tapered	16	12	1	37.00	32.83	25.13	19.75	18.47	19.13	19.55
			2	144.26	116.47	87.80	75.21	72.36	74.57	76.47
			3	312.30	258.11	196.53	165.14	157.58	162.18	166.13
Thin	12	12	1	32.13	27.56	21.00	17.13	16.22	16.80	17.17
			2	121.87	99.70	76.04	65.43	63.18	65.26	66.97
			3	256.08	214.80	166.42	142.66	137.53	142.23	145.94
Tapered	16	10	1	34.02	30.23	23.17	18.16	16.98	17.58	17.97
			2	133.60	107.85	81.25	69.60	66.97	69.03	70.78
			3	289.86	239.42	182.20	153.11	146.14	150.43	154.10
Thin	10	10	1	26.86	23.21	17.71	14.33	13.53	14.01	14.32
			2	102.69	83.70	63.62	54.66	52.73	54.43	55.84
			3	217.88	181.86	140.10	119.53	114.92	118.69	121.72

Table 3.19 First three natural frequencies (in Hz) of thick, thin and thickness-tapered simply supported 400-mm-long composite beams with 40 mm end delamination

Beam type	Number of plies		Mode number	Stacking sequence on the thick side (at the left end)						
	At the left end	At the right end		$[0]_{8s}$	$[15]_{8s}$	$[30]_{8s}$	$[45]_{8s}$	$[60]_{8s}$	$[75]_{8s}$	$[90]_{8s}$
Thick	16	16	1	39.84	34.13	26.05	21.44	20.36	21.09	21.56
			2	137.69	113.52	86.99	74.93	72.46	74.88	76.87
			3	298.03	250.29	194.24	167.37	162.18	168.08	172.58
Tapered	16	14	1	37.55	33.45	25.76	20.15	18.81	19.45	19.88
			2	133.17	108.17	81.87	69.82	67.00	68.95	70.67
			3	296.40	245.46	186.33	156.58	149.66	154.24	158.08
Thin	14	14	1	35.02	30.14	23.01	18.83	17.83	18.46	18.88
			2	121.81	100.11	76.48	65.77	63.50	65.57	67.29
			3	266.05	222.19	171.45	147.12	142.19	147.18	151.06
Tapered	16	12	1	35.17	31.36	24.16	18.87	17.61	18.22	18.61
			2	125.07	101.48	76.76	65.55	62.92	64.76	66.37
			3	277.63	228.60	173.60	145.77	139.27	143.51	147.08
Thin	12	12	1	30.15	26.09	19.96	16.20	15.30	15.84	16.19
			2	105.47	86.40	65.88	56.54	54.51	56.25	57.71
			3	232.21	192.98	148.22	126.66	122.09	126.24	129.52
Tapered	16	10	1	32.59	29.07	22.40	17.47	16.30	16.87	17.24
			2	116.67	94.57	71.50	61.11	58.69	60.40	61.91
			3	256.26	211.22	160.48	134.64	128.58	132.48	135.75
Thin	10	10	1	25.22	21.96	16.83	13.56	12.76	13.21	13.50
			2	88.70	72.37	55.16	47.25	45.50	46.92	48.12
			3	196.63	162.52	124.52	105.96	101.92	105.27	107.96

Table 3.20 First three natural frequencies (in Hz) of thick, thin and thickness-tapered simply supported 400-mm-long composite beams with 80 mm end delamination

Beam type	Number of plies		Mode number	Stacking sequence on the thick side (at the left end)						
	At the left end	At the right end		$[0]_{8s}$	$[15]_{8s}$	$[30]_{8s}$	$[45]_{8s}$	$[60]_{8s}$	$[75]_{8s}$	$[90]_{8s}$
Thick	16	16	1	30.57	25.94	20.33	16.53	15.61	16.17	16.53
			2	125.47	101.72	77.76	66.87	64.63	66.81	68.57
			3	267.77	215.14	174.05	149.53	144.57	149.59	153.54
Tapered	16	14	1	28.94	26.11	20.26	15.65	14.53	15.02	15.34
			2	118.90	95.84	72.12	61.64	59.36	61.24	62.82
			3	265.83	208.56	166.89	140.19	133.91	137.78	141.13
Thin	14	14	1	26.85	23.42	17.74	14.52	13.68	14.16	14.47
			2	110.66	89.93	72.48	58.59	56.59	58.47	60.01
			3	238.32	198.88	157.58	131.41	126.78	131.02	134.43
Tapered	16	12	1	27.46	24.79	19.24	14.85	13.78	14.25	14.55
			2	109.94	88.57	66.65	56.99	54.88	56.62	58.08
			3	250.46	206.86	157.19	132.02	126.11	129.77	132.93
Thin	12	12	1	23.10	20.29	15.59	12.49	11.73	12.15	12.41
			2	95.52	77.52	58.64	50.30	48.54	50.13	51.44
			3	207.47	172.95	132.71	113.13	108.90	112.40	115.30
Tapered	16	10	1	25.86	23.33	18.11	13.87	12.98	13.42	13.70
			2	100.68	81.11	61.03	53.37	50.26	51.85	53.18
			3	234.24	193.42	146.92	125.80	117.87	121.31	124.27
Thin	10	10	1	19.32	17.08	13.16	10.45	9.79	10.13	10.35
			2	80.09	64.86	48.98	41.96	40.48	41.79	42.87
			3	175.31	145.71	111.47	94.64	90.94	93.79	96.14

Table 3.21 First three natural frequencies (in Hz) of thick, thin and thickness-tapered simply supported 400-mm-long composite beams with 160 mm end delamination

Beam type	Number of plies		Mode number	Stacking sequence on the thick side (at the left end)						
	At the left end	At the right end		$[0]_{8s}$	$[15]_{8s}$	$[30]_{8s}$	$[45]_{8s}$	$[60]_{8s}$	$[75]_{8s}$	$[90]_{8s}$
Thick	16	16	1	24.49	21.36	16.33	13.16	12.39	12.84	13.12
			2	111.27	91.31	69.50	59.68	57.60	59.49	61.05
			3	243.32	201.84	154.94	133.04	128.53	132.99	136.46
Tapered	16	14	1	22.94	20.79	16.14	12.38	11.48	11.88	12.14
			2	106.17	86.24	65.10	55.49	53.28	54.88	56.25
			3	236.33	193.18	146.26	123.40	118.22	121.89	124.96
Thin	14	14	1	21.48	18.84	14.44	11.55	10.85	11.24	11.49
			2	98.10	80.32	61.03	52.33	50.46	52.09	53.44
			3	215.87	178.36	136.45	116.76	112.66	116.46	119.48
Tapered	16	12	1	21.60	19.59	15.23	11.67	10.82	11.19	11.43
			2	99.79	80.94	61.07	52.11	50.06	51.56	52.86
			3	219.30	179.39	135.80	114.51	109.66	113.07	115.92
Thin	12	12	1	18.45	15.96	12.66	9.93	9.31	9.64	9.85
			2	84.67	70.54	54.40	44.93	43.30	44.67	45.82
			3	187.33	156.88	117.75	100.38	96.72	99.90	102.47
Tapered	16	10	1	20.19	18.32	14.24	10.92	10.12	10.47	10.69
			2	93.05	75.35	56.84	48.54	46.65	48.06	49.27
			3	201.43	165.01	124.75	105.17	100.70	103.83	106.44
Thin	10	10	1	15.41	13.69	10.53	8.30	7.76	8.04	8.21
			2	71.00	57.93	43.88	37.52	36.12	37.25	38.20
			3	157.81	129.57	98.59	83.89	80.72	83.32	85.44

Table 3.22 First three natural frequencies (in Hz) of thick, thin and thickness-tapered simply supported 400-mm-long composite beams with 240 mm end delamination

From Tables 3.19 - 3.22, it is observed that the natural frequencies of thick, thin and thickness-tapered composite beams decrease with the increase in delamination length. The natural frequencies of the thick beam are the highest and that of the thin beam with 10 plies are the lowest, whereas the natural frequencies of the thickness-tapered beam fall in between the natural frequencies of thick and thin beams, as was observed in the previous chapter. For instance, in Table 3.21, the 1st natural frequency of the thick beam is 30.57 Hz, whereas the 1st natural frequency of the thickness-tapered beam with 4 plies dropped-off is 27.60 Hz, the 1st natural frequency of the thin beam with 12 plies is 23.10 Hz which is the lowest among the three. It can also be observed that the natural frequencies of the thickness-tapered and thin beams decrease with each layer reduction.

The graphical representation of the first three natural frequencies of thick, thin and thickness-tapered simply supported composite beams with end delamination is shown in Figure 3.19 for different delamination lengths and fiber orientation angles.

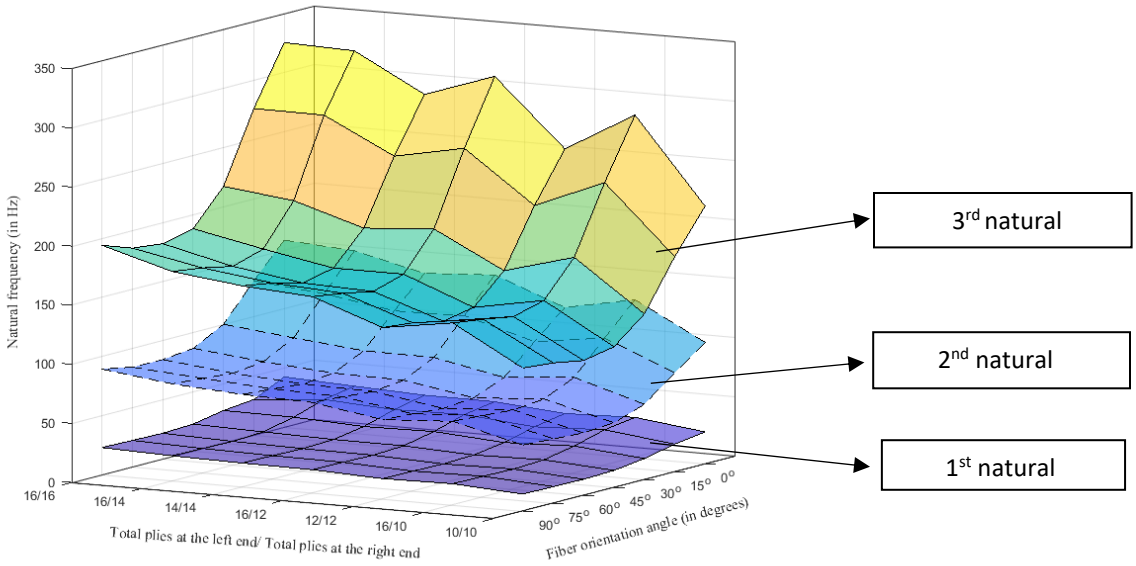

Figure 3.19 (a) Graphical representation of first three natural frequencies (in Hz) of thick, thin and thickness-tapered simply supported 400-mm-long composite beams with 40 mm end delamination

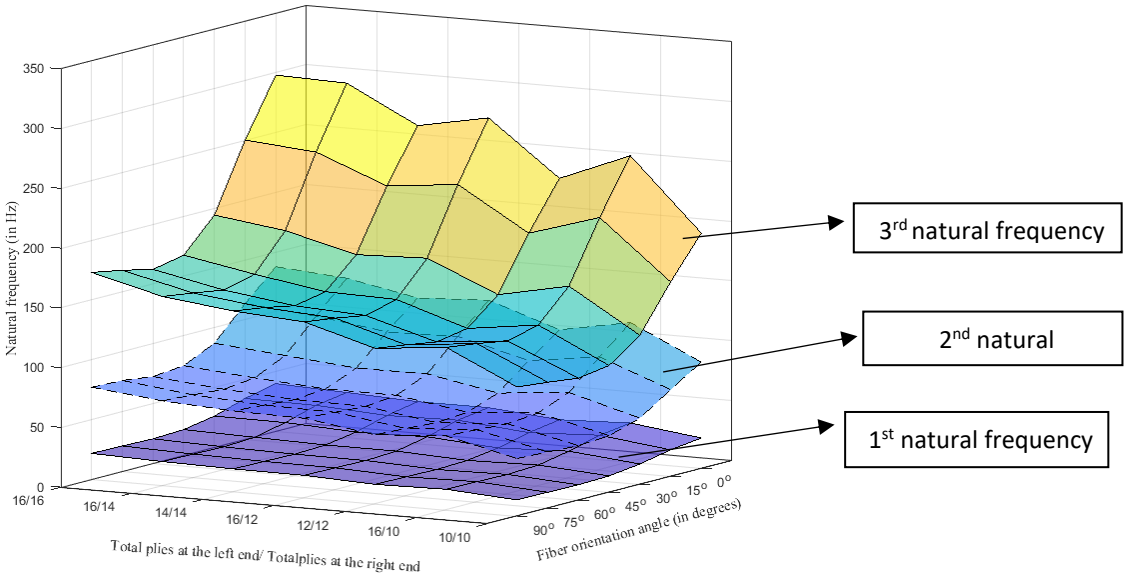

Figure 3.19 (b) Graphical representation of first three natural frequencies (in Hz) of thick, thin and thickness-tapered simply supported 400-mm-long composite beams with 80 mm end delamination

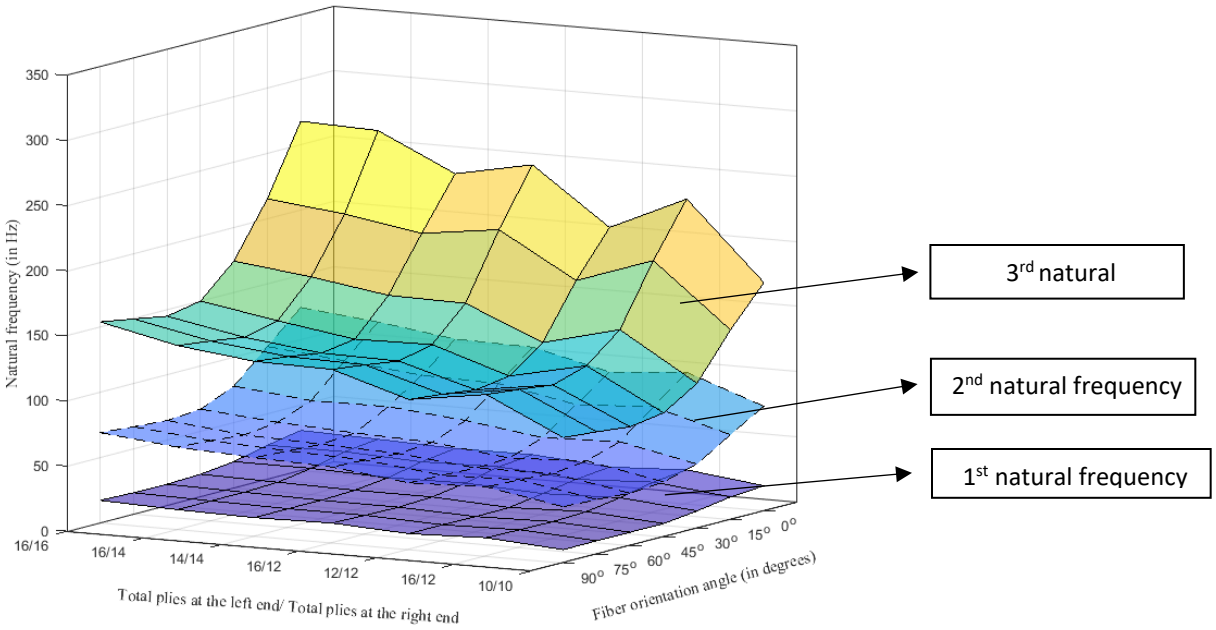

Figure 3.19 (c) Graphical representation of first three natural frequencies (in Hz) of thick, thin and thickness-tapered simply supported 400-mm-long composite beams with 160 mm end delamination

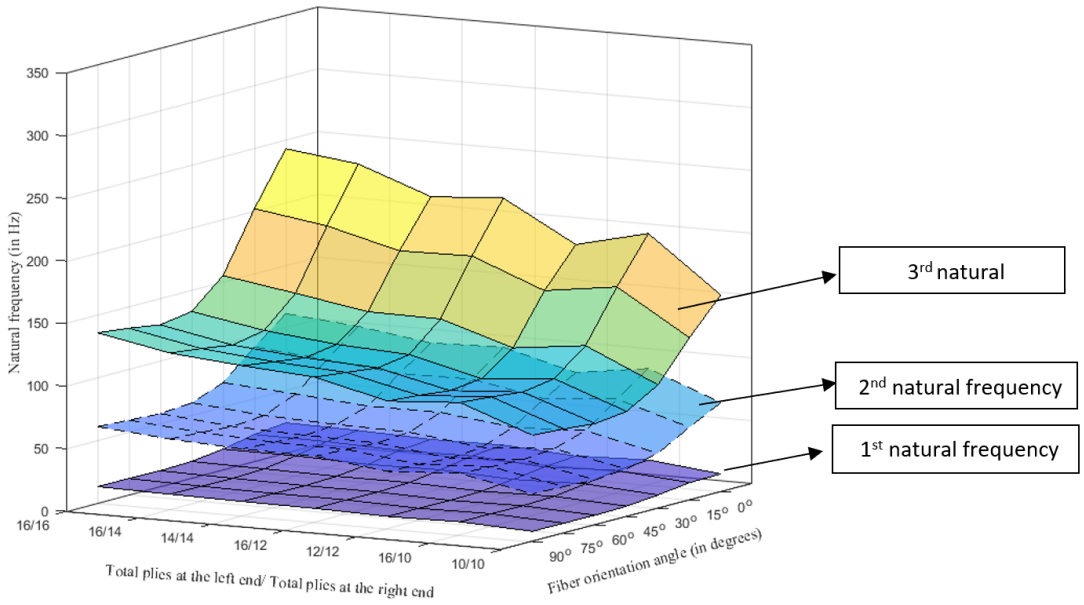

Figure 3.19 (d) Graphical representation of first three natural frequencies (in Hz) of thick, thin and thickness-tapered simply supported 400-mm-long composite beams with 240 mm end delamination

Figure 3.19 Graphical representation of first three natural frequencies (in Hz) of thick, thin and thickness-tapered simply supported 400-mm-long composite beams with end delamination

From Figure 3.19, it is observed that for any delamination length, the thick beam has the highest 3rd natural frequency, followed by the 3rd natural frequency of the tapered beam with 2 plies dropped-off and then the thin beam with 14 plies. With further layer reduction, the peaks and troughs can be observed on the 3rd natural frequency surface.

The peaks and troughs on the 3rd natural frequency surface represent the 3rd natural frequency of the tapered beams (with 4 and 6 plies dropped-off) and thin beams (with 14 and 12 plies), respectively. From this observation, it is evident that the 3rd natural frequency of thickness-tapered composite beams is higher than that of the thin beams but is lower than that of the thick beam. A similar variation is observed on the 2nd natural frequency surface as observed on the 3rd natural frequency surface. A proper scaling was not possible for the range of 1st natural frequency, due to which the 1st natural frequency surface appears to be monotonic.

3.9 Influences of the taper angle on the natural frequencies of the thickness-tapered composite beam with end delamination

In this section, the influence of taper angle (α) on the free vibration response of the thickness-tapered simply supported composite beam with end delamination is investigated for various fiber orientation angles. The length of the beam and number of plies dropped-off change the taper angle of the beam. The composite beams of four different lengths are considered for this comparative study. The ratio of delamination-length-to-beam-length is $1:4$ for all the cases discussed in this section. The thickness-tapered composite beams have $[\theta]_{8s}$ stacking sequence (where θ is the fiber orientation angle) on the thick side, whereas on the thin side the stacking sequence could be $[\theta]_{7s}$, $[\theta]_{6s}$, $[\theta]_{5s}$ $[\theta]_{4s}$ with 2, 4, 6, and 8 plies dropped-off, respectively.

The mechanical properties of the composite material are given in Table 3.1, whereas the interface parameters are given in Table 3.2. The geometric properties of the beam are given in Table 3.3. The number of plies and the thickness of the beam mentioned in Table 3.3 refer to the number of plies and the thickness on the thick side (at the left end) of the thickness-tapered beam.

The natural frequencies are determined from the modal analysis which are listed in Tables 3.23 - 3.26. The mesh of element size 4 mm is used to perform the analysis.

Number of plies		Taper angle (α)	Mode number	Stacking sequence on the thick side (at the left end)						
At the left end	At the right end			$[0]_{8s}$	$[15]_{8s}$	$[30]_{8s}$	$[45]_{8s}$	$[60]_{8s}$	$[75]_{8s}$	$[90]_{8s}$
16	14	0.0295°	1	35.60	31.86	24.61	19.17	17.86	18.46	18.86
			2	125.01	101.35	76.58	65.33	62.73	64.61	66.24
			3	297.01	243.60	184.53	155.33	148.71	153.36	157.21
16	12	0.0590°	1	33.52	30.01	23.19	18.04	16.80	17.38	17.75
			2	116.95	94.76	71.60	61.13	58.71	60.45	61.98
			3	275.63	226.20	171.39	144.16	137.97	142.29	145.86
16	10	0.0886°	1	31.23	27.97	21.60	16.80	15.65	16.18	16.54
			2	108.71	88.05	66.51	56.83	54.59	56.20	57.62
			3	253.48	208.20	157.81	132.62	126.87	130.83	134.10
16	8	0.1181°	1	28.67	25.65	19.81	15.40	14.35	14.85	15.17
			2	100.19	81.15	61.30	52.39	50.33	51.81	53.11
			3	230.35	189.43	143.66	120.59	115.30	118.88	121.85

Table 3.23 First three natural frequencies (in Hz) of the 400-mm-long thickness-tapered simply supported composite beams with 100 mm end delamination

Number of plies		Taper angle (α)	Mode number	Stacking sequence on the thick side (at the left end)						
At the left end	At the right end			$[0]_{8s}$	$[15]_{8s}$	$[30]_{8s}$	$[45]_{8s}$	$[60]_{8s}$	$[75]_{8s}$	$[90]_{8s}$
16	14	0.0393°	1	63.14	56.11	43.78	34.12	31.74	32.80	33.50
			2	221.68	178.42	136.23	116.31	111.59	114.80	117.65
			3	526.69	428.53	328.87	276.79	264.65	272.63	279.40
16	12	0.0787°	1	59.46	53.33	41.22	32.10	29.87	30.87	31.53
			2	207.38	167.91	127.32	108.82	104.44	107.41	110.09
			3	488.96	401.49	305.54	256.96	245.58	252.97	259.25
16	10	0.1181°	1	55.42	49.70	38.44	29.89	27.81	28.75	29.37
			2	192.76	156.01	118.31	101.19	97.11	99.86	102.34
			3	433.02	369.68	281.42	236.47	225.85	232.62	238.39
16	8	0.1575°	1	50.89	45.60	35.25	27.41	25.52	26.39	26.96
			2	177.63	143.78	109.02	93.30	89.53	92.05	94.33
			3	395.60	336.46	256.25	215.09	205.27	211.39	216.61

Table 3.24 First three natural frequencies (in Hz) of the 300-mm-long thickness-tapered simply supported composite beams with 75 mm end delamination

Number of plies		Taper angle (α)	Mode number	Stacking sequence on the thick side (at the left end)						
At the left end	At the right end			$[0]_{8s}$	$[15]_{8s}$	$[30]_{8s}$	$[45]_{8s}$	$[60]_{8s}$	$[75]_{8s}$	$[90]_{8s}$
16	14	0.0472°	1	90.73	81.44	63.07	49.19	45.70	47.19	48.20
			2	318.53	257.68	196.13	167.76	160.78	165.23	169.30
			3	756.51	620.70	474.27	399.59	381.47	392.53	402.19
16	12	0.0945°	1	85.46	76.75	59.44	46.28	43.01	44.43	45.37
			2	297.99	240.90	183.35	156.98	150.47	154.61	158.41
			3	702.54	576.78	440.78	371.02	354.02	364.27	373.22
16	10	0.1418°	1	79.67	71.54	55.39	43.09	40.05	41.38	42.27
			2	276.96	223.80	170.31	145.94	139.92	143.73	147.26
			3	646.52	531.32	406.12	341.47	325.63	335.02	343.24
16	8	0.1890°	1	73.17	62.94	50.80	39.51	36.74	37.98	38.80
			2	255.24	202.76	156.88	134.54	129.00	132.49	135.73
			3	480.05	387.48	369.89	310.66	296.03	304.50	311.94

Table 3.25 First three natural frequencies (in Hz) of the 250-mm-long thickness-tapered simply supported 250-mm-long composite beams with 62.5 mm end delamination

Number of plies		Taper angle (α)	Mode number	Stacking sequence on the thick side (at the left end)						
At the left end	At the right end			$[0]_{8s}$	$[15]_{8s}$	$[30]_{8s}$	$[45]_{8s}$	$[60]_{8s}$	$[75]_{8s}$	$[90]_{8s}$
16	14	0.0590°	1	141.32	127.10	98.59	76.96	71.39	73.66	75.21
			2	495.96	399.58	305.74	262.52	251.42	257.97	264.23
			3	1176.50	965.27	741.18	626.14	596.96	613.16	627.99
16	12	0.1181°	1	133.15	119.8	92.98	72.40	67.18	69.35	70.81
			2	463.99	373.50	285.41	245.53	235.32	241.39	247.23
			3	1093.30	897.36	684.74	581.32	554.17	569.15	582.83
16	10	0.1772°	1	124.16	111.72	86.56	67.40	62.57	64.61	65.98
			2	431.26	346.93	265.15	228.28	218.83	224.43	229.85
			3	1006.80	826.89	635.05	535.33	509.88	523.59	536.21
16	8	0.2363°	1	114.07	102.6	79.46	61.81	57.41	59.31	60.57
			2	397.41	319.68	244.29	210.86	201.73	206.86	211.84
			3	915.88	753.04	578.78	488.13	463.60	475.93	487.36

Table 3.26 First three natural frequencies (in Hz) of the 200-mm-long thickness-tapered simply supported composite beams with 50 mm end delamination

Tables 3.23 - 3.26 depict the influence of the beam length and taper angle (α) on the natural frequencies of end delaminated thickness-tapered simply supported composite beams with different number of plies dropped-off. The analysis is conducted on four different beam lengths for various fiber orientation angles. The taper angle of the beam increases with decrease in beam length and with increase in number of plies dropped-off.

It is observed that the natural frequencies of the beams with the same beam length decrease with the increase in number of plies dropped-off, i.e. with the corresponding increase in the taper angle value. For instance, in Table 3.26 the 1st natural frequencies of the 200-mm-long end delaminated beams with 2 and 8 plies dropped-off are 141.32 Hz and 114.07 Hz, respectively, for 0° fiber orientation angle.

Table 3.27 illustrates the natural frequencies of end delaminated thickness-tapered simply supported composite beams of different beam lengths with 8 dropped-off plies. The ratio of delamination-length-to-beam-length is 1: 4.

Number of plies at the right end	Beam length	Taper angle (α)	Mode number	Stacking sequence on the thick side (at the left end)						
				$[0]_{8s}$	$[15]_{8s}$	$[30]_{8s}$	$[45]_{8s}$	$[60]_{8s}$	$[75]_{8s}$	$[90]_{8s}$
8	400 mm	0.1181°	1	28.67	25.65	19.81	15.40	14.35	14.85	15.17
			2	100.19	81.15	61.30	52.39	50.33	51.81	53.11
			3	230.35	189.43	143.66	120.59	115.30	118.88	121.85
	300 mm	0.1575°	1	50.89	45.60	35.25	27.41	25.52	26.39	26.96
			2	177.63	143.78	109.02	93.30	89.53	92.05	94.33
			3	395.60	336.46	256.25	215.09	205.27	211.39	216.61
	250 mm	0.1890°	1	73.17	62.94	50.80	39.51	36.74	37.98	38.80
			2	255.24	202.76	156.88	134.54	129.00	132.49	135.73
			3	480.05	387.48	369.89	310.66	296.03	304.50	311.94
	200 mm	0.2363°	1	114.07	102.6	79.46	61.81	57.41	59.31	60.57
			2	397.41	319.68	244.29	210.86	201.73	206.86	211.84
			3	915.88	753.04	578.78	488.13	463.60	475.93	487.36

Table 3. 27 First three natural frequencies (in Hz) of the end delaminated thickness-tapered simply supported composite beams of different lengths with delamination-length-to-beam-length ratio of 1: 4 and with 8 plies dropped-off

From Table 3.27, it is observed that the natural frequencies of the end delaminated composite beams increase with the decrease in beam length, i.e. with the corresponding increase

in the taper angle value. For instance, in Table 3.27 the 1st natural frequencies of the composite beams of beam lengths 400 mm and 200 mm are 28.7 Hz and 114.07 Hz, respectively for 0° fiber orientation angle.

From Tables 3.23 - 3.27, it can be concluded that the natural frequencies of the beams of the same length decrease with the increase in the number of plies dropped-off, i.e. with the corresponding increase in the taper angle value, whereas by considering the beams with the same number of plies dropped-off, the short beams with higher taper angle have higher natural frequencies than that of the long beams.

Figure 3.20 depicts the influences of the taper angle and fiber orientation angle on the natural frequencies of thickness-tapered simply supported composite beams of different lengths with 8 plies dropped-off. The ratio of delamination-length-to-beam-length is 1: 4. The taper angle changes with the change in the beam length and the shortest beam has the highest taper angle. It can be concluded that the natural frequencies increase with an increase in taper angle. The highest natural frequencies are recorded for the beam with 0.2363° taper angle and $[0]_{8s}$ stacking sequence. The variations of all the three natural frequencies with the change in taper angle and fiber orientation angle remain the same. A proper scaling was not possible for the range of 1st natural frequency, due to which the 1st natural frequency surface appears to be monotonic.

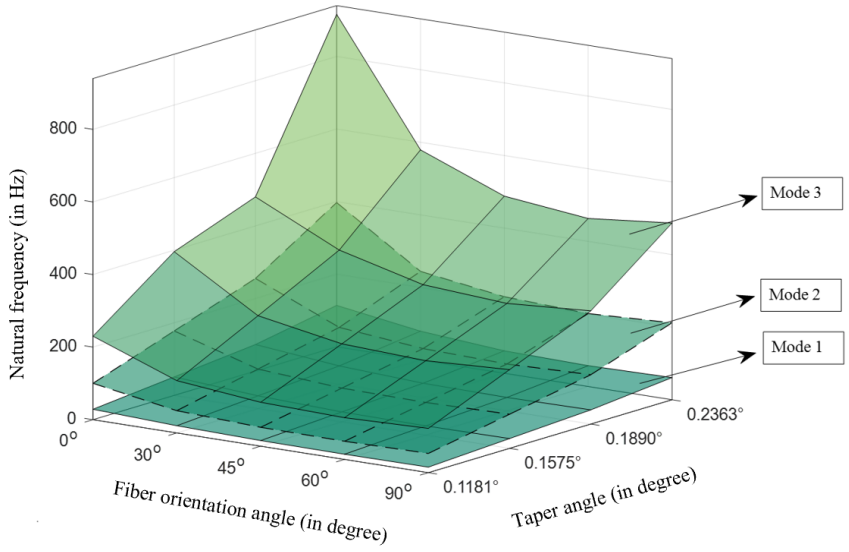

Figure 3.20 Graphical representation of the first three natural frequencies (in Hz) of the thickness-tapered simply supported composite beams of different beam lengths with 8 plies dropped-off and with delamination-length-to-beam-length ratio of 1: 4

3.10 Conclusion

In this chapter, the free vibration response of uniform and thickness-tapered simply supported composite beams with end and mid-span delaminations of different lengths, delamination locations, and stacking sequences were determined. The influences of delamination length and fiber orientation angle on the first three out-of-plane bending natural frequencies of end and mid-span delaminated uniform and thickness-tapered simply supported composite beams were investigated. Up to 20 mm end delamination, there was negligible influence of the delamination length on the natural frequencies of 400-mm-long uniform and thickness-tapered composite beams for any fiber orientation angle. The higher mode frequencies were more sensitive to the delamination length. The composite beams with 60° fiber orientation angle have minimum natural frequencies for any delamination length. With the increase in delamination length a significant decrease was observed in the 1^{st} natural frequency of the end delaminated composite beams as compared to that of the mid-span delaminated composite beams.

A free vibration analysis was conducted on the uniform composite beam with mid-span delamination between different plies. The natural frequencies of the composite beam were higher when delamination was away from the mid-plane. The highest natural frequencies were observed for the uniform composite beams with mid-span delamination at the interface between 14^{th} and 15^{th} plies. The large mid-span delamination located away from mid-plane leads to local buckling of the beam and convergence difficulties in the modal analysis.

The effect of layer reduction on the natural frequencies of the end delaminated simply supported composite beams was investigated. The natural frequencies of the thickness-tapered composite beams lie in between the natural frequencies of the thick and thin beams.

A comprehensive study was conducted to observe the influence of the taper angle on the natural frequencies of end delaminated thickness-tapered simply supported composite beams. It can be concluded that the natural frequencies of the beams of the same length decrease with the increase in the number of plies dropped-off, i.e. with the corresponding increase in the taper angle value, whereas by considering the beams with the same number of plies dropped-off, the short beams with higher taper angle have higher natural frequencies than that of the long beams.

Chapter 4

Free vibration response of rotating doubly tapered cantilever composite beams with delamination

4.1 Introduction

In the previous chapter, the free vibration response of the uniform and thickness-tapered simply supported composite beams with end and mid-span delaminations was determined and the influences of the delamination length, delamination location and fiber orientation angle on the natural frequencies of the delaminated beams were investigated. The delamination lengths having negligible effect on the natural frequencies of the uniform and thickness-tapered simply supported composite beams with end delamination were determined. The natural frequencies of the mid-span and end delaminated thickness-tapered simply supported composite beams were compared. The free vibration analysis of the uniform simply supported composite beams with mid-span delamination between different plies was also conducted. The influences of the layer reduction and taper angle on the natural frequencies of end delaminated simply supported composite beams were investigated.

In this chapter, the free vibration analyses of the rotating thickness-tapered and doubly tapered cantilever composite beams with end and mid-span delaminations are conducted. The natural frequencies of the delaminated rotating composite beams change significantly due to the change in the rotational velocity, delamination length, beam profile and stacking sequence. Various numerical studies are conducted to investigate the influences of the rotational velocity, delamination length and stacking sequence on the first three out-of-plane bending natural frequencies of the rotating thickness-tapered and doubly tapered cantilever composite beams with delamination. The influence of the double tapering on the natural frequencies of the end and mid-span delaminated beams is also investigated. The influences of the hub radius and the thickness taper angle on the natural frequencies of the rotating doubly tapered composite beams are also studied.

The FEA tool ANSYS® 19.0 Workbench platform has been chosen to perform the numerical studies presented in this chapter. ANSYS® Composite PrepPost (ACP) is used to model the composite beams and the natural frequencies of the composite beams are determined from the modal analysis. The SOLID185 finite element is used for the three-dimensional modeling of the delaminated beams to describe the out-of-plane bending vibrations and the CONTAC174 contact finite element is used to define surface to surface contact for modeling the cohesive interface. The mesh of element size 4 mm is used to conduct all the analyses presented in this chapter.

All the beams considered in this chapter are made up of Metyx® 600 Tex graphite-epoxy composite material. The mechanical properties of the composite are given in Table 4.1, whereas the interface parameters are given in Table 4.2. The geometric properties of the beams considered in this chapter are given in Table 4.3. The number of plies, thickness of the beam and width of the beam mentioned in Table 4.3 refer to the number of plies, thickness on the thick side (at the fixed end) and width on the thick side of the doubly tapered beam. The geometrical illustration of the rotating doubly tapered cantilever composite beam with end delamination is shown in Figure 4.1.

Mechanical properties of Metyx® 600 Tex graphite-epoxy	
Longitudinal modulus (E_1)	44.15 GPa
Transverse modulus (E_2)	12.30 GPa
$E_3 = E_2$	12.30 GPa
In-plane shear modulus (G_{12})	4.09 GPa
G_{13}=G_{12}	4.09 GPa
Density of a ply (ρ_p)	2026 kg/m^3
Major Poisson's ratio (υ_{12})	0.20
Minor Poisson's ratio (υ_{21})	0.018

Table 4.1 Mechanical properties of Metyx® 600 Tex graphite-epoxy [5]

Cohesive interface parameters [4]	
Maximum tangential traction	29.8 MPa
Critical energy release rate	774 J/m^2
Artificial damping coefficient	0.001
Delaminated interface parameters [5]	
Penalty stiffness of the delaminated interface	10^5

Table 4.2 Interface parameters of the cohesive and delaminated regions [4,5]

Geometric properties of the beam	
Length (L)	400 mm
Width (b_0)	20.5 mm
Individual ply thickness	0.206 mm
Number of plies at the fixed end	16
Thickness of the beam (h_0)	3.3 mm
Hub radius (R)	25 mm

Table 4.3 Geometric properties of the beam

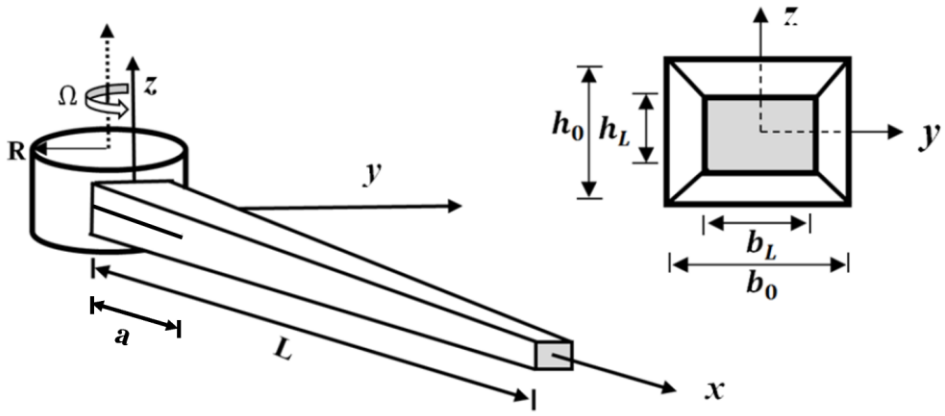

Figure 4.1 Geometrical representation of the rotating doubly tapered cantilever composite beam with end delamination

4.2 Free vibration response of rotating thickness-tapered composite beam with end mid-plane delamination

In this section, the first three out-of-plane bending natural frequencies of the rotating thickness-tapered cantilever composite beams with end mid-plane delamination are investigated. There are a total of 16 plies at the fixed end of the beam and at the free end there could be a total of 14, 12, 10 or 8 plies depending on the number of plies dropped-off. The modeling of the thickness-tapered beams was explained in the subsection 2.4.2 of the Chapter 2. The stacking sequences mentioned in the following tables refer to the stacking sequences at the fixed end of the beams. The analysis is conducted on the thickness-tapered composite beams with four different stacking sequences for various rotational velocities. The mechanical properties of the composite material were given in Table 4.1, whereas the interface parameters were given in Table 4.2. The geometric properties of the beam were given in Table 4.3. The number of plies and the thickness

of the beam mentioned in Table 4.3 refer to the number of plies and the thickness on the thick side (at the fixed end) of the thickness-tapered beam, respectively.

The first three out-of-plane bending natural frequencies of the end delaminated rotating thickness-tapered cantilever composite beams are determined from the modal analysis and are presented in Tables 4.4 - 4.11.

Number of plies		**Stacking sequence at the fixed end**	**Mode number**	**Rotational velocity (in rad/s)**				
At the fixed end	**At the free end**			**0**	**50**	**100**	**150**	**200**
16	14	$[90]_{8s}$	1	8.06	12.09	19.53	27.54	35.68
			2	47.87	52.15	63.25	78.26	95.26
			3	129.85	134.23	146.52	164.81	187.18
		$[0/90]_{4s}$	1	12.88	15.74	22.10	29.67	37.59
			2	76.63	79.27	86.99	98.63	112.61
			3	208.24	210.20	218.29	231.85	247.81
	12	$[90]_{8s}$	1	8.20	12.24	19.68	29.66	35.84
			2	45.86	50.20	61.38	98.50	93.30
			3	122.37	126.77	139.08	231.10	179.54
		$[0/90]_{4s}$	1	13.12	15.97	22.33	29.87	37.80
			2	73.28	76.06	83.83	95.38	109.47
			3	194.50	197.29	205.43	218.27	235.00
	10	$[90]_{8s}$	1	8.39	12.41	19.86	27.89	36.05
			2	43.76	48.16	59.42	74.41	91.21
			3	114.52	118.95	131.30	149.51	171.60
		$[0/90]_{4s}$	1	13.51	16.34	22.68	30.23	38.17
			2	70.63	73.43	81.26	92.84	106.91
			3	184.60	187.38	195.47	208.23	224.80
	8	$[90]_{8s}$	1	8.63	12.64	20.10	28.14	36.30
			2	41.53	46.01	57.36	72.31	88.97
			3	106.19	110.67	123.11	141.31	163.26
		$[0/90]_{4s}$	1	13.72	16.56	22.92	30.49	38.44
			2	66.79	69.65	77.59	89.25	103.32
			3	170.27	173.10	181.30	194.16	210.80

Table 4.4 First three natural frequencies (in Hz) of the 400-mm-long rotating thickness-tapered cantilever composite beams with 40 mm end delamination for $[90]_{8s}$ and $[0/90]_{4s}$ stacking sequences

Number of plies		Stacking sequence at the fixed end	Mode number	Rotational velocity (in rad/s)				
At the fixed end	At the free end			0	50	100	150	200
16	14	$[90]_{8s}$	1	8.01	12.00	19.32	27.24	35.34
			2	44.66	49.17	60.73	76.15	93.48
			3	113.61	119.08	133.90	154.89	179.50
		$[0/90]_{4s}$	1	12.80	15.64	21.92	29.37	37.20
			2	71.63	74.52	82.60	94.55	109.08
			3	182.75	186.19	196.08	211.33	230.66
	12	$[90]_{8s}$	1	8.17	12.15	19.48	27.40	35.49
			2	43.13	47.62	59.10	74.39	91.55
			3	107.65	113.00	127.51	148.10	172.28
		$[0/90]_{4s}$	1	13.03	15.84	22.10	29.52	37.32
			2	67.69	70.64	78.84	90.89	105.47
			3	167.02	170.62	180.92	196.64	216.38
	10	$[90]_{8s}$	1	8.36	12.34	19.67	27.59	35.68
			2	41.49	45.96	57.38	72.54	89.50
			3	101.47	106.69	120.87	141.05	164.78
		$[0/90]_{4s}$	1	13.46	16.26	22.51	29.94	37.77
			2	66.80	69.67	77.65	89.42	103.69
			3	163.15	166.47	176.01	190.73	209.40
	8	$[90]_{8s}$	1	8.60	12.57	19.91	27.83	35.91
			2	39.71	44.19	55.56	70.56	87.30
			3	94.97	100.07	113.92	133.66	156.92
		$[0/90]_{4s}$	1	13.67	16.47	22.73	30.16	37.98
			2	63.11	66.00	74.04	85.82	100.03
			3	149.47	152.82	162.43	177.19	195.83

Table 4.5 First three natural frequencies (in Hz) of the 400-mm-long rotating thickness-tapered cantilever composite beams with 80 mm end delamination for $[90]_{8s}$ and $[0/90]_{4s}$ stacking sequences

Number of plies		Stacking sequence at the fixed end	Mode number	Rotational velocity (in rad/s)				
At the fixed end	At the free end			0	50	100	150	200
16	14	$[90]_{8s}$	1	7.65	11.60	18.90	26.86	35.01
			2	34.10	40.39	54.80	72.22	90.74
			3	104.03	110.05	126.09	148.39	174.12
		$[0/90]_{4s}$	1	12.27	15.07	21.31	28.73	36.58
			2	55.43	59.50	70.21	84.88	101.63
			3	167.85	171.59	182.40	198.88	219.53
	12	$[90]_{8s}$	1	7.84	11.77	19.04	26.99	35.14
			2	33.02	39.23	53.43	70.61	88.88
			3	97.50	103.48	119.40	141.49	166.93
		$[0/90]_{4s}$	1	12.32	15.11	21.31	28.72	36.57
			2	49.52	53.96	65.38	80.58	97.61
			3	152.17	156.18	167.51	184.56	205.64
	10	$[90]_{8s}$	1	8.07	11.96	19.21	27.15	35.29
			2	31.94	38.03	51.99	68.88	86.88
			3	90.69	96.66	112.49	134.35	159.46
		$[0/90]_{4s}$	1	12.99	15.73	21.86	29.22	37.04
			2	51.39	55.40	65.90	80.23	96.53
			3	146.34	150.30	161.05	177.37	197.70
	8	$[90]_{8s}$	1	8.35	12.21	19.43	27.35	35.48
			2	30.86	36.80	50.45	67.02	84.69
			3	83.56	89.54	105.29	126.91	151.65
		$[0/90]_{4s}$	1	13.20	15.92	22.03	29.37	37.18
			2	47.60	51.72	62.39	76.76	92.98
			3	132.68	136.56	147.53	164.04	184.44

Table 4.6 First three natural frequencies (in Hz) of the 400-mm-long rotating thickness-tapered cantilever composite beams with 160 mm end delamination for $[90]_{8s}$ and $[0/90]_{4s}$ stacking sequences

Number of plies		Stacking sequence at the fixed end	Mode number	Rotational velocity (in rad/s)				
At the fixed end	At the free end			0	50	100	150	200
16	14	$[90]_{8s}$	1	6.91	11.13	18.63	26.68	34.87
			2	30.07	36.90	52.04	69.99	88.92
			3	85.70	93.78	114.03	140.20	168.71
		$[0/90]_{4s}$	1	11.15	14.17	20.67	28.27	36.31
			2	49.03	53.50	64.99	80.39	85.91
			3	140.21	145.27	148.35	179.75	191.42
	12	$[90]_{8s}$	1	7.11	11.27	18.75	26.79	34.98
			2	28.73	35.61	50.71	68.50	87.21
			3	81.51	89.46	109.29	134.82	162.63
		$[0/90]_{4s}$	1	11.20	14.23	20.75	28.35	36.33
			2	44.79	49.54	61.51	77.22	97.72
			3	122.76	128.42	143.82	165.76	204.27
	10	$[90]_{8s}$	1	7.35	11.45	18.89	26.93	35.12
			2	27.38	34.30	49.31	66.90	85.35
			3	77.17	84.96	104.30	129.12	156.17
		$[0/90]_{4s}$	1	11.55	14.52	20.98	28.55	36.50
			2	42.67	47.43	59.35	74.91	92.15
			3	119.03	124.33	138.80	159.50	183.82
	8	$[90]_{8s}$	1	7.64	11.68	19.08	27.10	35.29
			2	26.02	32.95	47.84	65.17	83.30
			3	72.63	80.20	98.93	122.95	149.18
		$[0/90]_{4s}$	1	11.88	14.81	21.22	28.77	36.71
			2	40.07	44.92	56.93	72.43	89.48
			3	110.36	115.66	130.05	150.45	170.66

Table 4.7 First three natural frequencies (in Hz) of the 400-mm-long rotating thickness-tapered cantilever composite beams with 240 mm end delamination for $[90]_{8s}$ and $[0/90]_{4s}$ stacking sequences

Number of plies		Stacking sequence at the fixed end	Mode number	Rotational velocity (in rad/s)				
At the fixed end	At the free end			0	50	100	150	200
16	14	$[0]_{8s}$	1	15.25	17.73	23.60	30.85	38.63
			2	90.40	92.73	99.40	109.61	122.46
			3	244.36	246.22	253.65	264.76	279.51
		$[-45/45]_{4s}$	1	8.34	12.31	19.72	27.74	35.90
			2	49.73	53.89	64.77	79.59	96.46
			3	135.68	139.87	151.74	169.53	191.44
	12	$[0]_{8s}$	1	15.53	18.01	23.87	31.13	38.92
			2	86.64	89.01	95.76	106.05	118.95
			3	230.42	232.79	239.73	250.86	265.59
		$[-45/45]_{4s}$	1	8.49	12.45	19.87	27.91	27.91
			2	47.62	51.84	62.81	77.64	77.64
			3	127.76	132.00	143.92	161.70	161.70
	10	$[0]_{8s}$	1	15.88	18.35	24.21	31.48	39.27
			2	82.69	85.10	91.94	102.33	115.28
			3	215.76	218.15	225.13	236.30	251.05
		$[-45/45]_{4s}$	1	8.67	12.63	20.06	28.10	28.10
			2	45.38	49.67	60.74	75.57	75.57
			3	119.43	123.71	135.71	153.51	153.51
	8	$[0]_{8s}$	1	16.33	18.79	24.64	31.91	39.72
			2	78.51	80.97	87.91	98.40	111.40
			3	200.20	202.61	209.67	220.91	235.71
		$[-45/45]_{4s}$	1	8.91	12.86	20.30	28.35	36.54
			2	43.06	47.43	58.59	73.41	89.98
			3	110.70	115.04	127.14	144.97	166.59

Table 4.8 First three natural frequencies (in Hz) of the 400-mm-long rotating thickness-tapered cantilever composite beams with 40 mm end delamination for $[0]_{8s}$ and $[-45/45]_{4s}$ stacking sequences

Number of plies		Stacking sequence at the fixed end	Mode number	Rotational velocity (in rad/s)				
At the fixed end	At the free end			0	50	100	150	200
16	14	$[0]_{8s}$	1	15.16	17.62	23.41	30.55	38.22
			2	84.18	86.65	93.69	104.38	117.73
			3	213.78	216.75	225.38	238.93	256.45
		$[-45/45]_{4s}$	1	8.31	12.23	19.54	27.47	35.56
			2	46.88	51.18	62.38	77.51	94.64
			3	119.95	125.00	139.08	159.32	183.33
	12	$[0]_{8s}$	1	15.45	17.91	23.70	30.85	38.52
			2	81.32	83.78	90.78	101.40	114.64
			3	202.57	205.48	213.92	227.19	244.35
		$[-45/45]_{4s}$	1	8.46	12.38	19.70	27.63	35.73
			2	45.20	49.51	60.67	75.70	92.67
			3	113.62	118.64	132.43	152.30	175.91
	10	$[0]_{8s}$	1	15.82	18.27	24.05	31.21	38.88
			2	78.26	80.72	87.69	98.26	111.40
			3	190.95	193.79	202.04	215.00	231.79
		$[-45/45]_{4s}$	1	8.65	12.57	19.89	27.83	35.92
			2	43.41	47.73	58.87	73.78	90.58
			3	107.12	112.03	125.53	145.01	168.20
	8	$[0]_{8s}$	1	16.28	18.72	24.50	31.66	39.33
			2	74.94	77.40	84.38	94.91	107.95
			3	178.75	181.52	189.57	202.22	218.63
		$[-45/45]_{4s}$	1	8.90	12.81	20.14	28.07	36.17
			2	41.48	45.83	56.95	71.74	88.34
			3	100.20	105.02	118.24	137.34	160.10

Table 4.9 First three natural frequencies (in Hz) of the 400-mm-long rotating thickness-tapered cantilever composite beams with 80 mm end delamination for $[0]_{8s}$ and $[-45/45]_{4s}$ stacking sequences

Number of plies		Stacking sequence at the fixed end	Mode number	Rotational velocity (in rad/s)				
At the fixed end	At the free end			0	50	100	150	200
16	14	$[0]_{8s}$	1	14.47	16.91	22.65	29.76	37.44
			2	64.31	67.88	77.51	91.16	107.13
			3	196.59	199.86	209.29	223.96	242.72
		$[-45/45]_{4s}$	1	7.97	11.85	19.11	27.06	35.21
			2	35.92	41.88	54.71	73.20	91.62
			3	108.55	114.19	129.74	151.60	177.03
	12	$[0]_{8s}$	1	14.83	17.25	22.96	30.04	37.70
			2	62.28	65.80	75.30	88.76	104.49
			3	184.31	187.56	169.18	211.48	230.08
		$[-45/45]_{4s}$	1	8.16	12.01	19.25	27.19	35.34
			2	34.73	40.68	54.57	71.56	89.74
			3	101.64	107.39	122.86	144.52	169.66
	10	$[0]_{8s}$	1	15.81	18.17	23.80	30.04	38.42
			2	58.20	61.56	70.68	88.76	98.74
			3	158.06	161.30	170.64	211.48	203.38
		$[-45/45]_{4s}$	1	8.38	12.22	19.43	27.36	35.50
			2	33.65	39.48	53.10	69.81	87.71
			3	94.53	100.27	115.68	137.16	162.00
	8	$[0]_{8s}$	1	15.81	18.17	23.80	30.82	38.42
			2	58.20	61.56	70.68	83.60	98.74
			3	158.06	161.30	170.15	185.06	203.38
		$[-45/45]_{4s}$	1	8.67	12.47	19.66	27.57	35.71
			2	32.49	38.19	51.52	67.91	85.50
			3	87.09	92.87	108.22	129.49	153.98

Table 4.10 First three natural frequencies (in Hz) of the 400-mm-long rotating thickness-tapered cantilever composite beams with 160 mm end delamination for $[0]_{8s}$ and $[-45/45]_{4s}$ stacking sequences

Number of plies		Stacking sequence at the fixed end	Mode number	Rotational velocity (in rad/s)				
At the fixed end	At the free end			0	50	100	150	200
16	14	$[0]_{8s}$	1	13.05	15.71	21.78	29.12	36.94
			2	56.89	60.79	71.15	85.53	102.13
			3	161.49	165.94	178.49	197.30	220.40
		$[-45/45]_{4s}$	1	7.22	11.34	18.81	26.86	35.05
			2	31.36	37.94	52.89	70.75	89.64
			3	90.29	97.93	117.57	143.26	171.48
	12	$[0]_{8s}$	1	13.43	16.05	22.05	29.36	37.17
			2	54.36	58.30	68.72	83.08	99.58
			3	153.63	158.01	170.35	188.80	211.39
		$[-45/45]_{4s}$	1	7.41	11.50	18.93	26.97	35.17
			2	29.92	36.63	51.53	69.24	87.92
			3	85.76	93.39	112.60	137.68	165.20
	10	$[0]_{8s}$	1	13.89	16.45	22.39	29.66	37.44
			2	51.79	55.77	66.23	80.55	96.92
			3	145.47	149.77	161.86	179.87	201.87
		$[-45/45]_{4s}$	1	7.66	11.69	19.09	27.12	35.32
			2	28.57	35.30	50.12	67.63	86.04
			3	81.46	88.87	107.56	131.89	158.62
	8	$[0]_{8s}$	1	14.45	16.95	22.81	30.03	37.79
			2	49.21	53.22	63.68	77.91	94.08
			3	136.94	141.13	152.88	170.35	191.65
		$[-45/45]_{4s}$	1	7.96	11.92	19.28	27.30	35.50
			2	27.12	33.88	48.59	65.09	83.95
			3	76.48	83.71	101.87	125.46	151.43

Table 4.11 First three natural frequencies (in Hz) of the 400-mm-long rotating thickness-tapered cantilever composite beams with 240 mm end delamination for $[0]_{8s}$ and $[-45/45]_{4s}$ stacking sequences

In Tables 4.4 - 4.11, the highest natural frequencies are observed for the end delaminated thickness-tapered composite beams with $[0]_{8s}$ stacking sequence, followed by the natural frequencies of the composite beams with $[0/90]_{4s}$ stacking sequence. The natural frequencies of the composite beams with $[90]_{8s}$ and $[-45/45]_{4s}$ stacking sequences are almost the same, but latter has slightly higher natural frequencies. For instance, the 1st, 2nd and 3rd natural frequencies of the rotating thickness-tapered composite beam with 240 mm end delamination and with 8 plies dropped-off for $[-45/45]_{4s}$ stacking sequence are 19.28 Hz, 48.59 Hz and 101.87 Hz, respectively, whereas the 1st, 2nd and 3rd natural frequencies of the rotating thickness-tapered composite beam

with 240 mm end delamination and with 8 plies dropped-off for $[90]_{8s}$ stacking sequence are 19.08 Hz, 47.84 Hz and 98.93 Hz, respectively, at 100 rad/s rotational velocity.

The natural frequencies increase with the increase in the rotational velocity but decrease with the increase in the delamination length. The lowest 1st natural frequency of 6.91 Hz is observed for the thickness-tapered composite beam with 240 mm end delamination and with 2 plies dropped-off for $[90]_{8s}$ stacking sequence at 0 rad/s rotational velocity, whereas the highest 1st natural frequency of 39.72 Hz is observed for the rotating thickness-tapered composite beam with 40 mm end delamination and with 8 plies dropped-off for $[0]_{8s}$ stacking sequence at 200 rad/s rotational velocity.

Figure 4.2 illustrates the influence of the rotational velocity on the natural frequencies of the 400-mm-long rotating thickness-tapered cantilever composite beams with 80 mm end delamination and with different number of plies at the free ends of the beams, for $[0/90]_{4s}$ stacking sequence.

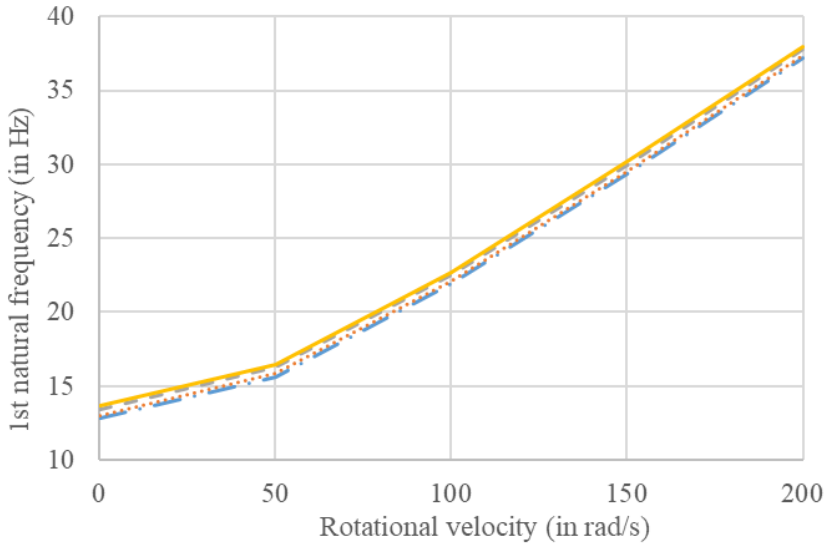

Figure 4.2 (a) 1st natural frequencies (in Hz) of the 400-mm-long rotating thickness-tapered cantilever composite beams with 80 mm end delamination and with different number of plies at the free ends of the beams for $[0/90]_{4s}$ stacking sequence

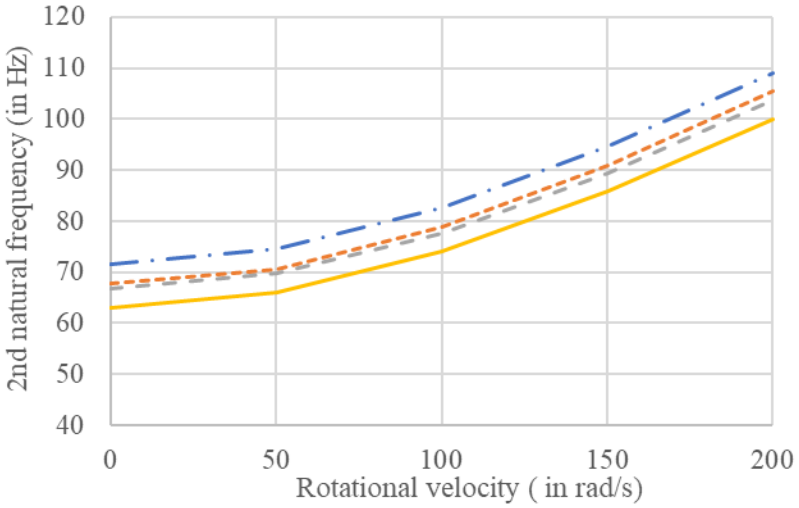

Figure 4.2 (b) 2nd natural frequencies (in Hz) of the 400-mm-long rotating thickness-tapered cantilever composite beams with 80 mm end delamination and with different number of plies at the free ends of the beams for $[0/90]_{4s}$ stacking sequence

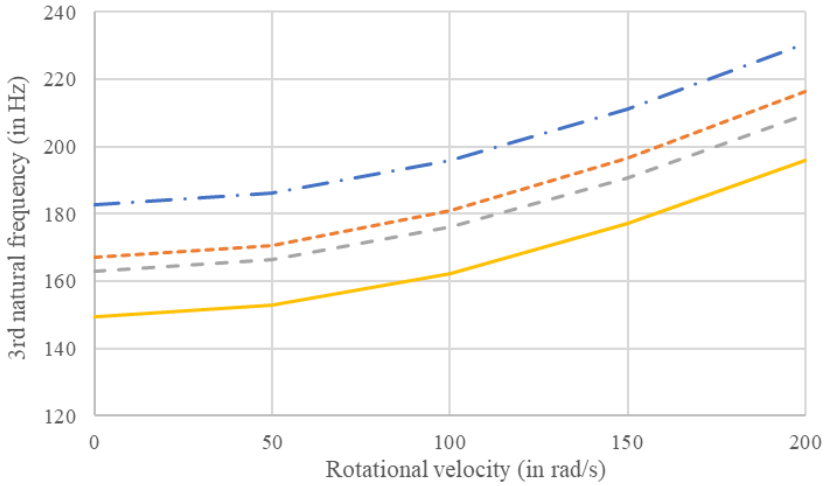

Figure 4.2 (c) 3rd natural frequencies (in Hz) of the 400-mm-long rotating thickness-tapered cantilever composite beams with 80 mm end delamination and with different number of plies at the free ends of the beams for $[0/90]_{4s}$ stacking sequence

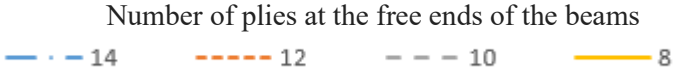

Figure 4.2 The first three natural frequencies (in Hz) of the 400-mm-long rotating thickness-tapered cantilever composite beams with 80 mm end delamination and with different number of plies at the free ends of the beams for $[0/90]_{4s}$ stacking sequence

Figure 4.2 shows the graphical representation of the first three natural frequencies of the 400-mm-long rotating thickness-tapered cantilever composite beams with 80 mm end delamination for $[0/90]_{4s}$ stacking sequence. It is observed that, all the three natural frequencies

are increasing with the increase in the rotational velocity. With the increase in the rotational velocity, the highest and the lowest rates of increase in the 1st natural frequency are seen for the thickness-tapered composite beams with 14 and 8 plies at the free ends of the beams, whereas the highest and the lowest rates of increase in the 2nd and 3rd natural frequencies are seen for the thickness-tapered composite beams with 8 and 14 plies at the free ends of the beams, respectively.

From Figure 4.2 (a), it is observed that the 1st natural frequencies of the rotating thickness-tapered cantilever composite beams with 80 mm end delamination and with different number of plies dropped-off are in close proximity for $[0/90]_{4s}$ stacking sequence for all the considered rotational velocities. The composite beam with 8 plies at the free end of the beam has the highest 1st natural frequency of 22.73 Hz, whereas the composite beam with 14 plies at the free end of the beam has the lowest 1st natural frequency of 19.323 Hz for $[0/90]_{8s}$ stacking sequence at 100 rad/s rotational velocity. The percentage increase of 177.8% is observed in the 1st natural frequency of the thickness-tapered composite beam with 8 plies dropped-off due to the increase in the rotational velocity from 0 rad/s to 200 rad/s.

In Figures 4.2 (b) and (c), the composite beam with 8 plies at the free end of the beam has the lowest 2nd and 3rd natural frequencies, whereas the composite beam with 14 plies at the free end of the beam has the highest 2nd and 3rd natural frequencies. For instance, the 2nd and 3rd natural frequencies of the composite beam with 80 mm end delamination and with 8 plies at the free end of the beam are 74.04 Hz and 162.43 Hz, respectively, whereas the 2nd and 3rd natural frequencies of the composite beam with 80 mm end delamination and with 14 plies at the free end of the beam are 82.60 Hz and 196.08 Hz, respectively, for $[0/90]_{4s}$ stacking sequence at 100 rad/s rotational velocity. The percentage increases of 58.5% and 31.0% are observed in the 2nd and 3rd natural frequencies, respectively, of the thickness-tapered composite beam with 8 plies dropped-off due to the increase in the rotational velocity from 0 rad/s to 200 rad/s for $[0/90]_{4s}$ stacking sequence.

For $[0/90]_{4s}$ stacking sequence, the percentage differences in the 1st, 2nd and 3rd natural frequencies of the thickness-tapered composite beams with 80 mm end delamination and with 8 and 14 plies at the free ends of the beams are 3.6%, 11.5% and 20.7%, respectively, at 100 rad/s rotational velocity, whereas for $[90]_{4s}$ stacking sequence, the percentage differences in the 1st, 2nd and 3rd natural frequencies of the thickness-tapered composite beams with 80 mm end

delamination and with 8 and 14 plies at the free ends of the beams are 3.0%, 9.3% and 17.5%, respectively, at 100 rad/s rotational velocity.

Figure 4.3 illustrates the influence of the thickness-tapering on the natural frequencies of the 400-mm-long thickness-tapered composite beams with 40 mm and 240 mm end delaminations for $[90]_{8s}$ stacking sequence at 100 rad/s rotational velocity.

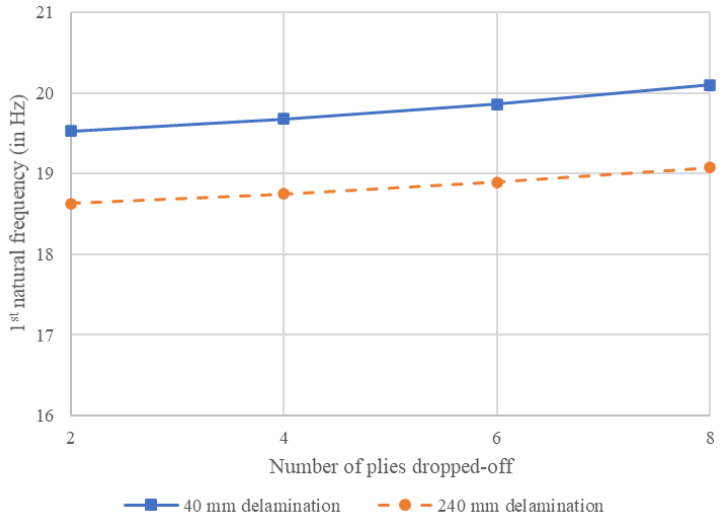

Figure 4.3 (a) The influence of the thickness-tapering on the 1st natural frequencies of the 400-mm-long rotating thickness-tapered composite beams with 40 mm and 240 mm end delaminations for $[90]_{8s}$ stacking sequence at 100 rad/s rotational velocity

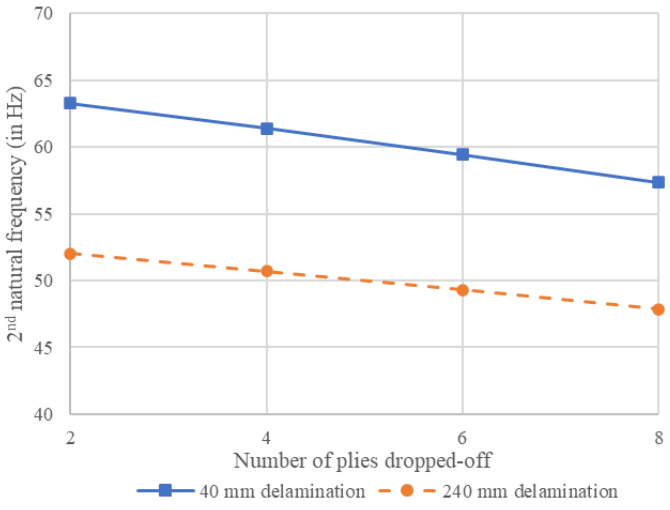

Figure 4.3 (b) The influence of the thickness-tapering on the 2nd natural frequencies of the 400-mm-long rotating thickness-tapered composite beams with 40 mm and 240 mm end delaminations for $[90]_{8s}$ stacking sequence at 100 rad/s rotational velocity

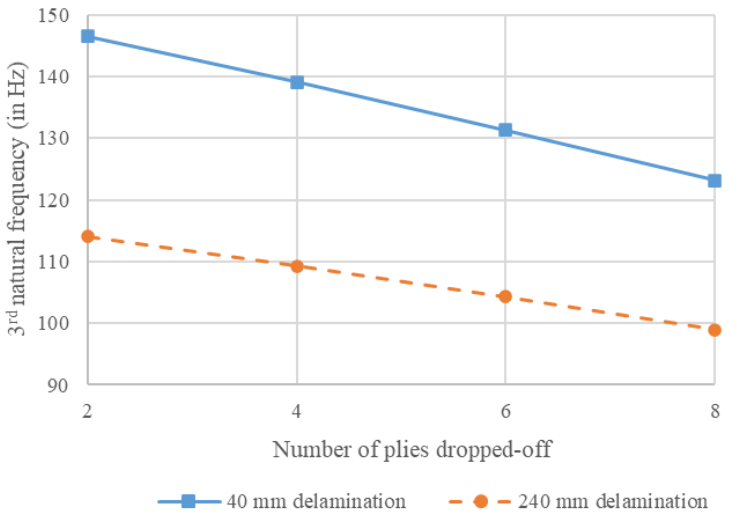

Figure 4.3 (c) The influence of the thickness-tapering on the 3rd natural frequencies of the 400-mm-long rotating thickness-tapered composite beams with 40 mm and 240 mm end delaminations for $[90]_{8s}$ stacking sequence at 100 rad/s rotational velocity

Figure 4.3 The influence of the thickness-tapering on the first three natural frequencies of the 400-mm-long rotating thickness-tapered cantilever composite beams with 40 mm and 240 mm end delaminations at 100 rad/s rotational velocity for $[90]_{8s}$ stacking sequence

From Figure 4.3, it is observed that with the increase in the number of plies dropped-off, the 1st natural frequencies of the rotating thickness-tapered cantilever composite beams increase linearly, whereas the 2nd and 3rd natural frequencies decrease linearly. The composite beam with a greater number of plies dropped-off has higher 1st natural frequency than the composite beam with a lesser number of plies dropped-off, which is due to the asymmetry in the cantilever boundary condition. For instance, the 1st, 2nd and 3rd natural frequencies of the thickness-tapered composite beam with 40 mm end delamination and with 2 plies dropped-off are 19.53 Hz, 63.25 Hz and 146.52 Hz, respectively, whereas the 1st, 2nd and 3rd natural frequencies of the thickness-tapered composite beam with 40 mm end delamination and with 8 plies dropped-off are 20.10 Hz, 57.36 Hz and 123.11 Hz, respectively, for $[90]_{8s}$ stacking sequence at 100 rad/s rotational velocity.

The rotating thickness-tapered composite beams with 40 mm end delamination have higher natural frequencies than the rotating thickness-tapered composite beams with 240 mm end delamination. The percentage differences between the 1st, 2nd and 3rd natural frequencies of the rotating thickness-tapered composite beams with 8 plies dropped-off and with 40 mm and 240

mm end delaminations are 5.3%, 19.8% and 24.4%, respectively, for $[90]_{8s}$ stacking sequence at 100 rad/s rotational velocity.

The first three mode shapes of the rotating thickness-tapered cantilever composite beam with 240 mm end delamination, and with 8 plies dropped-off for $[0/90]_{4s}$ stacking sequence at 200 rad/s rotational velocity are shown in Figure 4.4. The points of inflection of the mode shapes shown in Figure 4.4 are presented in Table 4.12.

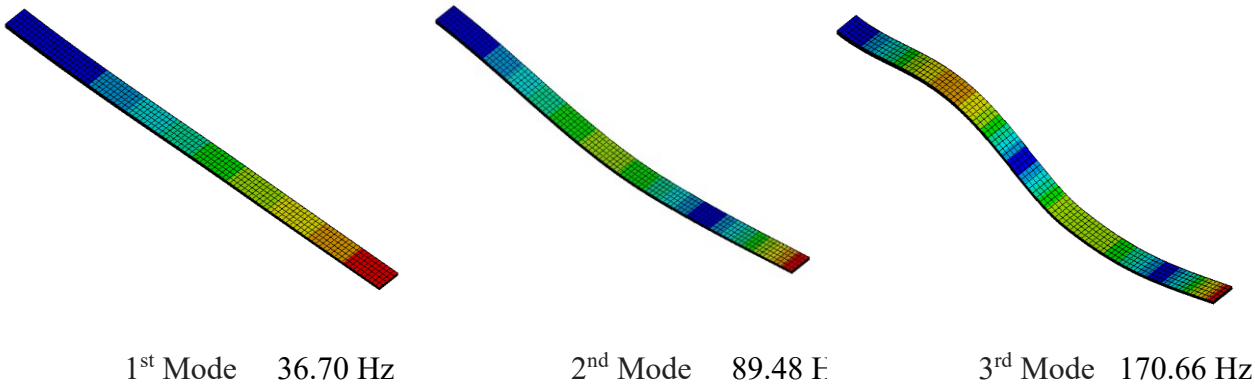

Figure 4.4 The pictorial representation of the first three mode shapes of the rotating thickness-tapered cantilever composite beam with 240 mm end delamination and with 8 plies dropped-off for $[0/90]_{4s}$ stacking sequence at 200 rad/s rotational velocity

Mode	Points of inflection of the mode shapes presented in Figure 4.4
1st Mode	0 mm
2nd Mode	0 mm, 185 mm
3rd Mode	0 mm, 110 mm, 245 mm

Table 4.12 The points of inflection of the mode shapes presented in Figure 4.4

4.3 Free vibration analysis of rotating doubly tapered composite beam with end mid-plane delamination

In this section, the natural frequencies of the rotating doubly tapered cantilever composite beams with end mid-plane delamination are investigated. There are a total of 16 and 8 plies at the fixed and free ends of the composite beams, respectively. The width of the beam is tailored to get different width-ratio values. The end delamination is modeled at the fixed end of the beam. The stacking sequences mentioned in the following tables refer to the stacking sequences at the fixed ends of the beams. In this study, the first three out-of-plane bending natural frequencies of the end

delaminated rotating doubly tapered cantilever composite beams are determined for four different delamination lengths and for four different stacking sequences at various rotational velocities. The mechanical properties of the composite material were given in Table 4.1, whereas the interface parameters were given in Table 4.2. The geometric properties of the beam were given in Table 4.3. The number of plies, thickness of the beam and width of the beam mentioned in Table 4.3 refer to the number of plies, thickness on the thick side (at the fixed end) and width on the thick side of the doubly tapered composite beam, respectively.

The first three out-of-plane bending natural frequencies of the 400-mm-long end delaminated rotating doubly tapered cantilever composite beams are determined from the modal analysis and are presented in Tables 4.13 - 4.20.

Number of plies at the fixed/free ends	Width-ratio value	Stacking sequence at the fixed end	Mode number	Rotational velocity (in rad/s)				
				0	50	100	150	200
16/8	0.1	$[90]_{8s}$	1	45.63	46.62	49.47	53.86	59.49
			2	164.18	165.10	167.85	172.35	178.46
			3	380.62	381.50	384.16	388.56	394.62
		$[0/90]_{4s}$	1	72.24	72.87	74.72	77.69	81.66
			2	261.32	261.88	263.59	266.42	270.33
			3	597.86	598.37	600.01	602.73	606.52
	0.5	$[90]_{8s}$	1	33.56	34.86	38.48	43.79	50.20
			2	140.01	141.27	144.98	150.97	158.97
			3	348.05	349.26	352.88	358.82	366.97
		$[0/90]_{4s}$	1	52.72	53.56	55.98	59.78	64.69
			2	224.61	225.39	227.72	231.56	236.83
			3	554.99	555.74	558.00	561.75	566.95
	1	$[90]_{8s}$	1	8.62	12.64	20.09	28.13	36.30
			2	41.53	46.01	57.35	72.31	88.96
			3	106.19	110.67	123.11	141.31	163.26
		$[0/90]_{4s}$	1	13.72	16.56	22.92	30.49	38.44
			2	66.79	69.65	77.59	89.25	103.32
			3	170.27	173.10	181.30	194.16	210.80

Table 4.13 The first three natural frequencies (in Hz) of the 400-mm-long rotating doubly tapered cantilever composite beams with 40 mm end delamination for $[90]_{8s}$ and $[0/90]_{4s}$ stacking sequences

Number of plies at the fixed/free ends	Width-ratio value	Stacking sequence at the fixed end	Mode number	Rotational velocity (in rad/s)				
				0	50	100	150	200
16/8	0.1	$[90]_{8s}$	1	45.44	46.51	49.38	53.66	59.26
			2	155.76	156.61	159.32	163.75	169.76
			3	337.03	337.91	340.80	345.56	352.12
		$[0/90]_{4s}$	1	72.19	72.79	74.60	77.516	81.40
			2	246.82	247.34	249.04	251.87	255.77
			3	527.12	527.66	529.53	532.64	536.96
	0.5	$[90]_{8s}$	1	32.77	34.08	37.73	43.05	49.45
			2	135.20	136.43	140.08	145.97	153.86
			3	310.97	312.31	316.31	322.87	331.83
		$[0/90]_{4s}$	1	51.99	52.82	55.24	59.032	63.91
			2	213.61	214.38	216.71	220.52	225.77
			3	487.49	488.35	490.95	495.25	501.21
	1	$[90]_{8s}$	1	8.60	12.57	19.90	27.83	35.91
			2	39.70	44.19	55.56	70.56	87.29
			3	94.96	100.07	113.92	133.66	156.92
		$[0/90]_{4s}$	1	13.66	16.46	22.73	30.16	37.98
			2	63.10	65.99	74.03	85.81	100.03
			3	149.47	152.82	162.43	177.19	195.83

Table 4.14 The first three natural frequencies (in Hz) of the 400-mm-long rotating doubly tapered cantilever composite beams with 80 mm end delamination for $[90]_{8s}$ and $[0/90]_{4s}$ stacking sequences

Number of plies at the fixed/free ends	Width-ratio value	Stacking sequence at the fixed end	Mode number	Rotational velocity (in rad/s)				
				0	50	100	150	200
16/8	0.1	$[90]_{8s}$	1	43.23	44.11	46.83	51.01	56.31
			2	122.78	123.21	126.83	132.65	140.39
			3	300.73	301.15	304.52	310.05	317.63
		$[0/90]_{4s}$	1	67.77	68.34	70.10	72.95	76.73
			2	187.42	188.17	190.59	194.54	199.95
			3	472.90	473.54	475.71	479.29	484.27
	0.5	$[90]_{8s}$	1	31.66	32.92	36.46	41.63	47.84
			2	104.33	105.97	110.87	118.58	128.60
			3	270.95	272.55	277.36	285.18	295.76
		$[0/90]_{4s}$	1	49.95	50.75	53.09	56.76	61.49
			2	161.03	162.12	165.41	170.74	177.93
			3	429.28	430.30	433.38	438.45	445.45
	1	$[90]_{8s}$	1	8.35	12.20	19.43	27.35	35.48
			2	30.85	36.80	50.45	67.02	84.69
			3	83.56	89.54	105.29	126.91	151.65
		$[0/90]_{4s}$	1	13.20	15.92	22.03	29.37	37.18
			2	47.60	51.72	62.39	76.76	92.98
			3	132.68	136.56	147.53	164.04	184.44

Table 4.15 The first three natural frequencies (in Hz) of the 400-mm-long rotating doubly tapered cantilever composite beams with 160 mm end delamination for $[90]_{8s}$ and $[0/90]_{4s}$ stacking sequences

Number of plies at the fixed/free ends	Width-ratio value	Stacking sequence at the fixed end	Mode number	Rotational velocity (in rad/s)				
				0	50	100	150	200
16/8	0.1	$[90]_{8s}$	1	37.33	38.39	41.48	46.15	51.94
			2	108.01	109.38	113.56	120.18	128.85
			3	255.48	256.86	261.26	268.41	278.06
		$[0/90]_{4s}$	1	57.39	57.98	60.08	63.42	67.79
			2	167.30	168.03	170.79	175.27	181.35
			3	386.21	387.06	389.05	393.98	400.76
	0.5	$[90]_{8s}$	1	28.53	29.90	33.67	39.11	45.66
			2	88.75	90.79	96.65	105.66	114.59
			3	235.06	237.11	243.20	252.96	263.14
		$[0/90]_{4s}$	1	44.22	45.10	47.68	51.69	56.80
			2	137.11	138.43	142.36	148.66	157.04
			3	357.44	358.84	363.00	369.82	379.13
	1	$[90]_{8s}$	1	7.64	11.68	19.08	27.10	35.29
			2	26.02	32.95	47.84	65.17	83.30
			3	72.63	80.20	98.93	122.95	149.18
		$[0/90]_{4s}$	1	11.88	14.81	21.22	28.77	36.71
			2	40.07	44.92	56.93	72.43	89.48
			3	110.36	115.66	130.05	150.45	174.26

Table 4.16 The first three natural frequencies (in Hz) of the 400-mm-long rotating doubly tapered cantilever composite beams with 240 mm end delamination for $[90]_{8s}$ and $[0/90]_{4s}$ stacking sequences

Number of plies at the fixed/free ends	Width-ratio value	Stacking sequence at the fixed end	Mode number	Rotational velocity (in rad/s)				
				0	50	100	150	200
16/8	0.1	$[0]_{8s}$	1	86.31	86.84	88.40	90.95	94.38
			2	307.72	308.20	309.66	312.08	315.44
			3	703.47	703.92	705.32	707.65	710.90
		$[45/-45]_{4s}$	1	47.99	48.94	51.67	55.90	61.28
			2	171.19	172.07	174.69	178.97	184.81
			3	392.63	393.48	396.00	400.17	405.93
	0.5	$[0]_{8s}$	1	62.09	62.81	64.90	68.23	72.62
			2	263.83	264.50	266.50	269.80	274.36
			3	649.32	649.96	651.90	655.12	659.59
		$[45/-45]_{4s}$	1	34.27	35.55	39.11	44.37	50.75
			2	146.49	147.70	151.29	157.08	164.84
			3	361.33	362.50	365.99	371.72	379.60
	1	$[0]_{8s}$	1	16.33	18.79	24.64	31.91	39.72
			2	78.51	80.97	87.91	98.40	111.40
			3	200.20	202.61	209.67	220.91	235.71
		$[45/-45]_{4s}$	1	8.91	12.86	20.30	28.35	36.54
			2	43.06	47.43	58.59	73.41	89.98
			3	110.70	115.04	127.14	144.97	166.59

Table 4.17 The first three natural frequencies (in Hz) of the 400-mm-long rotating doubly tapered cantilever composite beams with 40 mm end delamination for $[0]_{8s}$ and $[-45/45]_{4s}$ stacking sequences

Number of plies at the fixed/free ends	Width-ratio value	Stacking sequence at the fixed end	Mode number	Rotational velocity (in rad/s)				
				0	50	100	150	200
16/8	0.1	$[0]_{8s}$	1	85.88	86.39	87.94	90.45	93.84
			2	293.29	293.73	295.18	297.59	300.92
			3	630.35	630.79	632.34	634.92	638.51
		$[45/-45]_{4s}$	1	47.91	48.82	51.50	55.66	60.94
			2	164.10	164.86	167.46	171.72	177.51
			3	359.02	359.74	362.45	366.92	373.09
	0.5	$[0]_{8s}$	1	61.90	62.61	64.68	67.98	72.32
			2	253.45	254.10	256.08	259.34	263.85
			3	583.12	583.83	585.98	589.55	594.51
		$[45/-45]_{4s}$	1	33.98	35.26	38.81	44.04	50.36
			2	142.79	143.97	147.46	153.11	160.70
			3	331.55	332.80	336.55	342.72	351.16
	1	$[0]_{8s}$	1	16.28	18.72	24.50	31.66	39.33
			2	74.94	77.40	84.38	94.91	107.95
			3	178.75	181.52	189.57	202.22	218.63
		$[45/-45]_{4s}$	1	8.90	12.81	20.14	28.07	36.17
			2	41.48	45.83	56.95	71.74	88.34
			3	100.20	105.02	118.24	137.34	160.10

Table 4.18 The first three natural frequencies (in Hz) of the 400-mm-long rotating doubly tapered cantilever composite beams with 80 mm end delamination for $[0]_{8s}$ and $[-45/45]_{4s}$ stacking sequences

Number of plies at the fixed/free ends	Width-ratio value	Stacking sequence at the fixed end	Mode number	Rotational velocity (in rad/s)				
				0	50	100	150	200
16/8	0.1	$[0]_{8s}$	1	81.71	81.92	83.41	85.85	89.14
			2	228.39	228.81	230.76	234.00	238.45
			3	561.09	561.93	563.72	566.74	570.94
		$[45/-45]_{4s}$	1	45.18	45.76	48.42	52.52	57.73
			2	128.50	129.28	132.75	138.35	145.82
			3	313.14	314.06	317.31	322.65	329.97
	0.5	$[0]_{8s}$	1	59.93	60.52	62.53	65.72	69.92
			2	197.07	197.74	200.41	204.77	210.74
			3	512.00	512.84	515.40	519.66	525.55
		$[45/-45]_{4s}$	1	33.13	34.15	37.60	42.68	48.82
			2	111.37	112.39	117.08	124.48	134.14
			3	292.21	293.66	298.21	305.61	315.66
	1	$[0]_{8s}$	1	15.81	18.17	23.80	30.82	38.42
			2	58.20	61.56	70.68	83.60	98.74
			3	158.06	161.30	170.15	185.06	203.38
		$[45/-45]_{4s}$	1	8.67	12.47	19.66	27.57	35.71
			2	32.49	38.19	51.52	67.91	85.50
			3	87.09	92.87	108.22	129.49	153.98

Table 4.19 The first three natural frequencies (in Hz) of the 400-mm-long rotating doubly tapered cantilever composite beams with 160 mm end delamination for $[0]_{8s}$ and $[-45/45]_{4s}$ stacking sequences

Number of plies at the fixed/free ends	Width-ratio value	Stacking sequence at the fixed end	Mode number	Rotational velocity (in rad/s)				
				0	50	100	150	200
16/8	0.1	$[0]_{8s}$	1	70.50	71.03	72.75	75.52	79.24
			2	203.22	203.84	206.11	209.83	214.94
			3	479.14	479.20	481.56	485.45	490.86
		$[45/-45]_{4s}$	1	38.99	39.87	42.88	47.45	53.16
			2	112.54	113.61	117.68	124.14	132.63
			3	268.63	269.57	273.81	280.71	290.07
	0.5	$[0]_{8s}$	1	54.22	54.69	56.85	60.25	64.71
			2	168.87	169.41	172.48	177.78	184.83
			3	446.25	446.40	449.66	455.06	462.50
		$[45/-45]_{4s}$	1	29.72	31.05	34.72	40.06	46.47
			2	93.36	95.31	100.97	109.73	120.87
			3	250.96	252.89	258.73	268.12	280.64
	1	$[0]_{8s}$	1	14.45	16.95	22.81	30.03	37.79
			2	49.21	53.22	63.68	77.91	94.08
			3	136.94	141.13	152.88	170.35	191.65
		$[45/-45]_{4s}$	1	7.96	11.92	19.28	27.30	35.50
			2	27.12	33.88	48.59	65.09	83.95
			3	76.48	83.71	101.87	125.46	151.43

Table 4.20 The first three natural frequencies (in Hz) of the 400-mm-long rotating doubly tapered cantilever composite beams with 240 mm end delamination for $[0]_{8s}$ and $[-45/45]_{4s}$ stacking sequences

Tables 4.13 - 4.20 illustrate the natural frequencies of the 400-mm-long rotating doubly tapered cantilever composite beams with end mid-plane delamination. Tables 4.13 - 4.16 illustrate the natural frequencies of the composite beams with $[90]_{8s}$ and $[0/90]_{4s}$ stacking sequences, whereas Tables 4.17 - 4.20 illustrate the natural frequencies of the composite beams with $[0]_{8s}$ and $[-45/45]_{4s}$ stacking sequences.

From Tables 4.13 - 4.20, it is observed that the rotating doubly tapered composite beams with $[0]_{8s}$ stacking sequence have the highest natural frequencies, followed by the natural frequencies of the rotating doubly tapered composite beams with $[0/90]_{4s}$ stacking sequence. The natural frequencies of the doubly tapered beams with $[90]_{8s}$ and $[-45/45]_{4s}$ stacking sequences are almost the same, but the latter have slightly higher natural frequencies. The composite beams with $[90]_{8s}$ stacking sequence have the lowest natural frequencies. For instance, for $[-45/45]_{4s}$ stacking

sequence the 1st, 2nd and 3rd natural frequencies of the rotating doubly tapered composite beams with 240 mm end delamination and with width-ratio of value 0.1 are 42.88 Hz, 117.68 Hz and 273.81 Hz, respectively, at 100 rad/s rotational velocity, whereas for $[90]_{8s}$ stacking sequence the 1st, 2nd and 3rd natural frequencies of the rotating doubly tapered composite beams with 240 mm end delamination and with width-ratio of value 0.1 are 41.48 Hz, 113.56 Hz and 261.26 Hz, respectively, at 100rad/s rotational velocity. Similar observations were noted for the rotating thickness-tapered cantilever composite beams in the previous section.

It is also observed that the natural frequencies of the rotating doubly tapered composite beams increase with the decrease in the width-ratio value. For instance, in Tables 4.20 for $[0]_{8s}$ stacking sequence the 1st natural frequencies of the doubly tapered stationary cantilever composite beams with 240 mm end delamination and with width-ratio of values 0.1 and 1 are 70.5 Hz and 14.45 Hz, respectively.

Figure 4.5 illustrates the natural frequencies of the 400-mm-long rotating doubly tapered cantilever composite beams with 40 mm and 240 mm end delaminations and with 8 plies dropped-off for three different width-ratio values and for $[0/90]_{4s}$ stacking sequence.

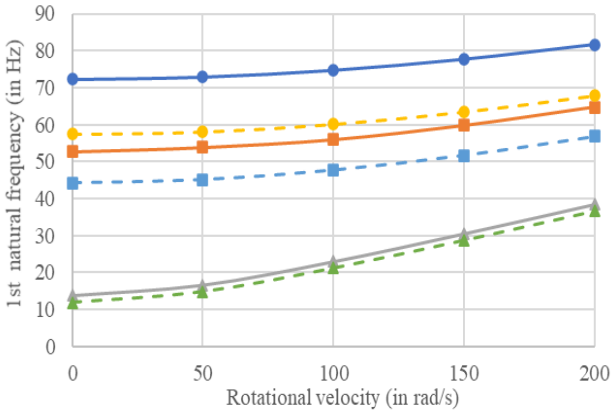

Figure 4.5 (a) 1st natural frequencies of the rotating doubly tapered cantilever composite beams with 40 mm and 240 mm end delaminations and with 8 plies dropped-off for $[0/90]_{4s}$ stacking sequence

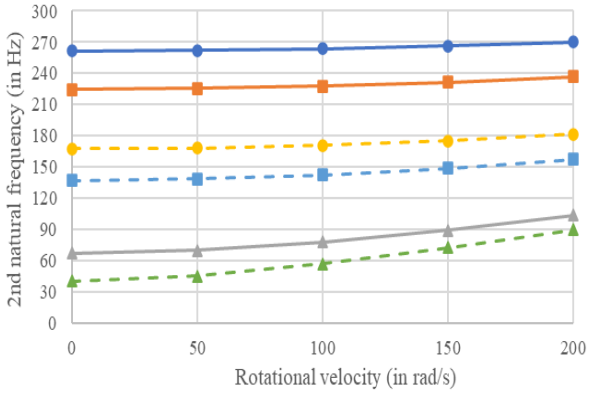

Figure 4.5 (b) 2nd natural frequencies of the rotating doubly tapered cantilever composite beams with 40 mm and 240 mm end delaminations and with 8 plies dropped-off for $[0/90]_{4s}$ stacking sequence

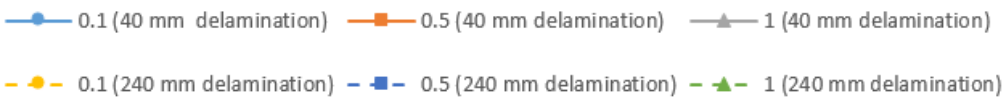

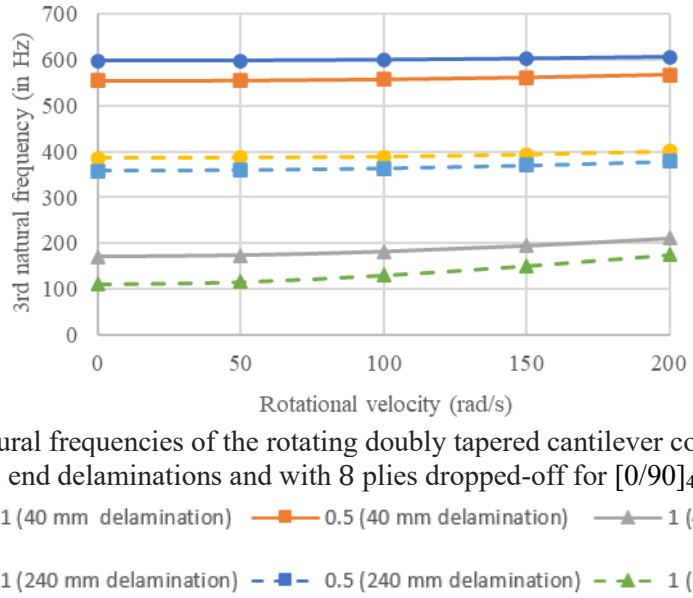

Figure 4.5 (c) 3rd natural frequencies of the rotating doubly tapered cantilever composite beams with 40 mm and 240 mm end delaminations and with 8 plies dropped-off for $[0/90]_{4s}$ stacking sequence

Figure 4.5 The first three natural frequencies of the 400-mm-long rotating doubly tapered cantilever composite beams with 40 mm and 240 mm end delaminations and with 8 plies dropped-off for $[0/90]_{4s}$ stacking sequence and for width-ratio values of 0.1, 0.5 and 1

From Figure 4.5, it is observed that the natural frequencies of the doubly tapered cantilever composite beams with 40 mm end delamination are higher than that of the rotating doubly tapered cantilever beams with 240 mm end delamination. The highest and the lowest natural frequencies are observed for the rotating doubly tapered composite beams with width-ratio of values 0.1 and 1, respectively.

In Figure 4.5, it is shown that the natural frequencies of the rotating doubly tapered composite beam with higher width-ratio value are more sensitive to the rotational velocity as compared to that of the doubly tapered beam with lower width-ratio value. For instance, in Figure 4.5 (a) the percentage increases in the fundamental frequencies of the rotating doubly tapered composite beams with 40 mm end delamination and with width-ratio of values 0.1, 0.5 and 1 due to the change in the rotational velocity from 0 rad/s to 200 rad/s are 13.3%, 22.7% and 180.1%, respectively, for $[0/90]_{4s}$ stacking sequence.

From Figure 4.5, it is also observed that the natural frequencies of the composite beam with the lower width-ratio value are more sensitive to the delamination length as compared to that of the beam with the higher width-ratio value. For instance, in Figure 4.5 (a) for $[0/90]_{4s}$ stacking sequence the percentage differences between the fundamental frequencies of the rotating doubly

tapered composite beams with 40 mm and 240 mm end delaminations are 7.46%, 14.84%, and 36.78% for 1, 0.5 and 0.1 width-ratios values, respectively, at 100 rad/s rotational velocity.

Figure 4.6 illustrates the percentage increases in the first three natural frequencies of the 400-mm-long rotating composite beams with 240 mm end delamination w.r.t. that of the first three natural frequencies of the 400-mm-long stationary composite beam with 240 mm end delamination. The analysis is conducted for three different width-ratio values and for $[0/90]_{4s}$ stacking sequence.

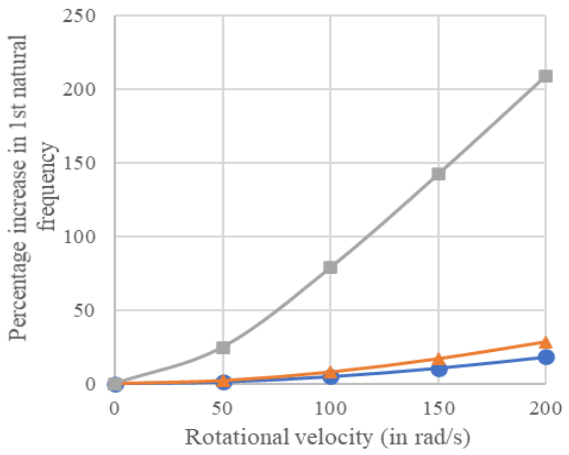

Figure 4.6 (b) Percentage increase in the 1st natural frequency vs rotational velocity

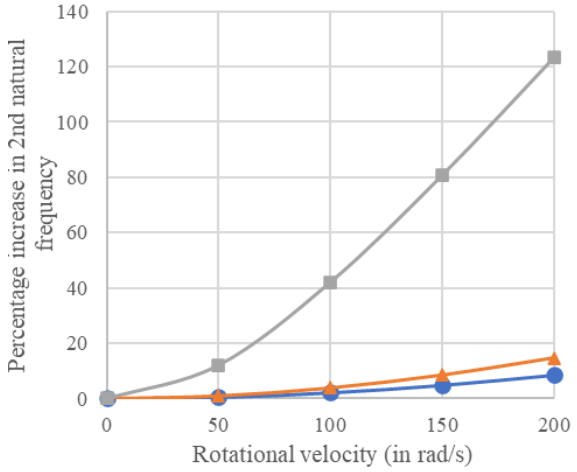

Figure 4.6 (b) Percentage increase in the 2nd natural frequency vs rotational velocity

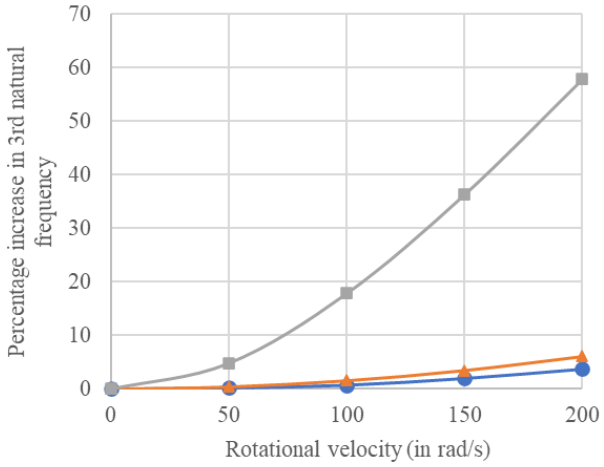

Figure 4.6 (c) Percentage increase in the 3rd natural frequency vs rotational velocity

Figure 4.6 The first three natural frequencies of the 400-mm-long rotating doubly tapered cantilever composite beams with 40 mm and 240 mm end delaminations and with 8 plies dropped-off for $[0/90]_{4s}$ stacking sequence and for width-ratio values of 0.1, 0.5 and 1

From Figure 4.6, it is observed that the natural frequencies of the 400-mm-long rotating doubly tapered cantilever composite beam with higher width-ratio value are more sensitive to the rotational velocity as compared to that of the composite beam with lower width-ratio value. In Figure 4.6 (a), the percentage increases in the 1st natural frequencies of the doubly tapered composite beams with width-ratio of value 0.1, 0.5, and 1 due to the increase in the rotational velocity from 0 rad/s to 200 rad/s are 18.1%, 28.4% and 208.05%, respectively, for $[0/90]_{4s}$ stacking sequence.

In Table 4.20, for $[-45/45]_{4s}$ stacking sequence the percentage increases in the 1st natural frequencies of the rotating doubly tapered composite beams with 240 mm end delamination and with width-ratio of values 0.1, 0.5 and 1 due to the increase in the rotational velocity from 0 rad/s to 200 rad/s are 36.5%, 60.42%, and 345.9%, respectively, whereas in Table 4.20, for $[0]_{8s}$ stacking sequence the percentage increases in the 1st natural frequencies of the rotating doubly tapered composite beams with 240 mm end delamination and with width-ratio of values 0.1, 0.5 and 1 due to the increase in the rotational velocity from 0 rad/s to 200 rad/s are 12.3%, 19.3%, and 161.5%, respectively.

4.4 Influence of the double taper ratio on the natural frequencies of rotating doubly tapered composite beams with end mid-plane delamination

In this section, the influence of the double tapering on the natural frequencies of the rotating doubly tapered cantilever composite beams with end mid-plane delamination is investigated. There are a total of 16 plies at the fixed end of the beam. The study is conducted for $[0]_{8s}$ and $[90]_{8s}$ stacking sequences at the fixed end of the beam and for 3 different delamination lengths. The mechanical properties of the composite material were given in Table 4.1, whereas the interface parameters were given in Table 4.2. The geometric properties of the beam were given in Table 4.3. The number of plies, thickness of the beam and width of the beam mentioned in Table 4.3 refer to the number of plies, thickness on the thick side (at the fixed end) and width on the thick side of the doubly tapered beam, respectively. The double taper ratio used in this analysis to study the influence of the double tapering in the composite beams is described as:

Double taper ratio = $\frac{s}{r_b}$

where "*s*" is number of plies dropped-off and "r_b" is width-ratio.

With the increase in the double taper ratio, the beam becomes narrower and thinner. Table 4.21 illustrates the width-ratio and the number of plies at the free end of the beam corresponding to the double taper ratio.

Number of plies at the free end	Width-ratio (r_b)	Double taper ratio
14	0.8	2.5
12	0.6	6.6
10	0.4	15
8	0.2	40

Table 4.21 The width-ratio values and the number of plies at the free end corresponding to the double taper ratio

The natural frequencies of the 400-mm-long rotating doubly tapered cantilever composite beams with end delamination of different lengths are obtained from the modal analysis and are presented in Tables 4.22 - 4.27. The graphical representations of the results are shown in Figures 4.7 and 4.8.

Number of plies at the fixed/free ends	Width-ratio	Double taper ratio	Mode number	Rotational velocity (in rad/s)				
				0	50	100	150	200
16/14	0.8	2.5	1	28.93	30.31	34.11	39.57	46.07
			2	147.46	148.75	152.57	158.73	166.99
			3	364.98	366.48	370.96	378.29	388.29
16/12	0.6	6.6	1	29.78	31.16	34.94	40.39	46.88
			2	142.98	144.25	148.04	154.16	162.36
			3	346.66	348.11	352.48	359.62	369.36
16/10	0.4	15	1	34.08	35.32	38.78	43.89	50.09
			2	145.15	146.29	149.67	155.16	162.55
			3	334.48	335.75	339.57	345.83	354.40
16/8	0.2	40	1	40.69	41.77	44.84	49.50	55.29
			2	146.29	147.25	150.29	155.23	161.90
			3	324.99	325.94	329.19	334.52	341.85

Table 4.22 Natural frequencies (in Hz) of the 400-mm-long rotating doubly tapered cantilever composite beams with 80 mm end delamination for $[90]_{8s}$ stacking sequence

Number of plies at the fixed/free ends	Width-ratio	Double taper ratio	Mode number	Rotational velocity (in rad/s)				
				0	50	100	150	200
16/14	0.8	2.5	1	26.86	28.27	32.10	37.58	44.08
			2	111.73	113.64	119.16	127.81	138.96
			3	332.34	334.06	339.18	347.53	358.83
16/12	0.6	6.6	1	28.66	29.92	33.62	38.98	45.35
			2	110.42	112.20	117.48	125.78	136.50
			3	314.83	315.68	320.61	328.62	339.49
16/10	0.4	15	1	32.72	33.77	37.16	42.17	48.25
			2	111.07	112.56	117.61	125.01	134.69
			3	299.84	300.49	312.28	319.41	329.20
16/8	0.2	40	1	38.77	39.84	42.83	47.36	53.00
			2	114.45	115.85	119.83	126.24	134.69
			3	288.21	289.53	293.32	299.57	308.10

Table 4.23 Natural frequencies (in Hz) of the 400-mm-long rotating doubly tapered cantilever composite beams with 160 mm end delamination for $[90]_{8s}$ stacking sequence

Number of plies at the fixed/free ends	Width-ratio	Double taper ratio	Mode number	Rotational velocity (in rad/s)				
				0	50	100	150	200
16/14	0.8	2.5	1	23.10	24.71	29.00	34.97	41.88
			2	97.09	99.32	105.75	115.63	128.13
			3	272.37	274.85	282.19	293.95	309.52
16/12	0.6	6.6	1	25.57	27.06	31.08	36.78	43.48
			2	95.96	98.04	104.03	113.28	125.02
			3	261.73	263.97	270.58	281.21	295.35
16/10	0.4	15	1	29.10	30.33	34.02	39.39	45.82
			2	96.02	97.86	103.31	111.76	122.57
			3	253.50	254.07	259.88	269.25	281.74
16/8	0.2	40	1	34.11	35.29	38.59	43.52	49.55
			2	99.12	100.76	105.49	112.91	122.51
			3	244.92	246.59	251.51	259.49	270.18

Table 4.24 Natural frequencies (in Hz) of the 400-mm-long rotating doubly tapered cantilever composite beams with 240 mm end delamination for $[90]_{8s}$ stacking sequence

Number of plies at the fixed/free ends	Width-ratio	Double taper ratio	Mode number	Rotational velocity (in rad/s)				
				0	50	100	150	200
16/14	0.8	2.5	1	54.62	55.36	57.54	60.98	65.47
			2	277.67	278.36	280.41	283.80	288.49
			3	686.57	687.38	689.78	693.77	699.30
16/12	0.6	6.6	1	56.33	57.07	59.23	62.65	67.12
			2	269.88	270.56	272.59	275.95	280.59
			3	653.24	654.02	656.36	660.23	665.60
16/10	0.4	15	1	64.04	64.70	66.68	69.82	73.99
			2	269.76	270.35	272.20	275.25	279.47
			3	626.76	627.42	629.47	632.87	637.59
16/8	0.2	40	1	76.49	77.06	78.78	81.56	85.28
			2	275.53	275.99	277.62	280.31	284.04
			3	608.12	608.54	610.28	613.17	617.19

Table 4.25 Natural frequencies (in Hz) of the 400-mm-long rotating doubly tapered cantilever composite beams with 80 mm end delamination for $[0]_{8s}$ stacking sequence

Number of plies at the fixed/free ends	Width-ratio	Double taper ratio	Mode number	Rotational velocity (in rad/s)				
				0	50	100	150	200
16/14	0.8	2.5	1	50.78	51.53	53.74	57.21	61.73
			2	210.77	211.78	214.80	219.73	226.44
			3	626.86	627.77	630.51	635.05	641.35
16/12	0.6	6.6	1	54.16	54.67	56.79	60.14	64.53
			2	207.29	208.09	210.98	215.70	222.15
			3	591.12	591.13	593.72	598.11	604.19
16/10	0.4	15	1	61.49	62.13	64.05	67.11	71.16
			2	208.84	209.67	212.21	216.39	222.11
			3	563.03	563.87	566.27	570.14	575.57
16/8	0.2	40	1	73.21	73.74	75.41	78.11	81.71
			2	214.61	215.19	217.37	220.95	225.87
			3	537.30	537.82	539.89	543.31	548.07

Table 4.26 Natural frequencies (in Hz) of the 400-mm-long rotating doubly tapered cantilever composite beams with 160 mm end delamination for $[0]_{8s}$ stacking sequence

Number of plies at the fixed/free ends	Width-ratio	Double taper ratio	Mode number	Rotational velocity (in rad/s)				
				0	50	100	150	200
16/14	0.8	2.5	1	44.45	45.31	47.79	51.67	56.63
			2	185.63	186.79	190.22	195.80	203.33
			3	516.04	517.33	521.19	527.52	536.25
16/12	0.6	6.6	1	48.35	49.14	51.47	55.13	59.86
			2	181.49	182.64	185.92	191.38	198.56
			3	494.20	495.33	498.85	505.04	512.95
16/10	0.4	15	1	54.78	55.51	57.62	60.97	65.35
			2	181.52	182.53	185.51	190.36	196.95
			3	475.90	476.99	480.11	485.28	492.40
16/8	0.2	40	1	64.88	65.12	66.96	69.94	73.88
			2	187.62	188.24	190.82	195.03	200.77
			3	462.23	462.66	465.29	469.64	475.65

Table 4.27 Natural frequencies (in Hz) of the 400-mm-long rotating doubly tapered cantilever composite beams with 240 mm end delamination for $[0]_{8s}$ stacking sequence

In sections 4.2 and 4.3, it was observed that the 2nd and 3rd natural frequencies of the composite beams decrease with the increase in the thickness-tapering and increase with the increase in the width-tapering. In the present study the combined effect of both the effects is noticeable.

From Tables 4.22 - 4.27, it is observed that with the increase in the double tapering or with the increase in the double taper ratio value the 2nd natural frequency of the doubly tapered composite beam remains almost the same, whereas the 3rd natural frequency decreases and the 1st natural frequency increases for any considered rotational velocity. For instance, in Table 4.27 for $[0]_{8s}$ stacking sequence and at 50 rad/s rotational velocity, the 1st, 2nd and 3rd natural frequencies of the rotating doubly tapered composite beam with 240 mm end delamination for double taper ratio of value 2.5 are 45.31 Hz, 186.63 Hz and 516.04 Hz, respectively, whereas the 1st, 2nd and 3rd natural frequencies of the considered beam for double taper ratio of value 40 are 65.12 Hz, 188.24 Hz and 462.66 Hz, respectively.

The influences of the rotational velocity and the double taper ratio on the 1st and 3rd natural frequencies of the 400-mm-long end delaminated doubly tapered composite beams are

shown in Figures 4.7 and 4.8, respectively. The influences of the rotational velocity and the double taper ratio on the 2nd natural frequency of the end delaminated doubly tapered composite beams are shown and compared to that of the 2nd natural frequency of mid-span delaminated doubly tapered beams in Figures 4.13 and 4.14 of section 4.6.

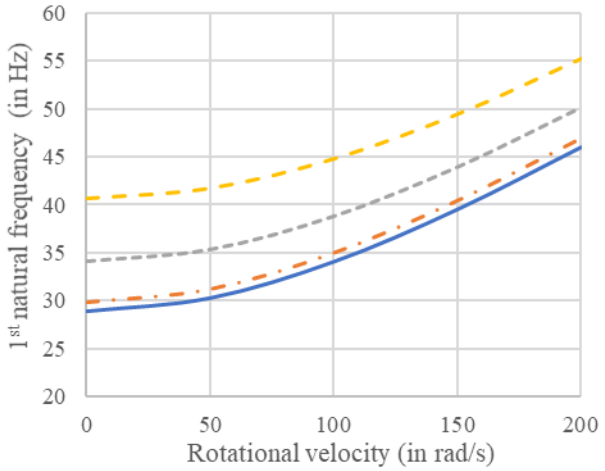

Figure 4.7 (a) 1st natural frequencies of the rotating doubly tapered cantilever composite beams with 80 mm end delamination and with $[90]_{8s}$ stacking sequence

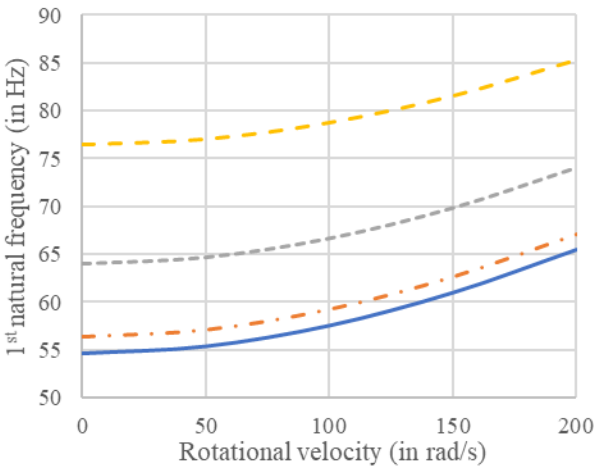

Figure 4.7 (b) 1st natural frequencies of the rotating doubly tapered cantilever composite beams with 80 mm end delamination and with $[0]_{8s}$ stacking sequence

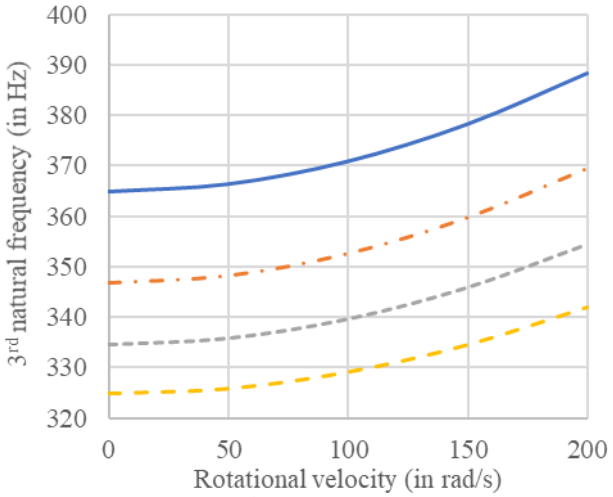

Figure 4.7 (c) 3rd natural frequencies of the rotating doubly tapered cantilever composite beams with 80 mm end delamination and with $[90]_{8s}$ stacking sequence

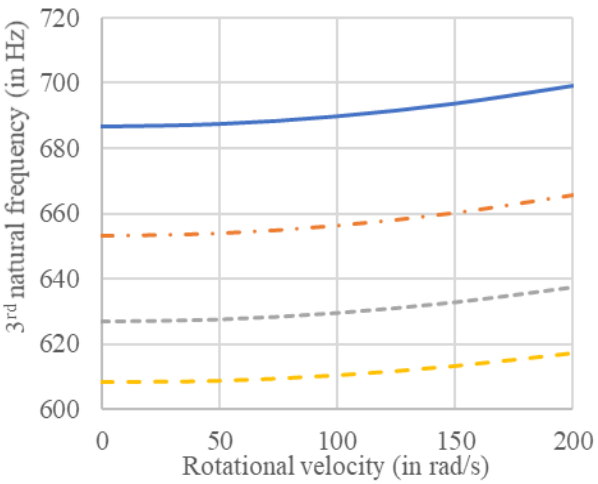

Figure 4.7 (d) 3rd natural frequencies of the rotating doubly tapered cantilever composite beams with 80 mm end delamination and with $[0]_{8s}$ stacking sequence

Figure 4.7 1st and 3rd natural frequencies (in Hz) of the 400-mm-long rotating doubly tapered cantilever composite beams with 80 mm end delamination and with $[90]_{8s}$ and $[0]_{8s}$ stacking sequences for different double taper ratio values at various rotational velocities

Figure 4.7 illustrates the 1st and 3rd natural frequencies of the 400-mm-long rotating doubly tapered cantilever composite beams with 80 mm end delamination and with different double taper ratio values for $[90]_{8s}$ and $[0]_{8s}$ stacking sequences.

In Figures 4.7, a slight increase is seen in the 1st and 3rd natural frequencies of the rotating doubly tapered cantilever composite beams up to 50 rad/s rotational velocity, but with further increase in the rotational velocity a comparatively sharper increase is seen in the 1st and 3rd natural frequencies. With the increase in the rotational velocity a higher increase is observed in the 1st and 3rd natural frequencies of the composite beams with $[90]_{8s}$ stacking sequence in comparison to that of the beams with $[0]_{8s}$ stacking sequence. For instance, in Figure 4.7 (a) and (c) for $[90]_{8s}$ stacking sequence the percentage increases in the 1st and 3rd natural frequencies of the doubly tapered composite beam with 80 mm end delamination and with double taper ratio of value 40 due to the increase in the rotational velocity from 0 rad/s to 50 rad/s are 2.6% and 0.3%, respectively, whereas the percentage increases in the 1st and 3rd natural frequencies of the considered beam due to the increase in the rotational velocity from 0 rad/s to 100 rad/s are 10.1% and 1.4%, respectively.

In Figures 4.7 (b) and (d), for $[0]_{8s}$ stacking sequence the percentage increases in the 1st and 3rd natural frequencies of the doubly tapered composite beam with 80 mm end delamination and with double taper ratio of value 40 due to the increase in the rotational velocity from 0 rad/s to 50 rad/s are 0.7% and 0.06%, respectively, whereas the percentage increases in the 1st and 3rd natural frequencies of the considered beam due to the increase in the rotational velocity from 0 rad/s to 100 rad/s are 2.9% and 0.35%, respectively.

In Figures 4.7 (a) and (b), the beam with the highest double taper ratio value has the highest 1st natural frequency, whereas the beam with the lowest double taper ratio value has the lowest 1st natural frequency. In Figures 4.7 (c) and (d), the beam with the lowest double taper ratio value has the highest 3rd natural frequency, whereas the beam with the highest double taper ratio value has the lowest 3rd natural frequency. For instance, in Figure 4.7 (b) for $[0]_{8s}$ stacking sequence and at 100 rad/s rotational velocity, the highest and the lowest 1st natural frequencies of 78.78 Hz and 57.54 Hz, respectively, are observed for the composite beams with double taper ratio of values 40 and 2.5, respectively, whereas for the same stacking sequence and at the same rotational velocity

the highest and the lowest 3rd natural frequencies of 689.89 Hz and 610.28 Hz, respectively, are observed for the composite beams with double taper ratio of values 2.5 and 40, respectively.

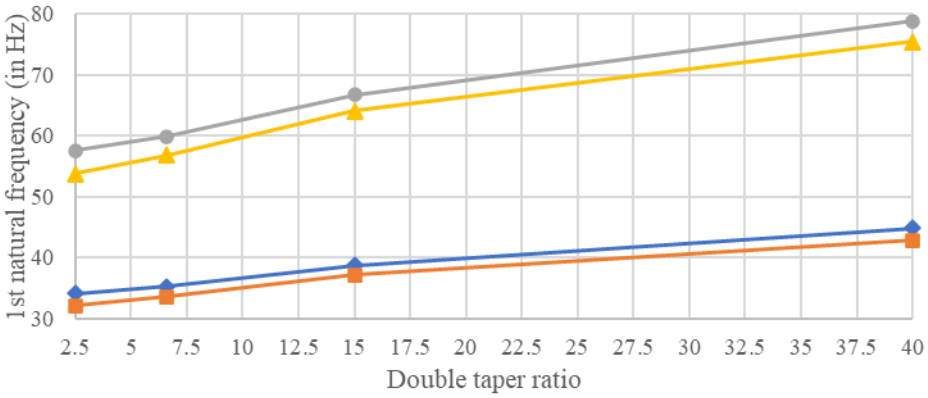

Figure 4.8 (a) The influence of the double taper ratio on the 1st natural frequencies of the rotating doubly tapered cantilever composite beams with end delaminations of lengths 80 mm and 160 mm for $[0]_{8s}$ and $[90]_{8s}$ stacking sequences at 100 rad/s rotational velocity

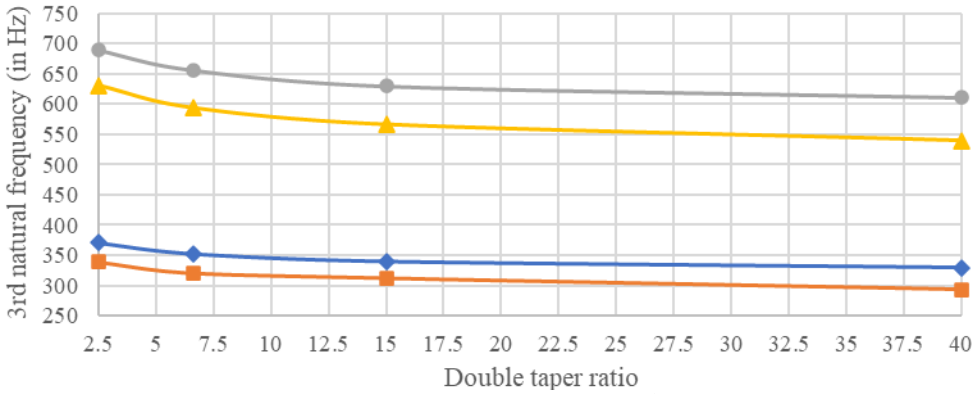

Figure 4.8 (b) The influence of the double taper ratio on the 3rd natural frequencies of the rotating doubly tapered cantilever composite beams with end delaminations of lengths 80 mm and 160 mm for $[0]_{8s}$ and $[90]_{8s}$ stacking sequences at 100 rad/s rotational velocity

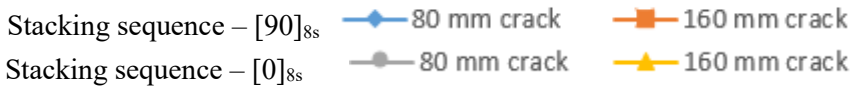

Figure 4.8 The influence of the double taper ratio on the 1st and 3rd natural frequencies of the 400-mm-long rotating doubly tapered cantilever composite beams with end delaminations of lengths 80 mm and 160 mm for $[0]_{8s}$ and $[90]_{8s}$ stacking sequence at 100 rad/s rotational velocity

Figure 4.8 illustrates the influence of the double taper ratio on the natural frequencies of the 400-mm-long rotating doubly tapered cantilever composite beams with end delaminations of lengths 80 mm and 160 mm for $[90]_{8s}$ and $[0]_{8s}$ stacking sequences at 100 rad/s rotational velocity.

From Figure 4.8, it is observed that with the increase in the double taper ratio value the 1st natural frequency of the beam increases, whereas the 3rd natural frequency of the beam decreases. The 1st and 3rd natural frequencies of the composite beam with $[0]_{8s}$ stacking sequence are higher than that of the composite beam with $[90]_{8s}$ stacking sequence. It is also observed that the 1st and 3rd natural frequencies of the beam with 160 mm end delamination are lower than that of the beam with 80 mm end delamination.

In Figure 4.8 (a) and (b), with the increase in the double taper ratio value from 2.5 to 40 the 1st natural frequencies of the rotating doubly tapered composite beams with 80 mm and 160 mm end delaminations increase by 31.4% and 33.4%, respectively, whereas the 3rd natural frequencies of the considered beams decrease by 12.6% and 9.3%, respectively, for $[90]_{8s}$ stacking sequence. For $[0]_{8s}$ stacking sequence, the 1st natural frequencies of the doubly tapered composite beams with 80 mm and 160 mm end delamination increase by 36.9% and 40.3%, respectively, whereas the 3rd natural frequencies of the considered beams decrease by 13.0% and 18.2%, respectively, due to the increase in the double taper ratio value from 2.5 to 40.

Figure 4.9 illustrates the first three mode shapes of the rotating doubly tapered composite beam with 240 mm end delamination and with double taper ratio of value 15, whereas Figure 4.10 illustrates the first three mode shapes of the rotating doubly tapered composite beam with 240 mm end delamination and with double taper ratio of value 2.5. The analysis is conducted for $[90]_{8s}$ stacking sequence at 100 rad/s rotational velocity. The points of inflection of the mode shapes are presented in Table 4.28.

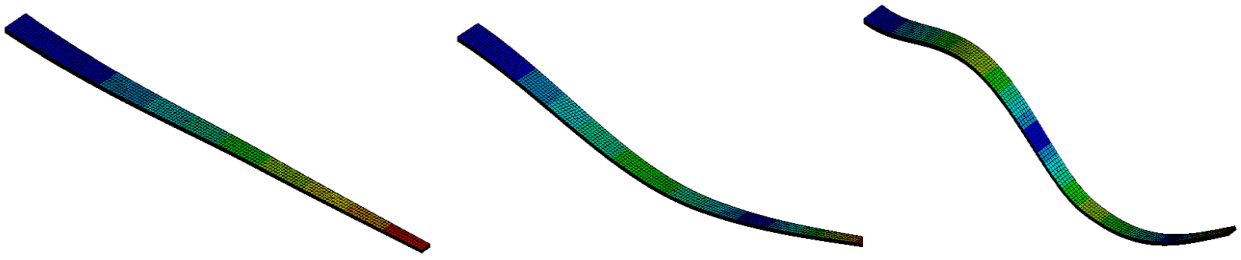

1st Mode shape 34.02 Hz 2nd Mode shape 103.31 Hz 3rd Mode shape 259.88 Hz

Figure 4.9 Pictorial representation of the first three mode shapes of the 400-mm-long rotating doubly tapered cantilever composite beam with double taper ratio of value 15 and with 240 mm end delamination for $[90]_{8s}$ stacking sequence and at 100 rad/s rotational velocity

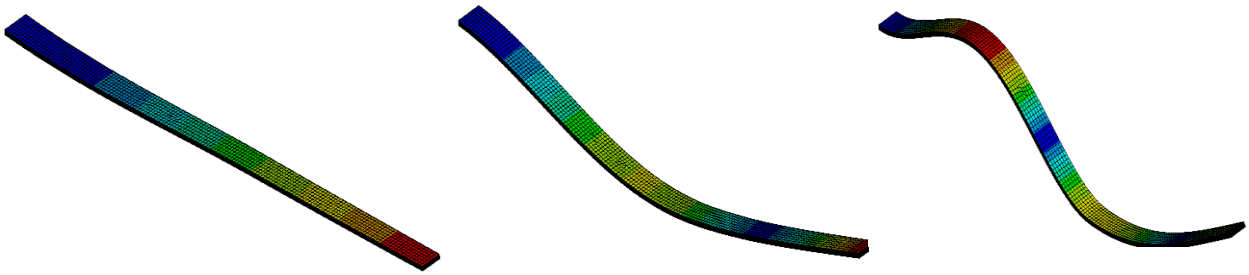

1st Mode shape 29.00 Hz 2nd Mode shape 105.75 Hz 3rd Mode shape 282.19 Hz

Figure 4.10 Pictorial representation of the first three mode shapes of the 400-mm-long rotating doubly tapered cantilever composite beam with double taper ratio of value 2.5 and with 240 mm end delamination for $[90]_{8s}$ stacking sequence and at 100 rad/s rotational velocity

Mode	Points of inflection of the mode shapes presented in Figure 4.9	Points of inflection of the mode shapes presented in Figure 4.10
1st Mode	0 mm	0 mm
2nd Mode	0 mm, 185 mm	0mm, 185mm
3rd Mode	0 mm, 110 mm, 245 mm	0 mm, 110 mm, 245 mm

Table 4.28 The points of inflection of the first three mode shapes of the rotating doubly tapered cantilever composite beam shown in Figures 4.9 and 4.10

From Table 4.28 and Figures 4.9 and 4.10, it is observed that the rotating doubly tapered composite beams with the same end delamination length, stacking sequence and rotational velocity have similar points of inflection and mode shapes irrespective of their double taper ratio values.

4.5 Influence of the double taper ratio on the natural frequencies rotating doubly tapered composite beams with mid-span mid-plane delamination

In this section, the influence of the double taper ratio on the natural frequencies of the rotating doubly tapered cantilever composite beams with mid-span mid-plane delamination is investigated for $[0]_{8s}$ and $[90]_{8s}$ stacking sequences. There are a total of 16 plies at the fixed end of the beam. The number of plies at the free end of the beams and width-ratio corresponding to the double taper ratio of the composite beams are given in Table 4.21. The mechanical properties of the composite material were given in Table 4.1, whereas the interface parameters were given in Table 4.2. The geometric properties of the beam were given in Table 4.3. The number of plies, thickness of the beam and width of the beam mentioned in Table 4.3 refer to the number of plies, thickness on the thick side (at the fixed end) and width on the thick side of the doubly tapered beam, respectively.

The natural frequencies of the 400-mm-long mid-span delaminated rotating doubly tapered cantilever composite beams obtained from the modal analysis are presented in Tables 4.29 - 4.34 for $[90]_{8s}$ and $[0]_{8s}$ stacking sequences. The graphical representations of the results are shown in Figures 4.11 and 4.12.

Number of plies at the fixed/free ends	Width-ratio	Double taper ratio	Mode number	Rotational velocity (in rad/s)				
				0	50	100	150	200
16/14	0.8	2.5	1	27.06	28.55	32.63	38.43	45.25
			2	155.48	156.79	160.76	167.17	170.39
			3	383.99	384.84	389.72	397.60	408.36
16/12	0.6	6.6	1	29.80	31.20	35.05	40.62	47.25
			2	152.40	153.67	157.45	163.51	171.66
			3	364.79	366.36	370.97	378.32	388.46
16/10	0.4	15	1	34.28	35.54	39.06	44.27	50.60
			2	150.81	151.99	155.49	161.15	168.75
			3	347.34	348.72	352.88	359.67	368.93
16/8	0.2	40	1	40.29	41.42	44.60	49.40	55.35
			2	154.14	155.23	158.43	163.48	170.16
			3	355.66	356.98	360.77	366.69	374.51

Table 4.29 Natural frequencies (in Hz) of the 400-mm-long rotating doubly tapered cantilever composite beam with 80 mm mid-span mid-plane delamination for $[90]_{8s}$ stacking sequence

Number of plies at the fixed/free ends	Width-ratio	Double taper ratio	Mode number	Rotational velocity (in rad/s)				
				0	50	100	150	200
16/14	0.8	2.5	1	25.91	27.50	31.77	37.77	44.75
			2	150.53	151.97	156.21	163.00	170.34
			3	290.56	292.84	299.54	310.32	324.75
16/12	0.6	6.6	1	28.54	30.03	34.08	39.87	46.70
			2	147.29	148.67	152.76	159.31	168.00
			3	278.57	280.67	286.87	296.89	310.33
16/10	0.4	15	1	30.22	31.68	35.67	41.43	48.24
			2	134.01	135.47	139.66	146.34	155.12
			3	249.24	251.35	257.27	266.83	279.63
16/8	0.2	40	1	37.88	39.12	42.54	47.66	53.94
			2	146.03	147.60	151.14	156.52	164.38
			3	259.06	260.82	265.53	273.39	284.08

Table 4.30 Natural frequencies (in Hz) of the 400-mm-long rotating doubly tapered cantilever composite beam with 160 mm mid-span mid-plane delamination for $[90]_{8s}$ stacking sequence

Number of plies at the fixed/free ends	Width-ratio	Double taper ratio	Mode number	Rotational velocity (in rad/s)				
				0	50	100	150	200
16/14	0.8	2.5	1	23.73	25.47	30.11	36.49	43.77
			2	134.80	136.48	141.67	149.84	160.46
			3	258.70	260.68	267.48	278.44	293.02
16/12	0.6	6.6	1	25.85	27.52	31.97	38.18	45.37
			2	131.01	132.74	137.78	145.66	155.92
			3	248.81	250.14	256.57	266.79	280.45
16/10	0.4	15	1	29.22	29.86	33.28	39.49	46.68
			2	118.80	121.00	126.06	133.99	144.22
			3	223.11	224.96	231.15	241.08	254.29
16/8	0.2	40	1	33.55	34.89	38.79	44.47	51.28
			2	129.54	130.82	135.09	142.02	150.77
			3	233.48	234.10	239.19	247.58	258.54

Table 4.31 Natural frequencies (in Hz) of the 400-mm-long rotating doubly tapered cantilever composite beam with 240 mm mid-span mid-plane delamination for $[90]_{8s}$ stacking sequence

Number of plies at the fixed/free ends	Width-ratio	Double taper ratio	Mode number	Rotational velocity (in rad/s)				
				0	50	100	150	200
16/14	0.8	2.5	1	51.02	51.83	54.19	57.90	62.71
			2	293.31	294.01	296.14	299.66	304.51
			3	720.58	721.38	723.98	728.29	734.27
16/12	0.6	6.6	1	56.29	57.05	59.25	62.74	67.30
			2	287.82	288.49	290.51	293.85	298.45
			3	685.58	686.43	688.87	692.91	698.52
16/10	0.4	15	1	60.33	61.05	63.19	66.58	71.04
			2	263.92	264.48	266.50	269.83	274.42
			3	605.04	605.79	608.15	612.07	617.51
16/8	0.2	40	1	76.43	76.69	78.46	81.31	85.12
			2	289.03	289.79	291.47	294.24	298.08
			3	627.00	628.96	630.88	634.09	638.54

Table 4.32 Natural frequencies (in Hz) of the 400-mm-long rotating doubly tapered cantilever composite beam with 80 mm mid-span mid-plane delamination for $[0]_{8s}$ stacking sequence

Number of plies at the fixed/free ends	Width-ratio	Double taper ratio	Mode number	Rotational velocity (in rad/s)				
				0	50	100	150	200
16/14	0.8	2.5	1	49.01	49.84	52.33	56.22	61.24
			2	284.53	285.25	287.53	291.29	296.47
			3	548.44	549.07	552.65	558.59	566.77
16/12	0.6	6.6	1	53.94	54.75	57.08	60.76	65.54
			2	278.17	278.90	281.10	284.73	289.72
			3	525.00	526.11	529.44	534.93	542.53
16/10	0.4	15	1	57.03	57.79	60.09	63.71	68.44
			2	252.96	253.76	256.03	259.76	264.87
			3	469.91	470.68	473.86	479.12	486.38
16/8	0.2	40	1	71.78	72.22	74.14	77.23	81.34
			2	275.85	276.18	278.09	281.26	285.61
			3	488.93	489.26	491.84	496.11	502.03

Table 4.33 Natural frequencies (in Hz) of the 400-mm-long rotating doubly tapered cantilever composite beam with 160 mm mid-span mid-plane delamination for $[0]_{8s}$ stacking sequence

Number of plies at the fixed/free ends	Width-ratio	Double taper ratio	Mode number	Rotational velocity (in rad/s)				
				0	50	100	150	200
16/14	0.8	2.5	1	51.29	52.09	48.52	52.78	58.18
			2	293.74	294.42	258.16	262.78	269.09
			3	488.27	489.43	493.06	499.10	507.41
16/12	0.6	6.6	1	48.91	49.75	52.36	56.43	61.64
			2	247.40	248.31	251.04	255.51	261.61
			3	469.29	469.73	473.15	478.79	486.57
16/10	0.4	15	1	51.35	52.23	54.82	58.85	64.04
			2	224.51	225.98	228.74	233.25	239.39
			3	418.99	421.07	424.41	429.90	437.46
16/8	0.2	40	1	63.41	63.99	66.21	69.74	74.37
			2	243.96	244.93	247.25	251.06	256.28
			3	437.75	439.84	442.58	447.10	453.36

Table 4.34 Natural frequencies (in Hz) of the 400-mm-long rotating doubly tapered cantilever composite beam with 240 mm mid-span mid-plane delamination for $[0]_{8s}$ stacking sequence

From Tables 4.29 - 4.34, it is observed that the 1st natural frequency of the 400-mm-long rotating doubly tapered composite beam with mid-span delamination increases with the increase in the double taper ratio value. The 2nd and 3rd natural frequencies of the considered beam decrease until the double taper ratio reaches the value of 15, but with further increase in the double taper ratio a slight increase is observed in the 2nd and 3rd natural frequencies. For instance, in Table 4.34 for $[0]_{8s}$ stacking sequence and at 50 rad/s rotational velocity, the 1st, 2nd and 3rd natural frequencies of the doubly tapered composite beam with 240 mm mid-span delamination and with double taper ratio of value 2.5 are 49.84 Hz, 285.25 Hz and 549.07 Hz, respectively, whereas at

the same rotational velocity the 1st, 2nd and 3rd natural frequencies of the considered beam with double taper ratio of value 15 are 57.79 Hz, 253.76 Hz and 470.68 Hz, respectively.

The influences of the rotational velocity and the double taper ratio on the 1st and 3rd natural frequencies of the mid-span delaminated doubly tapered composite beams are shown in Figures 4.11 and 4.12, respectively. The influences of the rotational velocity and the double taper ratio on the 2nd natural frequencies of the mid-span delaminated doubly tapered composite beams are shown and compared with that of the 2nd natural frequency of the end delaminated doubly tapered composite beams in Figures 4.13 and 4.14 of section 4.6.

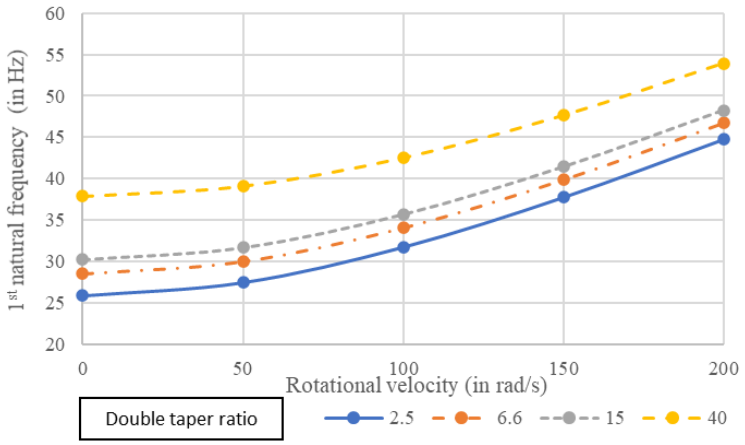

Figure 4.11 (a) 1st natural frequencies of the 400-mm-long rotating doubly tapered cantilever composite beams with 240 mm mid-span delamination for $[90]_{8s}$ stacking sequence

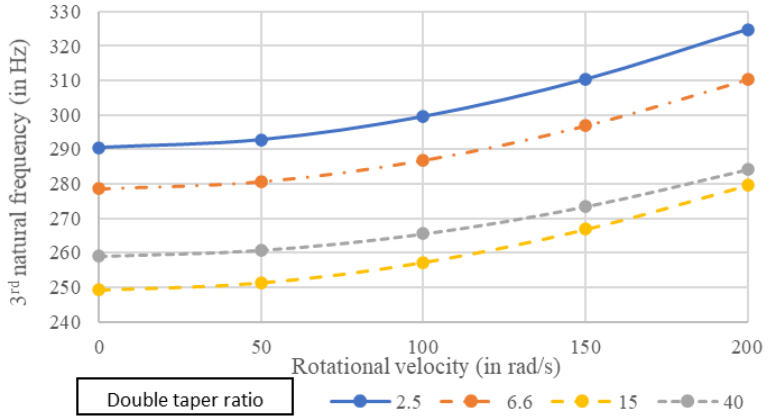

Figure 4.11 (b) 3rd natural frequencies of the 400-mm-long rotating doubly tapered cantilever composite beams with 240 mm mid-span delamination for $[90]_{8s}$ stacking sequence

Figure 4.11 1st and 3rd natural frequencies of the 400-mm-long rotating doubly tapered cantilever composite beams with 240 mm mid-span delamination and with $[90]_{8s}$ stacking sequence for different width-ratio values

Figure 4.11 illustrates the 1st and 3rd natural frequencies of the 400-mm-long rotating doubly tapered cantilever composite beams with 240 mm mid-span delamination and with $[90]_{8s}$ stacking sequence for various rotational velocities. The 1st and 3rd natural frequencies of all the beams with different double taper ratio values increase with the increase in the rotational velocity.

From Figure 4.11 (a), it is observed that the highest and the lowest 1st natural frequencies are observed for the composite beams with double taper ratio of values 40 and 2.5, respectively. For instance, at 100 rad/s rotational velocity the 1st natural frequencies of the composite beams with double taper ratio of values 40 and 2.5 are 38.79 Hz and 30.11 Hz, respectively.

In Figure 4.11 (a), for $[90]_{8s}$ stacking sequence the 1st natural frequencies of the rotating doubly tapered composite beams with 240 mm mid-span delamination and with double taper ratio of values 2.5, 6.6, 15 and 40 increase by 84.4%, 75.5%, 59.7% and 52.8%, respectively, due to the increase in the rotational velocity from 0 rad/s to 200 rad/s. In Table 4.34, for $[0]_{8s}$ stacking sequence the 1st natural frequencies of the rotating doubly tapered composite beams with 240 mm mid-span delamination and with double taper ratio of values 2.5, 6.6, 15 and 40 increase by 28.7%, 25.9%, 24.8% and 17.1%, respectively, due to the increase in the rotational velocity from 0 rad/s to 200 rad/s.

In Figure 4.11 (b), the highest and the lowest 3rd natural frequencies of 267.4 Hz and 231.1 Hz, respectively, are observed for the composite beams with 240 mm end delamination and with double taper ratio of values 2.5 and 15, respectively, for $[90]_{8s}$ stacking sequence at 100 rad/s rotational velocity.

The 3rd natural frequency of the composite beam with double taper ratio of value 40 is higher than that of the beam with double taper ratio of value 15, but with the increase in the rotational velocity the 3rd natural frequency curves of both the considered beams tend to converge. In Figure 4.11 (b), for $[90]_{8s}$ stacking sequence the percentage increases in the 3rd natural frequencies of the doubly tapered composite beams with 240 mm mid-span delamination and with double taper ratio of values 40 and 15 due to the increase in the rotational velocity from 0 rad/s to 200 rad/s are 10.73% and 13.97%, respectively.

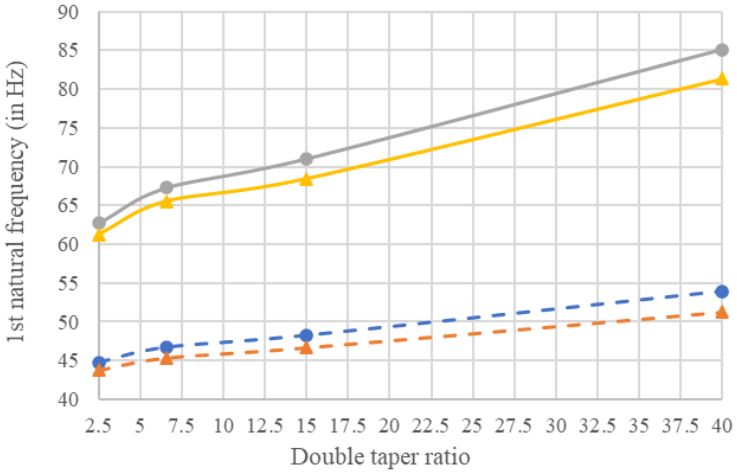

Figure 4.12 (a) The influence of the double taper ratio on the 1st natural frequencies of the rotating doubly tapered cantilever composite beams with 80 mm and 160 mm mid-span delaminations for $[0]_{8s}$ and $[90]_{8s}$ stacking sequences at 200 rad/s rotational velocity

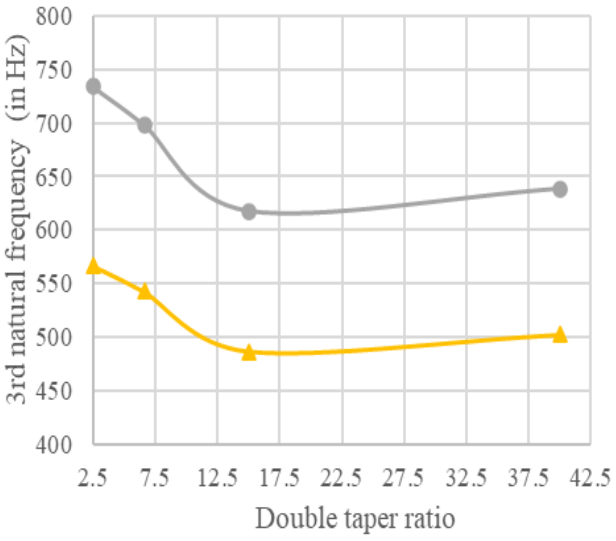

Figure 4.12 (b) The influence of the double taper ratio on the 3rd natural frequencies of the rotating doubly tapered cantilever composite beams with 80 mm and 160 mm mid-span delaminations for $[0]_{8s}$ stacking sequence at 200 rad/s rotational velocity

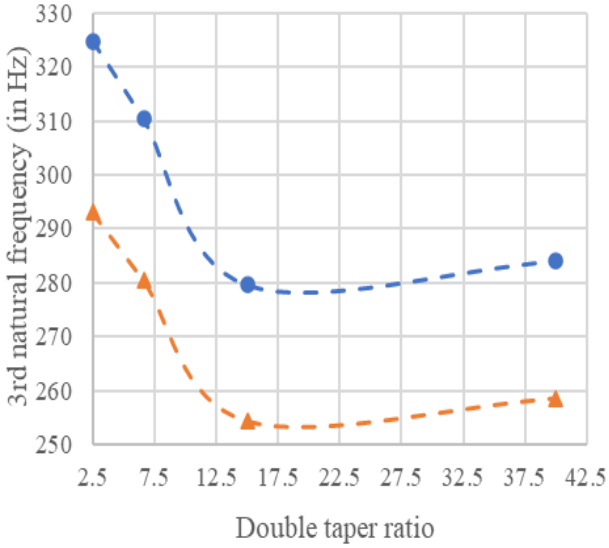

Figure 4.12 (c) The influence of the double taper ratio on the 3rd natural frequencies of the rotating doubly tapered cantilever composite beams with 80 mm and 160 mm mid-span delaminations for $[90]_{8s}$ stacking sequence at 200 rad/s rotational velocity

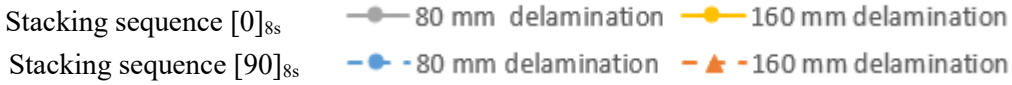

Figure 4.12 The influence of the 400-mm-long double taper ratio on the 1st and 3rd natural frequencies of the rotating doubly tapered cantilever composite beams with 80 mm and 160 mm mid-span delaminations for $[0]_{8s}$ and $[90]_{8s}$ stacking sequences at 200 rad/s rotational velocity

Figure 4.12 illustrates the influence of the 400-mm-long double taper ratio on the 1st and 3rd natural frequencies of the rotating doubly tapered cantilever composite beams with 80 mm and 160 mm mid-span delaminations for $[0]_{8s}$ and $[90]_{8s}$ stacking sequences at 200 rad/s rotational velocity.

In Figure 4.12 (a), the 1st natural frequencies of the rotating doubly tapered composite beams with mid-span delamination increase with the increase in the double taper ratio value for both considered stacking sequences. A sharp increase is seen in the 1st natural frequencies of the mid-span delaminated doubly tapered beams up to double taper ratio of value 6.6. With further increase in the double taper ratio value, the 1st natural frequencies of the considered beams increase linearly.

In Figures 4.12 (b) and (c), the 3rd natural frequencies of the rotating doubly tapered cantilever composite beams with mid-span delamination decrease sharply with the increase in double taper ratio of value up to 15 for both the considered stacking sequences. A slight increase is seen in the 3rd natural frequencies of the beams with further increase in the double taper ratio value.

4.6 Influence of the delamination location on the natural frequencies of rotating doubly tapered composite beams

In this section, the influence of the delamination location on the natural frequencies of the rotating doubly tapered cantilever composite beams is investigated. The natural frequencies of the rotating doubly tapered cantilever composite beams with 160 mm end and mid-span delaminations are shown in Figure 4.13. The analysis is conducted for $[90]_{8s}$ and $[0]_{8s}$ stacking sequences. The data representation for the plots presented in Figure 4.13 is done in Tables 4.23 and 4.26 for the doubly tapered beams with end mid-plane delamination and in Tables 4.30 and 4.33 for the doubly tapered beams with mid-span mid-plane delamination. The influence of the double taper ratio on the natural frequencies of the rotating doubly tapered cantilever composite beams with 240 mm end and mid-span delaminations is illustrated in Figure 4.14 for $[90]_{8s}$ stacking sequence at 200 rad/s rotational velocity. The data representation for the plots presented in Figure 4.14 is done in Tables 4.24 and 4.31 for the rotating doubly tapered composite beams with 240 mm end and mid-span delaminations, respectively.

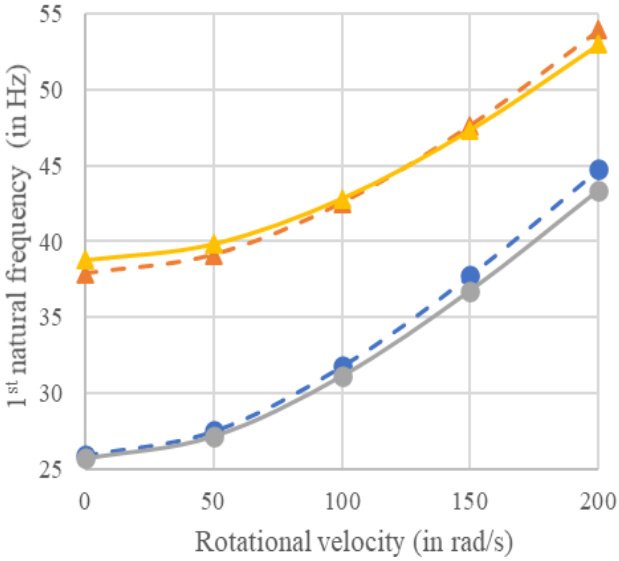

Figure 4.13 (a) Graphical illustration of the 1st natural frequencies of the rotating doubly tapered cantilever composite beams with 160 mm mid-span and end delaminations for $[90]_{8s}$ stacking sequence

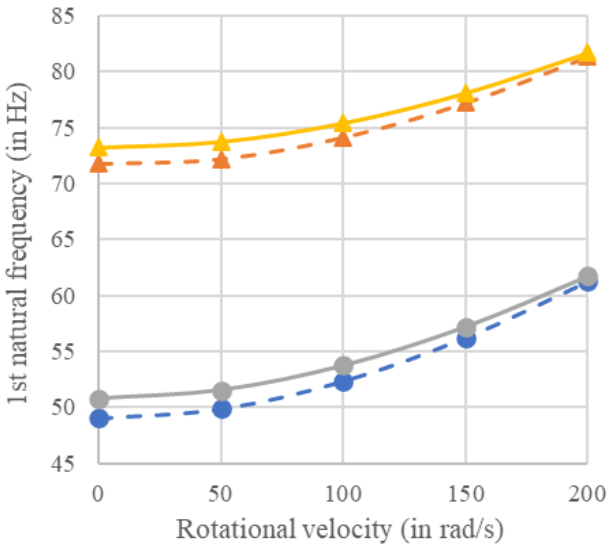

Figure 4.13 (b) Graphical illustration of the 1st natural frequencies of the rotating doubly tapered cantilever composite beams with 160 mm mid-span and end delaminations for $[0]_{8s}$ stacking sequence

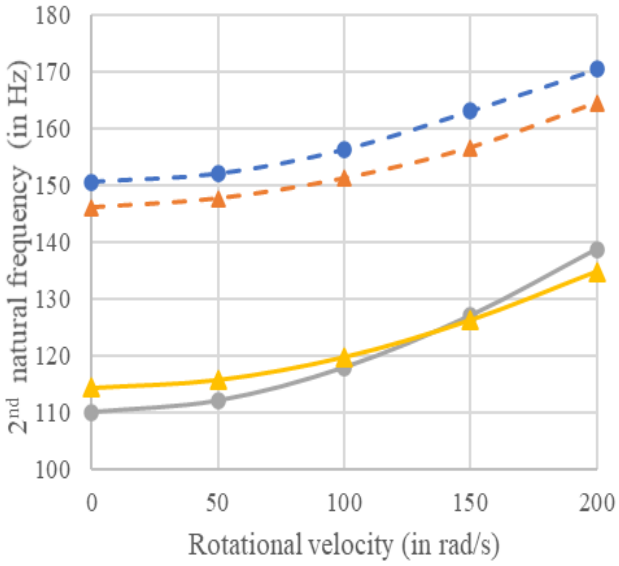

Figure 4.13 (c) Graphical illustration of the 2nd natural frequencies of the rotating doubly tapered cantilever composite beams with 160 mm mid-span and end delaminations for $[90]_{8s}$ stacking sequence

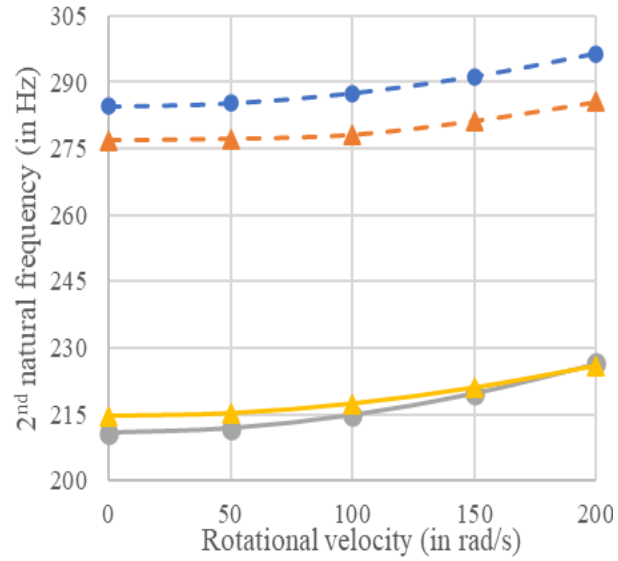

Figure 4.13 (d) Graphical illustration of the 2nd natural frequencies of the rotating doubly tapered cantilever composite beams with 160 mm mid-span and end delaminations for $[0]_{8s}$ stacking sequence

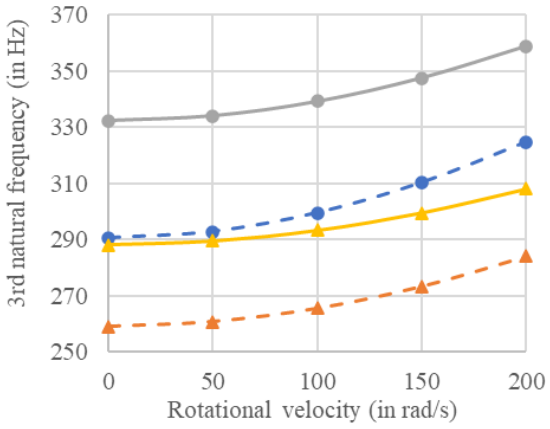

Figure 4.13 (e) Graphical illustration of the 3rd natural frequencies of the rotating doubly tapered cantilever composite beams with 160 mm mid-span and end delaminations for $[90]_{8s}$ stacking sequence

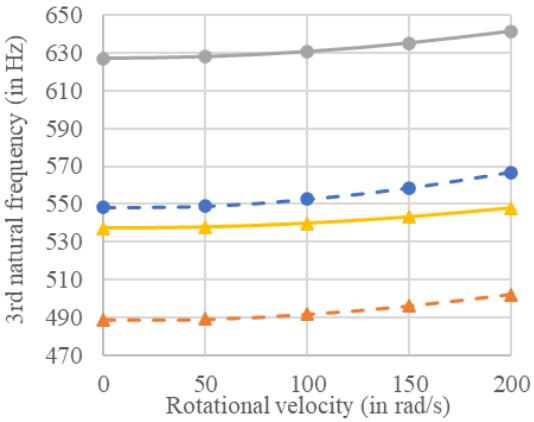

Figure 4.13 (f) Graphical illustration of the 3rd natural frequencies of the rotating doubly tapered cantilever composite beams with 160 mm mid-span and end delaminations for $[0]_{8s}$ stacking sequence

Figure 4.13 Graphical illustration of the first three natural frequencies of the 400-mm-long rotating doubly tapered cantilever composite beams with 160 mm mid-span and end delaminations for 2.5 and 40 double taper ratio values and for $[0]_{8s}$ and $[90]_{8s}$ stacking sequences

In Figures 4.13 (a) and (b), it is observed that the 1st natural frequencies of the beams with the same double taper ratio values are close, regardless of the delamination location. The 1st natural frequencies of the composite beams with double taper ratio of value 40 are higher than that of the composite beams with double taper ratio of value 2.5. For instance, in Figure 4.13 (a) for $[90]_{8s}$ stacking sequence and at 50 rad/s rotational velocity, the 1st natural frequencies of the end delaminated doubly tapered composite beams with double taper ratio of values 40 and 2.5 are 39.84 Hz and 28.27 Hz, respectively, whereas for the same stacking sequence and at the same rotational velocity the 1st natural frequencies of the mid-span delaminated doubly tapered composite beams with double taper ratio of values 40 and 2.5 are 39.12 Hz and 27.50 Hz, respectively. With the increase in the rotational velocity a higher increase is observed in the 1st natural frequency of the mid-span delaminated beams as compared to that of the end delaminated beams.

In Figures 4.13 (c) and (d), it is observed that the 2nd natural frequencies of the rotating doubly tapered composite beams with 160 mm mid-span delamination are higher than that of the rotating doubly tapered composite beams with 160 mm end delamination, for $[0]_{8s}$ and $[90]_{8s}$ stacking sequences. The mid-span delaminated beams with double taper ratio of value 2.5 have

higher 2nd natural frequencies than that of the mid-span delaminated beams with double taper ratio of value 40. For instance, in Figure 4.13 (d) for $[0]_{8s}$ stacking sequence and at 50 rad/s rotational velocity, the 2nd natural frequencies of the mid-span delaminated beams with double taper ratio of values 2.5 and 40 are 285.25 Hz and 276.78 Hz, respectively.

In Figures 4.13 (c) and (d), at low rotational velocities, the end delaminated beam with double taper ratio of value 2.5 has lower 2nd natural frequency than that of the end delaminated beam with double taper ratio of value 40, but with the increase in the rotational velocity a higher increase is seen in the 2nd natural frequency of the end delaminated beam with double taper ratio of value 2.5 as compared to that of the end delaminated beam with double taper ratio of value 40. For instance, in Figure 4.13 (c) for $[90]_{8s}$ stacking sequence and 160 mm end delamination length, the 2nd natural frequencies of the end delaminated doubly tapered composite beams with double taper ratio of values 2.5 and 40 at 0 rad/s rotational velocity are 111.73 Hz and 114.45 Hz, respectively, whereas the 2nd natural frequencies of the end delaminated doubly tapered composite beams with double taper ratio of values 2.5 and 40 at 200 rad/s are 138.96 Hz and 134.69 Hz, respectively. A percentage increases of 19.5% and 17.6% are observed in the 2nd natural frequencies of the rotating doubly tapered composite beams with double taper ratio of values 2.5 and 40, respectively, due to increase in the rotational velocity from 0 rad/s to 200 rad/s for $[90]_{8s}$ stacking sequence.

From Figures 4.13 (e) and (f), it is observed that the rotating doubly tapered composite beams with double taper ratio of value 2.5 have higher 3rd natural frequencies than that of the beams with double taper ratio of value 40. For instance, in Figure 4.13 (f) for $[0]_{8s}$ stacking sequence and at 100 rad/s rotational velocity, the 3rd natural frequencies of the end and mid-span delaminated composite beams with double taper ratio of value 2.5 are 630.5 Hz and 552.6 Hz, respectively, whereas the 3rd natural frequencies of the end and mid-span delaminated rotating doubly tapered composite beams with double taper ratio of value 40 are 539.8 Hz and 491.8 Hz, respectively.

With the increase in the rotational velocity, a higher increase is seen in the 3rd natural frequencies of the beams with mid-span delamination as compared to that of the beams with end delamination. For instance, in Figure 4.13 (f) for $[90]_{8s}$ stacking sequence, the percentage increases

in the 3rd natural frequencies due to the increase in the rotational velocity from 0 rad/s to 200 rad/s for the mid-span delaminated beams with double taper ratio of values 2.5 and 40 are 11.7% and 9.7%, respectively, whereas the percentage increases in the 3rd natural frequencies due to the increase in the rotational velocity from 0 rad/s to 200 rad/s for the end delaminated beams with double taper ratio of values 2.5 and 40 are 7.7% and 6.9%, respectively.

In Figure 4.13 (e) for $[90]_{8s}$ stacking sequence, the 3rd natural frequencies of the end and mid-span delaminated doubly tapered composite beams with double taper ratio of value 2.5 are higher than that of beams with double taper ratio of value 40. The highest 3rd natural frequency is observed for the mid-span delaminated beam with double taper ratio of value 2.5 followed by the 3rd natural frequency of the end delaminated beam with double taper ratio of value 2.5. The lowest value of 3rd natural frequency is observed for the end delaminated beam with a double taper ratio of value 40.

In Figure 4.13, due to the increase in the rotational velocity a sharper increase is observed in the natural frequencies of the beams with $[90]_{8s}$ stacking sequence in comparison to that of the beams with $[0]_{8s}$ stacking sequence.

Figure 4.14 illustrates the influence of the double taper ratio on the natural frequencies of the 400-mm-long doubly tapered composite beams with 240 mm mid-span and end delaminations at 200 rad/s rotational velocity and for $[90]_{8s}$ stacking sequence.

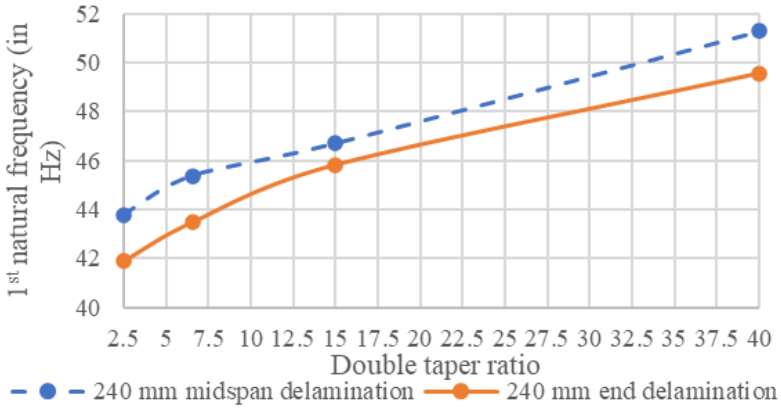

Figure 4.14 (a) The influence of the double taper ratio on the 1st natural frequencies of the 400-mm-long rotating doubly tapered composite beams with 240 mm mid-span and end delaminations at 200 rad/s rotational velocity

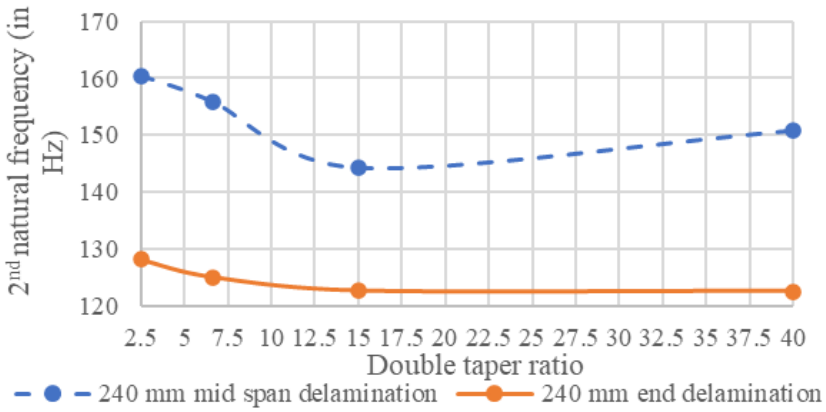

Figure 4.14 (b) The influence of the double taper ratio on the 2nd natural frequencies of the 400-mm-long rotating doubly tapered composite beams with 240 mm mid-span and end delaminations at 200 rad/s rotational velocity

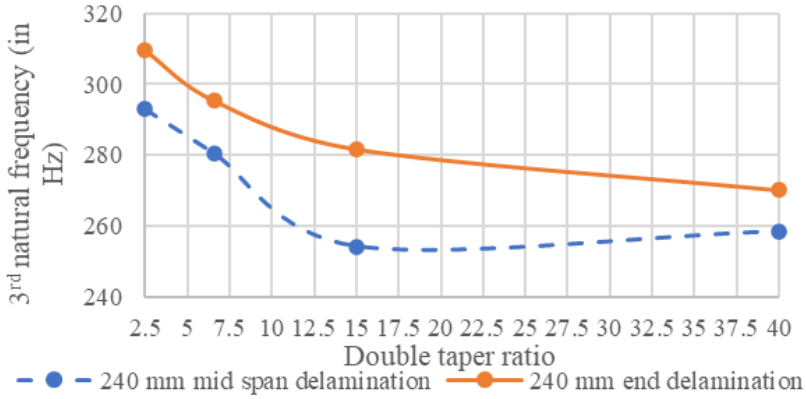

Figure 4.14 (c) The influence of the double taper ratio on the 3rd natural frequencies of the 400-mm-long rotating doubly tapered composite beams with 240 mm mid-span and end delaminations at 200 rad/s rotational velocity

Figure 4.14 The influence of the double taper ratio on the natural frequencies of the 400-mm-long rotating doubly tapered cantilever composite beams with 240 mm mid-span and end delaminations for $[90]_{8s}$ stacking sequence at 200 rad/s rotational velocity

From Figure 4.14 (a), it is observed that the 1st natural frequencies of the 400-mm-long rotating doubly tapered cantilever composite beams with 240 mm end and mid-span delaminations increase with the increase in the double taper ratio value, for $[90]_{8s}$ stacking sequence. The 1st natural frequency of the mid-span delaminated beam is higher than that of the end delaminated beam at 200 rad/s rotational velocity.

In Figures 4.14 (b) and (c), the 2nd and 3rd natural frequencies of the rotating doubly tapered composite beam with mid-span delamination decrease until the double taper ratio reaches the value of 15, a slight increase is observed in both the natural frequencies with further increase in the double taper ratio value. For instance, in Figure 4.14 (b) for $[90]_{8s}$ stacking sequence and at 200

rad/s rotational velocity, the 2nd natural frequencies of the mid-span delaminated doubly tapered beam for double taper ratio of values 2.5, 15 and 40 are 160.4 Hz, 144.2 Hz and 150.7 Hz, respectively, whereas the 3rd natural frequencies of the mid-span delaminated doubly tapered beam for double taper ratio of values 2.5, 15 and 40 are 293.01 Hz, 254.20 Hz and 258.54 Hz, respectively.

From Figures 4.14 (b) and (c), it is also observed that the 2nd and 3rd natural frequencies of the end delaminated doubly tapered composite beam decrease with the increase in the double taper ratio value, for $[90]_{8s}$ stacking sequence at 200 rad/s rotational velocity. With the increase in the double taper ratio value a higher decrease is seen in the 3rd natural frequency in comparison to that of the 2nd natural frequency of the end delaminated beam. For instance, the 2nd and 3rd natural frequencies of the end delaminated doubly tapered composite beam decrease by 4.3% and 11.7%, respectively, due to the increase in the double taper ratio value from 2.5 to 40.

4.7 Influence of the hub radius on the natural frequencies of rotating doubly tapered composite beams with end mid-plane delamination.

In this section, the influence of the hub radius on the natural frequencies of the rotating doubly tapered cantilever composite beams with end delaminations of different lengths is investigated for $[90]_{8s}$ and $[-45/45]_{4s}$ stacking sequences. The analysis is conducted on the doubly tapered composite beams with a total of 16 plies at the fixed end and 8 plies at the free end of the beam and with width-ratio of value 0.1. The hub is constantly rotating at 200 rad/s rotational velocity. The hub-radius-to-beam-length ratio (R/L) is used to discuss the results presented in Figures 4.15 and 4.16. The mechanical properties of the composite material were given in Table 4.1, whereas the interface parameters were given in Table 4.2. The geometric properties of the beam were given in Table 4.3. The number of plies, thickness of the beam and width of the beam mentioned in Table 4.3 refer to the number of plies, thickness on the thick side (at the fixed end) and width on the thick side of the doubly tapered beam, respectively. Figure 4.15 illustrates the natural frequencies of the 400-mm-long rotating doubly tapered cantilever composite beams with end delaminations of different lengths for different hub-radius-to-beam-length ratio values, at 200 rad/s rotational velocity. In Figure 4.15 the natural frequencies are plotted w.r.t. the values of the hub-radius-to-beam-length ratio (R/L).

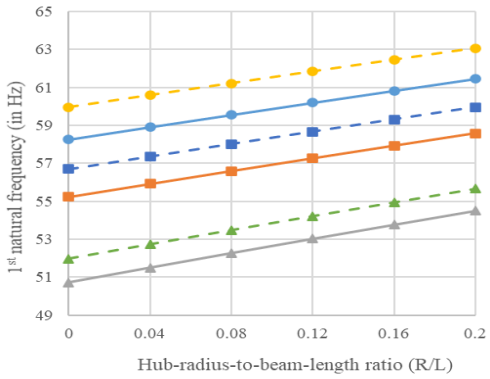

Figure 4.15 (a) The influence of the hub-radius-to-beam-length ratio (R/L) on the 1st natural frequencies of the rotating doubly tapered composite beams with end delamination at 200 rad/s rotational velocity

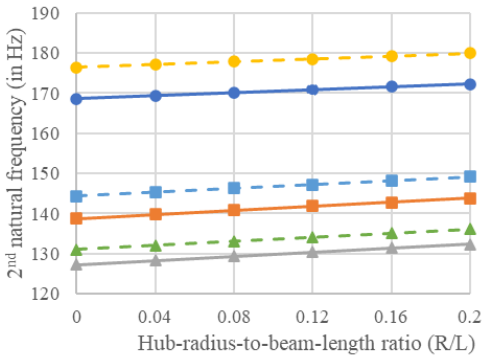

Figure 4.15 (b) The influence of the hub-radius-to-beam-length ratio (R/L) on the 2nd natural frequencies of the rotating doubly tapered composite beams with end delamination at 200 rad/s rotational velocity

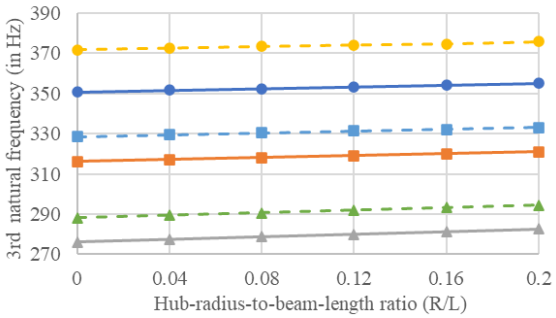

Figure 4.15 (c) The influence of the hub-radius-to-beam-length ratio (R/L) on the 3rd natural frequencies of the rotating doubly tapered composite beams with end delamination at 200 rad/s rotational velocity

Figure 4.15 The influence of the hub-radius-to-beam-length ratio (R/L) on the natural frequencies of the 400-mm-long rotating doubly tapered composite beams with end delamination of different lengths at 200 rad/s rotational velocity and for $[90]_{8s}$ and $[-45/45]_{4s}$ stacking sequences

From Figure 4.15, it is observed that all the three natural frequencies of the 400-mm-long doubly tapered composite beams with end delamination of different lengths increase linearly with the increase in the hub-radius-to-beam-length ratio value. A steep increase is observed in the lower mode frequencies as compared to the increase observed in the higher mode frequencies due to the increase in the hub-radius-to-beam-length ratio value. The natural frequencies of the beams with $[-45/45]_{4s}$ stacking sequence are higher than that of the beams with $[90]_{8s}$ stacking sequence. The

highest and the lowest natural frequencies are observed for the composite beams with 80 mm and 240 mm end delaminations, respectively, for both the considered stacking sequences.

Figure 4.16 illustrates the percentage increases in natural frequencies of the 400-mm-long end delaminated rotating doubly tapered composite beams due to the increase in the hub-radius-to-beam-length ratio value for $[-45/45]_{8s}$ stacking sequence. The analysis is conducted for three different end delamination lengths. The percentage increases in the natural frequencies of the end delaminated composite beams are calculated w.r.t. that of the end delaminated composite beam with the corresponding end delamination length and with the hub-radius-to-beam-length ratio of value 0.

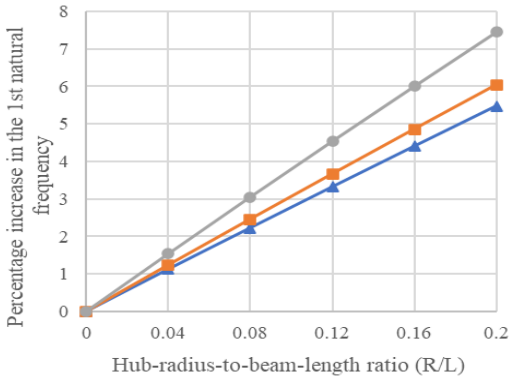

Figure 4.16 (a) The percentage increases in the 1st natural frequencies of the end delaminated rotating doubly tapered composite beams due to the increase in the hub-radius-to-beam-length ratio

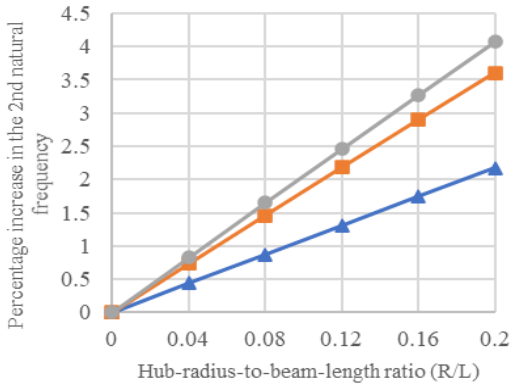

Figure 4.16 (b) The percentage increases in the 2nd natural frequencies of the end delaminated rotating doubly tapered composite beams due to the increase in the hub-radius-to-beam-length ratio

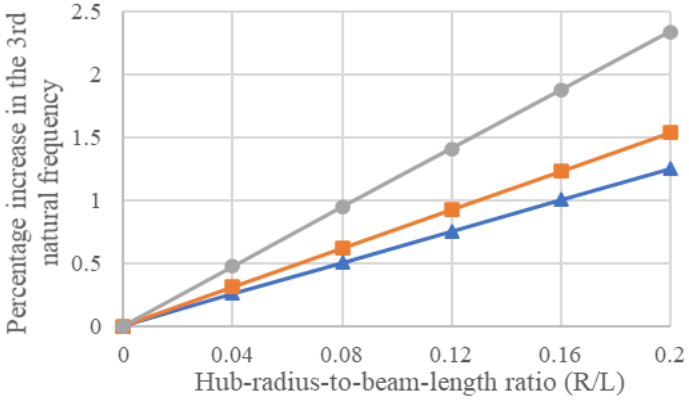

Figure 4.16 (c) The percentage increases in the 3rd natural frequencies of the end delaminated rotating doubly tapered composite beams due to the increase in the hub-radius-to-beam-length ratio

80 mm end crack 160 mm end crack 240 mm end crack

Figure 4.16 The percentage increases in the natural frequencies of the 400-mm-long end delaminated rotating doubly tapered cantilever composite beams with $[-45/45]_{4s}$ stacking sequence due to the increase in the hub-radius-to-beam-length ratio at 200 rad/s rotational velocity

From Figure 4.16, it is observed that the percentage increases in all the three natural frequencies of the considered beams are increasing linearly with the increase in the hub-radius-to-beam-length ratio. Higher percentage increases are seen in the lower mode frequencies of the beams as compared to the percentage increases in the higher mode frequencies of the beams. For instance, the percentage increases in the 1st and 3rd natural frequencies of the rotating doubly tapered composite beams with 160 mm end delamination due to the increase in the hub-radius-to-beam-length ratio value from 0 to 0.2 are 6.0% and 1.56%, respectively, for $[-45/45]_{4s}$ stacking sequence at 200 rad/s rotational velocity.

From Figure 4.16, it is also observed that with the increase in the hub-radius-to-beam-length ratio value the beam with larger delamination shows higher increase in the natural frequencies. For instance, the percentage increases in the 1st natural frequencies of the rotating doubly tapered composite beams with end delaminations of lengths 240 mm, 160 mm and 80 mm due to the increase in the hub-radius-to-beam-length ratio value from 0 to 0.2 are 7.4%, 6.0% and 5.3%, respectively, for $[-45/45]_{4s}$ stacking sequence at 200 rad/s rotational velocity.

4.8 Influence of the taper angle on the natural frequencies of the rotating doubly tapered composite beams with end mid-plane delamination

In this section, the influence of the taper angle (α) on the free vibration response of the rotating doubly tapered cantilever composite beams with end delamination is investigated for three different width-ratio values. There are a total of 16 plies at the fixed end of the beam and 8 plies at the free end of the beam. The taper angle of the beam changes due to the change in the beam length. The composite beams of four different lengths are considered for this comparative study. The ratio of delamination-length-to-beam-length is 1: 4 for all the cases discussed in this section. The analysis is conducted for $[90]_{8s}$ and $[0/90]_{4s}$ stacking sequences at the fixed end of the beam. The mechanical properties of the composite material were given in Table 4.1, whereas the interface parameters were given in Table 4.2. The geometric properties of the beam were given in Table 4.3. The number of plies, thickness of the beam and width of the beam mentioned in Table 4.3 refer to the number of plies, thickness on the thick side (at the fixed end) and width on the thick side of the doubly tapered beam. The natural frequencies of the rotating doubly tapered cantilever

composite beams with end delaminations are presented in Tables 4.35 - 4.42, for different taper angles and stacking sequences.

Taper angle	Number of plies		Width-ratio	Mode number	Rotational velocity (in rad/s)				
	At the fixed end	At the free end			0	50	100	150	200
0.1181°	16	8	0.1	1	45.28	46.23	48.99	53.25	58.61
				2	148.82	149.69	152.50	157.10	163.31
				3	313.09	314.06	317.26	322.59	329.81
			0.5	1	32.85	34.11	37.69	42.93	49.24
				2	130.97	132.18	135.91	141.92	149.96
				3	294.89	296.23	300.60	307.75	317.48
			1	1	8.57	12.51	19.79	27.68	35.77
				2	37.84	42.52	54.25	63.36	64.42
				3	88.90	94.52	109.49	130.32	154.40

Table 4.35 Natural frequencies (in Hz) of the 400-mm-long rotating doubly tapered cantilever composite beams of length 400 mm with 100 mm end delamination for $[90]_{8s}$ stacking sequence

Taper angle	Number of plies		Width-ratio	Mode number	Rotational velocity (in rad/s)				
	At the fixed end	At the free end			0	50	100	150	200
0.1575°	16	8	0.1	1	78.86	79.32	80.98	83.67	87.27
				2	275.37	275.39	277.01	279.69	283.41
				3	596.23	595.95	597.80	600.86	605.12
			0.5	1	56.90	57.66	59.88	63.38	67.96
				2	239.45	240.17	242.38	246.03	251.04
				3	551.71	552.54	555.14	559.45	565.42
			1	1	14.82	17.44	23.49	30.84	38.66
				2	69.70	72.54	80.49	92.26	105.14
				3	168.67	172.06	181.81	196.82	215.85

Table 4.36 Natural frequencies (in Hz) of the 400-mm-long rotating doubly tapered cantilever composite beams of length 300 mm with 75 mm end delamination for $[90]_{8s}$ stacking sequence

Taper angle	Number of plies		Width-ratio	Mode number	Rotational velocity (in rad/s)				
	At the fixed end	At the free end			0	50	100	150	200
0.1890°°	16	8	0.1	1	112.34	112.74	113.95	115.91	118.58
				2	402.47	402.88	404.11	406.03	408.70
				3	892.30	892.71	894.06	896.22	899.24
			0.5	1	80.79	81.28	82.90	85.51	89.03
				2	346.26	346.60	348.20	350.85	354.53
				3	814.92	815.32	817.19	820.30	824.63
			1	1	21.09	23.03	28.01	34.63	42.03
				2	101.97	104.02	109.96	119.21	131.07
				3	250.29	252.72	259.89	271.35	286.50

Table 4.37 Natural frequencies (in Hz) of the 400-mm-long rotating doubly tapered cantilever composite beams of length 250 mm with 62.5 mm end delamination for $[90]_{8s}$ stacking sequence

Taper angle	Number of plies		Width-ratio	Mode number	Rotational velocity (in rad/s)				
	At the fixed end	At the free end			0	50	100	150	200
0.2363°	16	8	0.1	1	174.56	174.59	175.38	176.71	178.53
				2	636.39	635.93	636.70	638.04	639.82
				3	1421.00	1420.70	1421.50	1423.00	1425.00
			0.5	1	125.22	125.50	126.57	128.34	130.77
				2	550.65	550.79	551.85	553.61	556.07
				3	1313.20	1313.30	1314.50	1316.60	1319.50
			1	1	32.59	33.91	37.57	42.93	49.40
				2	161.74	163.10	167.16	173.72	182.51
				3	397.06	397.26	397.88	398.92	400.36

Table 4.38 Natural frequencies (in Hz) of the 400-mm-long rotating doubly tapered cantilever composite beams of length 200 mm with 50 mm end delamination for $[90]_{8s}$ stacking sequence

Taper angle	Number of plies		Width-ratio	Mode number	Rotational velocity (in rad/s)				
	At the fixed end	At the free end			0	50	100	150	200
0.1181°	16	8	0.1	1	65.16	65.65	67.66	70.86	75.08
				2	212.63	213.01	215.00	218.27	222.78
				3	448.33	448.89	451.11	454.79	459.89
			0.5	1	47.09	47.98	50.64	54.74	59.97
				2	185.61	186.46	189.13	193.49	199.45
				3	418.78	419.71	422.77	427.82	434.78
			1	1	12.34	15.39	21.93	29.49	37.38
				2	54.17	57.53	66.64	79.60	94.81
				3	127.36	131.29	142.38	159.01	179.49

Table 4.39 Natural frequencies (in Hz) of the 400-mm-long rotating doubly tapered cantilever composite beams of length 400 mm with 50 mm end delamination for $[0/90]_{4s}$ stacking sequence

Taper angle	Number of plies		Width-ratio	Mode number	Rotational velocity (in rad/s)				
	At the fixed end	At the free end			0	50	100	150	200
0.1575°	16	8	0.1	1	113.69	114.01	115.18	117.10	119.74
				2	394.82	394.83	395.96	397.84	400.45
				3	855.40	855.41	856.68	858.80	861.76
			0.5	1	82.07	82.56	84.13	86.69	90.14
				2	342.82	343.27	344.81	347.38	350.94
				3	792.45	792.89	794.69	797.67	801.82
			1	1	21.42	23.33	28.22	34.75	42.07
				2	100.40	102.39	108.14	117.12	128.66
				3	242.85	245.19	252.06	263.05	273.01

Table 4.40 Natural frequencies (in Hz) of the 400-mm-long rotating doubly tapered cantilever composite beams of length 300 mm with 75 mm end delamination and $[0/90]_{4s}$ stacking sequence

Taper angle	Number of plies		Width-ratio	Mode number	Rotational velocity (in rad/s)				
	At the fixed end	At the free end			0	50	100	150	200
0.1890°	16	8	0.1	1	161.92	162.62	163.45	164.83	166.73
				2	580.17	580.41	581.20	582.53	584.39
				3	1278.90	1279.00	1279.90	1281.40	1283.50
			0.5	1	116.83	117.14	118.27	120.13	122.67
				2	500.62	500.85	501.95	503.79	506.35
				3	1176.40	1176.40	1177.70	1179.80	1182.80
			1	1	30.51	31.89	35.69	41.19	47.75
				2	147.46	148.88	153.07	159.81	168.80
				3	361.10	362.77	367.75	375.86	386.90

Table 4.41 Natural frequencies (in Hz) of the 400-mm-long rotating doubly tapered cantilever composite beams of length 250 mm with 62.5 mm end delamination for $[0/90]_{4s}$ stacking sequence

Taper angle	Number of plies		Width-ratio	Mode number	Rotational velocity (in rad/s)				
	At the fixed end	At the free end			0	50	100	150	200
0.2363°	16	8	0.1	1	252.21	252.19	252.74	253.65	254.92
				2	923.34	922.52	923.04	923.92	925.15
				3	2057.80	2054.50	2055.10	2056.10	2057.50
			0.5	1	181.05	181.24	181.99	183.22	184.94
				2	799.44	799.51	800.23	801.45	803.14
				3	1902.00	1901.90	1902.70	1904.10	1906.10
			1	1	47.16	48.08	50.74	54.87	60.14
				2	234.69	235.63	238.45	243.07	249.40
				3	582.73	583.83	587.16	592.66	600.26

Table 4.42 Natural frequencies (in Hz) of the 400-mm-long rotating doubly tapered cantilever composite beams of length 200 mm with 50 mm end delamination for $[0/90]_{4s}$ stacking sequence

From Tables 4.35 – 4.42, it is observed that the natural frequencies of the 400-mm-long rotating doubly tapered composite beams increase with the increase in the taper angle value or decrease in the beam length. For instance, in Tables 4.35 - 4.38 for 0.1 width-ratio value and for $[90]_{8s}$ stacking sequence at the fixed ends of the beams, the 1st natural frequencies of the doubly tapered stationary cantilever composite beams with taper angle of values 0.1181°, 0.1575°, 0.1890° and 0.2363° are 45.28 Hz, 78.86 Hz, 112.34 Hz and 174.56 Hz, respectively.

From Tables 4.35 – 4.42, it is also observed that for the given length of the rotating doubly tapered composite beam with end delamination, the natural frequencies decrease with the increase in the width-ratio value. For instance, in Table 4.42 for $[0/90]_{4s}$ stacking sequence at the fixed end of the beam and at 200 rad/s rotational velocity, the 1st natural frequencies of 200-mm-long 50-

mm-end-delaminated doubly tapered composite beam for the width-ratio of values 0.1, 0.5 and 1 are 254.92 Hz, 154.94 Hz and 60.14 Hz, respectively.

Figure 4.17 illustrates the influence of the taper angle on the natural frequencies of the end delaminated rotating cantilever composite beams with $[90]_{8s}$ and $[0/90]_{4s}$ stacking sequences for three different width-ratio values at 100 rad/s rotational velocity.

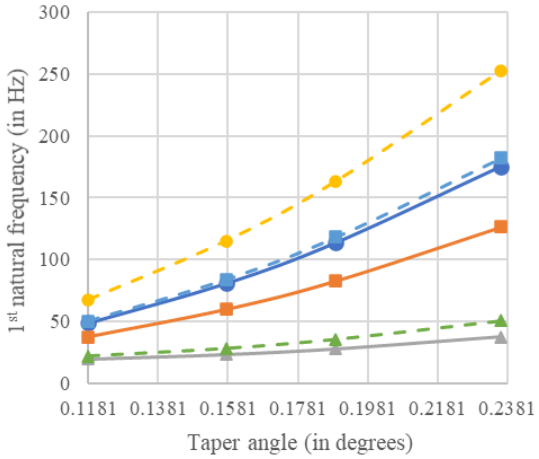

Figure 4.17 (a) The influence of the taper angle on the 1st natural frequencies (in Hz) of the rotating doubly tapered composite beams with end delamination at 100 rad/s rotational velocity

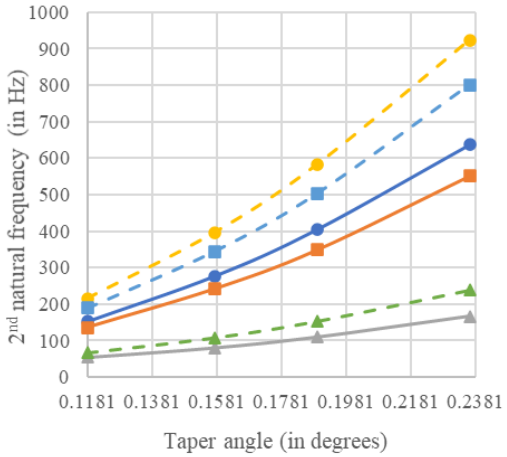

Figure 4.17 (b) The influence of the taper angle on the 2nd natural frequencies (in Hz) of the rotating doubly tapered composite beams with end delamination at 100 rad/s rotational velocity

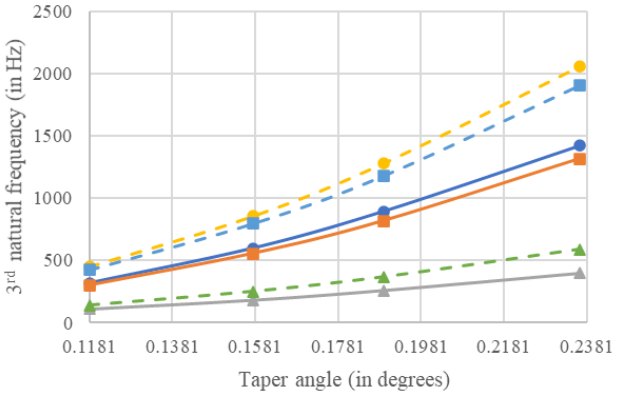

Figure 4.17 (c) The influence of the taper angle on the 3rd natural frequencies (in Hz) of the rotating doubly tapered composite beams with end delamination at 100 rad/s rotational velocity

Figure 4.17 The influence of the taper angle on the first three natural frequencies (in Hz) of the end delaminated rotating doubly tapered composite beams of different width-ratio values for $[90]_{8s}$ and $[0/90]_{4s}$ stacking sequences at 100 rad/s rotational velocity

From Figure 4.17, it is observed that the natural frequencies of the rotating doubly tapered cantilever composite beams increase linearly with the increase in the taper angle value. The natural frequencies of the beams with $[0/90]_{4s}$ stacking sequence are higher than that of the beams with $[90]_{8s}$ stacking sequence.

In Figure 4.17, a higher increase is observed in the natural frequencies of the beams with $[0/90]_{4s}$ stacking sequence than that of the beams with $[90]_{8s}$ stacking sequence due to the increase in the taper angle value. A higher increase is noted in the natural frequencies of the doubly tapered beams with lower width-ratio values as compared to that of the beams with higher width-ratio values. For instance, in Figure 4.17 (a) for $[0/90]_{4s}$ stacking sequence the percentage increases in the fundamental frequencies of the rotating doubly tapered composite beams with width-ratio of values 0.1, 0.5 and 1 due to the increase in the taper angle value from 0.1181° to 0.2281° are 273.8%, 259.0% and 131.7%, respectively, whereas for $[90]_{8s}$ stacking sequence the percentage increases in the fundamental frequencies of the rotating doubly tapered composite beams with width-ratio of values 0.1, 0.5 and 1 due to the increase in the taper angle value from 0.1181° to 0.2281° are 258.4%, 236.4% and 90.3%, respectively.

4.9 Conclusion

In this chapter, the free vibration response of the thickness-tapered and rotating doubly tapered cantilever composite beams with delaminations of different lengths and locations, and with different stacking sequences were determined for various rotational velocities. The influences of the delamination length, rotational velocity and stacking sequence on the first three out-of-plane bending natural frequencies of the end delaminated rotating thickness-tapered cantilever composite beams and end and mid-span delaminated rotating doubly tapered cantilever composite beams were investigated. The influences of the change in the geometrical parameters (number of plies dropped-off, width-ratio, double taper ratio and beam length) on the natural frequencies of the rotating thickness-tapered and doubly tapered composite beams were also studied.

All the three out-of-plane bending natural frequencies of the rotating thickness-tapered and doubly tapered composite beams with delaminations increase with the increase in the rotational velocity and decrease with the increase in the delamination length. The highest natural frequencies

of the thickness-tapered and doubly tapered composite beams were observed for $[0]_{8s}$ stacking sequence, followed by the natural frequencies of the composite beams with $[0/90]_{4s}$ stacking sequence. The natural frequencies of the composite beams with $[90]_{8s}$ and $[-45/45]_{4s}$ stacking sequences were almost the same, but the latter has slightly higher natural frequencies.

The 1st natural frequencies of the rotating thickness-tapered cantilever composite beams with end delamination increase linearly, whereas the 2nd and 3rd natural frequencies decrease linearly with the increase in the number of plies dropped-off. With the increase in the double taper ratio value the 2nd natural frequency of the end delaminated rotating doubly tapered composite beam remains almost the same, whereas the 3rd natural frequency decreases and the 1st natural frequency increases for any considered rotational velocity. With the increase in the double taper ratio value the 1st natural frequency of the mid-span delaminated rotating doubly tapered composite beam increases, whereas the 2nd and 3rd natural frequencies of the considered beam decrease until the double taper ratio reaches the value of 15, but with further increase in the double taper ratio value a slight increase was observed in both the natural frequencies.

The natural frequencies of the end delaminated rotating doubly tapered composite beams with higher width-ratio values were more sensitive to the rotational velocity, whereas the natural frequencies of the end delaminated rotating doubly tapered composite beams with lower width-ratio values were more sensitive to the delamination length. All the three natural frequencies of the end delaminated doubly tapered composite beams increase linearly with the increase in the hub-radius-to-beam-length ratio value. The beams with larger delamination show higher increase in the natural frequencies due to increase in the hub-radius-to-beam-length ratio value in comparison to that of the beams with smaller delamination.

The natural frequencies of the rotating doubly tapered composite beams increase with the increase in the taper angle value or decrease in the beam length. The natural frequencies of the rotating doubly tapered cantilever composite beams increase linearly with the increase in the taper angle value. A higher increase was noted in the natural frequencies of the doubly tapered beams with the lower width-ratio values as compared to that of the beams with the higher width-ratio values due to the increase in the taper angle value.

Chapter 5

Conclusion

5.1 Contribution

In the present thesis, the free vibration response of the stationary thickness-tapered simply supported composite beams and rotating doubly tapered cantilever composite beams with end and mid-span delaminations has been investigated. The vibration characteristics of the delaminated composite beams obtained by modal analysis using FEA tool ANSYS® have been analyzed. The first ply failure analyses have been conducted using Tsai-Wu failure criterion to determine the critically stressed locations prone to delamination in the stationary and rotating composite beams. The Mode-I and Mode-II delamination tests have been performed on the numerical models of Double Cantilever Beam (DCB) and End Notch Flexure (ENF) test samples based on Cohesive Zone Modeling (CZM) using ANSYS®. The load vs displacement curves for the DCB and ENF test samples were obtained, studied and verified with the available results. The natural frequencies of the intact and delaminated composite beams have been determined and verified where possible. The influences of the various system parameters on the free vibration response of the stationary and rotating delaminated composite beams have been studied for uniform, thickness-tapered and doubly tapered beam profiles, in the present thesis.

Comprehensive parametric studies have been conducted to investigate the influences of the delamination length and location, fiber orientation angle and taper angle on the natural frequencies of the stationary simply supported and rotating cantilever composite beams with delamination. The end delamination lengths having minimal effect on the natural frequencies of the stationary uniform and thickness-tapered simply supported composite beams have been determined. The thickness-wise locations of large mid-span delaminations between different plies of the laminate are determined, which lead to local buckling and cause convergence difficulties in the modal analysis. The influences of the thickness-tapering and layer reduction on the natural frequencies of the stationary simply supported composite beams have been studied. The natural frequencies of the composite beams with end and mid-span delaminations are compared and thoroughly investigated. The free vibration analyses of the thickness-tapered and doubly tapered

cantilever composite beams with end and mid-span delaminations have been conducted, at different rotational velocities and for various stacking sequences. Various numerical studies have been conducted to analyze the influences of the rotational velocity, double tapering and hub radius on the natural frequencies of the rotating doubly tapered cantilever composite beams with delamination.

The studies performed in the present thesis are helpful in developing economical delamination detection techniques for the stationary and rotating tapered composite structures based on their free vibration. The present thesis is also helpful for the safe designing of the stationary and rotating tapered composite structures by considering the influences of delamination length and location on the natural frequencies of the tapered composite structure to avoid failure due to resonance, when in service.

5.2 Conclusion

- The natural frequencies of the composite beams decrease with the increase in the delamination length.
- Up to 5% of the total beam length, the end delamination has minimal effect on the first three natural frequencies of the uniform and thickness-tapered simply supported composite beams, for any considered fiber orientation angle.
- Higher modes should be studied to investigate the effects of the end delamination of length lesser than 5% of the total beam length.
- The higher mode frequencies were more sensitive to the delamination length as compared to the lower mode frequencies.
- The delaminated composite beams with 0° and 60° fiber orientation angles have the highest and the lowest natural frequencies, respectively, for any considered delamination length.
- The composite beams with $[45]_{8s}$ and $[90]_{8s}$ stacking sequences have similar values of their effective stiffnesses in the longitudinal direction of the beam, resulting in close values of their natural frequencies.
- With the increase in the delamination length, a significant decrease was observed in the 1^{st} natural frequencies of the uniform and thickness-tapered composite beams with end delamination, as compared to that of the decrease in the 1^{st} natural frequencies of the uniform and thickness-tapered composite beams with mid-span delamination.

- The natural frequencies of the uniform simply supported composite beams were higher when the mid-span delamination was away from the mid-plane.
- The large mid-span delamination located away from the mid-plane leads to the local buckling of the beam and convergence difficulties in the modal analysis.
- Due to layer reduction in the laminated beams, the natural frequencies of the thickness-tapered beams were higher than those of the thin uniform beams and lower than those of the thick uniform beam, for the simply supported boundary condition. For the cantilever boundary condition, the 1^{st} natural frequencies of the thickness-tapered beams were higher than those of the thin and thick uniform beams, but the 2^{nd} and 3^{rd} natural frequencies of the thickness-tapered beams were higher than those of the thin beams but lower than those of the thick beam, which is due to asymmetry in the cantilever boundary condition.
- All the three out-of-plane bending natural frequencies of the rotating thickness-tapered and doubly tapered composite beams with delamination increase with the increase in the rotational velocity.
- With the increase in the number of plies dropped-off, the 1^{st} natural frequencies of the rotating thickness-tapered cantilever composite beams with end delamination increase linearly, whereas the 2^{nd} and 3^{rd} natural frequencies decrease linearly.
- With the increase in the double taper ratio value, the 2^{nd} natural frequency of the end delaminated rotating thickness-tapered composite beam remains almost the same, whereas the 1^{st} and 3^{rd} natural frequencies of the considered beam increases and decreases, respectively, for any considered rotational velocity.
- With the increase in the double taper ratio value, the 1^{st} natural frequency of the mid-span delaminated rotating thickness-tapered composite beam increases, whereas the 2^{nd} and 3^{rd} natural frequencies of the considered beam decrease until the double taper ratio reaches the value of 15, but with further increase in the double taper ratio value a slight increase was observed in both the natural frequencies.
- The natural frequencies of the end delaminated rotating thickness-tapered composite beams with higher width-ratio values were more sensitive to the rotational velocity, whereas the natural frequencies of the end delaminated rotating thickness-tapered composite beams with lower width-ratio values were more sensitive to the delamination length.

- All the three natural frequencies of the end delaminated rotating thickness-tapered composite beams increase linearly, due to the increase in the hub-radius-to-beam-length ratio value.
- With the increase in the hub-radius-to-beam-length ratio value, the rotating composite beams with larger delamination have higher increase in their natural frequencies in comparison to that of the beams with smaller delamination.
- The natural frequencies of the rotating thickness-tapered composite beams increase linearly due to the increase in the taper angle value or decrease in the beam length.
- With the increase in taper angle value, a higher increase was noted in the natural frequencies of the doubly tapered beams with lower width-ratio values as compared to those of the beams with the higher width-ratio values.
- With the increase in the rotational velocity, the natural frequencies of the rotating thickness-tapered and doubly tapered composite beams with end and mid-span delaminations of same length and with same beam profile increase by a similar amount, irrespective of their different delamination locations.
- The fundamental frequencies of the rotating thickness-tapered composite beams with end and mid-span delaminations of the same length are close, regardless of their different delamination locations.
- With the increase in the rotational velocity, a higher increase is observed in the natural frequencies of the thickness-tapered cantilever composite beams with delamination in comparison to those of the doubly tapered cantilever composite beams with delamination.
- With the increase in the end delamination length, a lower decrease is observed in the fundamental frequency of the rotating doubly tapered cantilever composite beam as compared to those of the stationary uniform and thickness-tapered simply supported composite beams.
- The 1^{st} and 2^{nd} natural frequencies of the rotating doubly tapered cantilever composite beams with end delamination of length 20% of the total beam length decrease by 0.2% - 0.5% and 4% - 7%, respectively, w.r.t. those of the corresponding rotating intact composite beams.
- The 1^{st} and 2^{nd} natural frequencies of the stationary uniform and thickness-tapered simply supported composite beams with end delamination of length 20% of the total beam length decrease by 4% - 8% and 14% - 17%, respectively, w.r.t. those of the corresponding stationary intact composite beams.

- It can be concluded that up to a certain end delamination length, the first two natural frequencies of the rotating doubly tapered cantilever composite beams are less sensitive to the end delamination as compared to those of the stationary uniform and thickness-tapered simply supported composite beams.
- With the increase in the mid-span delamination length, a higher decrease is observed in the fundamental frequency of the rotating doubly tapered cantilever composite beams as compared to those of the stationary uniform and thickness-tapered simply supported composite beams.

5.3 Recommendations for future work

The study of free vibration of stationary and rotating thickness-tapered and doubly tapered composite beams with delamination can be continued in the future studies based on the following recommendations:

- Free vibration analysis of stationary and rotating thickness-tapered and doubly tapered composite beams, and thickness-tapered composite plates with multiple delaminations can be conducted.
- The influence of delamination on the dynamic instability of delaminated rotating thickness-taperedthicknes composite beams can be investigated.
- Forced vibration analysis can be performed on the stationary and rotating thickness-tapered and doubly tapered composite beams with delamination.
- Damping can be introduced in the free vibration analysis of stationary and rotating doubly tapered composite beams with delamination.
- The influence of cohesive interface parameters on the local buckling of delaminated composite beams vibrating at their natural frequencies can be studied.

References

[1] D. A. Peters, “An Approximate Solution for the Free Vibrations of Rotating Uniform Cantilever Beams”, NASA Ames Research Center Moffett Field, 1973.
(Source- https://ntrs.nasa.gov/citations/19780025346)

[2] W. Boyce, E. William and G. Handelman, “Vibrations of Rotating Beams with Tip Mass”, *Zeitschrift für angewandte Mathematik und Physik ZAMP*, Vol. 12, pp. 369-392, 1961.
(Source- https://link.springer.com/content/pdf/10.1007/BF01600687.pdf)

[3] S. Putter and H. Manor, “Natural Frequencies of Radial Rotating Beams”, *Journal of Sound and Vibration*, Vol. 56, pp. 175-185. 1978.
(Source - https://doi.org/10.1016/S0022-460X(78)80013-3)

[4] H.H. Yoo, S.H. Lee and S.H. Shin, “Flap Wise Bending Vibration Analysis of Rotating Multi-Layered Composite Beams”, *Journal of Sound and Vibration*, Vol. 286, pp. 745–761, 2005.

[5] C. Kuo and S. Lin, “Modal Analysis and Control of a Rotating Euler-Bernoulli Beam Part I: Control System Analysis and Controller Design”, *Mathematical and Computer Modelling*, Vol. 27, No. 5, pp.75-92, 1998.

[6] T. Aksencer and M. Aydogdu, “Flapwise Vibration of Rotating Composite Beams”, *Composite Structures*, Vol. 134, pp. 672–679, 2015.

[7] R. Chandra and I. Chopra, “Experimental-Theoretical Investigation of the Vibration Characteristics of Rotating Composite Box Beams”, *Journal of Aircraft,* Vol. 29, No.4, pp. 657-664, 1992.

[8] Y. Qin, X. Li, E.C. Yang and Y.H. Li, “Flapwise Free Vibration Characteristics of a Rotating Composite Thin-Walled Beam under Aerodynamic Force and Hygrothermal Environment”, *Composite Structures*, Vol. 153, pp. 490-503, 2016.

[9] E. Carrera, M. Filippi and E. Zappino, “Free Vibration Analysis of Rotating Composite Blades via Carrera Unified Formulation”, *Composite Structures*, Vol. 106, pp. 317–325, 2013.

[10] M.L. Pavankishore and R.K. Behera, “Determination of Optimal Stacking Sequence for Modal Characteristics Evaluation of Composite Marine Propeller Blade”, *Journal of Mechanical Design and Vibration*, Vol. 2, No. 4, pp. 94-101, 2014.

[11] S. Seraj, “Free Vibration and Dynamic Instability Analyses of Doubly-Tapered Rotating Laminated Composite Beams”, M.A.Sc. Thesis, Concordia University, 2016.

[12] R. B. Abarcar and P. F. Cunniff, “The Vibration of Cantilever Beams of Fiber Reinforced Material”, *Journal of Composite Materials*, Vol. 6, pp. 504-516, 1972.

[13] K. Chandrashekhara, K. Krishnamurthy and S. Roy, “Free Vibration of Composite Beams Including Rotary Inertia and Shear Deformation”, *Journal of Composite Structures*, Vol. 14, pp. 269-279, 1990.

[14] H. Abromivich and A. Livshits, “Free Vibration of Non-symmetric Cross-ply Laminated Composite Beams”, *Journal of Sound and Vibration*, Vol. 176, No. 5, pp. 596-612, 1994.

[15] A. K. Miller and D. F. Adams, “An Analytic Means of Determining the Flexural and Torsional Resonant Frequencies of Generally Orthotropic Beams”, *Journal of Sound and Vibration*, Vol. 41, No. 4, pp. 433-449, 1975.

[16] J. R. Vinson and R. L. Sierakowski, The Behavior of Structures Composed of Composite Materials, 2nd Edition, Kluwer Academic Publishers, 2002.

[17] S. Krishnaswamy, K. Chandrashekhara and W. Z. B. Wu, “Analytical Solutions to Vibration of Generally Layered Composite Beams”, *Journal of Sound and Vibration*, Vol. 159, pp. 85-99, 1992.

[18] M. S. Nabi and N. Ganesan, “A Generalized Element for the Free Vibration Analysis of Composite Beams”, *Computers and Structures*, Vol. 51, No. 5, pp. 607-610, 1994.

[19] A. Zabihollah, “Vibration and Buckling Analysis of Tapered Composite Beams Using Conventional and Advanced Finite Element Formulations”, M.A.Sc. Thesis, Concordia University, 2003.

[20] H. Eftakher, “Free and Forced Vibrations of Tapered Composite Beams Including the Effects of Axial Force and Damping”, M.A.Sc. Thesis, Concordia University, 2008.

[21] S. Seraj and R. Ganesan, “Dynamic Instability of Rotating Doubly-Tapered Laminated Composite Beams under Periodic Rotational Speeds”, *Composite Structures*, Vol. 200, pp. 711-728, 2018.

[22] B. Arab, “Vibration Analysis of Thickness-Tapered Laminated Composite Square Plates Based on Ritz Method”, M.A.Sc. Thesis, Concordia University, 2019.

[23] P. Kumar, “Dynamic Response of Doubly-Tapered Laminated Composite Beams under Periodic and Non-Periodic Loadings”, M.A.Sc. Thesis, Concordia University, 2019.

[24] M.F. Kanninen, “An Augmented Double Cantilever Beam Model for Studying Crack Propagation and Arrest”, *International Journal of Fracture*, Vol. 9, pp. 83–92, 1973.

[25] E.F. Rybicki, D.W. Schmueser and J. Fox, “An Energy Release Rate Approach for Stable Crack Growth in the Free-Edge Delamination Problem”, *Journal of Composite Material*, Vol. 11, pp. 470–487, 1977.

[26] F.E. Penado, “A Closed Form Solution for the Energy Release Rate of the Double Cantilever Beam Specimen with an Adhesive Layer”, *Journal of Composite Material*, Vol. 27, pp. 383–407, 1993.

[27] K. Arakawa and K. Takahashi, “Interlaminar Fracture Analysis of Composite DCB Specimens”, *International Journal of Fracture*, Vol. 74, pp. 277–287, 1995.

[28] S. Zheng and C. Sun, “A Double Plate Finite Element Model for Impact Induced Delamination Problems”, *Composites Science and Technology*, Vol. 53, pp. 111-118, 1995.

[29] R. Krueger and T.K. O’Brien., “A Shell/3D Technique for the Analysis of Delaminated Composite Laminates”, *Composites Part A: Applied Science and Manufacturing*, Vol. 32, No.1, pp. 24 – 44, 2001.

[30] G. Alfano and M. A. Crisfield, “Finite Element Interface Models for the Delamination Analysis of Laminated Composites: Mechanical and Computational Issues”, *International Journal for Numerical Methods in Engineering*, Vol. 50, pp. 1701 – 1736, 2001.

[31] P. W. Harper and S. R. Hallett, “Cohesive Zone Length in Numerical Simulations of Composite Delamination”, *Engineering Fracture Mechanics*, Vol. 75, No. 16, pp. 4774 - 4792, 2008.

[32] S. Supreeth and S. B. Manjunath S. B., “Modeling and Analysis of Mode-I and Mode-II Delamination Onset in Composite Laminates”, *International Journal of Engineering Research in Mechanical and Civil Engineering*, Vol. 3, pp.14 – 21, 2018.

[33] H. Calliogllu and G. Atlihan, “Vibration Analysis of Delaminated Composite Beams using Analytical and FEM Models”, *Indian Journal of Engineering & Material Sciences*, Vol. 18, pp. 7-14, 2011.

[34] R.A. Jafri-Talookolaei and C. Della, “Dynamic Behavior of a Rotating Delaminated Composite Beam including Rotary Inertia and Shear Deformation Effects”, *Ain Shams Engineering Journal*, Vol. 6, pp. 1031 – 1044, 2015.

[35] https://doi.org/10.1016/S0020-7683(98)00325-4

[36] M. Swaminathan and J.S. Rao, “Vibrations of Rotating, Pre-Twisted and Tapered Blades”, *Mechanism and Machine Theory*, Vol. 12, No. 4, pp. 331-337, 1977.

[37] S. Khosravi, H. Arvin and Y. Kiani, “Vibration Analysis of Rotating Composite Beams Reinforced with Carbon Nanotubes in Thermal Environment”, *International Journal of Mechanical Sciences*, Vol. 164, Article 105187, 2019.

[38] E. Shafei, S. Faroughi and A. Reali, “Nonlinear Vibration of Anisotropic Composite Beams using Iso-Geometric Third-Order Shear Deformation Theory”, *Composite Structures*, Vol. 252, Article 112627, 2020

[39] A. Babu, P Sudhagar and R. Vasudevan, “Dynamic Characterization of Thickness Tapered Laminated Composite Plates”, *Journal of Vibration and Control,* Vol. 22, No.16, pp. 3555–3575, 2016.

[40] S. Ashok and P. Jeyaraj, “Static Deflection and Thermal Stress Analysis of Non-Uniformly Heated Tapered Composite Laminate Plates with Ply Drop-Off”, *Structures*, Vol. 15, pp. 307-319, 2018.

[41] R. K. Munian, D. R. Mahapatra and S. Gopalakrishnan, “Lamb Wave Interaction with Composite Delamination”, *Composite Structures*, Vol. 206, pp. 484-498, 2018.

[42] A.A. Mekonnen, K. Woo, M Kang et al., “Post-Buckling and Delamination Propagation Behavior of Composite Laminates with Embedded Delamination”, *Journal of Mechanical Science and Technology*, Vol. 34, pp. 1099–1110, 2020.

[43] M. Hassan, G. Hussain, A. Ali et al., “Effect of Pre-Rolling Temperature on the Interfacial Properties and Formability of Steel-Steel Bilayer Sheet in Single Point Incremental Forming”, *Journal of engineering manufacturing*, Vol. 235, pp. 406-416, 2020.

[44] Z. Zhang, J. Pan, W. Luo et al., “Vibration-Based Delamination Detection in Curved Composite Plates”, *Composites Part A: Applied Science and Manufacturing*, Vol. 119, pp. 261-274, 2019.

[45] H. Alidoost and J. Rezaeepazhand, “Instability of a Delaminated Composite Beam Subjected to a Concentrated Follower Force”, *Thin-Walled Structures*, Vol. 120, pp. 191-202, 2017.

[46] M. Imran, R. Khan and S. Badshah, “Finite Element Analysis to Investigate the Influence of Delamination Size, Stacking Sequence and Boundary Conditions on the Vibration Behavior of Composite Plate”, *Iranian Journal of Material Science and Engineering*, Vol. 16, pp. 11-21, 2019.

[47] A. Babu and R. Vasudevan, “Vibration Analysis of Rotating Delaminated Non-Uniform Composite Plates”, *Aerospace Science and Technology*, Vol. 60, pp. 172-182, 2017.

[48] M. Lezgy-Nazargah “Assessment of refined high-order global–local theory for progressive failure analysis of laminated composite beams”, *Acta Mechanica,* Vol. 228, No. 5, 2017, pp. 1923-1940.

[49] https://www.mm.bme.hu/~gyebro/files/ans_help_v182/ans_elem/Hlp_E_SHELL181.html

[50] https://www.mm.bme.hu/~gyebro/files/ans_help_v182/ans_elem/Hlp_E_SOLID185.html

[51] M. W. Hyer, Stress Analysis of Fiber-reinforced Composite Materials, WCB McGraw-Hill publishers, 1998.

[52] http://www.redbackaviation.com/understanding-rotor-blades-the-rotary-wing

[53] https://acs-composites.com/

[54] https://www.reddit.com/r/EngineeringPorn/comments/hmdwfp/genx_fan_blades/

[55] https://line.17qq.com/articles/mkwsnngsy.html

Appendix A

Pictorial illustration of applications of stationary and rotating composite beams

Figure A.1 Turbine blades for aircraft engines made up of composite material made up of composite material [54]

Figure A.2 Rotor blades for drone made from epoxy-graphite composite material [53]

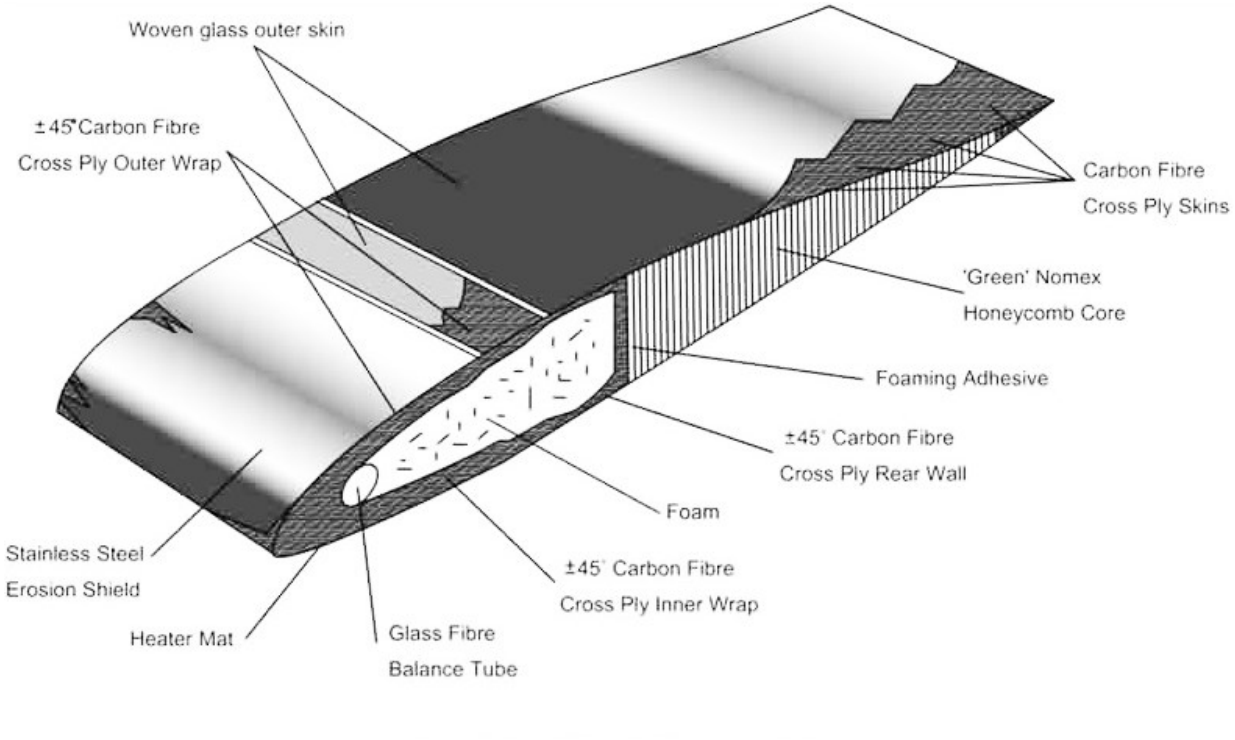

Figure A.3 Cross-section view of helicopter blade [52]

Figure A.4 Cross-section of aircraft wing [55]

Appendix B

Convergence study

468 elements	612 elements	1800 elements	7200 elements	ANSYS® Results available in Ref. [11]
101.91	101.86	101.82	101.79	101.80
636.87	633.02	630.08	628.2	629.00
1783.6	1754.3	1732.3	1718.3	1725.50

Table B.1 Convergence study of uniform composite beam for $[0]_{18s}$ stacking sequence using SOLID185 finite elements

Appendix C

Screenshots of the important steps required for modeling doubly tapered composite beams in ANSYS®

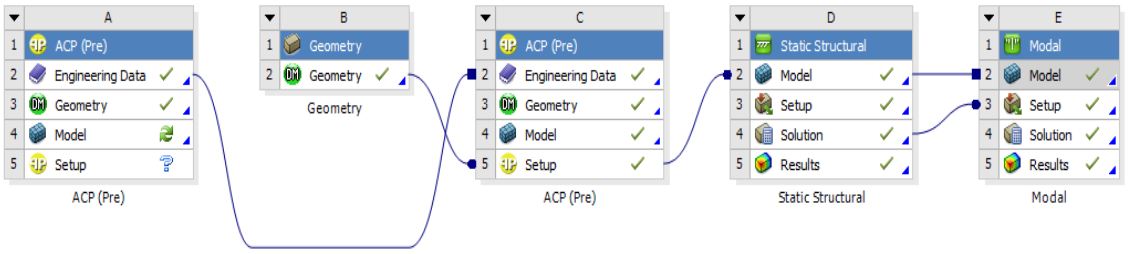

Figure C.1 Project schematic

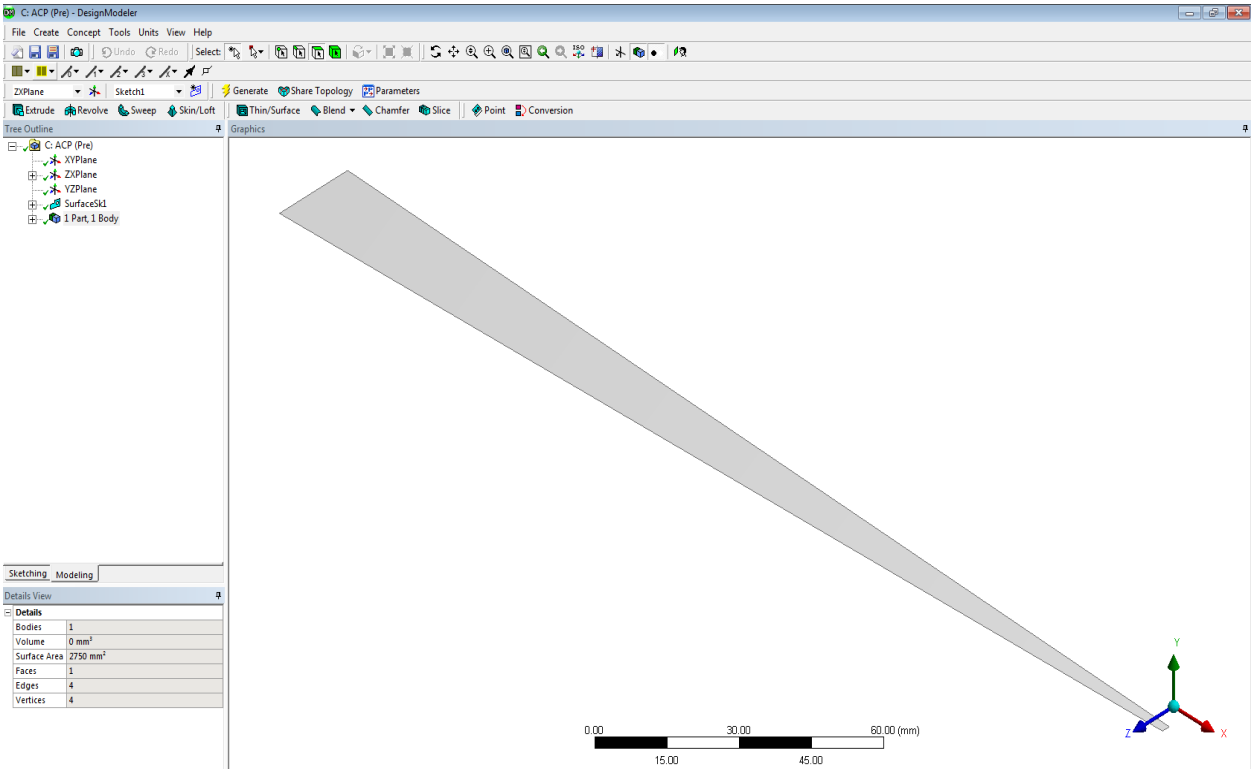

Figure C.2 Geometry of the plane surface required for the modeling of doubly tapered composite beam created in Design Modeler

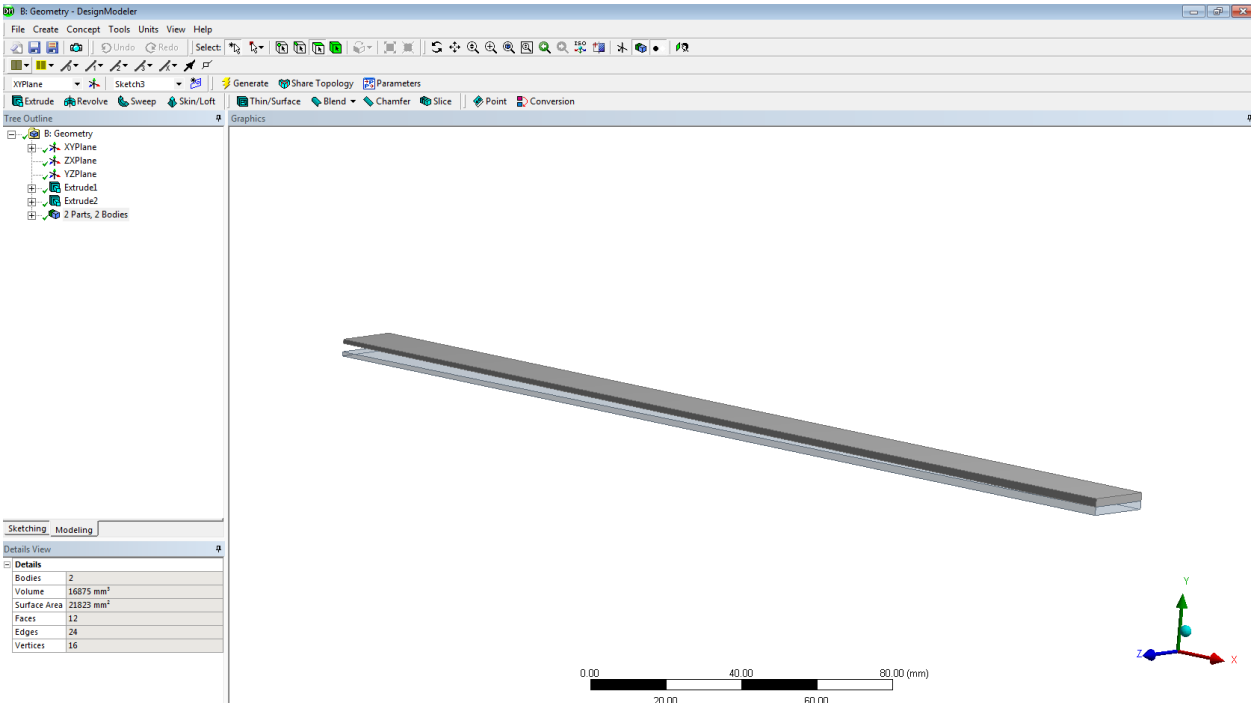

Figure C.3 Cut-off geometry required for the thickness-tapering of doubly tapered composite beam created in design modeler

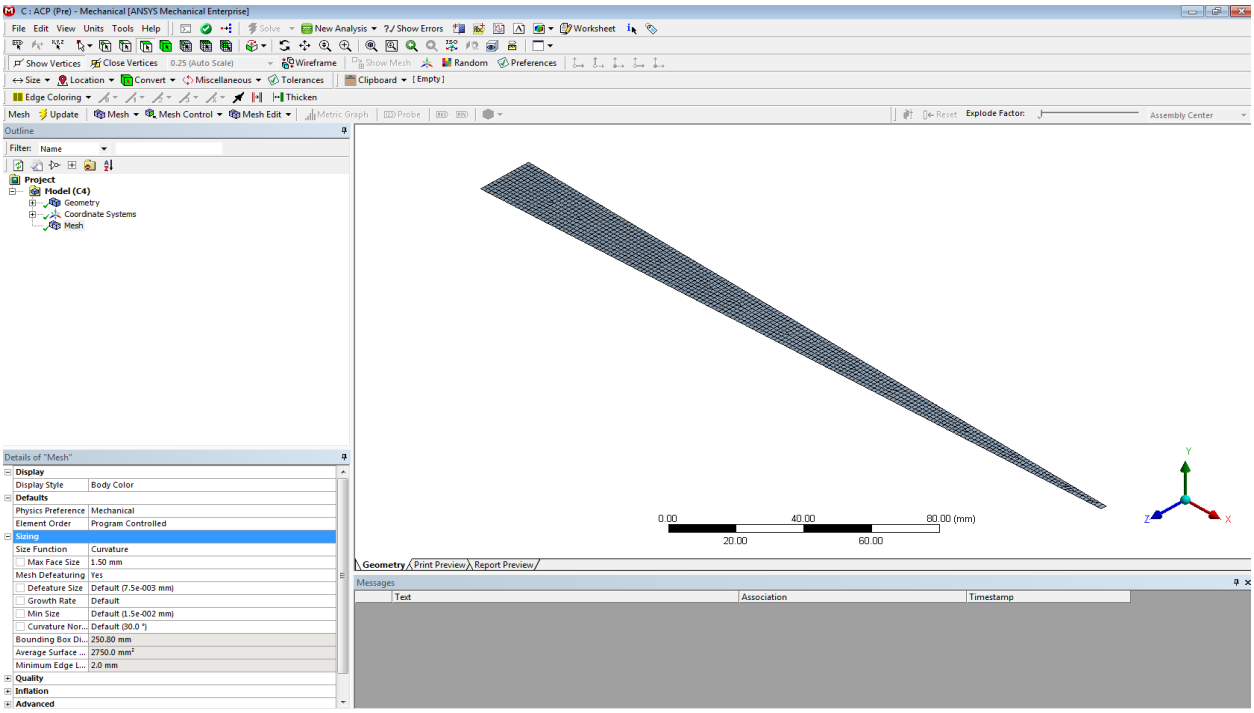

Figure C.4 Meshing of the plane surface done in Mechanical module of ACP (Pre)

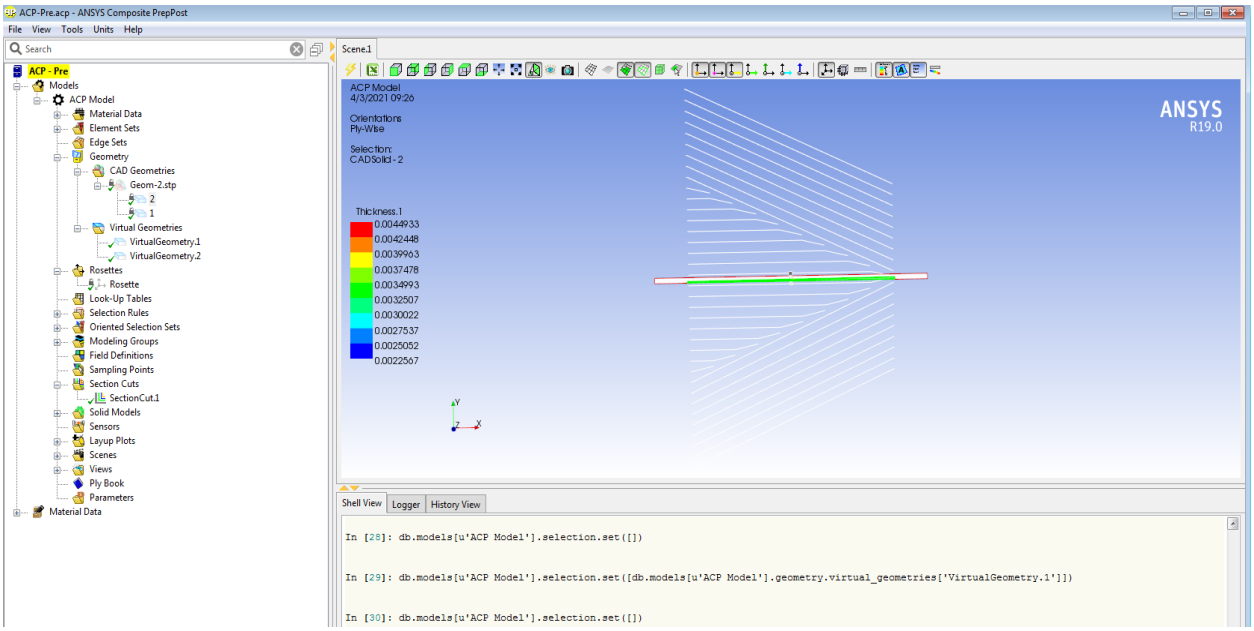

Figure C.5 Virtual geometries created in ACP using CAD geometries which are cut-off geometries imported from Design Modeler

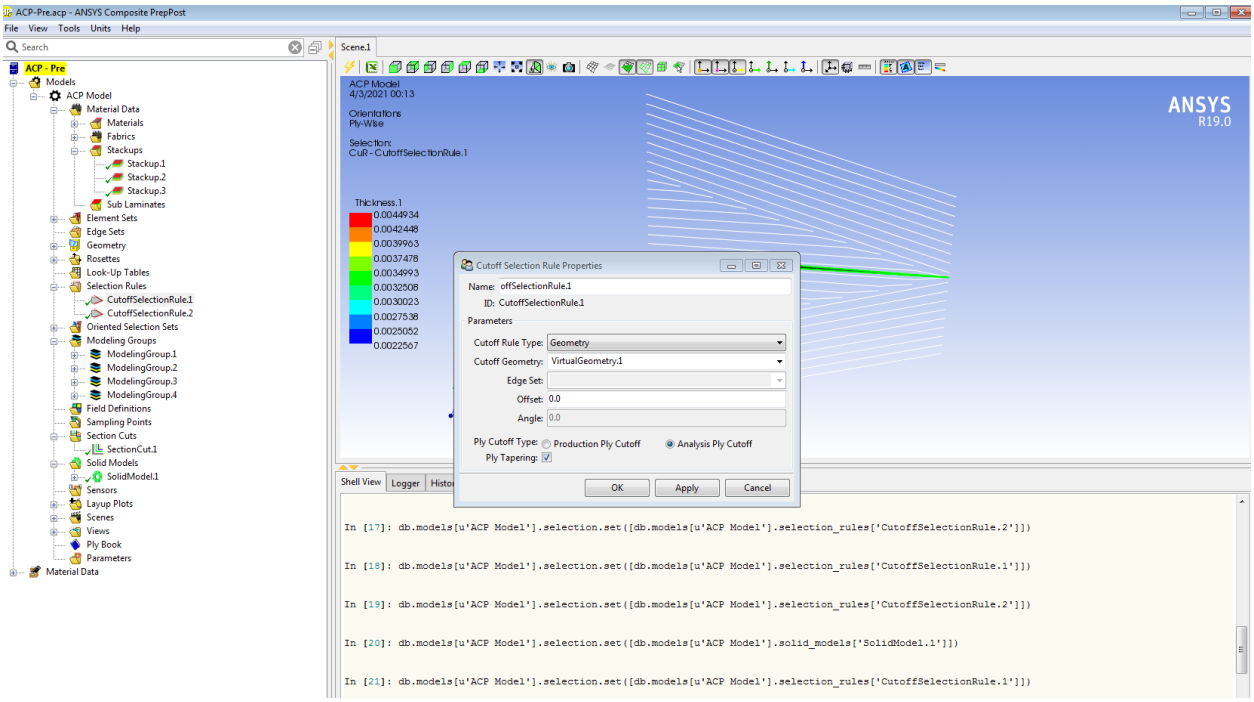

Figure C.6 Details of cut-off selection rule

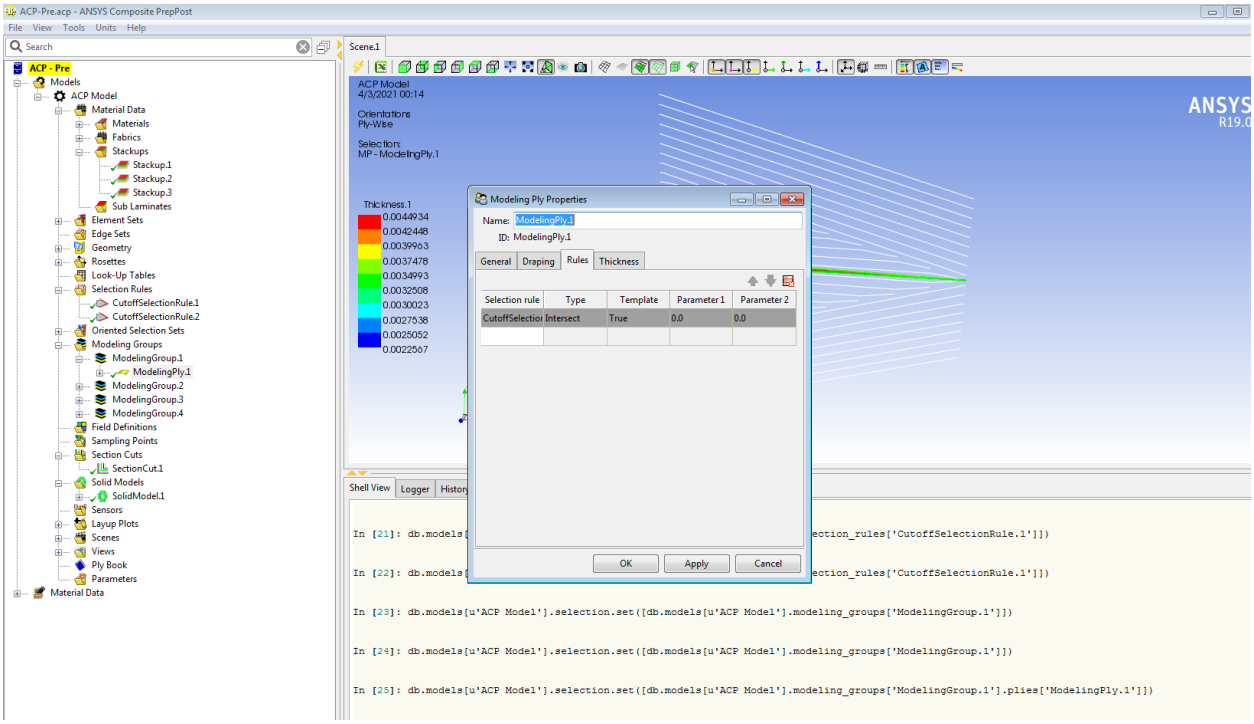

Figure C.6 Applying cut-off selection rule to the modeling of group of the plies to be dropped-off

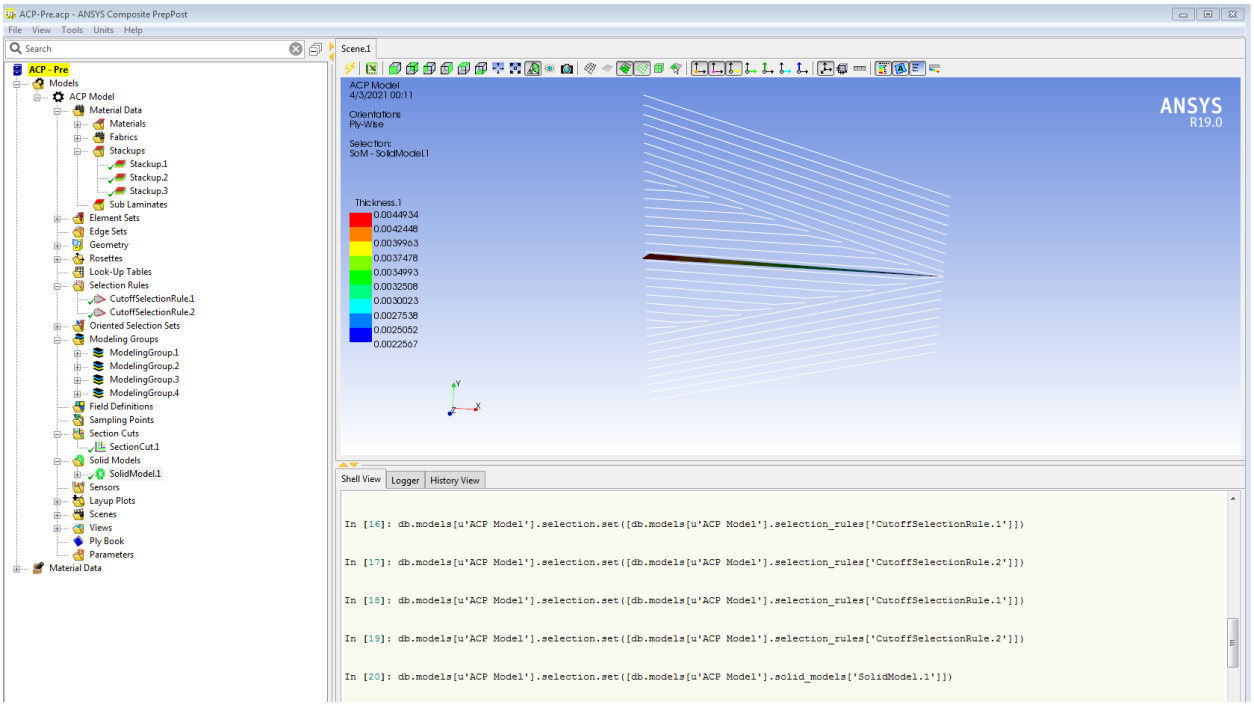

Figure C.7 Applying cut-off selection rule to the modeling of group of the plies to be dropped-off

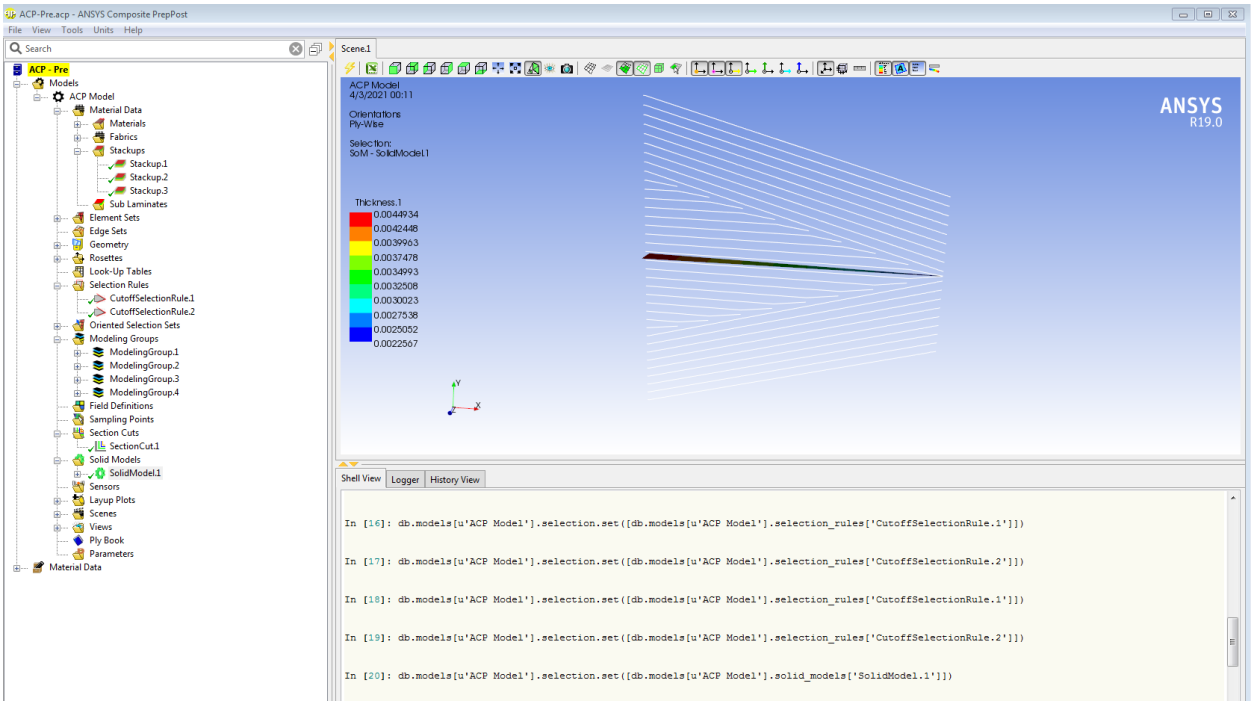

Figure C.7 Solid geometry and selection cut of doubly tapered composite beam

Appendix D

Screenshots of the important steps required for modeling cohesive zone for Mode-II delamination test

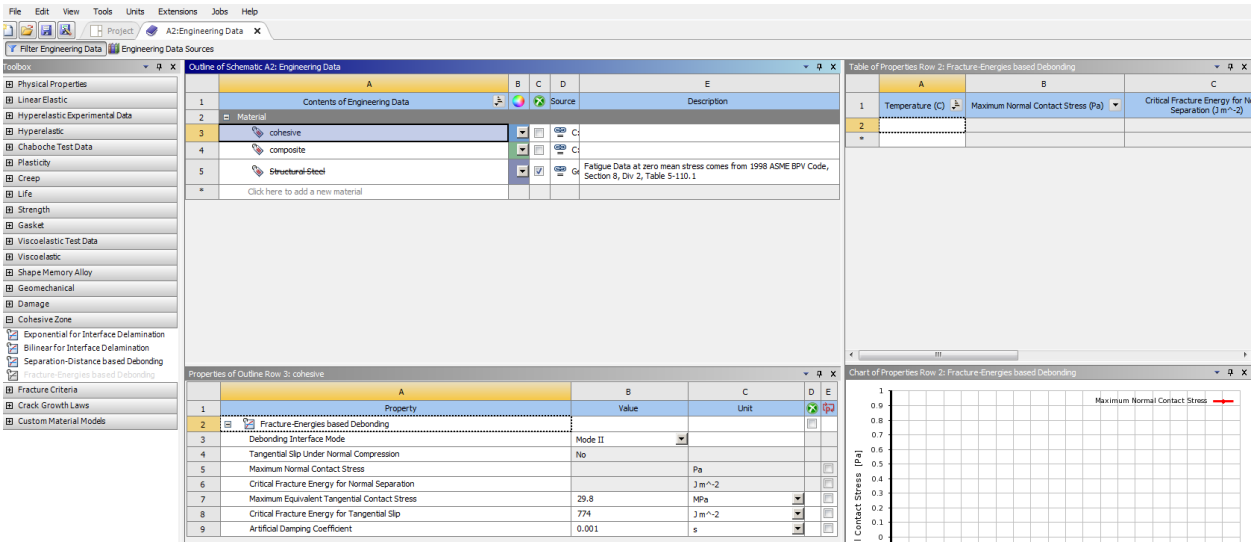

Figure D.1 Engineering properties of the cohesive zone

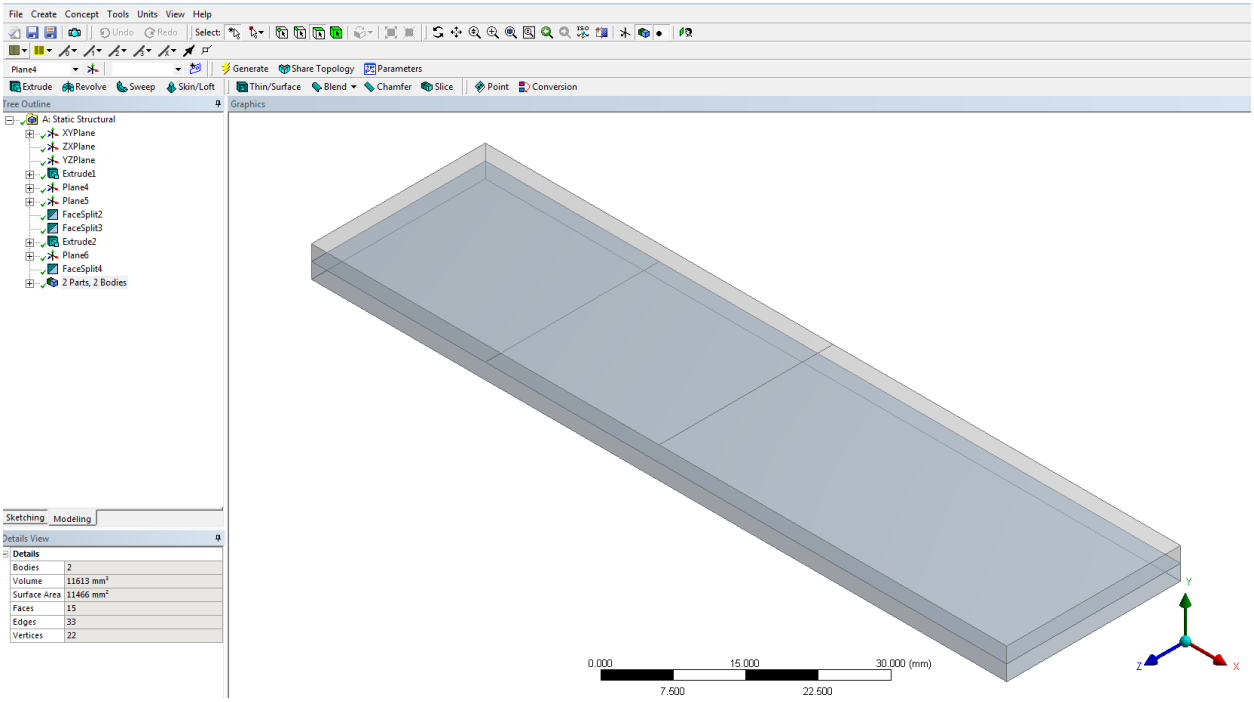

Figure D.2 Geometry of ENF test sample created in Design Modeler

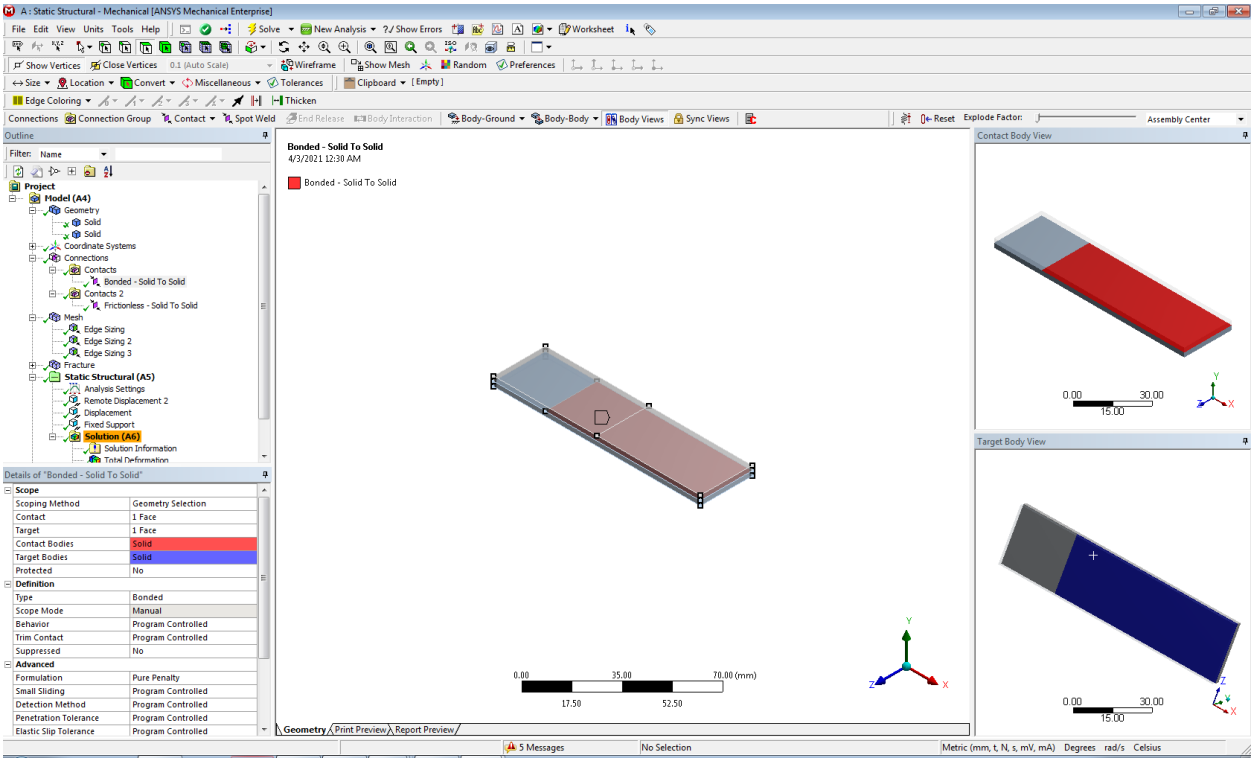

Figure D.3 Details of bonded region (cohesive interface)

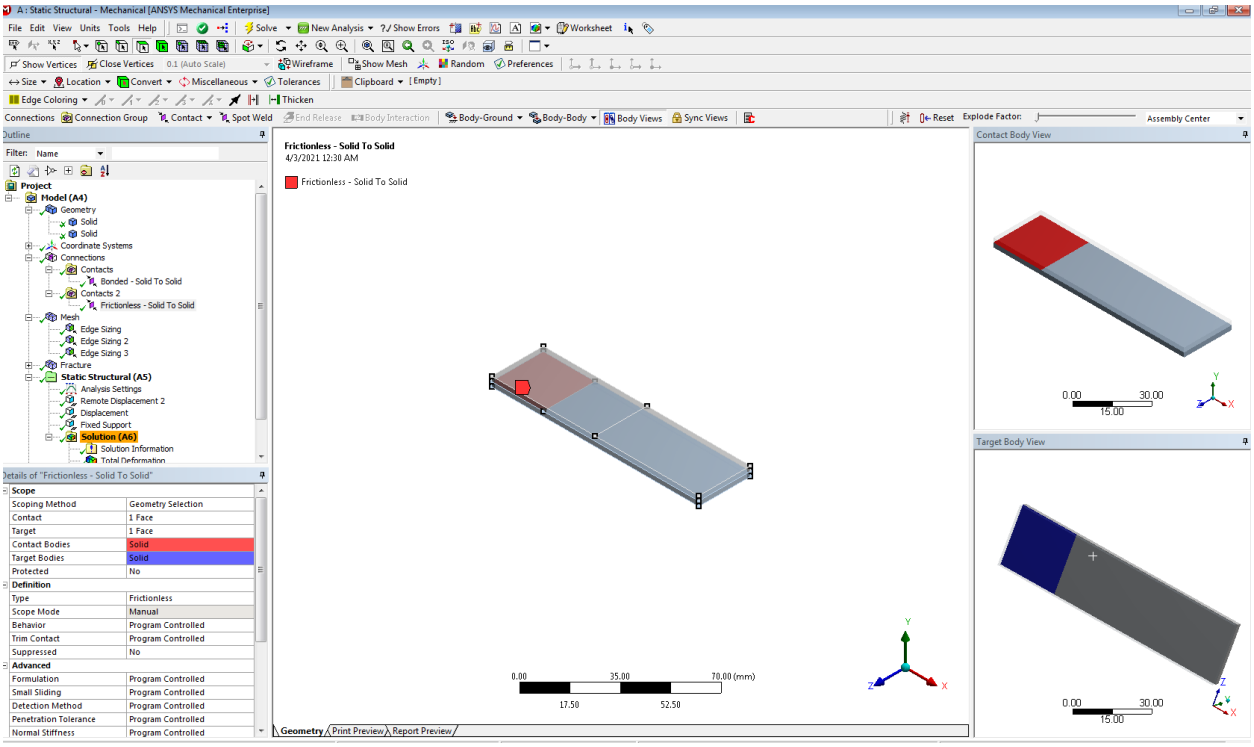

Figure D.4 Details of frictionless region (delaminated interface)

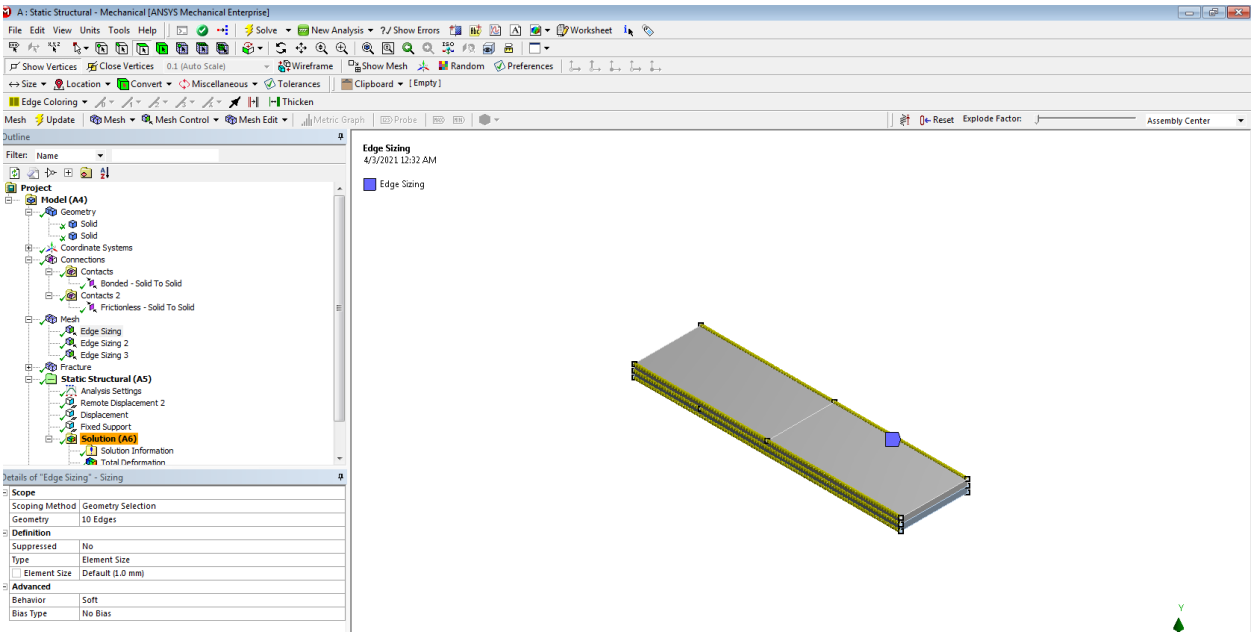

Figure D.5 Details of edge mesh along the length

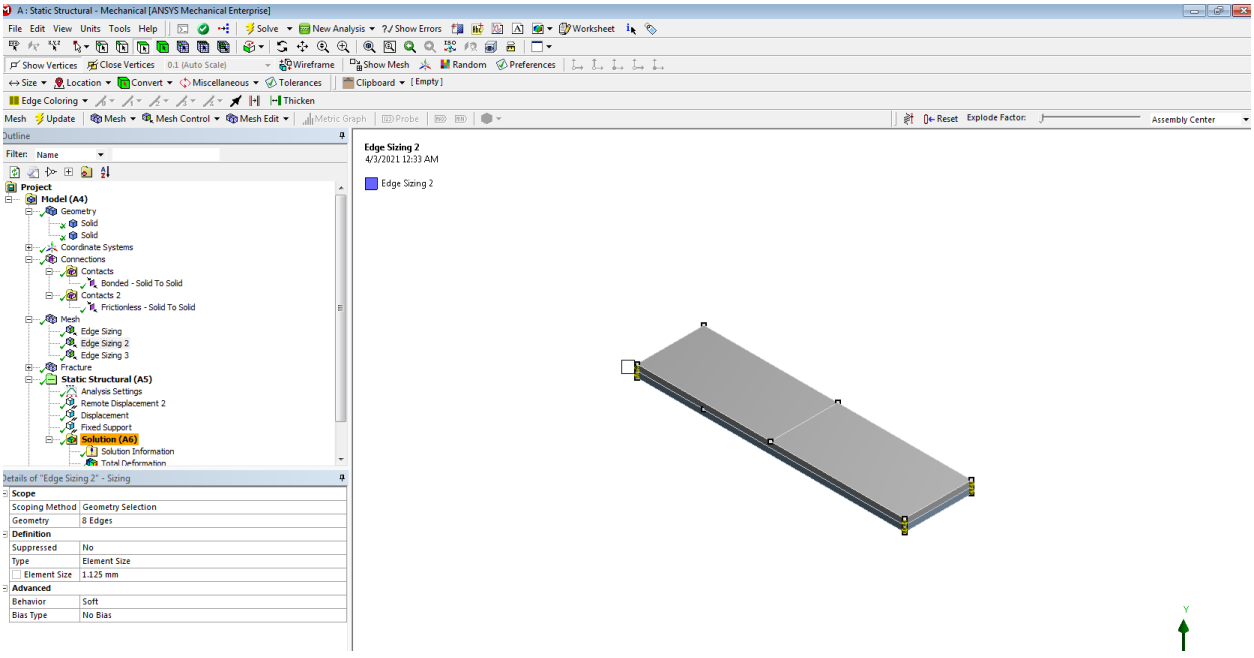

Figure D.5 Details of edge mesh along the thickness

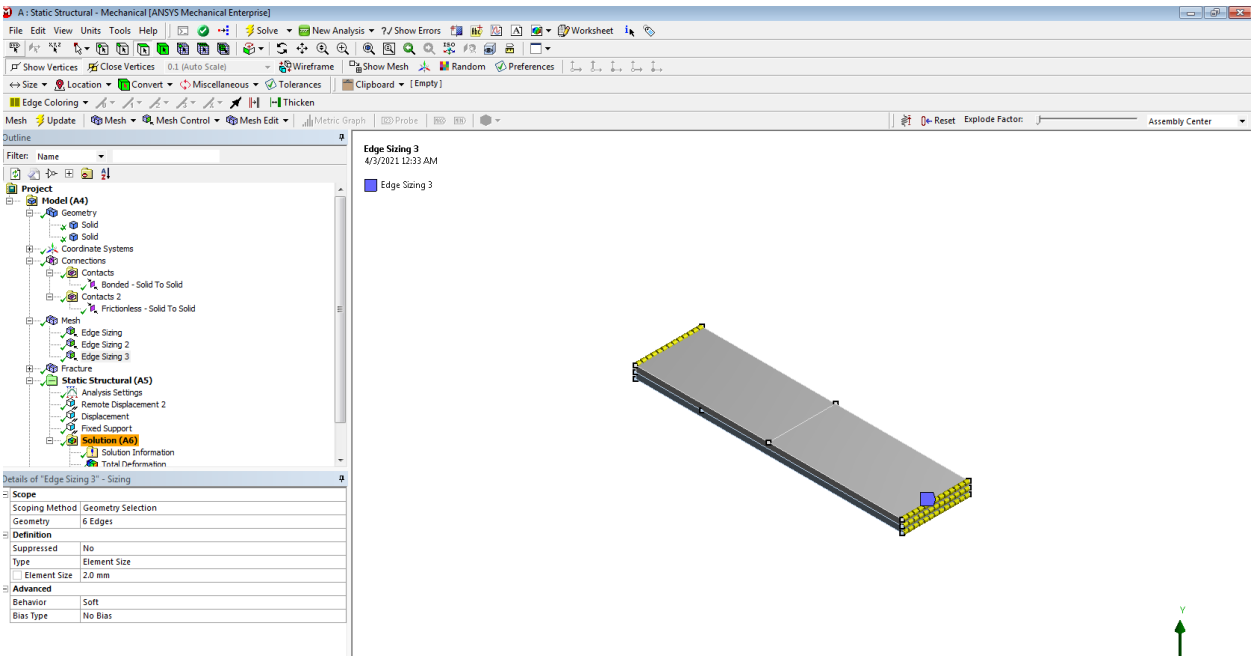

Figure D.6 Details of edge mesh along the width

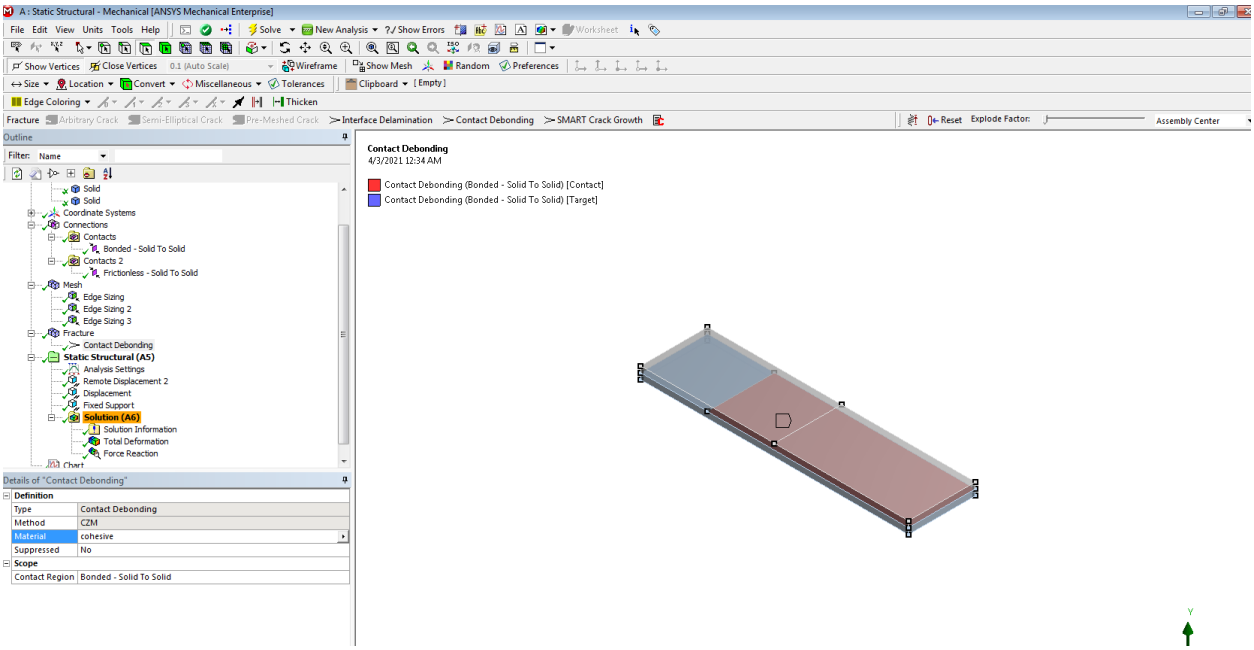

Figure D.6 Details of contact debonding

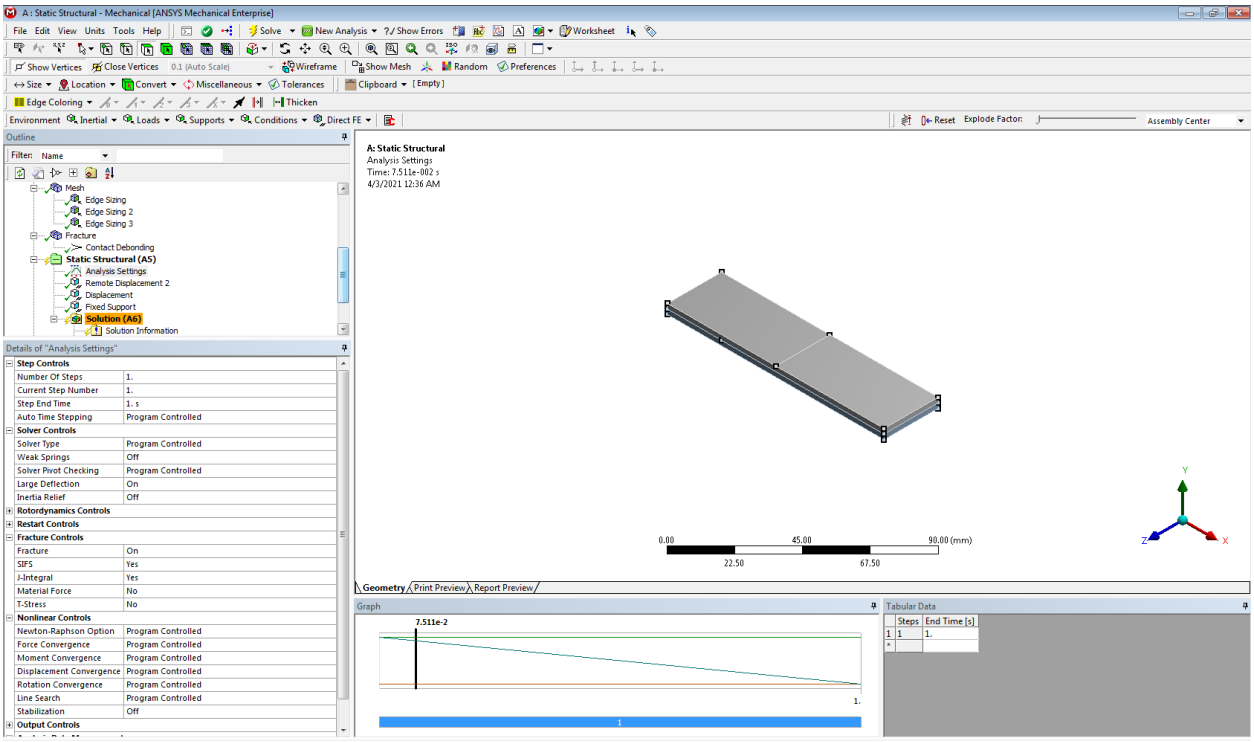

Figure D.7 Details of analysis settingsref..